



RU GRANT FINAL REPORT FORM

Please email a softcopy of this report to rcmo@usm.my

A	PROJECT DETAILS
i	Title of Research: Super acid functionalized ordered mesoporous catalysts for selective production of monoglycerides from glycerol: A pilot study
ii	Account Number: 1001/PJKIMIA/814181
iii	Name of Research Leader: Prof Dr Ahmad Zuhairi Abdullah
iv	Name of Co-Researcher: 1. Assoc Prof Dr Mohd Azmier Ahmad 2.
v	Duration of this research: a) Start Date : 15 December 2012 b) Completion Date : 14 December 2015 c) Duration : 36 months d) Revised Date (if any) : 14 August 2016
B	ABSTRACT OF RESEARCH
	<p><i>(An abstract of between 100 and 200 words must be prepared in Bahasa Malaysia and in English. This abstract will be included in the Report of the Research and Innovation Section at a later date as a means of presenting the project findings of the researcher/s to the University and the community at large)</i></p> <p>Abstract</p> <p>An increase in glycerol production is expected because of the increasing use of methyl esters (biodiesel). This increase can enhance the importance of glycerol as a cheap raw material for producing value-added products. Future scenarios for worldwide glycerol market will mostly be related to the supply and demand of glycerol and its application in other industries are first reviewed. Esterification of lauric acid with glycerol to selectively form monoglycerides (monolaurin and monopalmitin) was conducted using 12-tungstophosphoric acid (HPW) supported SBA-15 and sulfated zirconia SBA as catalysts. Via direct synthesis method, highly uniformed SBA-15 catalysts functionalized with 12-tungstophosphorus acid (HPW) were synthesized. Their characteristics were investigated using BET surface analysis, NH₃-TPD, FTIR, SEM, TEM, EDS and TGA. Surface defects were found in SBA-15 catalysts with high HPW loading (30-40 wt. %). High loadings also caused the deposition of HPW on the external surface and subject to oxidative decomposition to WO₃ that affected their acidity. HPW in mesopores had better thermal stability. High lauric acid conversion (70 %) and</p>

monolaurin yield (50 %) were shown in 6 h at 160 °C by the catalyst with 20 wt. % HPW. Lower yield was achieved at higher temperature. Its ordered mesoporosity evidently resulted in shape selectivity effect to suppress by-products formation. Effects of reaction temperature (150-170 °C), reactant ratios (1:1-5:1) and catalysts loadings (1-5 wt. %) were thoroughly elucidated. They were synthesized with HPW loadings of 10–40 wt. % and characterized for surface characteristic, acidity profile, surface morphology and elemental composition. A conversion of 95 % for lauric acid with monolaurin yield of 53 % were achieved while the excellent activity was successfully correlated with the characteristics. Effects of different reaction parameters including temperature (150-170 °C), reactant ratio (1:1-5:1) and catalyst loading (1-5 wt. %) were also elucidated. High turnover number (1,123–4,262) and turnover frequency (3.1–11.8 min⁻¹) were demonstrated by the catalysts. 40wt%-HPW/IM was the most suitable catalyst for this reaction. Optimization of lauric acid conversion and monolaurin yield catalysed by highly uniformed SBA-15 catalysts post impregnated with 12-tungstophosphorus acid (HPW) were elucidated via design of experiment (DoE): response surface methodology (RSM). Significance effect of factors including reaction time (t), reactant ratio (R) and temperature (T) were investigated, leading to development of response model monolaurin yield (R₂), respectively. Optimized monolaurin yield operating condition (50% yield at t=3.18 h, R=4.6 and T=175 °C) were found using developed model that showed both high accuracy (98% confidence level, small standard deviation and error) and repeatability (3 times). Comparison of optimized operating condition with other literature reported results showed superior performance of developed catalyst with significant reduction in reaction time needed for similar lauric acid conversion and monolaurin yield. The structural properties of the prepared catalysts were characterized using different characterization techniques. Sulfated zirconia was successfully incorporated with improved properties, such as larger mesopore surface area; the mesoporous structure was preserved as well. The highest yield of 79.1% was obtained during reaction over SZSBA-15 catalyst with 16 wt.% zirconium oxychloride loading and 3 h of reflux time. About 83.4% selectivity toward monolaurin was achieved at a high conversion of lauric acid (94.9 %), a lauric acid-to-glycerol molar ratio of 4.0, within 6 h, and at 160 °C. Product distribution was successfully elucidated. Multiple kinetic models including simple power law model and mechanism based models were investigated for selective esterification of glycerol with lauric acid using post impregnated 12-tungstophosphoric acid SBA-15. Rate equation for all suggested models and mechanisms were derived and appropriate experimental works were performed. The model best describe the studied reaction is found to be a combination of both nucleophilic substitution mechanism with Langmuir-Hinshelwood kinetic model with high accuracy and reliability of the model observed. The mechanism scheme describing the reaction from the bulk up to reactant molecular level and the interaction between reactant molecules on catalyst surface was outlined. Activation energy (E_a) of the studied reaction is found to be 35.62 kJ mol⁻¹ with the Arrhenius constant, A of 1141.2 L mol⁻¹ g_{cat}⁻¹ h⁻¹ shows 40wt%-HPW/IM to have relatively low activation energy compared with reported catalyst on the same or reaction.

Abstrak

Peningkatan dalam pengeluaran gliserol adalah dijangka kerana peningkatan penggunaan bahan api seperti ester metil (biodiesel). Peningkatan ini boleh meningkatkan pengeluaran gliserol sebagai bahan mentah yang murah untuk mengeluarkan produk nilai tambah. Senario masa depan untuk pasaran di seluruh dunia gliserol kebanyakannya akan berkaitan dengan bekalan dan permintaan gliserol dan aplikasinya dalam industri lain. Pengesteran selektif asid laurik dengan gliserol untuk membentuk monogliserida (monolaurin dan monopalmitin) telah dijalankan menggunakan asid 12-tungstophosphoric (HPW) disokong SBA-15 dan zirkonia tersulfat SBA sebagai pemangkin telah dikaji. Melalui kaedah sintesis langsung, pemangkin SBA-15 yang berstruktur sangat seragam yang difungsikan dengan asid 12-tungstophosphorus (HPW) telah disintesis. Ciri-ciri mereka telah disiasat menggunakan analisis BET permukaan, NH₃-TPD, FTIR, SEM, TEM, EDS dan TGA. Kecacatan permukaan ditemui pada pemangkin SBA-15 dengan muatan HPW tinggi (30-40 wt.%). Beban yang tinggi juga menyebabkan pemendapan HPW pada permukaan luar dan membawa kepada penguraian oksidatif kepada WO₃ yang menjejaskan keasidan. HPW dalam mesolintang mempunyai kestabilan haba yang lebih baik. Penukaran asid laurik yang tinggi (70%) dan hasil monolaurin yang baik (50%) telah ditunjukkan dalam 6 jam pada 160 °C oleh pemangkin dengan 20 wt. % HPW. Hasil yang lebih rendah telah dicapai pada suhu yang lebih tinggi. Mesoporositi mangkin ternyata mengakibatkan kesan kepemilihan bentuk untuk pembentukan produk. Kesan suhu tindak balas (150-170 °C), nisbah bahan tindak balas (1: 1-5: 1) dan pemangkin beban (. 1-5% berat) telah berjaya diperincikan. Mangkin-mangkin telah disintesis dengan beban HPW daripada 10-40 wt. % dan dicirikan bagi sifatnya permukaan, profil keasidan, permukaan morfologi dan komposisi unsur. Penukaran 95% asid laurik dengan hasil monolaurin 53% telah dicapai manakala aktiviti yang baik telah berjaya dihubungkan dengan ciri-ciri mangkin. Kesan parameter tindak balas berbeza termasuk suhu (150-170 °C), nisbah bahan tindak balas (1: 1-5: 1) dan muatan pemangkin (1-5% berat) juga telah dijelaskan. Jumlah perolehan yang tinggi dan kekerapan perolehan telah ditunjukkan oleh pemangkin. 40wt% -HPW/IM merupakan pemangkin yang paling sesuai untuk tindak balas ini. Optimisasi penukaran asid laurik dan hasil monolaurin oleh pemangkin SBA-15 yang sangat beruniform yang diimpregnasi dengan asid 12-tungstophosphorus (HPW) telah dijelaskan melalui reka bentuk eksperimen

kaedah gerak balas permukaan (RSM). Kesan faktor termasuk masa tindak balas (t), nisbah bahan tindak balas (R) dan suhu (T) telah disiasat, yang membawa kepada pembangunan hasil model sambutan monolaurin optimum, masing-masing. Hasil optimum monolaurin (50% hasil pada t = 3.18 jam, R = 4.6 dan T = 175 °C) telah didapati menggunakan model yang menunjukkan kedua-dua ketepatan yang tinggi (98% tahap keyakinan, sisihan piawai kecil dan kesilapan) dan kebolehulangan (3 kali). Perbandingan keadaan operasi dioptimumkan dengan maklumat yang dilaporkan menunjukkan prestasi unggul pemangkin yang dibangunkan dengan pengurangan ketara dalam masa tindak balas yang diperlukan untuk penukaran laurik asid dan hasil monolaurin yang sama. Sifat-sifat struktur pemangkin yang disediakan telah dicirikan menggunakan teknik-teknik pencirian yang berbeza. Sulfat zirkonia telah berjaya digabungkan dengan ciri-ciri yang lebih baik, seperti kawasan permukaan mesoliang lebih besar dan juga struktur mesoporous yang terpelihara. Hasil tertinggi 79.1% telah diperolehi semasa tindak balas menggunakan pemangkin SZSBA-15 dengan 16 wt. % muatan zirkonium oksiklorida dan masa refluks 3 jam. Kira-kira 83.4% kememilihan monolaurin telah dicapai pada penukaran yang tinggi asid laurik (94.9%), nisbah molar asid laurik kepada gliserol sebanyak 4.0, dalam masa 6 jam, dan pada 160 °C. Distribusi produk juga telah berjaya dijelaskan. Pelbagai model mudah termasuk model hukum kuasa dan model berasaskan mekanisme telah disiasat untuk pengesteran terpilih gliserol dengan asid laurik menggunakan asid 12-tungstophosphorik SBA-15. Persamaan kadar bagi semua model yang dicadangkan dan mekanisme diperolehi dan kerja-kerja eksperimen yang sewajarnya telah dilaksanakan. Model terbaik bagi menggambarkan tindakbalas yang dikaji didapati adalah gabungan kedua-dua mekanisme penggantian nukleofilik dengan model kinetik Langmuir-Hinshelwood dengan ketepatan dan kebolehpercayaan model yang tinggi. Skim mekanisme yang menggambarkan tindakbalas pukal sehingga bahan tindak balas peringkat molekul dan interaksi antara molekul bahan tindak balas pada permukaan mangkin telah dicadangkan. Tenaga pengaktifan (E_a) tindak balas yang dikaji didapati 35.62 kJ mol⁻¹ dengan pekali Arrhenius A 1141,2 L mol⁻¹ g_{cat}⁻¹ h⁻¹ menunjukkan mangkin 40wt%-HPW/IM mempunyai tenaga pengaktifan yang rendah berbanding dengan pemangkin dilaporkan bagi tindakbalas yang sama.

C BUDGET & EXPENDITURE

i	<p>Total Approved Budget : RM 211,000</p> <p style="text-align: center;"><u>Yearly Budget Distributed</u></p> <p>Year 1 : RM 90,000.00</p> <p>Year 2 : RM 58,100.00</p> <p>Year 3 : RM 62,400.00</p> <p>Total Expenditure : RM 210,974.92</p> <p>Balance : RM 25.08</p> <p>Percentage of Amount Spent (%) : 99.99</p> <p><i># Please attach final account statement (eStatement) to indicate the project expenditure</i></p>
---	--

ii Equipment Purchased Under Vot 35000

No.	Name of Equipment	Amount (RM)	Location	Status
1	Diaphragm pump	6,975	Environmental Lab, School of Chemical Engineering USM (0.16)	Still working
2	Magnetic heating stirrer plate	5,940	Environmental Lab, School of Chemical Engineering USM (0.16)	Still working
3	pH meter Schott	3,570	Environmental Lab, School of Chemical Engineering USM (0.16)	Broken. Writing Off
4	Memmert Oven 220C	3,250	Environmental Lab, School of Chemical Engineering USM (0.16)	Still working

Please attach the Asset/Inventory Return Form (Borang Penyerahan Aset/Inventori) – Appendix 1

D RESEARCH ACHIEVEMENTS																							
i	Project Objectives (as stated/approved in the project proposal)																						
	<table border="1"> <thead> <tr> <th>No.</th> <th>Project Objectives</th> <th>Achievement</th> </tr> </thead> <tbody> <tr> <td>1</td> <td>To design and fabricate a suitable integrated pilot reactor system for selective production of monoglycerides from glycerol.</td> <td>Achieved</td> </tr> <tr> <td>2</td> <td>To synthesize highly ordered mesoporous catalysts functionalized with super acid for selective production of monoglycerides by suppressing the formation of by-products.</td> <td>Achieved</td> </tr> <tr> <td>3</td> <td>To characterize physical, chemical and structural properties of the mesoporous catalyst materials for correlation with catalytic behaviors in the reaction.</td> <td>Achieved</td> </tr> <tr> <td>4</td> <td>To demonstrate the catalytic activity and stability of the mesoporous catalyst to selectively produce monoglycerides with effectiveness in achieving product separation goals to subsequently identify the optimum operation conditions.</td> <td>Achieved</td> </tr> <tr> <td>5</td> <td>To verify the overall feasibility of the optimized process based on the successful production of the desired product, economical consideration, practicality of the approach proposed, energy requirement, waste generation etc.</td> <td>Achieved</td> </tr> <tr> <td>6</td> <td>To develop a reliable mathematical model to accurately represent the reaction under various conditions for use in the scale up of the process.</td> <td>Achieved</td> </tr> </tbody> </table>	No.	Project Objectives	Achievement	1	To design and fabricate a suitable integrated pilot reactor system for selective production of monoglycerides from glycerol.	Achieved	2	To synthesize highly ordered mesoporous catalysts functionalized with super acid for selective production of monoglycerides by suppressing the formation of by-products.	Achieved	3	To characterize physical, chemical and structural properties of the mesoporous catalyst materials for correlation with catalytic behaviors in the reaction.	Achieved	4	To demonstrate the catalytic activity and stability of the mesoporous catalyst to selectively produce monoglycerides with effectiveness in achieving product separation goals to subsequently identify the optimum operation conditions.	Achieved	5	To verify the overall feasibility of the optimized process based on the successful production of the desired product, economical consideration, practicality of the approach proposed, energy requirement, waste generation etc.	Achieved	6	To develop a reliable mathematical model to accurately represent the reaction under various conditions for use in the scale up of the process.	Achieved	
No.	Project Objectives	Achievement																					
1	To design and fabricate a suitable integrated pilot reactor system for selective production of monoglycerides from glycerol.	Achieved																					
2	To synthesize highly ordered mesoporous catalysts functionalized with super acid for selective production of monoglycerides by suppressing the formation of by-products.	Achieved																					
3	To characterize physical, chemical and structural properties of the mesoporous catalyst materials for correlation with catalytic behaviors in the reaction.	Achieved																					
4	To demonstrate the catalytic activity and stability of the mesoporous catalyst to selectively produce monoglycerides with effectiveness in achieving product separation goals to subsequently identify the optimum operation conditions.	Achieved																					
5	To verify the overall feasibility of the optimized process based on the successful production of the desired product, economical consideration, practicality of the approach proposed, energy requirement, waste generation etc.	Achieved																					
6	To develop a reliable mathematical model to accurately represent the reaction under various conditions for use in the scale up of the process.	Achieved																					

ii	Research Output																
	a) Publications in ISI Web of Science/Scopus																
	<table border="1"> <thead> <tr> <th>No.</th> <th>Publication (authors, title, journal, year, volume, pages, etc.)</th> <th>Status of Publication (published/accepted/ under review)</th> </tr> </thead> <tbody> <tr> <td>1</td> <td>Hoo Peng Yong and Ahmad Zuhairi Abdullah (2014). Direct synthesis of mesoporous 12-tungstophosphoric acid SBA-15 catalyst for selective esterification of glycerol and lauric acid to monolaurate, Chemical Engineering Journal, 250, 274-287. (Publisher: Elsevier).</td> <td>Published</td> </tr> <tr> <td>2</td> <td>Zahra Gholami, Ahmad Zuhairi Abdullah, Keat Teong Lee (2014). Dealing with the surplus of glycerol production from biodiesel industry through catalytic upgrading to polyglycerols and other value-added products, Renewable and Sustainable Energy Reviews 2014, 39, 327-341. (Publisher: Elsevier).</td> <td>Published</td> </tr> <tr> <td>3</td> <td>Lilis Hermida, Ahmad Zuhairi Abdullah, Abdul Rahman Mohamed (2015). Deoxygenation of fatty acid to produce diesel-like hydrocarbons: A review of process conditions, reaction kinetics and mechanism, Renewable and Sustainable Energy Reviews, 42, 1223-1233. (Publisher: Elsevier).</td> <td>Published</td> </tr> <tr> <td>4</td> <td>Hoo Peng Yong and Ahmad Zuhairi Abdullah (2015). Kinetic modelling and mechanism study for selective esterification of glycerol with lauric acid using 12-tungstophosphoric acid post impregnated SBA-15, Industrial & Engineering Chemistry Research, 54, 7852-7858. (Publisher: American Chemical Society).</td> <td>Published</td> </tr> </tbody> </table>	No.	Publication (authors, title, journal, year, volume, pages, etc.)	Status of Publication (published/accepted/ under review)	1	Hoo Peng Yong and Ahmad Zuhairi Abdullah (2014). Direct synthesis of mesoporous 12-tungstophosphoric acid SBA-15 catalyst for selective esterification of glycerol and lauric acid to monolaurate, Chemical Engineering Journal, 250, 274-287. (Publisher: Elsevier).	Published	2	Zahra Gholami, Ahmad Zuhairi Abdullah, Keat Teong Lee (2014). Dealing with the surplus of glycerol production from biodiesel industry through catalytic upgrading to polyglycerols and other value-added products, Renewable and Sustainable Energy Reviews 2014, 39, 327-341. (Publisher: Elsevier).	Published	3	Lilis Hermida, Ahmad Zuhairi Abdullah, Abdul Rahman Mohamed (2015). Deoxygenation of fatty acid to produce diesel-like hydrocarbons: A review of process conditions, reaction kinetics and mechanism, Renewable and Sustainable Energy Reviews, 42, 1223-1233. (Publisher: Elsevier).	Published	4	Hoo Peng Yong and Ahmad Zuhairi Abdullah (2015). Kinetic modelling and mechanism study for selective esterification of glycerol with lauric acid using 12-tungstophosphoric acid post impregnated SBA-15, Industrial & Engineering Chemistry Research, 54, 7852-7858. (Publisher: American Chemical Society).	Published	
No.	Publication (authors, title, journal, year, volume, pages, etc.)	Status of Publication (published/accepted/ under review)															
1	Hoo Peng Yong and Ahmad Zuhairi Abdullah (2014). Direct synthesis of mesoporous 12-tungstophosphoric acid SBA-15 catalyst for selective esterification of glycerol and lauric acid to monolaurate, Chemical Engineering Journal, 250, 274-287. (Publisher: Elsevier).	Published															
2	Zahra Gholami, Ahmad Zuhairi Abdullah, Keat Teong Lee (2014). Dealing with the surplus of glycerol production from biodiesel industry through catalytic upgrading to polyglycerols and other value-added products, Renewable and Sustainable Energy Reviews 2014, 39, 327-341. (Publisher: Elsevier).	Published															
3	Lilis Hermida, Ahmad Zuhairi Abdullah, Abdul Rahman Mohamed (2015). Deoxygenation of fatty acid to produce diesel-like hydrocarbons: A review of process conditions, reaction kinetics and mechanism, Renewable and Sustainable Energy Reviews, 42, 1223-1233. (Publisher: Elsevier).	Published															
4	Hoo Peng Yong and Ahmad Zuhairi Abdullah (2015). Kinetic modelling and mechanism study for selective esterification of glycerol with lauric acid using 12-tungstophosphoric acid post impregnated SBA-15, Industrial & Engineering Chemistry Research, 54, 7852-7858. (Publisher: American Chemical Society).	Published															

5	Hoo Peng Yong and Ahmad Zuhairi Abdullah (2016). Optimization of monolaurin yield in selective esterification of glycerol with lauric acid catalyzed by post impregnated mesoporous HPW/SBA-15 catalyst, Korean Journal of Chemical Engineering, 33(4), 1200-1210. (Publisher: Springer).	Published
6	Ahmad Zuhairi Abdullah, Zahra Gholami, Muhammad Ayoub & Fatemeh Gholami (2016). Selective monolaurin synthesis through esterification of glycerol using sulfated zirconia-loaded SBA-15 catalyst, 203, 496-504. Chemical Engineering Communications. (Publisher: Taylor & Francis).	Published
7	Mohd Hizami Mohd Yusoff, Ahmad Zuhairi Abdullah (2016). Catalytic behavior of sulfated zirconia supported on SBA-15 as catalyst in selective glycerol esterification with palmitic acid to monopalmitin, Journal of Taiwan Institute of Chemical Engineers, 60, 199-204. (Publisher: Elsevier).	Published
8		

b) Publications in Other Journals

No.	Publication (authors,title,journal,year,volume,pages,etc.)	Status of Publication (published/accepted/ under review)
1	Lilis Hermida, Ahmad Zuhairi Abdullah, Abdul Rahman Mohamed (2013). Synthesis and characterization of mesostructured cellular foam (MCF) silica loaded with nickel nanoparticles as a novel catalyst, Materials Sciences and Applications, 4, 52-62. (Publisher: Scientific Research Publishing, USA).	Published
2	Lilis Hermida, Hadis Amani, Ahmad Zuhairi Abdullah and Abdul Rahman Mohamed (2016). Deoxygenation of palmitic acid to produce diesel-like hydrocarbons over nickel incorporated cellular foam catalyst: A kinetic study, Journal of Advanced Chemical Engineering, 6(1), 1-8. (Publisher: OMICS International, USA).	Published

c) Other Publications

(book, chapters in book, monograph, magazine, etc.)

No.	Publication (authors,title,journal,year,volume,pages,etc.)	Status of Publication (published/accepted/ under review)
1	Lilis Hermida, Ahmad Zuhairi Abdullah, Abdul Rahman Mohamed (2013). Nickel functionalized mesostructured cellular foam (MCF) silica as a catalyst for solventless deoxygenation of palmitic acid to produce diesel-like hydrocarbon, Materials and Processes for Energy: Communicating Current Research and Technological Developments, 312-319. Publisher: Formatex Research Center, Badajoz, Spain.	Published

d) Conference Proceeding

No.	Conference (conference name,date,place)	Title of Abstract/Article	Level (International/National)

Please attach a full copy of the publication/proceeding listed above

(Attached in the final report)

iii Other Research Output/Impact From This Project
(patent, products, awards, copyright, external grant, networking, etc.)

1. 1 Post-doctoral Fellow, Dr Shazia Sultana from Quaid-i-Azam University, Pakistan.
2. 1 Post-doctoral Fellow, Dr Hadis Amani.
3. Dana Inovasi Awal, "Feasibility demonstration of palm oil based monoglycerides production as halal emulsifiers using heterogeneous catalytic reactor system", RM : 50,000, Universiti Sains Malaysia. From 15 September 2014 to 14 September 2015 as project leader.
4. A Trans-Disiplinary Research Grant Scheme (TRGS 203/PJKIMIA/6762001) from the Ministry of Higher Education (Fasa 2/2014). Program Title: Production of valuable chemicals from crude glycerol using catalytic and biochemical methods. Project Title: Mesoporous composite catalyst for conversion of purified crude glycerol to lactic acid. 1 February 2015-31 January 2018.
5. Invited Talk (Plenary), International Conference on Environmental Research and Technology, 27-28 May 2015, Penang.
6. Invited Talk (Plenary). 11th Joint Conference on Chemistry, 15-16 September 2016, Purwokerto, Indonesia.
7. Invited Talk, International Conference on Biomass, 10-11 October 2016, Bogor, Indonesia.

E HUMAN CAPITAL DEVELOPMENT

a) Graduated Human Capital

Student	Nationality (No.)		Name
	National	International	
PhD	1	1	1. Hoo Peng Yong (Completed in 2016) 2. Mohd Hizami Mohd Yusoff (Completed in 2016)
MSc			1. Natasya Ghazali (Mixed mode) (Completed in 2012) 2. Syamima Nasrin Mohamed Salleh (910117-07-5464) (Completed in 2015)
Undergraduate			1. Siti Nuramirah Nor 'Azlan (2014-2015) 2. Dhivian A/L T. Nintiaselvan (2015-2016) 2. Lim Wei Mei (2015-2016)

b) On-going Human Capital

Student	Nationality (No.)		Name
	National	International	
PhD	-	-	1. 2.
MSc	-	-	1. 2.
Undergraduate	-	-	1. Kishor Kumar A/L A Murugan (2016-2017) 2.

c) Others Human Capital

Student	Nationality (No.)		Name
	National	International	
Post Doctoral Fellow		2	1. Dr Shazia Sultana (Pakistan) 2. Dr Hadis Amani (Iran)
Research Officer			1. 2.
Research Assistant	5	1	1. Syamima Nasrin Mohamed Salleh (910117-07-5464) 2. Helmi Amanullah (910128-07-5339) 3. Kartina Embong (911107-11-5594) 4. Muhammad Hazim Yaakob (911227-08-5289) 5. Yeoh Wei Jie (901018-07-5181) 6. Lilis Hermida (A1280176)
Others (.....)			1. 2.

F COMPREHENSIVE TECHNICAL REPORT

Applicants are required to prepare a comprehensive technical report explaining the project. The following format should be used (this report must be attached separately):

- Introduction
- Objectives
- Methods
- Results
- Discussion
- Conclusion and Suggestion
- Acknowledgements
- References

(Please see the attached technical reports on the details of works completed)

G PROBLEMS/CONSTRAINTS/CHALLENGES IF ANY

(Please provide issues arising from the project and how they were resolved)

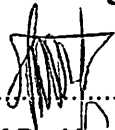
1. Long queue for the analytical services
2. Calibration for the GC analysis often resulted in erroneous results

H RECOMMENDATION

(Please provide recommendations that can be used to improve the delivery of information, grant management, guidelines and policy, etc.)

- i. To continue with a single line budget policy for internal grants.
- ii. To encourage inclusion of external researcher in the proposal
- iii. Successful projects should receive higher priority to secure next grant for continuation of the work.

Project Leader's Signature:



.....
Name : Prof Dr Ahmad Zuhairi Abdullah

Date : 30 September 2016

PROFESSOR DR AHMAD ZUHAIRI ABDULLAH
School of Chemical Engineering,
Universiti Sains Malaysia, Engineering Campus,
Nibong Tebal, Penang, Malaysia.

I COMMENTS, IF ANY/ENDORSEMENT BY PTJ'S RESEARCH COMMITTEE

Good research output and human capital
development outcome -

Jh 18/10/16

Signature and Stamp of Chairperson of PTJ's Evaluation Committee

Name : PROFESOR AZLINA HARUN @KAMARUDDIN
Dekan
Pusat Pengajian Kejuruteraan Kimia
Kampus Kejuruteraan
Date : Universiti Sains Malaysia, Seri Ampangan
14300 Nibong Tebal, Seberang Perai Selatan
Pulau Pinang.

Jh 18/10/16

Signature and Stamp of Dean/ Director of PTJ

Name : PROFESOR AZLINA HARUN @KAMARUDDIN
Dean
Pusat Pengajian Kejuruteraan Kimia
Kampus Kejuruteraan
Date : Universiti Sains Malaysia, Seri Ampangan
14300 Nibong Tebal, Seberang Perai Selatan
Pulau Pinang.



BORANG PENYERAHAN ASET / INVENTORI

A. BUTIR PENYELIDIK

1. NAMA PENYELIDIK : PROF DR AHMAD ZUHAIRI ABDULLAH
 2. NO STAF : 0424/14
 3. PTJ : PP KEJURUTERAAN KIMIA
 4. KOD PROJEK : 1001/PJKIMIA/814181
 5. TARIKH TAMAT PENYELIDIKAN : 14 OGOS 2016

B. MAKLUMAT ASET / INVENTORI

BIL	KETERANGAN ASET	NO HARTA	NO. SIRI	HARGA (RM)
1	Diaphragh Pump	AK00007090	3376109	6,975
2	Magnetic Heating Stirrer Plate	AK00007091	07-359093	5,940
3	pH Meter Schott	AK00007092	13031305	3,570
4	Oven Memmert 220C	AK00007130	B113.0034	3,250

0.16
0.16
Lupus
0.16

C. PERAKUAN PENYERAHAN

Saya dengan ini menyerahkan aset/ inventori seperti butiran B di atas kepada pihak Universiti:

PROFESOR DR AHMAD ZUHAIRI ABDULLAH
 (Pusat Pengajian Kejuruteraan Kimia,
 Universiti Sains Malaysia, Kampus Kejuruteraan,
 14300 Nibong Tebal, Pulau Pinang, Malaysia)

Tarikh: 04/10/2016

D. PERAKUAN PENERIMAAN

Saya telah memeriksa dan menyemak setiap alatan dan didapati :

- Lengkap
 Rosak
 Hilang : Nyatakan.....
 Lain-lain : Nyatakan

Diperakukan Oleh :

Tandatangan)
 Pegawai Aset PTJ

MOHD. YUSOF BIN ISMAIL
 Peninggal Juruara JA38
 Pusat Pengajian Kejuruteraan Kimia
 Kampus Kejuruteraan
 Universiti Sains Malaysia
 Seri Asempagan

Nama :
 Tarikh : 12/10/2016

*Nota : Sesalanan borang yang telah lengkap perlulah dikemukakan kepada Unit Pengurusan Harta, Jabatan Bendahari dan Pejabat RCMO untuk tujuan rekod.

Nickel functionalized mesostructured cellular foam (MCF) silica as a catalyst for solventless deoxygenation of palmitic acid to produce diesel-like hydrocarbons

Lilis Hermida^{1,2}, Ahmad Zuhairi Abdullah^{1,*} and Abdul Rahman Mohamed¹

¹ School of Chemical Engineering, Universiti Sains Malaysia, 14300 Nibong Tebal, Penang, Malaysia

² Department of Chemical Engineering, Universitas Lampung, Bandar Lampung 35145, Lampung, Indonesia

*E-mail: chzuhairi@eng.usm.my *Tel: +604-594 1013

Mesostructured cellular foam (MCF) silicas synthesized at different conditions were incorporated with nickel to synthesize nickel functionalized MCF catalysts. Morphologies of the MCF silicas and the catalysts were characterized using nitrogen adsorption-desorption, scanning electron microscope (SEM) and energy dispersive X-ray (EDX). Activities of the catalysts were evaluated based on solventless deoxygenation of palmitic acid for 6 h at 300 °C under inert atmosphere in a semi batch reactor for production of n-pentadecane and 1-pentadecene as hydrocarbon fuels. Palmitic acid conversion of 86.4% with n-pentadecane selectivity of 31.8 % and 1-pentadecene selectivity of 29.2 % was achieved by a catalyst using TEOS amount of 9.2 ml and aging time of 3 days in the MCF syntheses. The highest activity of the catalyst was attributed to the highest nickel content together with the smallest nickel particles dispersed in the catalyst.

Keywords: mesostructured cellular foam; silica; nickel incorporation; deoxygenation; palmitic acid; hydrocarbon fuels.

1. Introduction

Diesel fuel demand is predicted to grow from 24 million barrels per day in 2009 to 34 million barrels per day by 2030 as reported in OPEC World Oil Outlook [1]. Diesel fuel is derived from fossil fuel source which is non-renewable and the amount is finite. Therefore, the increasing demand of diesel fuel leads to an important development of biomass-based technologies to produce biofuels. Biomass, a renewable source, is biological material from living organisms such as, trees, crops, animals, plants, co-product from industrial process and wastes from agriculture and industries [2]. Biomass supplies are not limited since trees, animals and crops are biologically reproducible and waste will always exist.

Palm fatty acid distillate (PFAD) is a co-product of the physical refining of crude palm oil (CPO) to produce refined, bleached and deodorized (RBD) palm oil in which CPO is obtained from oil palm fruits through an oil mill, as can be seen in Fig. 1. The RBD palm oil is usually used for production of vegetable oil and can also be used in the manufacture of margarine, shortening, ice cream and condensed milk [3]. PFAD contains more than 90 % palmitic acid [4]. So far, PFAD is mostly used as a raw material for laundry soap industries [4]. The use of PFAD as feedstock for production of biofuels, as value-added products, has more advantages in terms of price and availability, especially in Malaysia and Indonesia, as these countries are the world's top-two largest CPO producers [4,5].

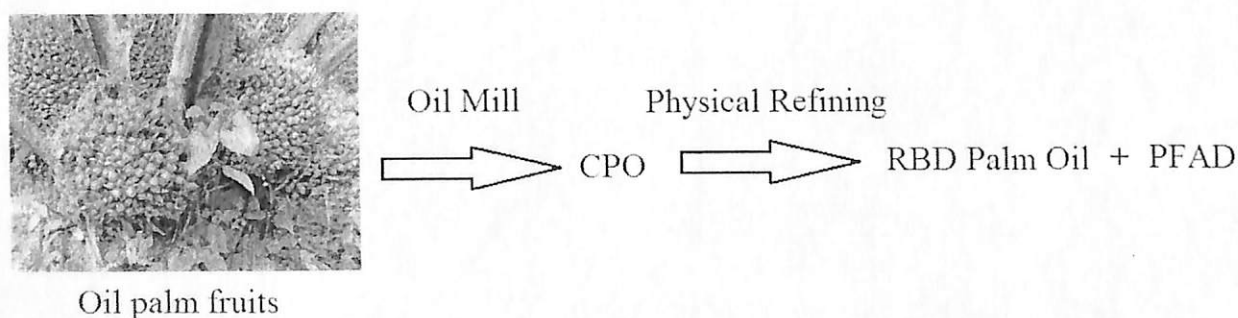


Fig. 1 Palm fatty acid distillate (PFAD) as a co-product of physical refining process of CPO to RBD palm oil

Production of biofuels from various renewable feedstocks has been extensively studied for many years. Transesterification of vegetable oil with methanol is commonly used for production of biodiesel which is a prominent biofuel. Biodiesel contains fatty acid methyl esters (FAMES) and is usually used in a mixture with diesel fuel [6]. Next-generation biofuel could be diesel like-hydrocarbons produced by catalytic deoxygenation of fatty acids over metal supported catalysts. The catalytic deoxygenation of fatty acids is a potential technology that generates linear corresponding n-alkanes (paraffins) and alkenes (olefins) through decarboxylation and decarbonation [7], respectively, as can be seen in Fig. 2. Meanwhile, CO₂ and CO are formed as gaseous products. The n-alkanes and alkenes are

hydrocarbons that are similar to those found in diesel fuel derived from fossil fuel resources, for example n-heptadecane and 1-heptadecene from stearic acid deoxygenation, n-pentadecane and 1-pentadecene from palmitic acid deoxygenation, etc. [8]. As such, the diesel like-hydrocarbons can be directly used and fully compatible with existing diesel engines without modification.

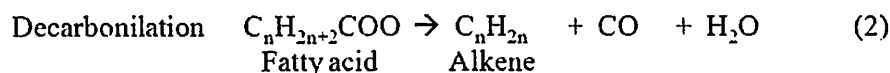
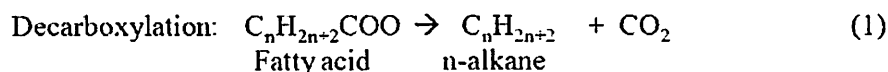


Fig. 2. Deoxygenation of fatty acid through decarboxylation and decarbonilation

Deoxygenation of steric acid and palmitic acid over several active metals such as Pd supported on various supports (silica, activated carbon and mesoporous carbon Sibunit) have been successfully carried out at 300 °C [9,10]. Due to the high price of Pd, researchers has also investigated several catalysts with different active sites (hydrotacites and nickel) and different supports (MgO/Al₂O₃ and Al₂O₃), as alternative catalysts [11-14]. A series of hydrotalcite catalysts with different ratios of magnesium oxide to alumina (MgO/Al₂O₃) have been investigated for deoxygenation of oleic acid at 300-400 °C. Subsequently, deoxygenation of triolein over Ni supported on alumina (Al₂O₃) catalysts has been studied at 350 °C. However, the process generated various types of hydrocarbon fuels such as heptanes, octane, nonane and heptadecane due to the occurrence of cracking reaction during the deoxygenation. Besides due to the application of higher temperatures, this could be due to small pore diameters (below 20 Å) of the alumina (Al₂O₃) based catalysts. According to the literatures, the effective catalysts having mesopore sizes (20 – 500 Å) are required for reactions involving bulky molecules such as fatty acid to diminish diffusion limitation of reactants and products during the reaction [15-17].

Mesostructured cellular foam (MCF) is a class of three-dimensional (3D) hydrothermally robust materials with ultra-large pore size (up to 500 Å) [18]. Owing to their larger pore sizes, MCF materials have advantages in terms of better diffusion of reactants and products. However, there has been limited information about the utilization of MCF silica as supports for loading of catalytically active component. Therefore, in the present study catalyst made from various MCF silicas have been incorporated with inexpensive metal i.e. nickel for deoxygenation of palmitic acid, as a representative of PFAD, to produce diesel-like hydrocarbons i.e. n-pentadecane and 1-pentadecene.

2. Experimental

2.1 Preparation of MCF silica supports

Various MCF silica support materials were prepared according to a previously reported procedure [19] with modification in terms of the tetraethyl ortho silicates (TEOS) amount (from 9.2 to 35 ml) and aging time (from 1 to 3 days), as given in Table 1. In a typical synthesis, 4 g of Pluronic 123 (P123) was dissolved in 70 ml of 1.6 M HCl. Then, 3.4 ml of trimethylbenzene (TMB) was added, and the resulting solution was heated to 40 °C with rapid stirring to synthesize a microemulsion (template). After stirring for 2 h, TEOS (*T*) was added to the solution and stirred for 5 min. Then, the solution was transferred into a poly-ethylene bottle and kept at 40 °C in an oven for 20 h for formation of pre-condensed silica foam. After that, the mixture was removed from the oven and then NH₄F.HF (46 mg in 5 ml of deionised water) was added to the mixture with slow mixing. Then, it was aged at 80 °C in an oven for certain duration (*D*). After cooling, the mixture was filtered and then dried at 100 °C for 12 h. After that, calcination was carried out in static air at 300 °C for 0.5 h and 500 °C for 6 h to remove the template. Hereafter, the synthesis materials will be donated as MCF (*aT-bD*), where *a* is the amount of TEOS and *b* is duration of aging time.

Table 1 Modification used in the synthesis of MCF silica support materials

No	Supports	Amount of TEOS (<i>T</i>), ml	Aging time (<i>D</i>), day
1	MCF(9.2T-2D)	9.2	2
2	MCF(12.5T-2D)	12.5	2
3	MCF(16T-2D)	16	2
4	MCF(9.2T-1D)	9.2	1
5	MCF(9.2T-3D)	9.2	3

2.2 Incorporation of nickel (Ni) into MCF silica materials

The MCF silica supports were functionalized with nickel using a deposition-precipitation method adopted from literature [20]. In the procedure, 250 ml of an aqueous solution containing 10.156 g of $\text{Ni}(\text{NO}_3)_2 \cdot 6\text{H}_2\text{O}$ and 0.3 ml of HNO_3 69 % wt/wt was prepared. In a typical preparation, 40 ml of the aqueous solution was used for dissolving 6.3 g of urea at room temperature to make a urea solution and 210 ml of the aqueous solution was mixed with 1.9 g of the MCF support to make a suspension. The suspension was heated at 40 °C, and then mixed with the urea solution under rapid mixing. After that, the mixture was heated to 90 °C for 2 h under static condition. After cooling, the mixture was filtered and the solid was washed three times with 20 ml of hot distilled water (~50 °C) followed by drying at 100 °C for 12 h. Then, the solids were calcined in static air at 300 °C for 6 h. Then the calcined samples were reduced at 550 °C for 2.5 h under hydrogen stream, and then cooled to room temperature in nitrogen flow to obtain nickel functionalized MCF catalysts. The catalysts are designated NiMCF(*a*T-*b*D)(R) in which *a* is the amount of TEOS and *b* is duration of aging time in the synthesis of MCF supports, as given in Table 2.

Table 2 Modification used in the synthesis of MCF silica materials

No	Supports	Catalysts
1	MCF(9.2T-2D)	NiMCF(9.2T-2D)(R)
2	MCF(12.5T-2D)	NiMCF(12.5T-2D)(R)
3	MCF(16T-2D)	NiMCF(16T-2D)(R)
4	MCF(9.2T-1D)	NiMCF(9.2T-1D)(R)
5	MCF(9.2T-3D)	NiMCF(9.2T-3D)(R)

2.3 Characterization

Nitrogen adsorption-desorption isotherm data were obtained using a Quanta-chrome Autosorb 1C automated gas sorption analyzer operated at liquid nitrogen temperature to estimate average cell pore size, average window pore size, specific pore volume and specific surface area (S_{BET}). Average cell pore size was evaluated using Barrett-Joyner-Halenda (BJH) method from the adsorption branch of the isotherm data. Meanwhile, average window pore size was evaluated using BJH method from the desorption branch. S_{BET} was calculated using Brunauer-Emmett-Teller (BET) method. Samples were also analyzed using Leo Supra 50 VP field emission scanning electron microscope (SEM), equipped with an Oxford INCAx act, energy dispersive X-ray (EDX) microanalysis system, to obtain SEM images and chemical compositions. Prior to the analysis, samples were mounted on stubs with double-sided adhesive tape. Then, the samples were coated with high purity gold and observed at room temperature.

2.4 Solventless deoxygenation of palmitic acid

Solventless deoxygenation of palmitic acid was performed in a semibatch mode in which CO_2 and CO gases produced during the reaction was continuously removed. The deoxygenation was carried out in a 250 mL three-necked flask reactor equipped with a magnetic stirring bar, reflux condenser and a tube to pass pure nitrogen flow to reaction mixture. During the deoxygenation reaction, the nitrogen stream swept the evolved gases through the condenser and a trap containing 50 ml of 1 M sodium hydroxide. The reactor was placed on a hot plate.

Palmitic acid (4.5 g) and catalyst (0.45 g) were first added into the reactor. Before the reaction was started, nitrogen flow was passed through the reaction mixture for about 30 min. Then, the reaction mixture was heated to 300 °C and maintained for 6 h to perform deoxygenation of palmitic acid without solvent under rapid stirring and nitrogen flow. The liquid product was collected and analyzed by means of an Agilent Technology 7890A GC system equipped with a flame ionization detector and a non-polar capillary column (GsBP-5). Palmitic acid conversion was calculated based on the amount of palmitic acid converted in the reaction divided by initial number of moles of palmitic acid loaded into the reactor. The selectivity was calculated as the number of moles of product recovered divided by the number of moles of palmitic acid that had reacted.

3. Results and discussion

3.1 Characterization of nickel functionalized MCF catalysts

Schematic cross section of MCF silica as reported in the literature is of strut-like structure as given in Fig. 3, which shows that the cells of the MCF structure are framed by the silica struts [18]. The disordered array of silica struts are composed of uniform-sized spherical cells interconnected by window pores. Surface characteristics of MCF materials prepared with different TEOS amounts and aging times and the corresponding nickel functionalized MFC catalyst using nitrogen adsorption-desorption can be seen in Table 3.

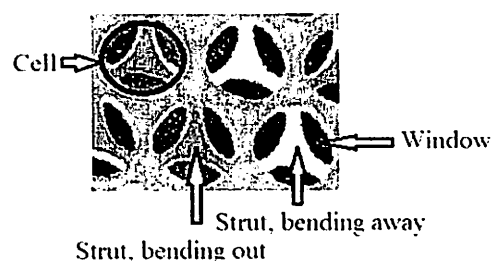


Fig. 3. Schematic cross section of MCF silica adopted from Schmidt-Winkel *et al* [18]

Table 3 Surface characteristics of MCF materials and corresponding nickel functionalized MCF catalysts

Supports	S_{BET} , m^2/g	V_{pore} , cm^3/g	d_{cell} , \AA	d_{window} , \AA	Catalysts	S_{BET} , m^2/g	V_{pore} , cm^3/g	d_{cell} , \AA	d_{window} , \AA
MCF(9.2T-2D)	375	2.24	232	130	NiMCF(9.2T-2D)(R)	281	1.02	184	125
MCF(12.5T-2D)	404	1.62	231	102	NiMCF(12.5T-2D)(R)	324	1.05	230	100
MCF(16T-2D)	336	1.41	235	102	NiMCF(16T-2D)(R)	309	0.92	235	100
MCF(9.2T-1D)	394	1.85	235	125	NiMCF(9.2T-1D)(R)	253	0.93	233	153
MCF(9.2T-3D)	378	2.12	235	158	NiMCF(9.2T-3D)(R)	307	1.09	234	90

d_{cell} and d_{window} pore are the cell and window pore diameters, respectively, determined using the BJH method,

S_{BET} is the surface area determined based on the BET method, and

V_{pore} is the total pore volume determined at a relative pressure of 0.9948

When using the same aging time (2 days) in the MCF support synthesis, the increase in TEOS amount from 9.2 ml to 12.5 ml resulted in an increase in total surface area of the MCF silica material. However, its pore volume, cell size and window pore size decreased to suggest that the thicknesses of the MCF walls increased. Further increase in TEOS amount from 12.5 ml to 16 ml was found to decrease the total surface area and the pore volume. Meanwhile, the cell size increased but the window pore size was virtually unchanged. The main reason for the above phenomenon was attributed to a higher number TMB/P123 microemulsion phase that interacted with protonated silicate species leading to the formation of the ‘soft silica’-coated TMB/P123 microemulsion phase. Then, condensation of silica in the walls led to a higher the formation of Si-O-Si linkages in the form of mesostructure in the MCF. Meanwhile, the use of an extra TEOS amount in the synthesis interrupted the condensation of silica network. This resulted in a detrimental effect to the formation of mesostructure in the MCF [21]. This behaviour was similar to that in the synthesis of SBA-15 silica materials [22].

For the use of the same TEOS amount (9.2 ml), window pore size in MCF silica supports increased with increasing aging time whilst cell size remained stable, as suggested by data in Table 3. This result could be attributed to the ‘soft silica’-coated TMB/P123 composite droplets that experienced an increase in size and consequently expanded the window pore size. At the same time, condensation of silica in the walls took place with the formation of Si-O-Si linkages to solidify the inorganic network, and subsequently the materials with increased pore size gradually rigidified [18, 21]. As longer aging duration was allowed, the larger window pore size in MCF structure would be obtained. As a result, the highest window pore size (158 Å) was achieved at aging time of 3 days as longest aging duration in the synthesis of MCF supports.

Deposition-precipitation method generally involves the conversion of a highly soluble metal precursor into another substance which specifically precipitates onto a support and not in the solution [23]. Incorporation of nickel into MCF silica supports using deposition-precipitation method resulted in some changes in textural parameters such as total surface area, total pore volume, cell size and window pore size, as can be seen in Table 3. Mechanism of nickel incorporation into MCF silica has been previously reported [24]. The mechanism was assumed to be analogous to nickel incorporation into Spherosil as reported in the literature [25]. It is suggested that the changes in the textural parameters were affected by the partial dissolution of siliceous pore and by the deposition of nickel particles [25]. Table 3 generally shows that incorporation of nickel into MCF supports resulted in decreases in total surface area, pore volume, cell size and window pore size due to deposition of nicks. However, for MCF(9.2T-1D) support prepared at TEOS amount of 9.2 ml and an aging time of 1 day, the window pore size increased from 125 Å to 153 Å after the incorporation of nickel. This behaviour was most likely due to a greater consumption of the siliceous pore walls during the deposition-precipitation [24].

All nitrogen adsorption-desorption isotherm curves, as shown in Fig. 4, are of type IV characterized by hysteresis in multilayer range of physisorption isotherms, which is often associated with capillary condensation (the pore filling process) in mesopore structure [26]. The functionalization of MCF supports with nickel resulted in a reduction in the

nitrogen adsorption-desorption isotherm curves of nickel functionalized MCF catalysts. However, the forms of the curves did not appreciably change after functionalization with nickel. This observation indicated that total pore volume experienced a decrease but the mesoporosity of the MCF materials was maintained after they were incorporated with nickel as suggested in the literature [27]. Mesoporosity are pores with diameter between 20 and 500 Å [26]. The results were in agreement with the surface characteristic results in Table 3 in which all nickel functionalized MCF catalysts had window pore sizes (from 90 to 153 Å) in the range of mesoporosity. Window pores are gates for reactants access to the cell where the active centres were mostly located in the catalysts [28]. The mesoporosity of catalysts is needed for reactions involving bulky molecules of fatty acids to reduce diffusion limitations faced by reactants and products within the catalyst pores during the process to consequently increase the their activities [15-17].

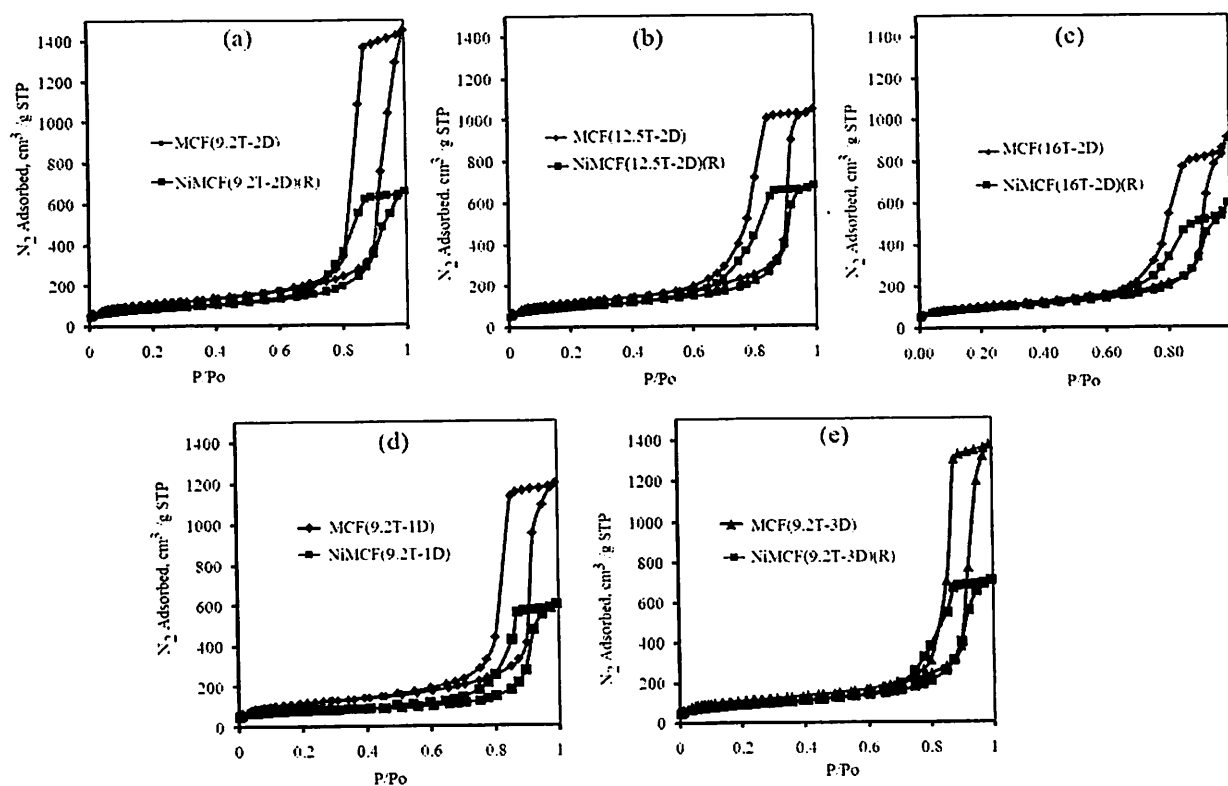


Fig. 4 Nitrogen adsorption-desorption isotherm of (a): MCF(9.2T-2D) support and NiMCF(9.2T-2D)(R) catalyst, (b): MCF(12.5T-2D) support and NiMCF(12.5T-2D)(R) catalyst, (c): MCF(16T-2D) support and NiMCF(16T-2D)(R) catalyst, (d): MCF(9.2T-1D) support and NiMCF(9.2T-1D)(R) catalyst, (e): MCF(9.2T-3D) support and NiMCF(9.2T-3D)(R) catalyst.

Morphologies of nickel functionalized MCF catalysts were examined using SEM. The results are shown in Fig. 5. The morphology of the nickel functionalized MCF catalysts was strongly influenced by the structural characteristics of the supports. For catalysts using MCF supports prepared at the same aging time (2 days), the increase in TEOS amount resulted in thicker and larger sizes of nickel particles to present in the catalysts. At TEOS amount of 9.2 in the MCF synthesis, uniform nickel nanoparticles in the form of nanoworms were observed in NiMCF(9.2T-2D)(R) catalyst. Meanwhile, nickel particles in the form of layered and platelet structures were observed in NiMCF(9.2T-2D)(R) and NiMCF(9.2T-2D)(R) catalysts using MCF supports prepared at TEOS amount of 12.5 ml and 16 ml, respectively. This result was attributed to a higher density of silanol groups (Si-OH) in the MCF support. As such, more $\text{Ni}(\text{OH})_2(\text{OH})_4$ complex reacted with the silanol groups in the MCF supports during the deposition-precipitation process to increase the nickel particle sizes, as suggested in the literature [24, 29]. Meanwhile, for catalysts using the same TEOS amount (9.2 ml) in the MCF syntheses, sizes of nickel particles present in the catalysts slightly decreased with the increase in aging time. Nickel nanoparticles in the form of nanoworms dispersed in NiMCF(9.2T-1D)(R) catalyst prepared using MCF support with an aging time of 1 day were slightly larger compared to those in NiMCF(9.2T-2D)(R) and NiMCF(9.2T-3D)(R) catalysts prepared using MCF support at aging times of 2 and 3 days, respectively.

Chemical compositions of the catalysts were determined using EDX, as can be seen in Fig. 6. NiMCF(9.2T-2D)(R) catalyst using MCF support prepared at TEOS amount of 9.2 ml was found to contain metallic nickel 5.3 wt. % with the same aging time (2 days) in the MCF synthesis. When the TEOS amount was increased from 9.2 ml to 12.5 ml, the metallic nickel content in the catalyst decreased to 3.1 wt. %. These observations suggested that the use of TEOS amount of 9.2 ml in the MCF synthesis led to homogeneous distribution of nickel inside and outside the cells in

NiMCF-9.2T(R) catalyst. This can be confirmed by the surface characteristic results in Table 3 where the deposition of the MCF(9.2T-2D) support with nickel resulted in higher reductions in cell size from 232 to 184 Å and in window pore size from 130 to 125 Å. Meanwhile, the use of TEOS amount of 12.5 ml in the MCF synthesis resulted in NiMCF(12.5T-2D)(R) catalysts with metallic nickel in the form of layered and platelet structures that could be mainly distributed outside the cells in the catalysts. However, further increase in TEOS amount from 12.5 to 16 ml resulted in NiMCF(16T-2D)(R) with a higher content of metallic nickel (14.1 wt. %) due to larger and thicker sizes of metallic nickel particles which were in the form of layered and platelet structures. Surface characteristic results in Table 3 confirm that there were no appreciable changes in cell sizes of MCF(12.5T-2D) and MCF(16T-2D) after the nickel incorporation, which suggested that the metallic nickel particles were mainly located outside the cells.

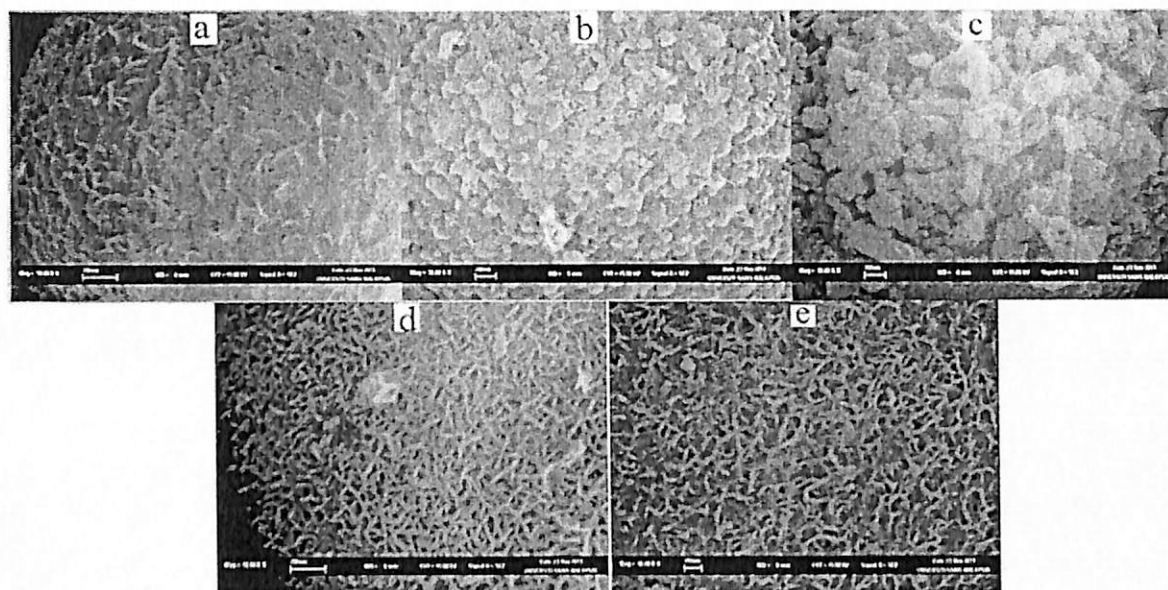


Fig. 5 SEM images of (a): NiMCF(9.2T-2D)(R), (b): NiMCF(12.5T-2D)(R), (c): NiMCF(16T-2D)(R), (d): NiMCF(9.2T-1D)(R) and (e): NiMCF(9.2T-3D)(R) catalysts.

Furthermore, at the same TEOS amount (9.2 ml) in the MCF support syntheses, the increase in aging time was found to increase the amount of nickel compositions present in the catalyst, as can be seen in Fig. 6. The highest amount of nickel was found to be 17.57 wt. % in the NiMCF(9.2T-3D)(R) catalyst that used MCF support prepared at the longest aging time (3 days). It was envisioned that window pore size of MCF material used as a support was the main factor that influenced the nickel nanoparticle incorporation. The window pore size of MCF support prepared using an aging time of 3 days (MCF(9.2T-3D)) support was the highest among them. Then, window pore size of MCF(9.2T-2D) was higher than that of MCF(9.2T-1D), as presented in Table 3. As such, most of nickel nanoparticles were easily introduced through the window pore size of MCF(9.2T-3D) support. It can be concluded in this study that larger window pore size of MCF support resulted in easier incorporation of nickel nanoparticles with smaller sizes. Hence, a suitable support was necessary for obtaining a high dispersion of nickel species with small sizes.

3.2 Solventless deoxygenation of palmitic acid over nickel functionalized MCF catalysts

Catalytic performances of nickel functionalized MCF catalysts with different surface characteristics and nickel compositions were evaluated for deoxygenation of palmitic acid at 300 °C in solvent free condition under nitrogen flow for 6 h in a semi batch mode. Conversions of palmitic acid and selectivities of desirable products (n-pentadecane and 1-pentadecane) recorded during the experimental runs are shown in Table 4. NiMCF(9.2T-2D)(R) catalyst exhibited a higher palmitic acid conversion of 59 % compared to NiMCF(12.5T-2D)(R) and NiMCF(16T-2D)(R) catalysts using MCF support prepared at an aging time of 2 days. The higher palmitic acid conversion exhibited by NiMCF(9.2T-2D)(R) catalyst was attributed to small nickel nanoparticles dispersed in the catalyst, albeit it had the second highest nickel content among the catalysts using MCF support prepared at aging time of 2 days, as confirmed from SEM and EDX results in Fig. 5 and Fig. 6, respectively. Meanwhile, for the same MCF preparation in terms of TEOS amount (9.2 ml), NiMCF(9.2T-3D)(R) achieved the conversion of 86.4 % which was the highest active catalyst. Besides the small nickel nanoparticles dispersed in NiMCF(9.2T-3D)(R) catalyst, this was due to the highest nickel content, i.e. 17.57 wt. %, in the catalyst, as confirmed in EDX results in Fig. 6. Metallic nickel species were active sites to produce n-alkane and alkene in fatty acid deoxygenation through decarboxylation and decarbonilation reaction [12]. It is also reported in

the literature that for most metal supported catalysts, smaller active metal particles dispersed in the support may also lead to the higher catalytic activity in the reaction [30].

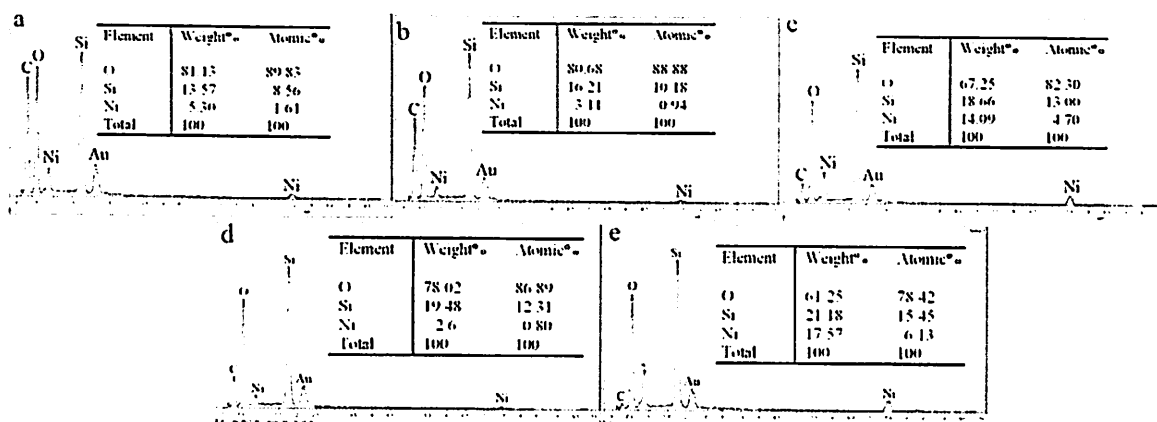


Fig. 6 EDX analysis results for chemical compositions of (a): NiMCF(9.2T-2D)(R), (b): NiMCF(12.5T-2D)(R), (c): NiMCF(16T-2D)(R), (d): NiMCF(9.2T-1D)(R) and (e): NiMCF(9.2T-3D)(R) catalysts

Table 4 Reaction results of solventless deoxygenation of palmitic acid over nickel functionalized MCF catalysts at 300 °C for 6 h.

Catalysts	Palmitic acid conversion, %	n-Pentadecane selectivity, %	1-Pentadecene selectivity, %
NiMCF(9.2T-2D)(R)	59.0	22	23.4
NiMCF(12.5T-2D)(R)	3.1	45	42.5
NiMCF(16T-2D)(R)	33.4	16	17.5
NiMCF(9.2T-1D)(R)	52.0	21	21.7
NiMCF(9.2T-3D)(R)	86.4	31.8	29.2

Furthermore, Table 4. also shows that selectivities of n-pentadecane performed by NiMCF(9.2T-2D)(R), NiMCF(16T-2D)(R) and NiMCF(9.2T-1D)(R) catalysts were a bit lower than those of 1-pentadecene in the palmitic acid deoxygenation. This result suggests that palmitic acid deoxygenation through decarboxylation was less selective than that through decarbonilation. On the other hand, palmitic acid deoxygenation over NiMCF(12.5T-2D)(R) and NiMCF(9.2T-3D)(R) catalysts gave a bit higher n-pentadecane selectivity compared to 1-pentadecene as the deoxygenation through decarboxylation was more intense than that through decarbonilation.

4. Conclusions

Preparation of MCF silica supports with different characteristics by varying TEOS amount and aging time was successfully carried out. With the same aging time in the MCF preparation, the increase in TEOS amount resulted in an increase in total surface area but its pore volume, cell size and window pore size experienced decreases due to a higher formation of Si-O-Si linkages. Further increase in TEOS amount caused a detrimental effect to the formation of the mesostructure in the MCF as condensations of the silica network were interrupted. Meanwhile, with the same TEOS amount in MCF preparation, the increase in aging time resulted in an increase in window pores size in the MCF materials attributed to an increase in size of the silica composites.

Incorporation of nickel into MCF supports was carried out using deposition-precipitation and then reduction process. The morphology of nickel functionalized MCF catalyst was strongly influenced by the structural characteristics of the MCF silica supports. With the same aging time in the MCF preparation, the increase in TEOS amount resulted in an increase in size of nickel particles that were dispersed in MCF silica due to a higher density of silanol groups (Si-OH) that reacted with nickel complex during the deposition-precipitation process. Meanwhile, with the same TEOS amount in the MCF preparation, the increase in aging time seemed to decrease the size of nickel particles dispersed in the catalysts but the amount of nickel content increased.

Among the MCF silica materials, MCF prepared using TEOS amount of 9.2 ml and aging time of 3 days MCF(9.2T-3D) was the most promising support for incorporation of nickel as the NiMCF(9.2T-3D)(R) catalyst obtained exhibited the highest palmitic acid conversion (86.4 %) with n-pentadecane selectivity of 31.8 % and 1-pentadecene selectivity of 29.2 % in solventless deoxygenation of palmitic acid at 300 °C under nitrogen flow for 6 h. The highest catalytic activity of NiMCF-9.2T(R) was attributed to the smallest nickel particle dispersed in the nickel functionalized MCF catalysts together with the highest nickel content (17.57 wt. %) as confirmed in SEM and EDX results

Acknowledgements A Research University (814181) grant from Universiti Sains Malaysia and aSciencefund (6013381) from MOSTI to support this research work are gratefully acknowledged. Lilis Hermida also thanks the Directorate General of Higher Education (DIKTI), Ministry of National Education of Indonesia for her PhD scholarship.

References

- [1] Diesel will lead global fuel demand growth-OPEC. Available at: <http://in.reuters.com/article/2009/07/08/opec-diesel-idINL859107920090708> Accessed November, 2012.
- [2] Biomass. SJD Partner Limited-Sustainable energy provider page. Available at: <http://www.sjdpartners.com/content/biomass> Accessed January, 2013.
- [3] Palm oil, available at: <http://www.oilinfat.com/page0031.aspx> Accessed January, 2013.
- [4] Top AGM. Production and utilization of palm fatty acid distillate (PFAD). *Lipid Technology*. 2010; 22 (1):11-13.
- [5] World's top producers target higher CPO output this year. Available at: <http://biz.thestar.com.my/news/story.asp?file=/2012/1/20/business/20120120075710> Accessed January 2013
- [6] Kikhtyanin OV, Rubanov AE, Ayupov AB, Echevsky GV. Hydroconversion of sunflower oil on Pd/SAPO-31 catalyst. *Fuel*. 2010;89:3085–3092.
- [7] Lestari S, Arvela PM, Beltramini J, Lu GQM, Murzin DY. Transforming triglycerides and fatty acids into biofuels. *Chemistry & Sustainability*. 2009; 2:1109 – 1119.
- [8] Identity and analysis of total petroleum hydrocarbon. Total petroleum hydrocarbon page. Available at: <http://www.bvsde.paho.org/bvstox/i/fulltext/toxprofiles/total.pdf> Accessed January, 2013.
- [9] Snare M, Kubickova I, Malki-Arvela P, Eränen K, Yu D. Heterogeneous catalytic deoxygenation of stearic acid for production of biodiesel. *Industrial & Engineering Chemistry Research*. 2006;45:5708-5715.
- [10] Lestari S, Malki-Arvela P, Simakova I, Beltramini J, Max Lu G Q, Murzin DY. Catalytic deoxygenation of stearic Acid and palmitic acid in semibatch mode. *Catalysis Letter*. 2009;130:48–51.
- [11] Na JG, Yi BE, Kim JN, Yi KB, Park SY, Park JH, Kim JN, Ko CH. Hydrocarbon production from decarboxylation of fatty acid without hydrogen. *Catalysis Today*. 2010;156;2010:44-48.
- [12] Roh HS, Eum IH, Jeong DW, Yi BE, Nab JG, Ko CH. The effect of calcination temperature on the performance of Ni/MgO-Al₂O₃ catalysts for decarboxylation of oleic acid. *Catalysis Today*. 2011;164:457–460.
- [13] Morgan T, Grubb D, Santillan-Jimenez E, Crocker M. Conversion of triglycerides to hydrocarbons over supported metal catalysts. *Topic in Catalysis*. 2010;53:820-829.
- [14] Morgan T, Santillan-Jimenez E, Harman-Ware AE, Ji Y, Grubb D, Crocker M. Catalytic deoxygenation of triglycerides to hydrocarbons over supported nickel catalysts. *Chemical Engineering Journal*. 2012;189-190:346-355.
- [15] Wilson K and Clark JH. Solid acids and their use as environmentally friendly catalysts in organic synthesis. *Pure and Applied Chemistry*. 2000;72:1313–1319.
- [16] Perez-Pariente J, Diaz I, Mohino F, Satre E. Selective synthesis of monoglycerides by using functionalized mesoporous catalysts. *Applied Catalysis A: General*. 2003; 254:173- 188.
- [17] Bossaert WD, Vos DED, Rhijn WMV, Bullen, J, Grobet, PJ, Jacobs PA. Mesoporous sulfonic acids as selective heterogeneous catalysts for the synthesis of monoglycerides. *Journal of Catalysis*. 1999;182:156–164.
- [18] Schmidt-Winkel P, Lukens WW, Yang P, Margolese DL, Lettow JS, Ying JY, Stucky GD. Microemulsion templating of siliceous mesostructured cellular foams with well-defined ultralarge mesopores. *Chemistry of Materials*. 2000;12:686-696.
- [19] Han Y, Lee SS, Ying JY. Siliceous mesocellular foam for high-performance liquid chromatography: Effect of morphology and pore structure, *Journal of Chromatography A*. 2010;1217:4337–4343.
- [20] Nares R, Ramirez J., Gutierrez-Alejandre A., Cuevas R.,(2009). Characterization and hydrogenation activity of Ni/Si(Al)-MCM-41 catalysts prepared by deposition-precipitation. *Industrial & Engineering Chemistry Research*. 2009;48:1154–1162.
- [21] Schmidt-Winkel P, Glinka CJ, Stucky GD. Microemulsion templates for mesoporous silica. *Langmuir*. 2000;16:356-361.
- [22] Abdullah AZ, Kamaruddin AH, Razali N, Abdullah H, Bhatia S. Elucidation of interactive effects of synthesis conditions on the characteristics of mesoporous silicas templated using polyoxide surfactant, *Science and Technology of Advanced Materials*. 2007;8: 249–256.
- [23] Louis C. Deposition-precipitation of supported metal catalysts. In: J.Regalbuto, Ed., *Catalyst Preparation Science and Engineering*. New York. Taylor and Francis; 2007:319-340.
- [24] Hermida L, Abdullah AZ, Mohamed AR . Synthesis and characterization of mesostructured cellular foam (MCF) silica loaded with nickel nanoparticles as a novel catalyst. *Materials Sciences and Application*. 2013; 4:52-62
- [25] Iler R (eds.). *The Chemistry of Silica*, New York: John Wiley & Sons; 1979.
- [26] Sing KSW. Adsorption methods for the characterization of porous materials. *Advances in Colloid and Interface Science*. 1998; 76-77:3-11.
- [27] Na-Chiangmai C, Tiengchad N, Kittisakmontree P, Mekasuwandumrong O, Powell J, Panpranot J. Characteristics and catalytic properties of mesocellular foam silica supported Pd nano particles in the liquid-phase selective hydrogenation of phenylacetylene. *Catalysis Letters*. 2011;141(8):1149-1155.
- [28] Kim J, Desch RJ, Thiel SW, Guliants VV, Pinto NG. Adsorption of biomolecules on mesostructured cellular foam silica: Effect of acid concentration and aging time in synthesis. *Microporous and Mesoporous Materials*. 2012;149(1):60-68.
- [29] Hermida L, Abdullah AZ, Mohamed AR . Structure characteristics and catalytic activity of nickel supported on mesostructured cellular foam (MCF) silica for decarboxylation of palmitic acid: Effect of TEOS. *Proceedings of International Conference on Environmental Research and Technology*. Penang, Malaysia; 30 May-1 June 2012.
- [30] Do DD. Adsorption science and technology. *Proceedings of the Second Pacific Basin Conference on Adsorption Science and Technology*, Singapore. World Scientific Publishing . Singapore; 2000.

Synthesis and Characterization of Mesostructured Cellular Foam (MCF) Silica Loaded with Nickel Nanoparticles as a Novel Catalyst

Lilis Hermida^{1,2}, Ahmad Zuhairi Abdullah^{1*}, Abdul Rahman Mohamed¹

¹School of Chemical Engineering, Universiti Sains Malaysia, Penang, Malaysia; ²Department of Chemical Engineering, Universitas Lampung, Lampung, Indonesia.
Email: chzuhairi@eng.usm.my

Received October 5th, 2012; revised October 25th, 2012; accepted November 23rd, 2012

ABSTRACT

This work investigated the possibility of incorporation of nickel into several mesostructured cellular foam (MCF) silica supports prepared at various aging times (1, 2, and 3 days) by using deposition-precipitation method followed by reduction process and to look for the best support to obtain supported nickel catalyst with highest nickel loading and smallest size of nickel nanoparticles. Analyses using nitrogen adsorption-desorption, transmission electron microscopy (TEM), X-ray diffraction (XRD), scanning electron microscopy (SEM) and energy dispersive X-ray (EDX) showed that MCF silica prepared at aging time of 3 days was the best support as the corresponding nickel functionalized MCF catalyst had the highest nickel content (17.57 wt%) and the smallest size of nickel nanoparticles (1 - 2 nm) together with high porosity (window pore size of 90 Å). The result was attributed to the highest window pore size in the MCF support which allowed more nickel nanoparticles to be incorporated.

Keywords: Mesostructured Cellular Foam; Amorphous Materials; Nanostructures; Sol-Gel Growth; Surface Properties

1. Introduction

Supported nickel catalysts as heterogeneous catalysts have attracted research attentions because of their potential application in many important petrochemical industries such as hydrogenation, deoxygenation, methanation, reforming, and hydrocracking. Besides good nickel particle dispersion in the catalyst support, pore size is a crucial variable affecting the catalyst performance as the activity usually relies on the presence of accessible active centres located in the internal pore of the catalysts [1]. Larger-pore sizes of the catalyst provide better diffusion of reactants and products during the course of reaction [2]. Therefore, high dispersion of small particles of nickel and high porosity of the catalyst are always desirable. Catalyst support may play a more active role in increasing the dispersion and stability of metal particles [3]. The main function of catalyst support is to achieve a fine dispersion of nickel nanoparticles and to prevent the nanoparticles from aggregating and the latter relies on confining nanosized environment of the catalyst [4].

Mesoporous silica materials such as MCM-41, SBA-15 and HMS with high porosity (pore size of up to 100 Å) have been widely studied as catalyst supports for incor-

poration of sulphated metal oxides [5,6], platinum nanoparticles [7] and propyl sulfonic acid [8-10]. These mesoporous silica materials have also been extensively used as supports for incorporation of nickel particles. Nickel functionalized mesoporous silicas have been successfully applied for hydrochlorination of chlorobenzene [11] and catalytic reforming of methane with carbon dioxide to produce synthesis gas (syngas) [12,13]. By using direct synthesis [2,12], post synthesis-grafting and impregnation methods [13] for incorporation of nickel, mesoporous silica materials (MCM-41, SBA-15, HMS) would form catalysts with good dispersion of nickel particles at nickel contents below 6 wt%. However, higher nickel loadings could lead to structural collapse and a significant drop in the well-defined framework mesoporosity because of local blockage of pore channel and agglomeration of nickel nanoparticles. This could result in diffusion limitation of reactants as well as the products to consequently reduce the activity of the catalyst. Recently, MCM-41 was incorporated with nickel particles using deposition-precipitation method followed by a reduction process that resulted in catalyst with good nickel particles dispersion at high nickel loading of 12.8 wt% [14]. However, the supported MCM 41 nickel catalyst had low porosity (average pore diameter of 39 Å) that would not

*Corresponding author.

be suitable for reactions involving bulky molecules such as hydrogenation of edible or non edible oil and deoxygenation of fatty acid. These reactions require catalysts with pore diameters of above 50 Å to diminish diffusion limitation of reactants and products [15]. Besides that, catalysts derived from MCM-41 support faced serious drawback of low hydrothermal stability [16-18].

Mesoporous cellular foam (MCF) silica is a very interesting new mesoporous silica material. It is a class of three-dimensional (3D) materials with ultra-large mesopores (up to 500 Å) that are hydrothermally robust [19-22]. In terms of the textural and framework structures, MCF materials are composed of uniform spherical cells interconnected by window pores with a narrow size distribution [19]. Owing to their 3D mesopore system with pore sizes substantially larger than those of MCM-41 or SBA-15 or HMS mesostructures, this material seems to be a very promising candidate to be used as catalytic support as it provides a better diffusion of reactants and products. This allows them to better overcome mass transfer limitations in many reactions [20,23]. However, there has been limited information about the utilization of MCF silicas as supports for loading of catalytically active component. Also, report addressing the dispersion of nickel particle on mesoporous cellular foam (MCF) silica is hardly found in the literature so far.

In the present study, MCF silica materials with different mesostructure characteristics have been prepared at various aging times (1, 2 and 3 days) and used as supports for nickel incorporation. The incorporation of nickel particle in the MCF silica has been carried out using deposition and precipitation (DP) method followed by a reduction process. The aims of this study are to investigate the influence of MCF support characteristics on surface and structural characteristics of nickel functionalized MCF catalysts. Thus, the best MCF support can be identified in order to obtain a catalyst with highest content of nickel nanoparticles together with high porosity. MCF silica supports and the corresponding nickel functionalized MCF catalysts have been characterized using nitrogen adsorption-desorption, TEM, SEM-EDX and XRD analyses.

2. Experimental Procedure

2.1. Synthesis of MCF Supports

MCF silica materials with different structures were synthesized according to a previously reported procedure [24] with modification with regards to the amount of acidic solution, the use of aging temperature and aging times. In a typical synthesis, 4 g of Pluronic 123 was dissolved in 70 ml of 1.6 M HCl. Then, 6.8 ml of trimethylbenzene (TMB) was added, and the resulting solution was heated

to 40°C with rapid stirring to synthesize the microemulsion (template). After stirring for 2 h, 9.2 ml of tetraethyl orthosilicate (TEOS) was added to the solution and stirred for 5 min. Then, the solution was transferred to a poly-ethylene bottle and kept at 40°C in an oven for 20 h for the formation of pre-condensed silica foam. After that, the mixture was removed from the oven and then NH₄F·HF solution (92 mg in 10 ml DI water) was added to the mixture under slow mixing. Then, the mixture was aged at 80°C in an oven for certain aging times. Three samples prepared using the synthesis procedure were MCF-1D that was aged for 1 day, MCF-2D that was aged for 2 days and MCF-3D that was aged for 3 days. After cooling, the mixture was filtered and the collected solid was then dried at 100°C for 12 h. After that, calcination was carried out in static air at 300°C for 0.5 h and 500°C for 6 h to remove the template. The calcined MCF silica materials were used as supports for Ni incorporation.

2.2. Nickel Incorporation into MCF Supports

MCF-1D, MCF-2D and MCF-3D materials were then functionalized with nickel using a deposition-precipitation method adopted from Nares *et al.* [14]. In the functionalization reaction, 250 ml of an nickel nitrate solution was prepared by dissolving 10.156 g of Ni(NO₃)₂·6H₂O and 0.3 ml of HNO₃ (69%wt/wt) with distilled deionize water. Then, 40 ml of the nickel nitrate solution was used for dissolving 6.3 g urea at room temperature to produce a urea solution and 210 ml of the nickel nitrate solution was mixed with 1.9 g of MCF silica materials to make a suspension. The suspension was then heated at 40°C during which the urea solution was added under rapid mixing. After that, the mixture was heated to 90°C for 2 h under static condition. After cooling, the mixture was filtered and the collected solid was washed three times with 20 ml hot distilled water (~50°C) and then dried at 100°C for 12 h. The solid was subsequently calcined in static air at 300°C for 6 h. The calcined solids are designated as NiMCF-1D(C), NiMCF-2D(C) and NiMCF-3D(C). The samples were then reduced at 550°C for 2.5 h under hydrogen stream and subsequently cooled to room temperature under nitrogen flow. The reduced samples are designated as NiMCF-1D(R), NiMCF-2D(R) and NiMCF-3D(R).

2.3. Characterization of Nickel Loaded MCF

Nitrogen adsorption-desorption isotherms were obtained using a Quanta-chrome Autosorb 1C automated gas sorption analyzer at liquid nitrogen temperature. Prior to the experiments, the samples were degassed ($p < 10^{-1}$ Pa) at 270°C for 6 h. The amounts of nitrogen gas adsorbed over a range of partial pressures were measured to obtain

a graph known as an adsorption isotherm, whilst desorption isotherm was obtained by measuring the quantities of nitrogen desorbed from the sample as the relative pressure was gradually lowered. Specific surface area (S_{BET}) was calculated using the BET method, while pore size distribution was obtained using the Barrett-Joyner-Halenda (BJH) model applied to the adsorption and desorption isotherms data.

The samples were also used for SEM/EDX imaging using a Leo Supra 50 VP field emission SEM, equipped with an Oxford INCA X act, which was an energy dispersive X-ray microanalysis system. Prior to analysis, samples were mounted on stubs with double-sided adhesive tape. Then, the samples were coated with high purity gold and observed at room temperature.

TEM images were obtained by means of a Philips CM 12 transmission electron microscope. About 0.08 g of each sample was first dissolved in 5 ml of 100% ethanol. The solution was then shaken for a moment and subsequently a small amount of the solution was taken using a micropipette and dropped on a metal grid for the analysis.

X-ray diffraction (XRD) analysis was performed using a Siemens 2000 X system to obtain XRD patterns of the catalysts at different stages of synthesis in order to identify the different phases in the materials. The observation was made on the calcined and reduced catalyst samples. The diffraction patterns were recorded using Cu-K α radiation at 2θ angles ranging from 10° - 100° .

3. Results and Discussion

Table 1 summarizes textural properties of various MCF silica supports prepared at different aging times as well as those of the corresponding nickel functionalized MCF catalysts after the reduction process. The textural properties were derived based on nitrogen adsorption-desorption data using Barrett, Joyner and Halenda (BJH) method to obtain the average cell size (d_{cell}) and window pore size ($d_{\text{window pore}}$). Specific surface area (S_{BET}) was evaluated using Brunauer, Emmett and Teller (BET) method. Meanwhile, total pore volume (V_{pore} , cm^3/g) was calculated as the amount of nitrogen adsorbed at $P/P_0 = 0.9948$. The window pore size in MCF silica supports increased with increasing aging time whilst cell size remained stable, as suggested by data in Table 1. This result could be attributed to the "soft silica"-coated TMB/P123 microemulsion droplets (composite droplets) that experienced an increase in size and consequently expanded the window pore size in the composite droplets during the aging step at 80°C . At the same time, condensation of silica in the walls took place with the formation of Si-O-Si linkages to solidify the inorganic network, and subsequently the materials with increased pore size

gradually rigidified [25,26]. As longer duration of aging was allowed, the larger window pore size in MCF structure would be obtained. The highest window pore size (158 \AA) was achieved with an aging time of 3 days in the synthesis of MCF supports. The increase in window pore size with the increase in aging time in the synthesis of MCF silica materials was also observed by the other researchers who studied the effects of acid concentration and aging time in preparation of MCF used for adsorption of biomolecules [27].

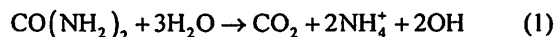
Table 1 also shows that the total surface area of MCF silica support slightly decreased from 394 to 375 cm^2/g when the aging time was increased from 1 day to 2 days. The reduction in the BET surface areas with increasing aging time might be ascribed to the enlargement of window pore sizes and the formation of denser framework walls [25,26]. However, the total surface area slightly increased from 375 to 378 cm^2/g if the aging time was increased from 2 days to 3 days. The increase in aging time from 1 day to 2 days resulted in an increase in total pore volume from 1.85 to 2.24 cm^3/g . Further increase in aging time to 3 days caused a slight decrease of the total pore volume to 2.12 cm^3/g .

Incorporation of nickel into MCF silica supports resulted in some changes in textural parameters such as total surface area, total pore volume, cell size and window pore size as can be seen in Table 1. The incorporation of nickel into MCF silica support was carried out using deposition-precipitation method at 90°C for 2 h. The solid sample was then collected, dried at 100°C , calcined at 300°C and finally reduced at 550°C . Deposition-precipitation method generally involves the conversion of a highly soluble metal precursor into another substance which specifically precipitates onto a support and not in solution [28]. In this study, silica (from MCF material) was suspended into the solution containing nickel nitrate salt, urea and nitric acid at room temperature. Deposition-precipitation was started when the temperature of the suspension reached 90°C . This condition led to urea hydrolysis (Equation (1)) that resulted in the for-

Table 1. Nitrogen adsorption-desorption result of MCF silica supports and the corresponding nickel functionalized nickel MCF catalysts.

Sample	S_{BET} (m^2/g)	V_{pore} (cm^3/g)	d_{cell} (\AA)	d_{window} (\AA)
MCF-1D	394	1.85	235	125
MCF-2D	375	2.24	232	130
MCF-3D	378	2.12	235	158
NiMCF-1D(R)	253	0.93	233	153
NiMCF-2D(R)	281	1.02	184	125
NiMCF-3D(R)	307	1.09	234	90

mation OH⁻ and a gradual increase in pH [29]. The function of nitric acid was to better regulate the changes in pH by neutralizing the released OH⁻ ion so that the suspension pH was maintained. It was suggested in the literature that the released OH⁻ ions also hydrolyzed the nickel hexa-aqua complex ([Ni(OH₂)₆]²⁺) in the suspension to generate nickel hydroxo-aqua complexes [29] as given in Equation (2).



Furthermore, mechanism of nickel incorporation into silica derived from porous silicas Spherosil with high surface area *i.e.* S_{BET} = 356 m²/g (Rhone-Poulenc, France, purity > 99.5%, XOA400) using the deposition-precipitation method has been proposed in the literature [30] and it is assumed to be analogous to nickel incorporation into MCF silica in this study. The mechanism can be briefly explained as follows: As the pH in the suspension was increased, silica derived from MCF support became negatively charged and the pH was higher than its point of zero charge (PZD ~pH 2). As such MCF silica would electrostatically adsorb the nickel hexa-aqua ([Ni(OH₂)₆]²⁺) which was in equilibrium with nickel(II) hydroxo-aqua complexes of [Ni(OH)(OH₂)₅]⁺ and Ni(OH)₂(OH₂)₄ as given in Equation (2). As the Ni(OH)₂(OH₂)₄ complex approached to the surface of MCF silica, it reacted with silanol groups (Si-OH) in MCF silica via hydrolytic adsorption which is a heterocondensation reaction. Then, it further reacted with the another Ni(OH)₂(OH₂)₄ complex to form nickel phyllosilicate layer on MCF silica via olation reaction which is formation of a hydroxo bridge between two metal centres as can be seen in Figure 1.

It has been reported in the literature that the basic medium could also cause partial silica dissolution as OH⁻ ions which are catalysts for silica depolymerisation [31], as can be seen in Figure 2. The silica dissolution also released Si(OH)₃⁻ ions that were further hydrolyzed to silicic acid (Si(OH)₄). Furthermore, the silicic acid can react with Ni(OH)₂(OH₂)₄ complex in the suspension via a heterocondensation reaction to form Si-O-Ni monomers as proposed in the literature [30]. These monomers can polymerize and grow on the surface of MCF silica leading to the formation of nickel phyllosilicate on its surface. After the deposition-precipitation stage, the sample was dried at 100°C for 12 h and then calcined at 300°C for 6 h in order to eliminate water more efficiently before the reduction step. No decomposition of nickel phyllosilicate on MCF silica could occur during the drying step at 100°C and subsequently in the calcinations step at

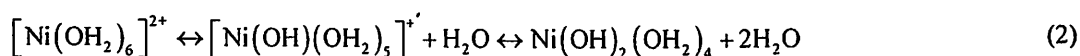
300°C as suggested in the literature [32]. Decomposition of the nickel phyllosilicate into NiO on silica only occurred when the calcination temperature exceeded 300°C until 600°C. It was reported in the literature that with more efficient elimination of water from the sample, smaller size metal nanoparticles on the silica can be produced after the reduction process [33].

Figure 3 schematically shows the mechanism of nickel nanoparticles formation during the reduction process which was adopted from Buratin *et al.* [30,32]. There were two steps in the mechanism of nickel particles formations that can be proposed *i.e.* the decomposition step and the reduction step. When the calcined samples *i.e.* NiMCF-1D(C), NiMCF-2D(C) and NiMCF-3D(C) were heated at 550°C under hydrogen stream for 2.5 h, nickel phyllosilicate in the calcined samples would be decomposed to NiO and silicate. Then, NiO would be reduced to Ni nanoparticles.

From the mechanisms of deposition-precipitation, MCF silica dissolution and formation of nickel particles that have been elucidated above, it can be concluded the changes in the textural parameters after the incorporation of nickel into MCF silica supports were affected by the partial dissolution of siliceous pore walls occurring during deposition-precipitation and by the deposition of nickel particles. Similar behaviour was also observed by Nares *et al.* [14] who used MCM-41 as the silica support. Table 1 shows that after the nickel incorporations, textural parameters of MCF silica supports generally decreased most probably due to the deposition of nickel on pore walls or on the surface of the MCF silica supports. However, for MCF-1D support prepared at an aging time of 1 day, window pore size increased from 125 Å to 153 Å after the incorporation of nickel. This behaviour was most likely due to a greater consumption of the siliceous pore walls during the deposition-precipitation.

MCF silica materials are made up of spherical cells interconnected by window pores in which the window pores are gates for accommodating active sites in the spherical cells. The reduction of total pore volume of MCF silica supports after the functionalization can be confirmed on the basis of the pore size distribution curves which include the size distributions of cells and window pores. The size distributions of cells in the samples were evaluated using the BJH method from the adsorption branch of the isotherm of the sample. Meanwhile, the size distributions of cells window pores of a sample were evaluated using BJH method from the desorption branch.

The size distributions of window pores of MCF silica



NiMCF-3D(R) catalysts with lower isotherm curves but no appreciable change in the form of the isotherm was observed (Figure 5). This observation indicated that total pore volume experienced a decrease but the mesoporosity of the MCF materials was maintained after functionalization. This result was comparable with that reported by Na-Chiangmay *et al.* [42] who observed that functionalization of MCF material with Pd had no significant influence on the structure of mesoporous support material. Furthermore, it was noted that, the incorporation of nickel into MCF-3D material resulted in the highest adsorption in NiMCF-3D(R) as compared to those in NiMCF-1D(R) and NiMCF-2D(R). The result suggested the lowest densification of the silica walls in NiMCF-3D(R).

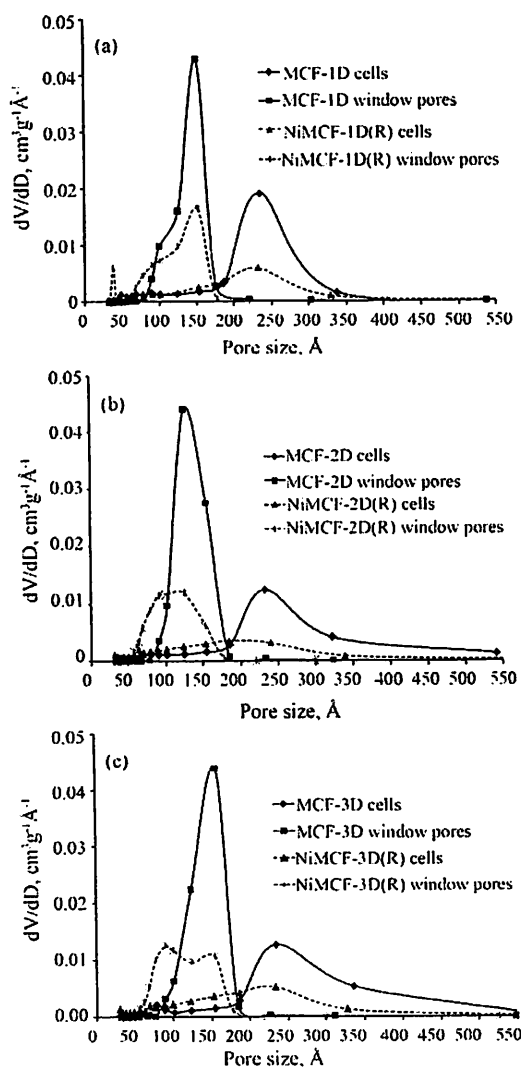


Figure 4. Cell and window pore size distribution of (a) MCF-1D and NiMCF-1D(R), (b) MCF-2D and NiMCF-2D(R), (c) MCF-3D and NiMCF-3D(R).

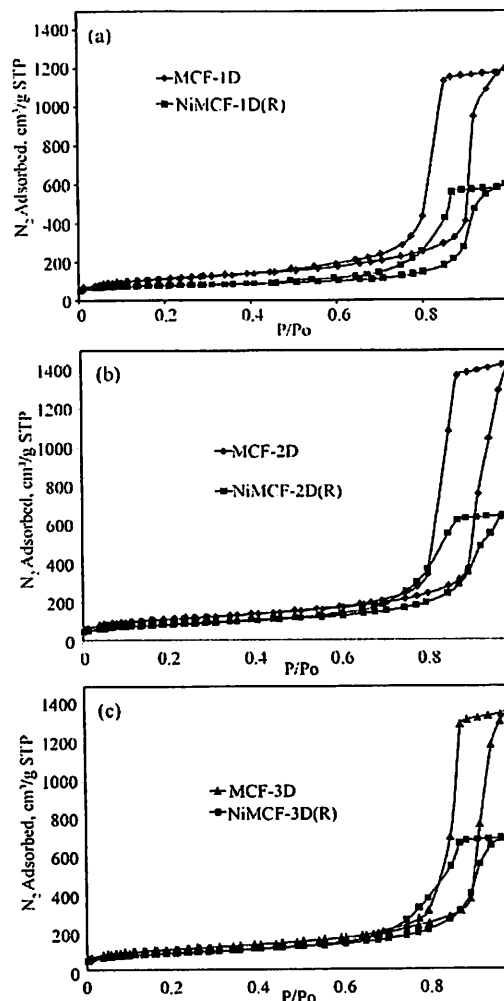


Figure 5. Nitrogen adsorption-desorption isotherm of (a) MCF-1D and NiMCF-1D(R), (b) MCF-2D and NiMCF-2D(R), (c) MCF-3D and NiMCF-3D(R).

Figure 6(a) shows the scanning electron microscope (SEM) image of MCF-3D material that clearly confirmed a spherical particle of MCF-3D with a size of about 5 μm in diameter. A higher magnification SEM image (Figure 6(b)), and transmission electron microscope (TEM) image (Figure 6(c)) show that MCF-3D possessed a mesoporous structure with cell size of about 240.5 \AA (24.05 nm). This result was consistent with the average cell size (235 \AA) obtained from nitrogen adsorption-desorption data (Table 1). The TEM image also confirmed a disordered array of silica struts that are composed of uniform-sized spherical cells interconnected by window pores with a narrow size distribution which is the characteristic structural feature of MCF material [19,26]. It has been reported in the literature that schematic cross section of MCF material is of strutlike structure. Figure 6(d) clearly shows that the cells of the MCF structure

were framed by the silica struts [26]. The wall thickness of the MCFs estimated through TEM analysis was about 5 nm. This result was in agreement with the thick, robust framework walls as observed in MCF-type mesoporous silica [26].

Morphology of various MCF silica materials (MCF-1D, MCF-2D and MCF-3D) which were incorporated with nickel using deposition-precipitation method, followed by reduction process was examined by means of SEM while the chemical composition was determined using EDX. The results are shown in Figure 7 and they indicate that morphology and chemical composition of the nickel incorporated MCF catalysts were strongly influenced by the characteristics of supports *i.e.* MCF silica materials. Nickel nanoparticles in the form of nanoworms dispersed in NiMCF-1D(R) catalyst prepared using MCF support with an aging time of 1 day had larger sizes compared to those in NiMCF-2D(R) and NiMCF-3D(R) catalysts prepared using MCF support with aging times of 2 and 3 days, respectively.

The SEM analysis results also show that all nickel functionalized MCF catalysts synthesized in this study still had highly porous structures. These results were in agreement with results from nitrogen adsorption-desorption isotherms curves in Figure 5 which indicated the meso-porosity of all resulted nickel functionalized MCF catalysts. Besides that, SEM analysis results in Figure 7 was also in agreement with results from Table 1 confirming that all nickel functionalized MCF catalysts had average window pore sizes of above 50 Å. These sizes made them suitable for the application in reactions involving bulky molecules [15]. This is because the window pores are gates for reactants or products access to the cell where the active centres were mostly located in the catalysts derived from MCF silica material [27].

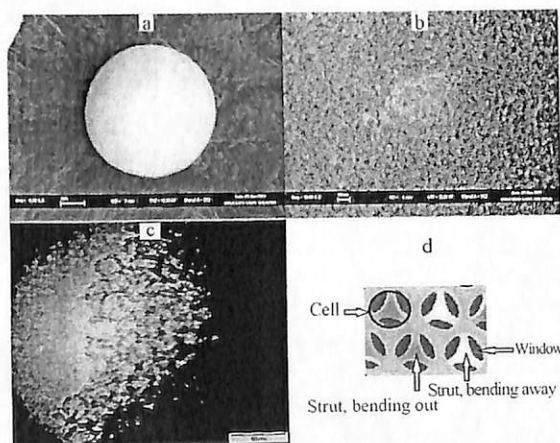


Figure 1. (a) SEM image of MCF-3D showing its morphology; (b) A higher magnification image showing the morphology of the MCF-3D surface; (c) TEM image of MCF-3D (d) Schematic cross section of MCF material [26].

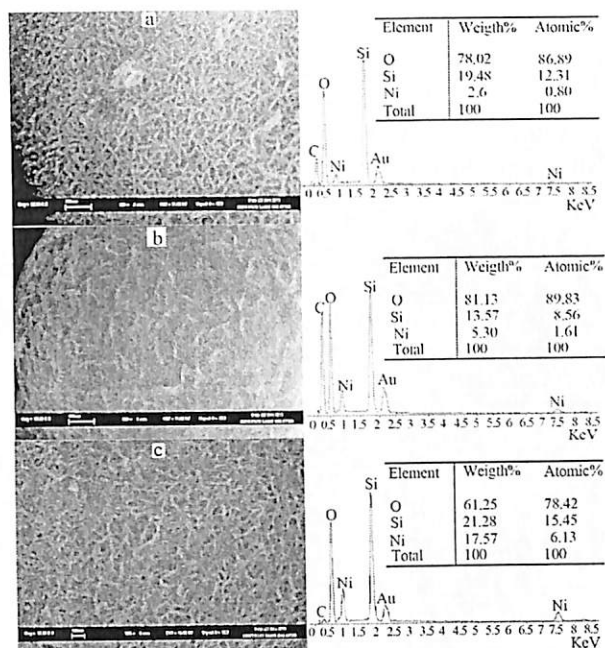


Figure 7. SEM images (left) together with chemical compositions (right) of (a) NiMCF-1D(R), (b) NiMCF-2D(R) and (c) NiMCF-3D(R).

Furthermore, it is observed from SEM images in Figure 7 that NiMCF-1D(R) catalyst had the highest porous structure as shown in Figure 7. The second highest porous structure was the NiMCF-3D(R) catalyst. Whereas NiMCF-1D(R) had the highest porous structure, it contained the lowest amount of nickel composition *i.e.* 2.6 wt%. Meanwhile, the highest amount of nickel incorporation was in the NiMCF-3D(R) catalyst *i.e.* 17.57 wt%. The amount of nickel nanoparticles dispersed in the MCF materials in this study decreased in the order of NiMCF-3D(R) > NiMCF-2D(R) > NiMCF-1D(R).

The amount of nickel composition in NiMCF-3D(R) catalyst in this study was higher than that in nickel functionalized HMS, SBA-15 or MCM-41 catalyst as reported in the literature [11-13]. The maximum amounts of nickel composition that were incorporated into the HMS and SBA-15 materials were only about 6 wt% and 5 wt%, respectively. Higher loadings of nickel detrimental to the mesostructure of the catalyst [11]. Meanwhile, nickel functionalized MCM-41 reaching a nickel composition of 12.8 wt% with an average nickel nanoparticles size of 3.38 nm has been reported in the literature [14]. However, synthesized nickel functionalized MCM-41 had an average pore diameter of 40 Å which could have limitation in reactions involving bulky molecules. Besides that, nickel supported mesoporous catalysts derived from MCM-41 materials had lower hydrothermal stability [16-18].

It was envisioned that window pore size of MCF material used as a support was the main factor that influenced the nickel nanoparticle incorporation. The window pore size of MCF support prepared using an aging time of 3 days (MCF-3D) was the highest among the others and window pore size of MCF-2D was higher than that of MCF-1D, as presented in Table 1. As such, most of nickel nanoparticles were easily introduced through the window pore size of MCF-3D support. This resulted in the highest amount of nickel nanoparticles in the NiMCF-3D(R). It can be concluded in this study that larger window pore size of MCF support resulted in the easier incorporation of nickel nanoparticle with smaller sizes. Hence, a suitable support was necessary for obtaining a high dispersion of nickel species with small size and high porous structure. This result was consistent with that reported by Subagyo *et al.* [43] who incorporated polyethyleneimine (PEI) into MCF silica material that was used as adsorbent for CO₂. They observed that the larger window pores in MCF material allowed more PEI to be incorporated.

The dispersion of nickel nanoparticles in MCF silica supports was further determined through TEM analysis and the results are shown in Figure 8. In general, it is noted that nickel nanoparticles (dark spots) were successfully dispersed on the support and no bulk particles (size of above 10 nm) were observed. This result indicated that drying at 100°C for h and calcinations at 300°C for 3 h attempted this study were efficient enough to remove water from the catalysts before the reduction step to consequently result in small nickel nanoparticles dispersed in the catalysts as suggested in the literature [33].

It can also be noted that, for the NiMCF-3D (R) prepared using MCF support prepared at an aging time of 3 days, a narrow nickel particle size distribution and small nickel particles with a mean particle size about 1 - 2 nm were observed. The mean nickel nanoparticle size in NiMCF-3D(R) in this study was smaller compared to that in NiMCM-40 as reported by Nares *et al.* [14]. The NiMCM-40 catalyst contained 13 wt% of nickel particles with a mean size of 3.38 nm. However, for NiMCF-1D(R) and NiMCF-2D(R) prepared using MCF host prepared at aging times of 1 and 2 days, respectively, nickel nanoparticles with sizes much larger (about 3 - 5 nm) and irregular shape were found to be dispersed on the supports as shown in Figures 7(a) and (b), respectively. The size of nickel nanoparticles dispersed on the MCF materials increased in the order of NiMCF-3D(R) > NiMCF-2D(R) > NiMCF-1D(R). This result was in agreement with the SEM-EDX analysis result.

Figure 9 shows XRD patterns of all catalysts produced after the calcinations step (*i.e.* NiMCF-1D(C), NiMCF-2D(C), NiMCF-3D(C)) and after the reduction

step (*i.e.* NiMCF-1D(R), NiMCF-2D(R), NiMCF-3D(R)). For the calcined catalyst samples, all of XRD patterns display peaks at $2\theta = 23^\circ$, 33° and 60° as can be seen in Figure 9(a). According to literatures, the peak at $2\theta = 23^\circ$ is a characteristic of amorphous silica [11,14]. Thus, the results suggested that the framework of the samples was amorphous. Meanwhile, peaks at $2\theta = 23^\circ$ and 60° are attributed to nickel phyllosilicates [14,44] that were detected in all the calcined catalyst samples. This result confirmed that nickel phyllosilicates in dried catalyst samples did not completely decompose into nickel oxide during the calcinations that was carried out at 300°C in this study [32].

Meanwhile, for all reduced catalyst samples, a new peak at $2\theta = 44^\circ$ was detected as can be seen in Figure 9(b). This peak was ascribed to metal nickel as reported in the literature [14,44]. Diffraction peaks at $2\theta = 23^\circ$ and 60° due to nickel phyllosilicates were clearly observed in NiMCF-1D(R) and NiMCF-2D(R) catalysts. This result indicated that for the NiMCF-1D(R) and NiMCF-2D(R), the reduction process at 550°C for 2.5 h under H₂ stream was not sufficient to completely convert nickel phyllosilicates into nickel metal through decomposition step and reduction step as shown in Figure 3. Similar behaviour has been reported for Ni/SiO₂ catalyst in which nickel phyllosilicates were still detected after the reduction process that was carried out at 450°C under H₂ stream [30].

Noticeably, for the reduced catalysts of NiMCF-3D(R) prepared using MCF support at an aging time of 3 days, only minor diffraction peaks at $2\theta = 23^\circ$ and 60° attributed to nickel phyllosilicates were observed. This result

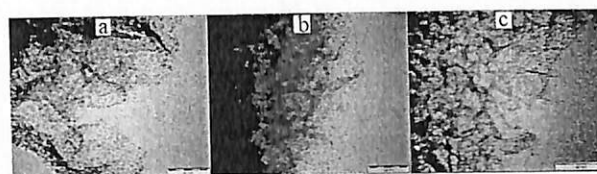


Figure 8. TEM images of (a) NiMCF-1D(R), (b) NiMCF-2D(R) and (c) NiMCF-3D(R).

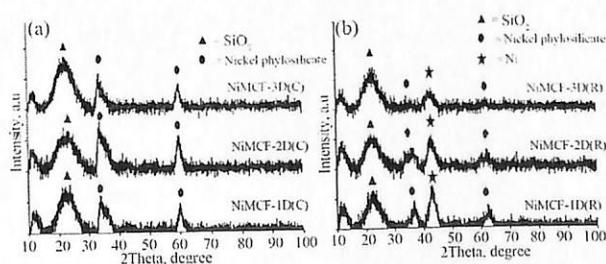


Figure 9. XRD patterns of (a) calcined catalyst samples of NiMCF-1D(C), NiMCF-2D(C), NiMCF-3D(C) and (b) reduced catalyst samples of NiMCF-1D(R), NiMCF-2D(R), NiMCF-3D(R).

confirmed that most of the nickel phyllosilicates were converted into nickel metal during the reduction process. Besides that, XRD pattern of the NiMCF-3D(R) displayed a weaker and broader peak at $2\theta = 44^\circ$ compared to that of NiMCF-1D(R) and NiMCF-2D(R) catalysts.

This result suggested nickel particles dispersed in NiMCF-3D(R) catalyst were of smaller sizes compared than those in NiMCF-1D(R) and NiMCF-2D(R). This observation was also consistent with SEM and TEM results.

It has been suggested that minor amount of unreduced nickel ions on the silica support could remain at the interface of nickel metal-silica surface as proved by some experimental and theoretical studies [45-49]. This condition was due to strong interaction between nickel phyllosilicate and silica surface [50]. These nickel ions attached to the silica surface would act as grafting sites for the metal nanoparticles. The nanoparticles could stabilize the dispersion of nickel particles to prevent them from aggregating or undergoing sintering during high temperature treatment [30].

4. Conclusions

Incorporation of nickel nanoparticles into MCF silica materials prepared at an aging temperature of 80°C and various aging times (1, 2 and 3 days) was successfully carried out. The increase in aging time resulted in an increase in window pores size in the MCF materials. Meanwhile, total surface area and pore volume were found to decrease. Nickel nanoparticle incorporation into the MCF silica materials was achieved using a deposition-precipitation method at 90°C for two hours followed by a reduction process for 2.5 h at 550°C . The window size was the critical dimension controlling the nickel nanoparticle incorporation. Among the MCF silica with various window pore sizes used in this study, the MCF support with an aging time of 3 days (MCF-3D) achieved the highest window pore size. As such, more nickel nanoparticles were incorporated into the MCF-3D support through the window pore size. The corresponding nickel functionalized MCF (NiMCF-3D(R)) catalyst had the highest nickel content (17.57 wt%) and the smallest sizes of nickel nanoparticles (1 - 2 nm) together with high porosity as confirmed in SEM and EDX results.

5. Acknowledgements

Research university (RU) grant from Universiti Sains Malaysia to support this research work is gratefully acknowledged. Lilis Hermida also thanks the Directorate General of Higher Education (DIKTI), Ministry of National Education of Indonesia for her PhD scholarship.

REFERENCES

- [1] T. Maschmeyer, "Derivatized Mesoporous Solids," *Current Opinion in Solid State and Materials Science*, Vol. 3, No. 1, 1998, pp. 71-78. doi:10.1016/S1359-0286(98)80068-5
- [2] T. M. Lancaster, S. S. Lee and J. Y. Ying, "Effect of Surface Modification on the Reactivity of MCF-Supported IndaBOX," *Chemical Communications*, Vol. 28, 2005, pp. 3577-3577. doi:10.1039/b506205e
- [3] W. F. Taylor, D. J. C. Yates and J. H. Sinfelt, "Catalysis over Supported Metals. II. The Effect of the Support on the Catalytic Activity of Nickel for Ethane Hydrogenolysis," *Journal of Physical Chemistry*, Vol. 68, No. 10, 1964, pp. 2962-2966. doi:10.1021/j100792a038
- [4] K. Niu, D. Shi, W. Dong, M. Chen and N. Zhongbin, "Chelating Template-Induced Encapsulation of NiO Cluster in Mesoporous Silica via Anionic Surfactant-Templated Route," *Journal of Colloid and Interface Science*, Vol. 362, No. 1, 2011, pp. 74-80. doi:10.1016/j.jcis.2011.06.038
- [5] L. Hermida, A. Z. Abdullah and A. R. Mohamed, "Post Synthetically Functionalized SBA-15 with Organosulfonic Acid and Sulfated Zirconia for Esterification of Glycerol to Monoglyceride," *Journal of Applied Sciences*, Vol. 10, No. 24, 2010, pp. 3199-3206. doi:10.3923/jas.2010.3199.3206
- [6] V. Degirmenci, A. Yilmaz and D. Uner, "Selective Methane Bromination over Sulfated Zirconia in SBA-15 Catalysts," *Catalysis Today*, Vol. 142, No. 1-2, 2009, pp. 30-33. doi:10.1016/j.cattod.2009.01.011
- [7] T. Huang and W. Tu, "Modification of Functionalized Mesoporous Silica on the Formation and the Catalytic Performance of Platinum Nanocatalysts," *Applied Surface Science*, Vol. 255, No. 17, 2009, pp. 7672-7678. doi:10.1016/j.apsusc.2009.04.134
- [8] L. Hermida, A. Z. Abdullah and A. R. Mohamed, "Synthesis of Monoglyceride through Glycerol Esterification with Lauric Acid over Propyl Sulfonic Acid Post-Synthesis Functionalized SBA-15 Mesoporous Catalyst," *Chemical Engineering Journal*, Vol. 174, No. 2-3, 2011, pp. 668-676.
- [9] R. I. Kureshy, I. Ahmad, K. Pathak, N. H. Khan, S. H. R. Abdi and R. V. Jasra, "Sulfonic acid Functionalized Mesoporous SBA-15 as an Efficient and Recyclable Catalyst for the Synthesis of Chromenes from Chromanols," *Catalysis Communications*, Vol. 10, No. 5, 2009, pp. 572-575. doi:10.1016/j.catcom.2008.10.035
- [10] L. Hermida, A. Z. Abdullah and A. R. Mohamed, "Effect of Functionalization Conditions of Sulfonic Acid Grafted SBA-15 on Catalytic Activity in the Esterification of Glycerol to Monoglyceride: a Factorial Design Approach," *Journal of Porous Materials*, Vol. 19, 2012, pp. 835-846. doi:10.1007/s10934-011-9538-x
- [11] J. Chen, J. Zhou, R. Wang and J. Zhang, "Preparation, Characterization, and Performance of HMS-Supported Ni Catalysts for Hydrodechlorination of Chlorobenzene," *Industrial and Engineering Chemistry Research*, Vol. 48,

- No. 8, 2009, pp. 3802-3811.
- [12] D. Liu, R. Lau, A. Borgna and Y. Yang, "Carbon Dioxide Reforming of Methane to Synthesis Gas over Ni-MCM-41 Catalysts," *Applied Catalysis A: General*, Vol. 358, No. 2, 2009, pp. 110-118. doi:10.1016/j.apcata.2008.12.044
- [13] D. Liu, X. Y. Quek, H. H. A. Waha, G. Zeng, Y. Li and Y. Yang, "Carbon Dioxide Reforming of Methane over Nickel-Grafted SBA-15 and MCM-41 Catalysts," *Catalysis Today*, Vol. 148, No. 3-4, 2009, pp. 243-250. doi:10.1016/j.cattod.2009.08.014
- [14] R. Nares, J. Ramirez, A. Gutierrez-Alejandre and R. Cuevas, "Characterization and Hydrogenation Activity of Ni/Si(Al)-MCM-41 Catalysts Prepared by Deposition Precipitation," *Industrial and Engineering Chemistry Research*, Vol. 48, No. 3, 2009, pp. 1154-1162. doi:10.1021/ie800569j
- [15] M. Nele, A. Vidal, D. I. L. Bhering, J. V. Pinto and V. M. M. Salim, "Preparation of High Loading Silica Supported Nickel Catalyst: Simultaneous Analysis of the Precipitation and Aging Steps," *Applied Catalysis A: General*, Vol. 178, No. 2, 1999, pp. 177-189. doi:10.1016/S0926-860X(98)00285-3
- [16] R. Ryoo and S. Jun, "Improvement of Hydrothermal Stability of MCM-41 Using Salt Effects during the Crystallization Process," *The Journal of Physical Chemistry B*, Vol. 101, No. 3, 1997, pp. 317-320. doi:10.1021/jp962500d
- [17] S. Inagaki, Y. Sakamoto, Y. Fukushima and O. Terasaki, "Pore Wall of a Mesoporous Molecular Sieve Derived from Kanemite," *Chemistry of Materials*, Vol. 8, No. 8, 1996, pp. 2089-2095. doi:10.1021/cm960115v
- [18] K. A. Koyano and T. Tatsumi, "Synthesis of Titanium-Containing MCM-41," *Microporous Materials*, Vol. 10, No. 4-6, 1997, pp. 259-271. doi:10.1016/S0927-6513(97)00016-3
- [19] P. Schmidt-Winkel, *et al.*, "Mesocellular Siliceous Foams with Uniformly Sized Cells and Windows," *Journal of the American Chemical Society*, Vol. 21, No. 1, 1999, pp. 254-255. doi:10.1021/ja983218i
- [20] J. S. Lettow, *et al.*, "Hexagonal to Mesocellular Foam Phase Transition in Polymer-Templated Mesoporous Silicas," *Langmuir*, Vol. 16, No. 22, 2000, pp. 8291-8295. doi:10.1021/la000660h
- [21] D. T. On and S. Kaliaguine, "Zeolite-Coated Mesoporous Cellular Silica Foams," *Journal of the American Chemical Society*, Vol. 125, No. 3, 2003, pp. 618-619. doi:10.1021/ja028656a
- [22] Q. Li, Z. Wu, D. F. Eng, B. Tu and D. J. Zhao, "Hydrothermal Stability of Mesoporous Cellular Silica Foams," *The Journal of Physical Chemistry C*, Vol. 114, No. 11, 2010, pp. 5012-5019. doi:10.1021/jp9100784
- [23] Y. J. Han, J. T. Watson, G. D. Stucky and A. Butler, "Catalytic Activity of Mesoporous Silicate-Immobilized Chloroperoxidase," *Journal of Molecular Catalysis B*, Vol. 17, No. 1, 2002, pp. 1-8. doi:10.1016/S1381-1177(01)00072-8
- [24] Y. Han, S. S. Lee and J. Y. Ying, "Siliceous Mesocellular Foam for High-Performance Liquid Chromatography: Effect of Morphology and Pore Structure," *Journal of Chromatography A*, Vol. 1217, No. 26, 2010, pp. 4337-4343. doi:10.1016/j.chroma.2010.04.041
- [25] P. Schmidt-Winkel, C. J. Glinka and G. D. Stucky, "Microemulsion Templates for Mesoporous Silica," *Langmuir*, Vol. 16, No. 2, 2000, pp. 356-361. doi:10.1021/la9906774
- [26] P. Schmidt-Winkel, *et al.*, "Microemulsion Templating of Siliceous Mesoporous Cellular Foams with Well-Defined Ultralarge Mesopore," *Chemistry of Materials*, Vol. 12, No. 3, 2000, pp. 686-696. doi:10.1021/cm991097v
- [27] J. Kim, R. J. Desch, S. W. Thiel, V. V. Gulians and N. G. Pinto, "Adsorption of Biomolecules on Mesoporous Cellular Foam Silica: Effect of Acid Concentration and Aging Time in Synthesis," *Microporous and Mesoporous Materials*, Vol. 149, No. 1, 2012, pp. 60-68. doi:10.1016/j.micromeso.2011.08.031
- [28] C. Louis, "Deposition-Precipitation of Supported Metal Catalysts," In: J. Regalbuto, Ed., *Catalyst Preparation Science and Engineering*, Taylor and Francis, Inc., New York, 2007, pp. 319-340.
- [29] P. Burattin, M. Che and C. Louis, "Molecular Approach to the Mechanism of Deposition-Precipitation of the Ni(II) Phase on Silica," *The Journal of Physical Chemistry B*, Vol. 102, No. 15, 1998, pp. 2722-2732. doi:10.1021/jp980018k
- [30] R. Iler, "The Chemistry of Silica," John Wiley & Sons, New York, 1979.
- [31] P. Burattin, M. Che and C. Louis, "Ni/SiO₂ Materials Prepared by Deposition-Precipitation: Influence of the Reduction Conditions and Mechanism of Formation of Metal Particles," *The Journal of Physical Chemistry B*, Vol. 104, No. 45, 2000, pp. 10482-10489. doi:10.1021/jp0003151
- [32] P. Burattin, M. Che and C. Louis, "Metal Particle Size in Ni/SiO₂ Materials Prepared by Deposition-Precipitation: Influence of the Nature of the Ni(II) Phase and of Its Interaction with the Support," *The Journal of Physical Chemistry B*, Vol. 103, No. 30, 1999, pp. 6171-6178. doi:10.1021/jp990115t
- [33] G. A. Martin, C. Mirodatos and H. Praliaud, "Chemistry of Silica-Supported Catalysts: Preparation, Activation and Reduction," *Applied Catalysis*, Vol. 1, No. 6, 1981, pp. 367-382. doi:10.1016/0166-9834(81)80054-1
- [34] M. Piumetti, *et al.*, "Novel Vanadium-Containing Mesocellular Foams (V-MCF) Obtained by Direct Synthesis," *Microporous and Mesoporous Materials*, Vol. 142, No. 1, 2011, pp. 45-54. doi:10.1016/j.micromeso.2010.11.010
- [35] Y. M. Liu, *et al.*, "Structure and Catalytic Properties of Vanadium Oxide Supported on Mesocellular Silica Foams (MCF) for the Oxidative Dehydrogenation of Propane to Propylene," *Journal of Catalysis*, Vol. 239, No. 1, 2006, pp. 125-136. doi:10.1016/j.jcat.2005.12.028
- [36] A. Koriakin, K. M. Ponvel and C. H. Lee, "Denitrogenation of Raw Diesel Fuel by Lithium-Modified Mesoporous Silica," *Chemical Engineering Journal*, Vol. 162, No.

- 2, 2010, pp. 649-655. doi:10.1016/j.ccej.2010.06.014
- [37] X. Yan, *et al.*, "Amine-Modified Mesoporous Silica Foams for CO₂ Capture," *Chemical Engineering Journal*, Vol. 168, No. 2, 2011, pp. 918-924. doi:10.1016/j.ccej.2011.01.066
- [38] Y. M. Liu, *et al.*, "Chromium Supported on Mesoporous Silica Foam (MCF) for Oxidative Dehydrogenation of Propane," *Catalysis Letters*, Vol. 106, No. 3-4, 2006, pp. 145-152. doi:10.1007/s10562-005-9622-4
- [39] K. S. W. Sing, "Adsorption Methods for the Characterization of Porous Materials," *Advances in Colloid and Interface Science*, Vol. 76-77, 1998, pp. 3-11. doi:10.1016/S0001-8686(98)00038-4
- [40] T. J. Barton, *et al.*, "Tailored Porous Materials," *Chemistry of Materials*, Vol. 11, No. 10, 1999, pp. 2633-2656. doi:10.1021/cm9805929
- [41] K. S. W. Sing, *et al.*, "Reporting Physisorption Data for Gas/Solid System-With Special Reference to the Determination of Surface and Porosity," *Pure and Applied Chemistry*, Vol. 57, No. 4, 1985, pp. 603-618. doi:10.1351/pac198557040603
- [42] C. Na-Chiangmai, *et al.*, "Characteristics and Catalytic Properties of Mesoporous Silica Supported Pd Nano Particles in the Liquid-Phase Selective Hydrogenation of Phenylacetylene," *Catalysis Letters*, Vol. 141, No. 8, 2011, pp. 1149-1155. doi:10.1007/s10562-011-0593-3
- [43] D. J. N. Subagyono, Z. Liang, G. P. Knowles and A. L. Chaffee, "Amine Modified Mesoporous Siliceous (MCF) as a Sorbent for CO₂," *Chemical Engineering Research and Design*, Vol. 89, No. 9, 2011, pp. 1647-1657. doi:10.1016/j.cherd.2011.02.019
- [44] P. Burattin, M. Che and C. Louis, "Characterization of the Ni(II) Phase Formed on Silica Upon Deposition-Pre-
cipitation," *The Journal of Physical Chemistry B*, Vol. 101, No. 36, 1997, pp. 7060-7074. doi:10.1021/jp970194d
- [45] T. Huizinga and R. Prins, "ESR Investigations of Platinum Supported on Alumina and Titania," *The Journal of Physical Chemistry*, Vol. 87, No. 1, 1983, pp. 173-176. doi:10.1021/j100224a037
- [46] P. Turlier, H. Praliaud, P. Moral, G. A. Martin and J. A. Dalmon, "Influence of the Nature of the Support on the Reducibility and Catalytic Properties of Nickel: Evidence for a New Type of Metal Support Interaction," *Applied Catalysis*, Vol. 19, No. 2, 1985, pp. 287-300. doi:10.1016/S0166-9834(00)81751-0
- [47] L. Bonneviot, M. Che, D. Olivier, G. A. Martin and E. J. Freund, "Electron Microscopy and Magnetic Studies of the Interaction between Nickel and Silica: Considerations on Possible Anchoring Sites," *The Journal of Physical Chemistry*, Vol. 90, No. 10, 1986, pp. 2112-2127. doi:10.1021/j100401a026
- [48] H. Haberlandt and F. J. Ritschl, "Quantum Chemical Investigation of Support-Metal Interaction and Their Influence on Chemisorptions. 2. Strong Metal Support Interaction in H-Ni-MO_x (M = Ti, Si)," *The Journal of Physical Chemistry*, Vol. 90, No. 18, 1986, pp. 4322-4330. doi:10.1021/j100409a020
- [49] M. Che, D. Masure and P. Chaquin, "Theoretical Study of the Formation of Oxide-Supported Metal Particles: Strength of the Chemical Glue as Represented by Transition Metal Ions at the Metal-Oxide Interface," *The Journal of Physical Chemistry*, Vol. 97, No. 35, 1993, pp. 9022-9027. doi:10.1021/j100137a030
- [50] J. W. E. Coenen, "Characterization of the Standard Nickel Silica Catalyst Euroni-1: III. Investigations of Catalyst-Structure," *Applied Catalysis*, Vol. 75, No. 1, 1991, pp. 193-223. doi:10.1016/S0166-9834(00)83132-2



Direct synthesis of mesoporous 12-tungstophosphoric acid SBA-15 catalyst for selective esterification of glycerol and lauric acid to monolaurate



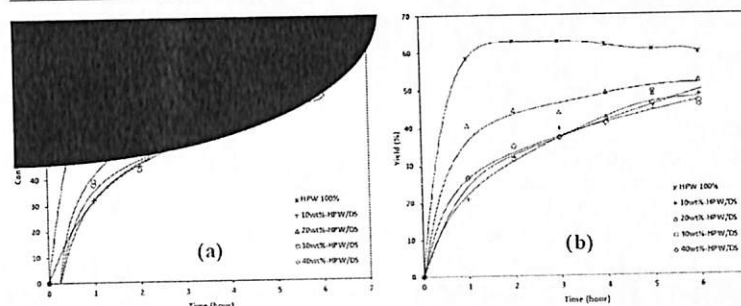
Peng-Yong Hoo, Ahmad Zuhairi Abdullah*

School of Chemical Engineering, Universiti Sains Malaysia, Nibong Tebal, Penang, Malaysia

HIGHLIGHTS

- Direct synthesis method of 12-tungstophosphoric acid SBA-15 catalyst.
- Surface characteristics retention at anions concentration below 20 wt.%.
- Formation of tungsten oxides at anions concentration above 20 wt.%.
- Direct esterification of glycerol with lauric acid to monolaurate.
- Elucidation of effects of process variables.

GRAPHICAL ABSTRACT



ARTICLE INFO

Article history:

Received 12 January 2014
Received in revised form 21 March 2014
Accepted 9 April 2014
Available online 18 April 2014

Keywords:

12-Tungstophosphoric acid
Mesoporous SBA-15 catalyst
Glycerol esterification
Direct synthesis
Monolaurate selectivity

ABSTRACT

Via direct synthesis method, highly uniformed SBA-15 catalysts functionalized with 12-tungstophosphorus acid (HPW) were synthesized. Their characteristics were investigated using BET surface analysis, NH_3 -TPD, FTIR, SEM, TEM, EDS and TGA. Surface defects were found in catalysts with high HPW loading (30–40 wt.%). High loadings also caused the deposition of WO_3 that affected their acidity. HPW in mesopores had better thermal stability. High lauric acid conversion (70%) and monolaurin yield (50%) were shown in 6 h at 160 °C by the catalyst with 20 wt.% HPW. Lower yield was achieved at higher temperature. Its ordered mesoporosity evidently resulted in shape selectivity effect to suppress by-products formation. Effects of reaction temperature (150–170 °C), reactant ratios (1:1–5:1) and catalysts loadings (1–5 wt.%) were thoroughly elucidated.

© 2014 Elsevier B.V. All rights reserved.

1. Introduction

Glycerol is produced as a by-product from oleochemical, soap making and biodiesel industries [1,2]. Its oversupply worldwide nowadays has affected its supply-demand relationship and by producing more value-added chemicals from it, more demand for this substance could be created [2]. Generally, monoglyceride can be synthesized using direct esterification of glycerol with fatty acid

in the presence of acidic catalyst at low temperature (363–393 K) [3]. Traditionally, sulfuric acid, phosphoric acid and organic sulfonic acid are used in the process [2]. The products mixtures usually contain 40–60% of monoglyceride, 35–45% of diglyceride and triglyceride, some salts and other by-products together with the homogeneous catalysts used [4]. Therefore, further expensive product purification processes such as molecular distillation, neutralization and discoloration are generally needed [4]. Another issue in this reaction is to achieve high selectivity to monoglycerides at high conversion as deep esterification reactions usually occur. Thus, heterogeneous catalysts that can show shape selectivity effect need to be designed.

* Corresponding author. Tel.: +60 4 599 6411; fax: +60 4 5941013.
E-mail address: chzuhairi@usm.my (A.Z. Abdullah).

Attempts to use catalysts based on acidic resin [5,6], zeolites [7], clay [8] and ordered mesoporous material [9] have been made. For the acidic active component of the catalyst, Keggin-type heteropoly acids (HPA) e.g. 12-tungstophosphoric acid (HPW, $H_3PW_{12}O_{40}$) is one of the potential materials with significantly higher Brønsted acidity compared to mineral acid catalysts [10]. Meanwhile, SBA-15 support generally shows highly ordered hexagonal mesophase, high hydrothermal stability, high surface area ($800\text{ m}^2/\text{g}$) and average mesopores size (60 \AA) [11]. It also has long mesopores with the width to length aspect ratio of 1:1000 that could provide high surface area within the mesopores that is particularly useful in many acid catalyzed reactions [12].

HPW have been introduced into SBA-15 and used for bifunctional conversion of *n*-decane [13]. The directly synthesized 30 wt.% HPW-SBA-15 catalyst showed 85.1% conversion and >70% yield. Different HPAs such as tungstophosphoric acid (PW), molybdophosphoric acid (PMo) and tungstosilicic acid (SiW) have also been incorporated into SBA-15. Tropecelo et al. [14] found that the HPW incorporated SBA-15 was the best catalyst with 96% conversion in palmitic acid esterification with methanol. Brahmkhatri and Patel [15] investigated the potential of similar catalyst in bio-diesel production. It consistently showed over 90% conversion as well as high reusability potential. However, reports on the use of this type of catalyst in glycerol esterification reactions are hardly found in literature. On top of that, several modifications of similar catalyst have been attempted to address and evaluate the leaching problem of such catalysts [16,17].

In this study, the behavior of HPW incorporated SBA-15 in glycerol esterification with lauric acid to selectively form glycerol monolaurate has been attempted. Particular focus has been given to shape selectivity effect in this catalyst. Correlations between catalyst characteristics and the catalytic behaviors have been established. In addition, effects of process variables such as HPW loadings, reaction temperature and reactant ratio have also been characterized.

2. Experimental

2.1. Synthesis of catalysts

HPW was incorporated into SBA-15 through a direct synthesis method outlined by Gagea et al. [13]. 1.92 g of Pluronic P123 (Sigma-Aldrich, Germany) was dissolved in 40 g of deionized water and 30 g of 4 M of HCl (R & J Chemicals) under stirring at $35\text{ }^\circ\text{C}$. The mixture was then heated up to $60\text{ }^\circ\text{C}$ and added with appropriate amounts of HPW solution. The HPW solution was prepared beforehand with the desired amount of HPW dissolved in 5 g of deionized water. The HPW solution was then added into the polymer mixture drop-wise under vigorous stirring.

The mixture was kept under stirring at $60\text{ }^\circ\text{C}$ for another 24 h. Then, 4 g of tetraethyl orthosilane (TEOS, Alfa Aesar) was added into the mixture under rapid stirring for 30 min. The formation of white precipitate could be immediately observed and the mixture was then transferred into a PE bottle and subjected to an aging process for 24 h at $80\text{ }^\circ\text{C}$ under static condition. The solution was then removed from the bottle, washed with deionized water and filtered. The filtered white solid was then dried in an oven at $60\text{ }^\circ\text{C}$ for 12 h followed by at $100\text{ }^\circ\text{C}$ for another 12 h. The dried powder was then sent for calcination in a furnace at a ramping rate of $2\text{ }^\circ\text{C}/\text{min}$ from room temperature to $300\text{ }^\circ\text{C}$ and maintained there for 30 min, followed by $500\text{ }^\circ\text{C}$ for another 6 h in air. The catalysts are denoted as *M* wt.%-HPW/DS in which the value of *M* could be 10, 20, 30 and 40.

2.2. Characterization of the catalysts

By using a Quanta-chrome Autosorb 1C surface analyzer operated at liquid nitrogen temperature, surface analysis of all synthesized catalysts were performed. Temperature programmed desorption of ammonia (NH_3 -TPD) by means of Micromeritics Autochem II system allowed characterization of acidity in the catalysts. Meanwhile, the detection of specific chemical bonds within the catalysts was achieved by mean of a Shimadzu IRPrestige-21 Fourier-transformed infrared (FTIR) system.

For surface morphology analysis, a Quanta™ FEG 450 scanning electron microscope (SEM) system operated at 5.00 kV was used while the surface elemental analysis (EDS) was done using an Oxford Silicone Drift Detector (SDD) X-Max. Besides that, Philips CM12 transmission electron microscope (TEM) with Docu Version 3.2 image analysis enabled the characterization of mesoporous channels in the catalysts. Lastly, thermal gravimetric analysis (TGA) was achieved by means of an STA 6000 from Perkin-Elmer, USA.

2.3. Catalytic activity study

All the catalysts synthesized were tested for selective esterification of glycerol (R & J Chemicals) with lauric acid (R & J Chemicals) to selectively form glycerol monolaurin. The reaction was carried out in a batch system that consisted of a heating mantle with stirring and a three-necked flask as the reaction vessel. One of the necks was connected to a vacuum pump and another neck was dedicated to a thermocouple for temperature measurement. After the reaction, the product mixtures were analyzed using a gas chromatograph (Agilent Technologies 7890A GC system) equipped with a CP-Sil 5CB ($15\text{ m} \times 0.32\text{ mm} \times 0.1\text{ mm}$) column. The lauric acid conversion and monolaurin selectivity were calculated based on calculation methods proposed by Hermida et al. [18].

3. Results and discussion

3.1. Characterization of catalysts

3.1.1. Surface analysis

All catalysts synthesized using direct synthesis method had high total surface area i.e. in the range of $169\text{--}521\text{ m}^2/\text{g}$ (Table 1). The surface area was found to decrease with increasing HPW loading. Thus, the introduction of HPW anions into the silica matrix would significantly change the surface characteristics. In this case, when more HPW anions were introduced, more deposition especially on the external surface occurred. Thus, a reduction in the surface area resulted [13]. On top of that, it is seen from SEM images that at higher HPW loading (40 wt.%), agglomeration of HPW crystal and tungsten oxide formed on the surface could drastically decrease the total surface area due to partial pore blockage.

Though the total surface area of all catalysts in this study decreased with higher HPW loading, the micropores and mesopores surface area did not always follow the same trend. Both microporosity and mesoporosity of these catalysts showed a non-systematic trend especially for 20 wt.%-HPW/DS. Interestingly, a drastic drop in total surface area of 20 wt.%-HPW/DS was observed, with much higher micropores area and lower mesopores area as compared with 30 wt.%-HPW/DS. These observations suggested that some abnormalities occurred in the pores that formed. On top of that, all catalysts showed reductions in both micropores and mesopores areas. Such phenomenon can be explained as more HPW anions being introduced into the silica support, the deposition of HPW on pores surface would reduce the pore size. Thus, an increase in microporosity could be observed with higher HPW

Table 1
Surface characteristics of SBA-15 and catalysts synthesized.

Catalyst	Total surface area (m ² /g) ^a	Micropore area (m ² /g) ^b	External surface area (m ² /g) ^b	Micropore volume (cm ³ /g) ^b	Total pore volume (cm ³ /g) ^c	Average pore size (Å) ^d
SBA-15	640	169	471	0.078	0.65	61
10 wt.-%-HPW/DS	521	99	422	0.045	0.75	59
20 wt.-%-HPW/DS	368	113	255	0.057	0.20	45
30 wt.-%-HPW/DS	348	78	270	0.036	0.42	45
40 wt.-%-HPW/DS	169	43	127	0.022	0.20	60

^a From BET desorption method.

^b From t-plot method.

^c From BJH desorption method.

^d From BJH desorption method.

loading, while both micropores and mesopores area experienced decreases in all cases.

In this study, the HPW anions were deposited within the mesopores of the SBA-15 support (as shown by a decrease in total and mesopores surface area). With that, the deposition of such large HPW anions would definitely cause the mesopores of the catalyst to be occupied by more amount of HPW, leading to a decrease in the average pore size of the catalyst. However, at higher HPW loading (30 wt.%), the oxidation of some HPW anions to much smaller tungsten trioxide would lessen the congestion effect within these pores and channels. This contributed to less severe effect to the drop in average pore size and thus compensating the effect of clogging due to the retained Keggin HPW. At higher HPW loading (40 wt.%), the high loading of HPW would have completely seal off certain channels and pores within the catalyst, making them undetectable during the BET analysis. At the same time, more tungsten trioxide was formed and deposited on the external surface of the catalyst, thus forming secondary pores that could have much higher pore size. All these reasons would ultimately cause the increase in the average pore size as reported in Table 1.

3.1.2. Adsorption isotherm

All catalysts synthesized showed the standard mesoporous Type IV isotherm (Fig. 1) according to the IUPAC classification characterized by a step increase from relative pressure of 0.2 to 0.4 due to capillary condensation [19]. With a closure at around $P/P_0 = 0.45$, most of them had narrow hysteresis loop (hysteresis type H1) except 30 wt.-%-HPW/DS (hysteresis type H2). Exceptionally, 30 wt.-%-HPW/DS showed narrow closure that represent large pores or voids found in the materials as is shown by some typical gel type materials [18]. However, the synthesized 30 wt.-%-HPW/DS was a silica solid with HPW deposited on the SBA-15 support. Such findings could be due to the disorder (surface roughness, chemical heterogeneity, pore wall defects) of the catalysts or heavily blocked pores or agglomeration of HPW crystal near the pore mouth, causing a sudden drop in N₂ desorbed near $P/P_0 = 0.48$ during desorption [20].

Comparatively, 10 wt.-%-HPW/DS had the most similar isotherm in terms of intensity and hysteresis shape as compared with the virgin SBA-15 support, suggesting that at low HPW loadings, HPW anions were successfully incorporated without significant changes in the surface characteristics. However, for 20 wt.-%-HPW/DS, the intensity dropped to suggest that its pores were much more crowded as compared to that at lower loading. The drop in intensity could reflect the fact that increased amount of smaller pores was demonstrated by 20 wt.-%-HPW/DS compared to 10 wt.-%-HPW/DS. Such observation was shared with catalyst with even higher HPW anion loading, i.e. 40 wt.-%-HPW/DS, though much lower intensity could be observed for the later one.

Based on the Barrett–Joyner–Halenda (BJH) method, pore size distributions of all catalysts are plotted in Fig. 2. It was used for

$P/P_0 > 0.35$ with the assumption that capillary condensation mechanism occurred. From the figure, it can be concluded that all synthesized catalysts had narrow and small pore size distribution range (within mesopores range, i.e. 20–500 Å). Such observation suggested that the pores formed within the catalysts were highly consistence in their pore sizes [20]. However, a small peak could also be found at lower pore size (30–40 Å) for SBA-15, 10 wt.-%-HPW/DS and 40 wt.-%-HPW/DS. Such peak is mainly due to the 'tensile strength effect' that could cause some errors during the N₂ desorption measurement [13]. Such observation could also be due to the formation of smaller, inter-channel pores that have formed between the long, hexagonal mesopores in SBA-15 which is also referred to as the bridge opening [21,22].

3.1.3. NH₃-TPD

The NH₃ desorption profiles of all catalysts synthesized using direct synthesis method are plotted in Fig. 3. Only results up to 500 °C is reported due to the known decomposition of HPW at a temperature of 485 °C [23]. It was found that the all three 10 wt.-%-HPW/DS, 20 wt.-%-HPW/DS and 40 wt.-%-HPW/DS demonstrated similar trend in the NH₃ desorption profiles. At low temperature, the amount of NH₃ desorbed increased with increasing temperature. As desorption became inhibited at higher temperature, more NH₃ was allowed to be desorbed from the catalysts surface with active acid sites at higher temperature. At low temperatures (100–200 °C), it was found that all catalysts experienced maximum NH₃ desorption at the temperature range of 150–177 °C, suggesting these acid sites were the mild acid sites contributed by the supported HPW anions within the mesopores [24].

The TCD signal intensity continued to rise for all catalysts except 30 wt.-%-HPW/DS and reached their maximums in a range of 255–307 °C. A wide peak from 100 to 300 °C detected in the TCD signal for 30 wt.-%-HPW/DS could have been masked by peak at higher temperature. Such peak could be related to the pore blockage within the catalyst, or due to the fact that some HPW anions could be unreachable due to isolation of HPW anions by the silica walls. Blocked HPW anions or channels containing active acid sites would trap the adsorbed NH₃ so that more energy was required for the adsorbed NH₃ to be desorbed from the pores and detected by the equipment.

On top of that, due to the decomposition of HPW at high temperature (485 °C), a slight increase in the intensity in all four desorption curves was detected. Due to the decomposition of HPW anions, destruction of the acid sites might occur. The acid sites would not be able to hold the NH₃ on the surface and thus were desorbed from the pores. Another peak with lower intensity could be found from all 4 catalysts at much higher temperatures (550–600 °C). This observation provided a proof to the claim that most acid site were situated within the pores. All available acid sites were categorized into weak, medium and strong acids sites according to their respective NH₃ desorption temperature range [25–27]. Generally, catalyst acidity increased with increasing

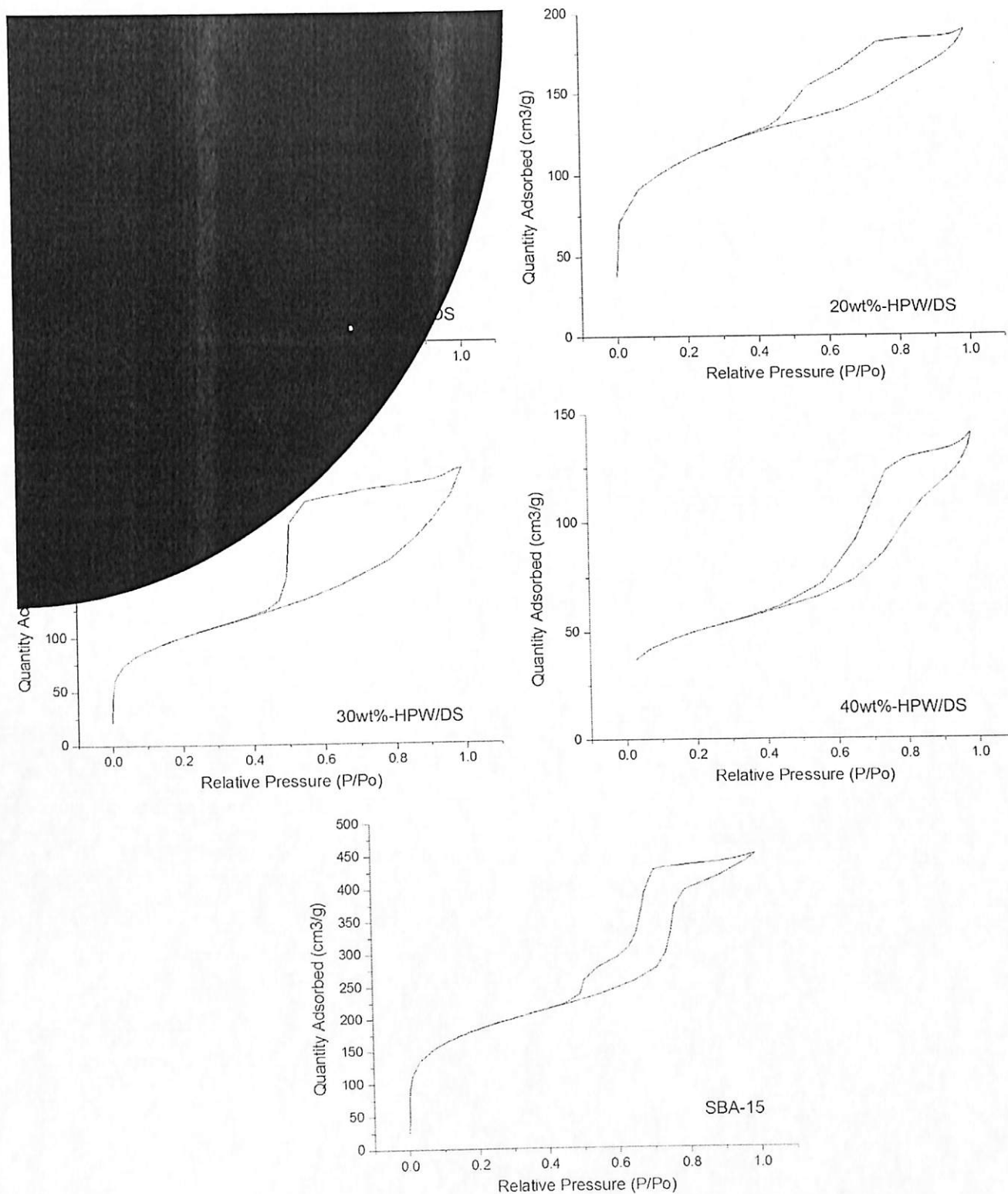


Fig. 1. Isotherm profiles of SBA-15, 10 wt.%-HPW/DS, 20 wt.%-HPW/DS, 30 wt.%-HPW/DS, 40 wt.%-HPW/DS.

HPW loading in the following order: 10 wt.%-HPW/DS < 20 wt.%-HPW/DS < 40 wt.%-HPW/DS < 30 wt.%-HPW/DS. It is generally understood that an increase in the number of acid sites causes the increase in the catalyst acidity. The decline in the acidity in

40 wt.%-HPW/DS could be attributed to the partial pore blockage at high HPW loading and loss of HPW acidity due to oxidation of HPW anions that formed tungsten trioxide that does not exert any acidity.

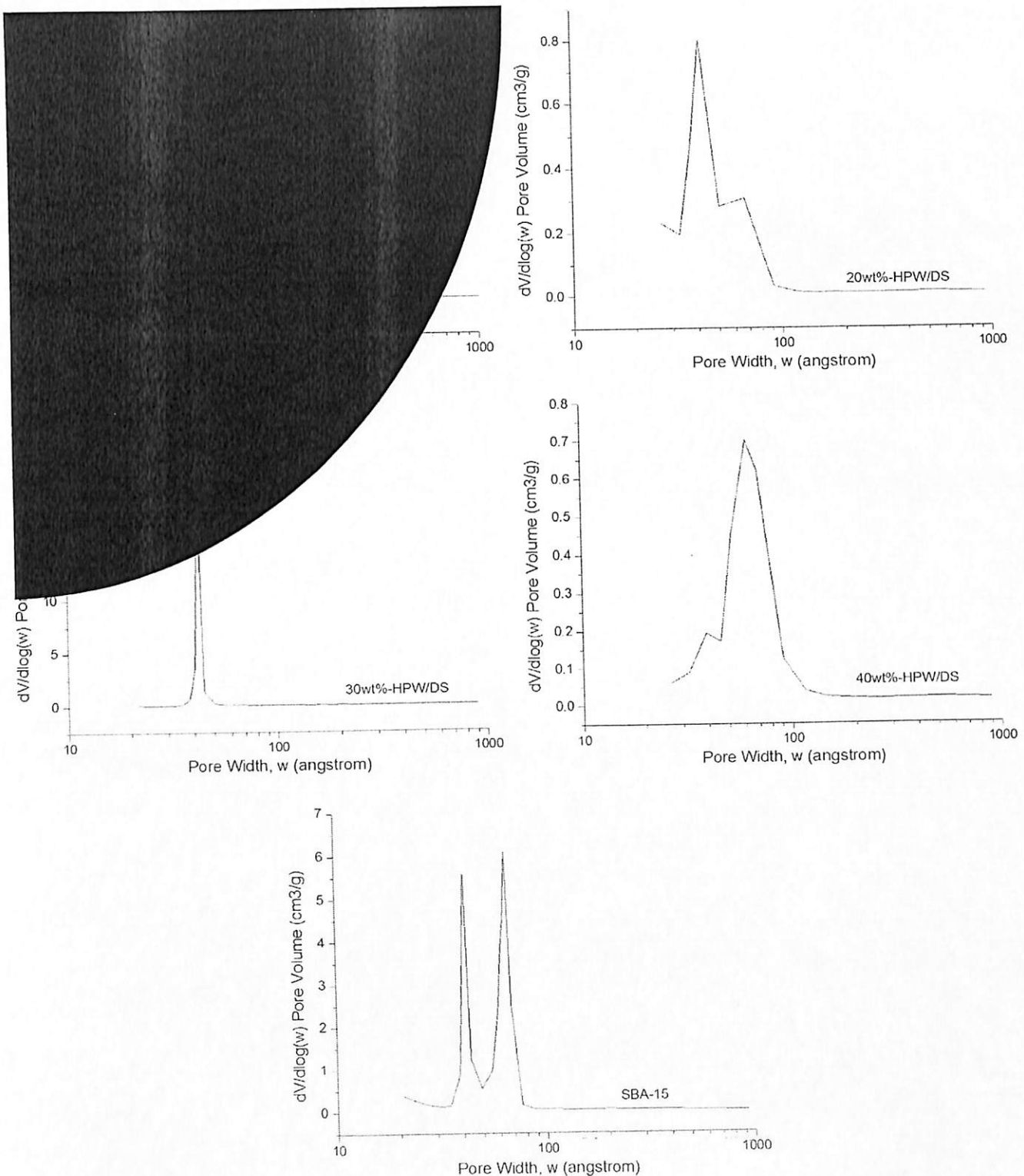


Fig. 2. BJH pore size distributions of SBA-15, 10 wt.%-HPW/DS, 20 wt.%-HPW/DS, 30 wt.%-HPW/DS, 40 wt.%-HPW/DS.

3.1.4. FTIR

The FTIR spectra (400–4000 cm^{-1}) for pure HPW, SBA-15, and all catalysts synthesized are shown in Fig. 4(a). Similarly, typical bands for Si–O–Si in condensed silica network of classic SBA-15 could be identified i.e. asymmetric stretching of Si–O–Si at a broad band of 1220–1076 cm^{-1} , symmetric Si–O–Si stretching Si–O–Si at 802 cm^{-1} and bending vibration of Si–O–Si at

459 cm^{-1} as shown in the vertical dotted lines [15]. These bands represent the properly formed condensed silica network in all catalysts that suggested mesopores structure was retained even though high HPW loadings were used (as high as 40 wt.%).

One interesting finding would be the condensed Si–OH band that was detected at 3453 cm^{-1} as this band represents the hydrogen bonds that was formed through polar interactions between

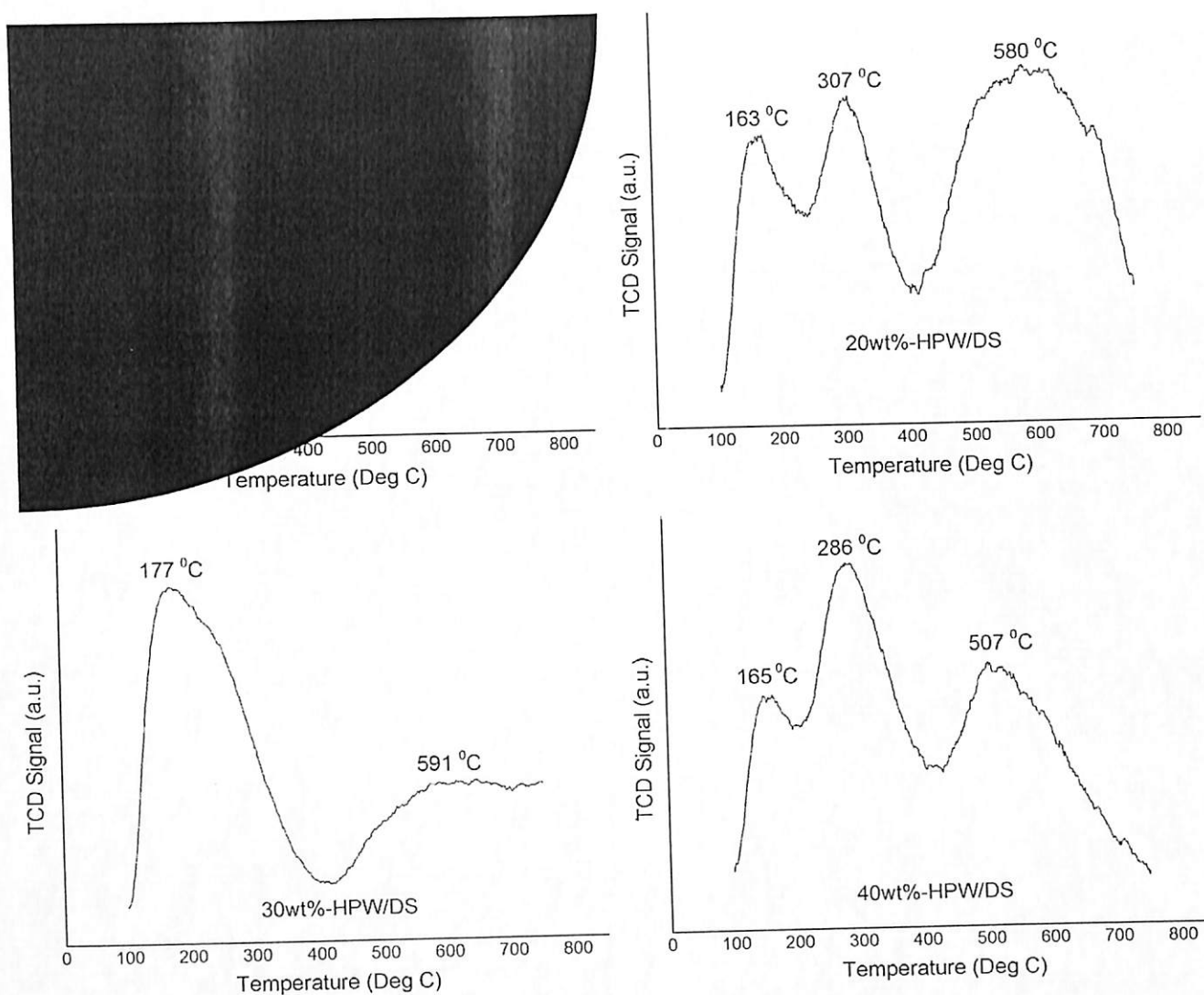


Fig. 3. NH_3 -TPD profiles of 10 wt.-%-HPW/DS, 20 wt.-%-HPW/DS, 30 wt.-%-HPW/DS and 40 wt.-%-HPW/DS.

Si—OH water molecules. It could also be due to other polar components that were hydrogen bonded to the Si—OH bond [28]. The presence of water molecules was detected in the virgin SBA-15 and all the 4 synthesized catalysts as indicated by the band at 1639 cm^{-1} . Generally, increments in intensity for this band were observed after the addition of HPW. Humidity in the air can cause adsorption of water molecules into the support material with hydrophilic Si—OH groups. High intensity shown by 10 wt.-%-HPW/DS could be associated with the availability of Si—OH in the support. On top of that, due to the hydrophilic nature of HPW itself, the supported catalyst would then have higher tendency to adsorb water molecules from the surrounding.

At higher HPW loading, the adsorption of water molecules should be more (and hence lower hydrophobicity) compared to catalysts with lower loading. Such explanation was clearly demonstrated by 30 wt.-%-HPW/DS. However, the intensity of such band dropped drastically in the case of 40 wt.-%-HPW/DS. Its yellowish appearance signified that the HPW supported onto SBA-15 underwent significant decomposition to tungsten trioxide (WO_3) causing the destruction of its Keggin structure. Due to high hydrophobicity of WO_3 , lower amount of water was adsorbed by the supported catalyst. However, 20 wt.-%-HPW/DS sample demonstrated very

interesting observation as the increase of magnitude in the intensity of adsorbed H_2O band was the lowest. As the color of the catalyst remained white, it was suggested that no significant HPW change into WO_3 occurred. Such observation suggested that at lower loading (10–20 wt.-%), most of the HPW anions situated within the pores that might have better protection from the thermal effect during calcination.

More detailed FTIR spectra of all catalysts are shown in Fig. 4(b). The characteristic bands of HPW anions including typical bands attributed to the vibrations of asymmetric P—O at central tetrahedral at 1087 cm^{-1} , terminal asymmetric oxygen ($\text{W}=\text{O}_d$) at 988 cm^{-1} , corner shared asymmetric oxygen ($\text{W}-\text{O}_b-\text{W}$) at 883 cm^{-1} and edge shared oxygen ($\text{W}-\text{O}_c-\text{W}$) at 802 cm^{-1} are detected [29]. A very weak band representing symmetric $\text{W}-\text{O}-\text{W}$ can also be found at 513 cm^{-1} . Due to low concentration of HPW in the catalysts, the bands below 600 cm^{-1} is hardly identified due to the dilution effect of silica [30]. All these bands indicate that the complex structure of HPW anions introduced into the support was retained and no significant structural change could be identified.

On top of that, obvious red shift of $\text{W}=\text{O}_d$ band can be identified as well. From the original band at 988 cm^{-1} shown by pure HPW,

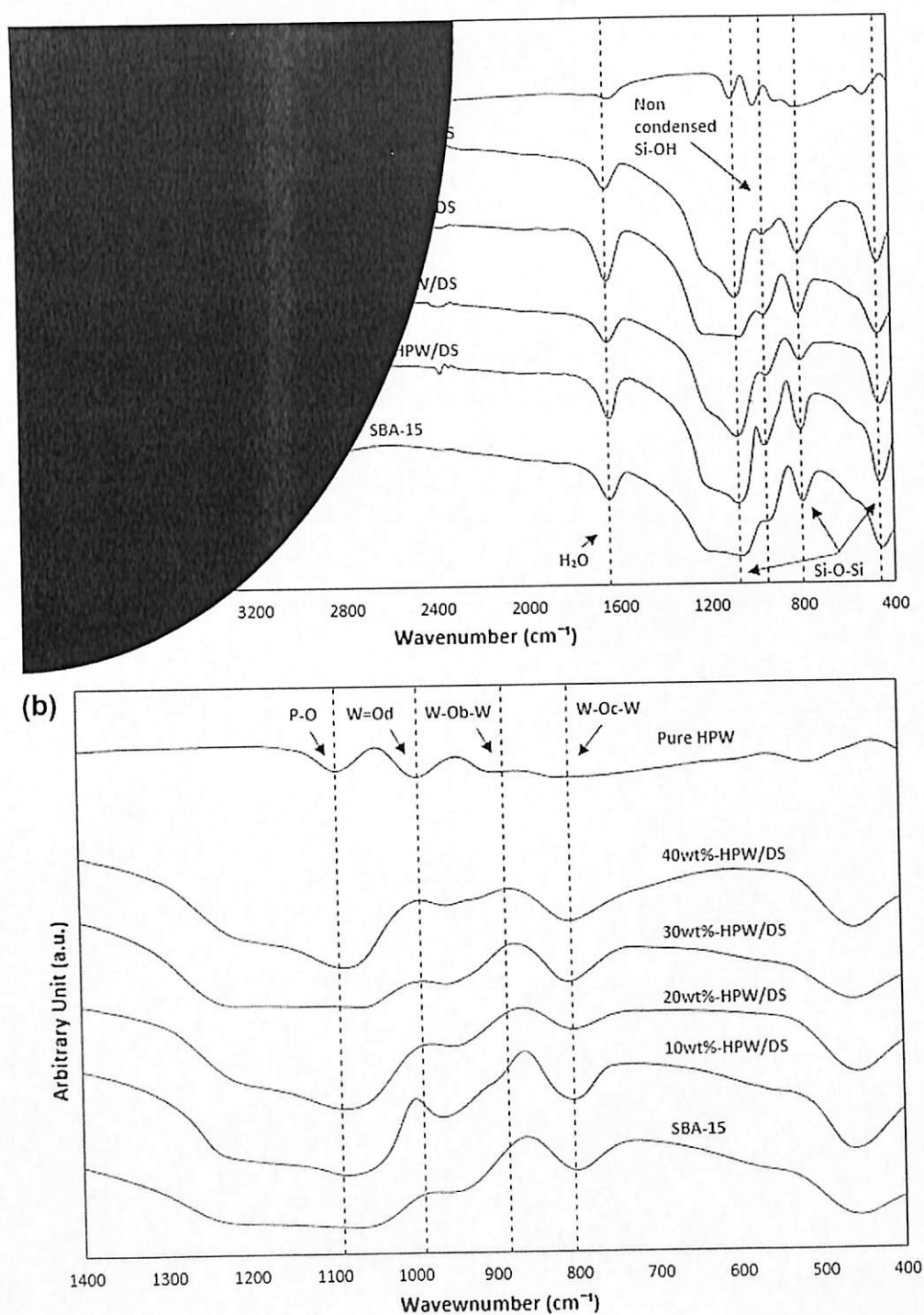


Fig. 4. (a) FTIR spectra of the synthesized catalysts, and (b) detailed FTIR spectra between 400 and 1400 cm^{-1} .

the band is red shifted to 961 cm^{-1} for both 30 wt.%-HPW/DS and 40 wt.%-HPW/DS, 953 cm^{-1} for 20 wt.%-HPW/DS and finally to 957 cm^{-1} for 10 wt.%-HPW/DS. This, again could be used as the evidence for the occurrence of interaction between HPW anions with the SBA-15 support [31]. Keggin structure of HPW anion is known to be electron-rich polyoxoanions. Thus, it is a strong acid due to its ability to donate electron to Lewis sites through the terminal $\text{W}=\text{O}_d$ bonds. The red shift of $\text{W}=\text{O}_d$ bands suggested that the interaction of the Keggin HPW anions might have occurred in the support, and acted as strong electron donor due to the presence

of the $\text{W}=\text{O}_d$ bonds [32]. Furthermore, the band of $\text{W}-\text{O}_b-\text{W}$ at 883 cm^{-1} was nowhere to be found in all 4 supported catalysts. Such an observation might be due to masking effect by other high intensity bands such as the high intensity bands around $850\text{--}900 \text{ cm}^{-1}$.

3.1.5. SEM/EDS

All SEM images captured for SBA-15 and all catalysts synthesized are shown in Fig. 5. SBA-15 shows the typical SBA-15 long fiber-like mesoporous channel structure which indicate

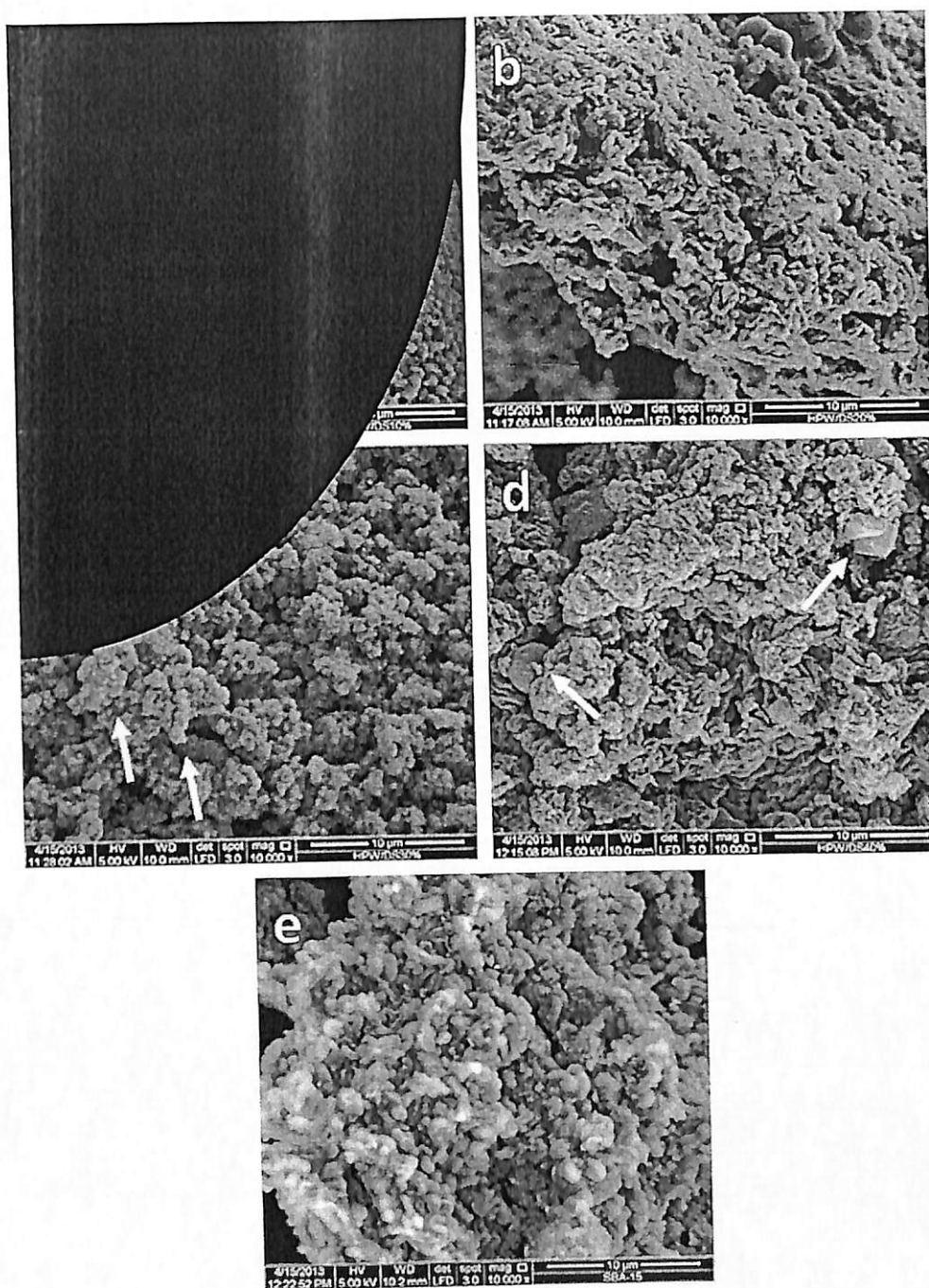


Fig. 5. SEM images for (a) 10 wt.%-HPW/DS, (b) 20 wt.%-HPW/DS, (c) 30 wt.%-HPW/DS, (d) 40 wt.%-HPW/DS and (e) SBA-15 samples (magnification 10k \times).

the successful synthesis of mesopores as predicted [33]. On top of that, hexagonal morphology attributed to the aggregation of hexagonal particles and stacking on each other is also seen [15]. In this work, the addition of HPW anions was performed even before the complete formation of mesoporous structure and addition of silica source. Thus, theoretically, most of the HPW anions were trapped between the mesoporous template (P123) and silica formed on them later. Calcination would then remove all P123 template leaving behind HPW on the mesoporous catalyst. For catalysts with higher HPW loadings such as 30 wt.%-HPW/DS and 40 wt.%-HPW/DS, the formation of HPW crystal could be seen in both SEM images in Fig. 5(c and d). Lesser HPW crystal could be seen

in 30 wt.%-HPW/DS sample while large portion of HPW crystal could be seen attaching on the external surface of 40 wt.%-HPW/DS samples.

For catalysts with lower loadings such as 10 wt.%-HPW/DS and 20 wt.%-HPW/DS, there was no visible presence of crystalline HPW on the surface. Interestingly, all SEM images show similarity in terms of shape and surface morphology with virgin SBA-15 except for the 10 wt.%-HPW/DS sample. The long fiber-like structure could still be found on 10 wt.%-HPW/DS, and the structure of this sample was found to be more uniform as compared to that of virgin SBA-15. This sample had a rod-like structure rather than a fiber-like structure that could be found on other catalysts in this study

[13]. Such surface morphology might be due to the aggregation of hexagonal particles stacking on top of each other during the introduction of silica source. Besides, at lower concentration, the P123 micelles could have less repulsion with the P123 micelles that had already been surrounded by HPW anions. Thus, stacking of micelles was facilitated to result in a more packed structure as shown in Fig. 5(a).

Similarly, SEM image of 20 wt.%-HPW/DS shows the typical fiber-like surface morphology with no crystal formed on the surface. Long fiber-like mesopores channels can clearly be seen as compared with the rest of the catalysts. This suggested that no HPW crystals were formed on the external surface of the catalysts. With most of HPW anions attached to P123, repulsive effect in between P123 micelles and attached P123 micelles would be greater than that at lower loading (10 wt.%). Thus, the mesopores that formed later would not be as packed compared to those in 10 wt.%-HPW/DS sample. On the other hand, high concentration of HPW anions in P123-HPW mixture resulted in more P123-HPW micelles to be formed. However, the size of the mesopores channels might restrict the inclusion of higher loading of HPW in the internal channels to force the excess HPW anions to deposit on the external surface as observed in the SEM images.

Specific elements on the external surface of the catalysts such as silicon (Si), oxygen (O), phosphorus (P), tungsten (W) were successfully detected from EDS analysis and the results are tabulated in Table 2. SBA-15 contained only Si and O on its surface without any P or W to be found. It was known that HPW anions consist of $PW_{12}O_{40}$ and that Keggin type HPW anions were believed to be "sandwiched" in between layers of silica of the catalyst. However, the actual weight percentage of successfully trapped HPW anions in the catalysts could not be accurately calculated due to the overlapping of the amount of O atom in both HPW anions and SBA-15.

It was interesting to see the trend of increasing difference in between designated HPW loading with the detected one. At 10 wt.%, the difference between the designated HPW loading and detected one was only 1.74%, while for the other catalysts, it was 6.07% (20 wt.%), 13.49% (30 wt.%) and 3.83% (40 wt.%). As not all HPW anions were deposited on the external surface of the catalyst, the missing HPW% could have been deposited in the internal pores. As higher concentration of HPW solution was used for the synthesis of catalysts with higher HPW loadings, the HPW anions would have been more dispersed in the reaction mixture, thus allowing more HPW anions to be introduced into the internal mesopores. On the other hand, interestingly, at the highest catalyst loading i.e. 40 wt.%, the difference between the detected and designated one was surprisingly low. Such phenomenon could be explained as most HPW anions could have formed tungsten oxide (WO_3) on the surface, so that more W elements could be found on the external surface.

In this study, it was understood that there was a possibility that the retained Keggin HPW anions could have been "sandwiched" in between silica particles of the catalysts due to the catalyst formation mechanism proposed [13]. Should an analysis such as XRF is

done, it would only show the total or bulk concentration of the catalysts, including those that might have been trapped within the particles. As the active acid sites that are available for the selective esterification reaction are of interest in this study, EDS was deemed to be more appropriate in measuring the elemental composition on the surface of the catalysts. On top of that, XRF is mostly suitable for samples with homogeneous or "smooth" surface finishing. Thus, it might cause result inaccuracy in this study that involved materials with non-homogeneous composition.

3.1.6. TEM

Most of the catalysts except 20 wt.%-HPW/DS had long and highly ordered mesoporous channels, which are similar to that of the virgin SBA-15 as shown in Fig. 6(e). Such a finding suggested that the formation of highly ordered mesopores channels were formed even with the introduction of HPW anions in the synthesis method. It was however, the effect of HPW anions addition before silica source (TEOS) that could have some effect on the structure. At very low HPW anions concentration (10 wt.%), the mesoporous and micropores were found to be abundantly available from the sample tested in TEM analysis.

The channel pore sizes found from the TEM images further verified the result gained from surface analysis earlier. Similarly, even at high HPW anions concentration (30 wt.% and 40 wt.%), the straight long mesopores channels were found as well. Interestingly, 20 wt.%-HPW/DS sample did not show obvious mesopores or micropores channels as shown in other TEM images from other catalysts. Such an observation suggested that highly ordered mesopores channels might not be satisfactorily formed in 20 wt.%-HPW/DS.

3.1.7. TGA

During the TGA analysis, drastic drops in weight for all the catalysts including SBA-15 can be observed from room temperature up to 100 °C due to the evaporation of adsorbed water molecules. SBA-15 suffered the largest weight loss (17.5 wt.%) followed by 10 wt.%-HPW/DS (13.9 wt.%), 20 wt.%-HPW/DS (9.1 wt.%), 30 wt.%-HPW/DS (10.8 wt.%) and 40 wt.%-HPW/DS (7.2 wt.%) (Fig. 7). Weight loss of catalyst due to adsorbed water was found to be more at lower loading (10 wt.%). This result suggested that more water was adsorbed by SBA-15 and 10 wt.%-HPW/DS due to more vacant Si—OH bonds available in the materials, making them slightly more hydrophilic to adsorb water.

As concluded in FTIR and SEM analyses, tungsten trioxide was formed on the surface of 40 wt.%-HPW/DS. As tungsten trioxide is hydrophobic, it was responsible for lesser adsorbed water molecules in 40 wt.%-HPW/DS. As for 30 wt.%-HPW/DS, although tungsten trioxide formation could be detected on the catalyst, significant portion of the HPW anions could maintain their Keggin structure. As the anions are hydrophilic, they would attach more readily to the surface of the catalysts. Consequently, more water molecules might be attracted to it as demonstrated by the TGA result of 20 wt.%-HPW/DS.

Table 2
Results of EDS analysis on the catalyst samples.

Catalyst	Component		Si	P	W	P + W					
	O						wt.%	at%	wt.%	at%	wt.%
	wt.%	at%									
SBA-15	67.28	78.31	32.72	21.69	0.00	0.00	0.00	0.00	0.00		
10 wt.%-HPW/DS	60.79	76.77	30.94	22.26	0.13	0.09	8.13	0.89	8.26		
20 wt.%-HPW/DS	56.45	75.70	29.62	22.63	0.08	0.06	13.84	1.62	13.93		
30 wt.%-HPW/DS	55.92	76.43	27.57	21.46	0.25	0.18	16.26	1.93	16.51		
40 wt.%-HPW/DS	45.72	76.98	18.11	17.37	0.49	0.43	35.68	5.23	36.17		

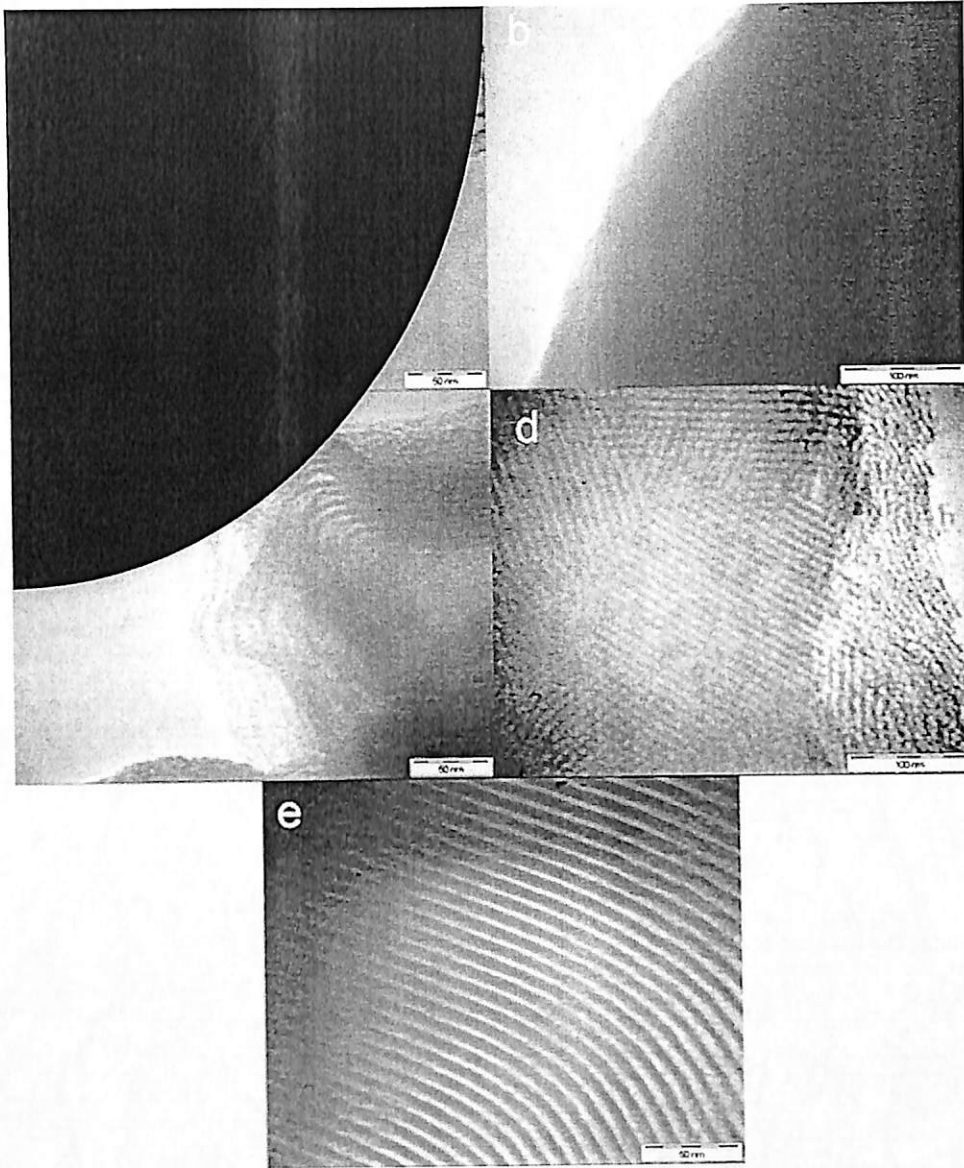


Fig. 6. TEM images of (a) 10 wt.-%-HPW/DS, (b) 20 wt.-%-HPW/DS, (c) 30 wt.-%-HPW/DS, (d) 40 wt.-%-HPW/DS and (e) SBA-15.

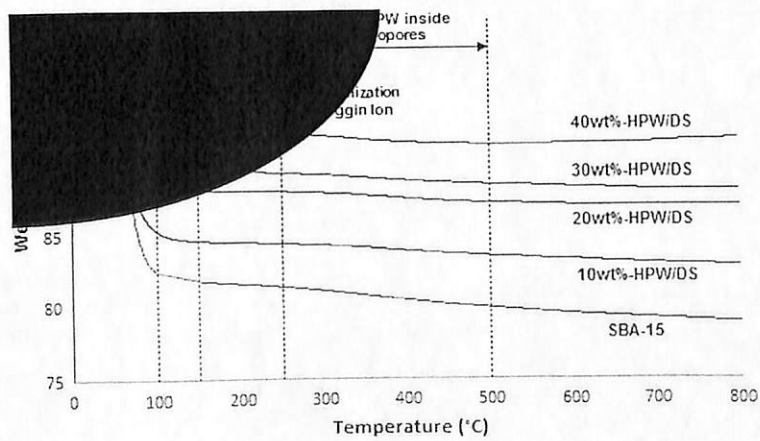


Fig. 7. TGA profiles of 10 wt.-%-HPW/DS, 20 wt.-%-HPW/DS, 30 wt.-%-HPW/DS and 40 wt.-%-HPW/DS samples.

For SBA-15, it suffered from only insignificant weight loss (2.31 wt.%) between 150 °C and 450 °C and it was mainly due to the evaporation of residual organic components such as the P123 directing templates in the catalyst. From 450 °C to 800 °C, SBA-15 experienced a gradual weight% drop of 1.23 wt.%. Such weight lost could be result from the condensation of silanol groups in SBA-15 to form siloxane bonds [15]. As for the rest for the catalysts, no significant weight drop was observed until 150 °C. From 150 °C to 250 °C, slight drops in weight were observed for all catalysts. The weight loss in this region was due to the loss of water molecules of crystallization of HPW to form HPW Keggin ion [23].

Another interesting region would be from 250 °C to 500 °C. Brahmkhatri and Patel [15] attributed it to the removal of water embedded in HPW molecules that were located inside the mesopores. In all synthesized catalysts, only small, gradual weight losses could be observed. Thus, it was concluded that the HPW anions were mainly located in the mesopores of the catalyst. This made water molecules in the mesopores channels to have difficulty to escape from the mesopores channels. This also suggested high stability of HPW anions within these catalysts.

According to Rocchiccioli-Deltcheff and his group [23], pure HPW could be decomposed by 485 °C. Thus, any loss of weight at temperatures above this could be explained as decomposition of HPW. However, there was almost no weight loss for all the synthesized catalyst. Thus, it was concluded that the HPW anions did not undergo significant decomposition until 800 °C. This observation suggested that these catalysts were very thermally stable catalysts without significant occurrence of HPW decomposition. Lower weight loss was experienced by catalysts with higher loadings (30 wt.% and 40 wt.%-HPW/DS). It was mainly due to the formation of extremely thermal stable tungsten trioxide in the catalysts.

3.2. Catalytic performance

3.2.1. Effect of HPW loading on SBA-15

Effects of HPW loading (between 10 and 40 wt.%) in the catalysts on the conversion and monolaurin yield were investigated. In this study, the other reaction variables such as catalysts loading, reaction temperature, reaction time, reactant ratio were fixed at 2.5 wt.%, 160 °C, 6 h, 4:1, respectively. From the lauric acid conversion profile (Fig. 8(a)), high activity, as represented by steeper slope at the beginning of the reaction (0–3 h) was demonstrated by all catalysts. Pure HPW (homogeneous) used for comparison clearly showed the highest conversion (97%) in 6 h as compared to the solid catalysts that only showed conversions between 70% and 75%. In this case, the homogeneous catalyst was actually in the same phase with the reactants. As HPW can also dissolve in glycerol which is a polar substance, it was well dispersed in the mixture to effectively act as the catalyst.

Despite the general expectation that higher activity should be observed for catalysts with higher amount of active acid sites, it was however 20 wt.%-HPW/DS that showed the highest activity initially while 10 wt.%-HPW/DS showed the lowest activity. With low HPW anions loading, understandably 10 wt.%-HPW/DS would show low reactivity compared other solid catalysts due to low amount of active acid sites available. Despite higher HPW anion loadings, 30 wt.%-HPW/DS and 40 wt.%-HPW/DS demonstrated reduced activity compared with 20 wt.%-HPW/DS. For instance, to reach 60% of conversion, 20 wt.%-HPW/DS only required about 3 h, while the two catalysts required up to 4 h.

Results in Fig. 8 suggest that at loadings HPW higher than 20 wt.%, their mesopores might have been significantly blocked, causing acid sites embedded in those mesopores to be inaccessible during the reaction [13]. Significant portion of the HPW anions had been deposited on external the surface of the catalyst as proposed by both SEM and EDX images earlier. Furthermore, HPW anions

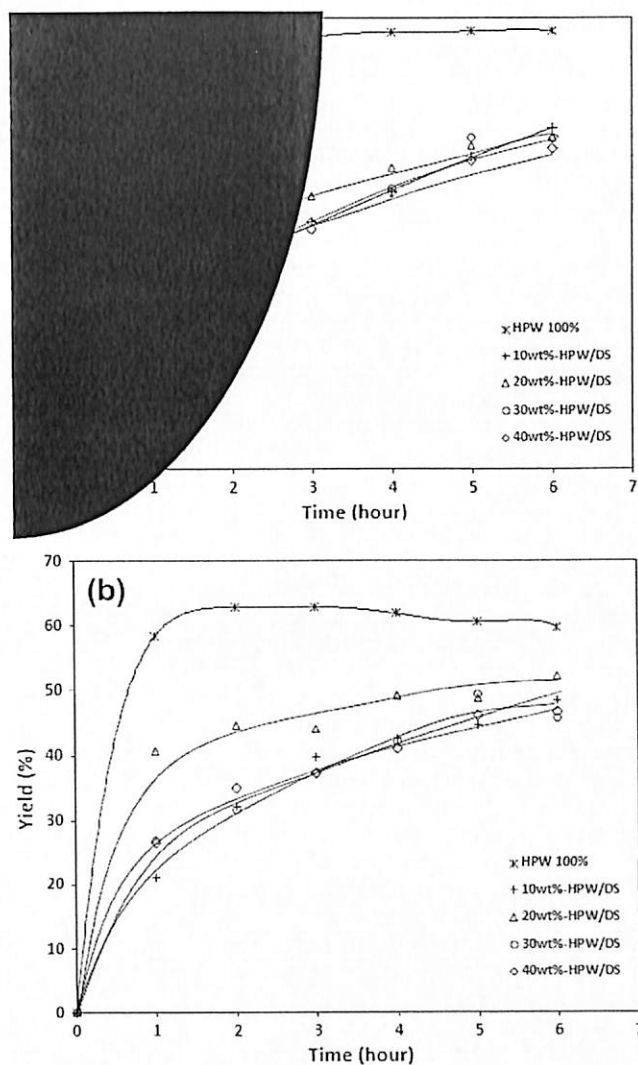


Fig. 8. Profiles of (a) conversion, and (b) monoglyceride yield shown by pure HPW, 10 wt.%-HPW/DS, 20 wt.%-HPW/DS, 30 wt.%-HPW/DS and 40 wt.%-HPW/DS.

might have been easily oxidized to tungsten oxides during calcination, as suggested by yellowish appearance of 30 wt.%-HPW/DS and 40 wt.%-HPW/DS catalysts causing the HPW to lose its Keggin structure [13]. Thus, the activities of the two catalysts were significantly lower as compared to that of 20 wt.%-HPW/DS, in which, most HPW anions were still located in the mesopores of the catalyst.

In this study, the effect of HPW loading on the selective formation of monolaurin was also scrutinized. Generally, homogeneous HPW catalyst and all the solid catalysts demonstrated moderate selectivities towards monolaurin (45–60% monoglyceride yield) (Fig. 8(b)). Thus, homogeneous HPW catalyst did not really lead to selective formation of monolaurin despite its high activity based on conversion. However, 20 wt.%-HPW/DS stood up to be the only solid catalyst that surpassed 50% of monolaurin yield. Upon chemical equilibrium achieved after about 4 h, the yield shown by 20 wt.%-HPW/DS did not differ much until the end of the reaction (6 h). As for the rest, after the reaction achieved equilibrium at about 5 h, the yield seemed to be leveled off.

The monoglyceride yield profile further verified the argument on the significant blockage of mesopores and inaccessibility of reactants to the active HPW anions sites within mesopores of

30 wt.-%-HPW/DS and 40 wt.-%-HPW/DS catalysts. The low monoglyceride yields of 30 wt.-%-HPW/DS and 40 wt.-%-HPW/DS catalysts indicated the conversion of monoglyceride to di- or triglyceride through further esterification reaction steps. Interestingly, the monoglyceride yield of 10 wt.-%-HPW/DS suffered a slight decrease by nearly 5% at the end of reaction. Despite an increase in conversion with time, the lauric acid actually further reacted with monolaurin to form higher by-products. However, the reaction was not really favored due to larger molecular sized products that were involved. However, the retardation effect on the external large pores could be minimal as compared to that within the internal mesopores of SBA-15 catalysts [6]. On the other hand, 20 wt.-%-HPW/DS did not suffer from progressive drop in monoglyceride yield at the end of the reaction, despite its high activity. This suggests that the shape selectivity effect was in highest in 20 wt.-%-HPW/DS as compared to the other catalysts. This was ascribed to its relatively more ordered mesoporosity as suggested by surface analysis and TEM results.

It was found in this study that the conversion using direct synthesized catalysts were significantly lower than that achieved using sulfonic acid functionalized SBA-15 catalysts (94% conversion) [34]. However, Hermida and co-workers [34] used much longer reaction time (20 h with reflux) compared with only 6 h maximum in this study. In another study, zeolite with tin-organic framework was also used and 40% of conversion with high monoglyceride selectivity (>98%) were achieved [35]. However, the monoglyceride yield was only about 40%. It could be due to limited access to the internal small pores and most reaction could occur on the external surface area. Thus, 20 wt.-%-HPW/DS catalyst demonstrated quite promising results as compared to other catalyst system investigated recently. Its relatively larger internal mesopores would allow significant access of reactants to the active sites while at the same time playing a role in hindering the formation of larger by-products.

3.2.2. Effect of reaction temperature

Using 20 wt.-%-HPW/DS, effect of reaction temperature were studied using different reaction temperatures between 150 °C and 170 °C while the rest of process variables were fixed (4:1, 2.5 wt.-% catalyst loading and continuous stirring). As shown in Fig. 9(a), increasing reaction temperature led to corresponding increases in both reactivity and conversion. At the beginning of the reaction, very low activity (based on slope of the curve) was observed at 150 °C. At low temperature, the energy possessed by reactant molecules were lower so that it decreased the possibility of effective collision in two ways, i.e. by decreasing the kinetic energy in reactant molecules and decreasing the potential energy of molecules. Thus, it was harder to exceed the activation energy needed for successful conversion [36]. Similarly, at higher reaction temperatures i.e. 160 °C and 170 °C, higher activity was observed, with only slight different in activities. Such findings also verified that the activation energy in the esterification of glycerol with lauric acid is of positive value as the rate of reaction increased with increasing temperature.

With 10 °C increase, the rate of reaction between 160 °C and 170 °C did not differ much at the beginning of the reaction. However, the reaction at 170 °C showed significantly higher rate compared with that at 160 °C (86% compared to 60% conversion in 6 h). This result could be due to the fact that more products or by-products were formed at higher temperature. For by-products i.e. di- and triglycerides to form, higher energy was needed to overcome the energy barrier to form larger molecules. It was also needed to overcome steric hindrance of large molecules to be formed. Furthermore, the ordered mesopores of the catalyst would play the role in shape catalysis so that the favorable product was monolaurin.

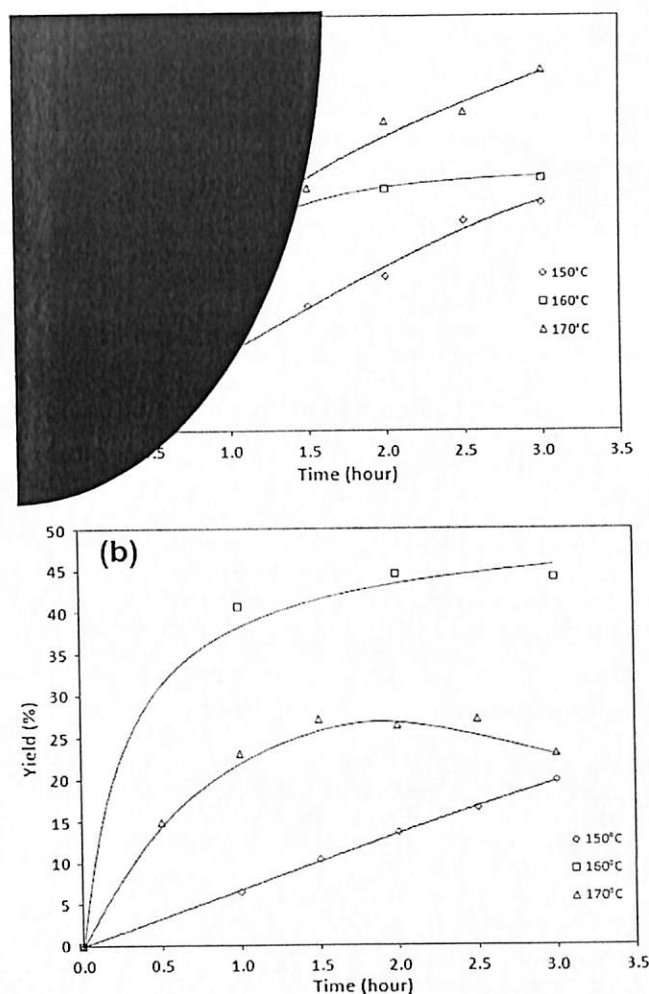


Fig. 9. Profiles of (a) conversion, and (b) monoglyceride yield for 20 wt.-%-HPW/DS at different reaction temperatures.

As shown in Fig. 9(b), the monolaurin yield at 160 °C was way higher than those of 150 °C and 170 °C, with over 45% yield compared with 20–30% yield achieved at the other 2 temperatures. Such a finding provided evidence for the suggestion that at higher reaction temperature, more by-products other than the monoglyceride were formed. The yield profile at 170 °C showed a clear reduction in the monoglyceride yield after 2 h to indicate that more monoglyceride was used to form other by-products. On the other hand, at low temperature i.e. 150 °C, the yield was low due to low conversion despite monolaurin was the main substance in the product mixture. Thus, increasing temperature could only be beneficial in increasing the conversion while the effect to monolaurin yield could be detrimental.

3.2.3. Effect of reactant ratio

Next, the effect of glycerol to lauric acid ratio (R) towards conversion and selectivity of monoglyceride were studied by using reactant ratios in the range of 1:1–5:1 while maintaining the rest of the experimental parameters. Generally, at higher reactant ratio, the rate of reaction was found to increase as demonstrated by steeper slope in Fig. 10(a). With increasing reactant concentration, Le Chatelier's principle suggested that the esterification of glycerol with lauric acid would shift to form more products. It was however, towards the end of the reaction, all runs with different reactant ratios achieved almost the same conversions between 64% and

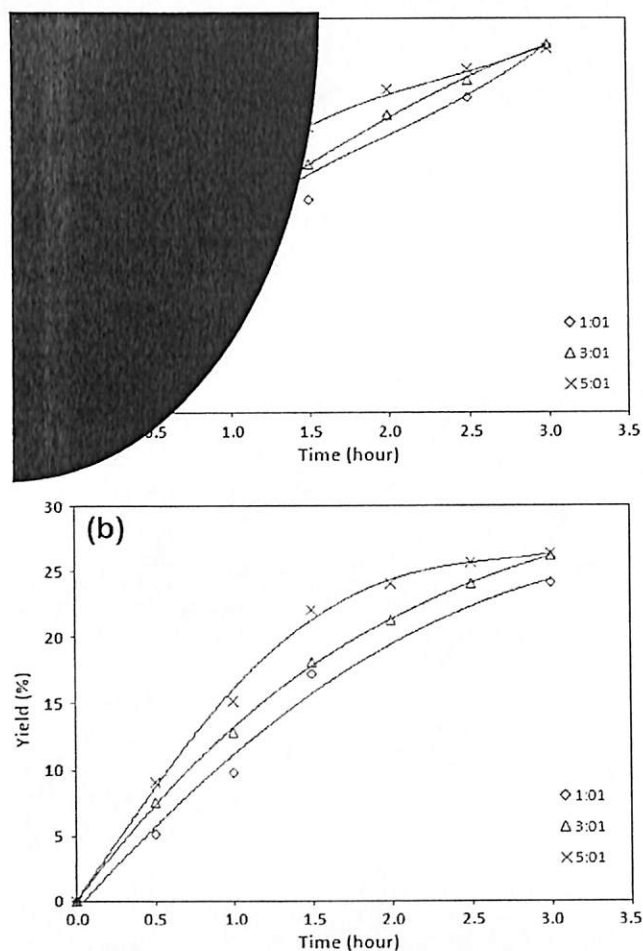


Fig. 10. Profiles of (a) conversion, and (b) monoglyceride yield for 20 wt.%-HPW/DS at different reactant ratios.

65%. This observation suggested that despite higher ratio of reactant used, it only benefited the early stage of the reaction, during which both reactants were at high concentrations and available for the reaction. As the conversion proceeded, the excess reactant concentration dropped while the limiting reactant concentration was way too low to affect the reaction [6].

On the other hand, from Fig. 10(b), monoglyceride yield was found to be higher at the beginning of the reaction for higher R value as compared with runs with lower R value. However, the yields achieved using different reactant ratios were found to be very similar at the end of reaction. Thus, it could be concluded that the reactant ratio affected the initial rate of reaction but did not have much impact on the final selectivity towards monoglyceride in this study. It was somehow similar with conversion trend as discussed earlier. It was obvious when minimal reactant ratio could result in similar outcome compared to higher reactant ratio, it should always be used for the consideration of production cost saving [3].

3.2.4. Effect of catalyst loading

Then, 20 wt.%-HPW/DS was used at different loadings with respect to the amount of lauric acid in the reactor while the rest of the parameters fixed (160 °C, 4:1, continuous stirring). The catalyst loading with respect to limiting reactant, i.e. lauric acid was varied from 1 wt.% to 5 wt.%. From Fig. 11(a), a change in catalyst loading did not have much effect on rate of reaction at the beginning of the reaction. It was however, after 1.5 h, significant

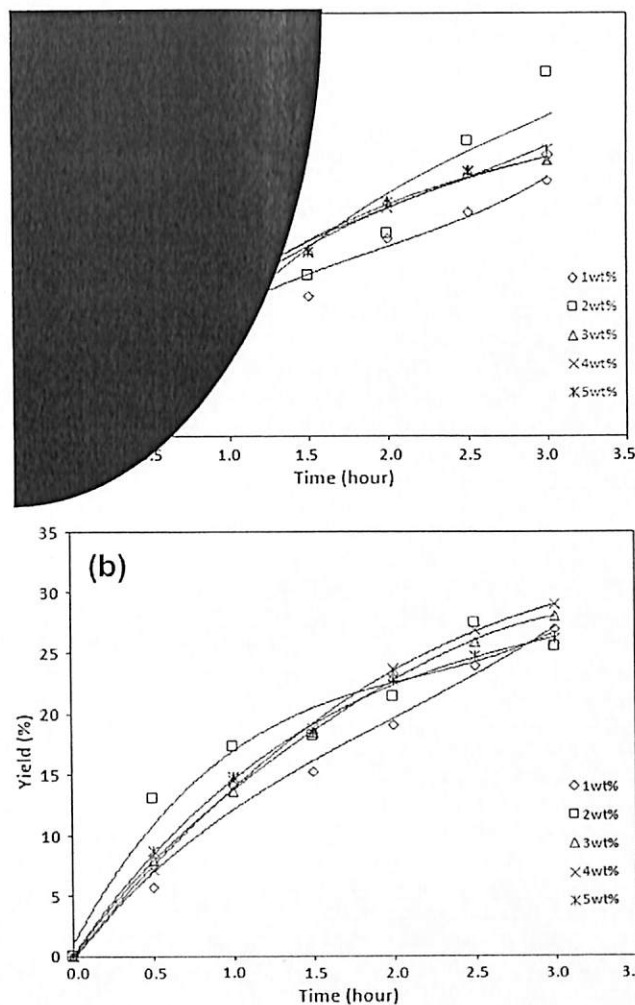


Fig. 11. Profiles of (a) conversion, and (b) monoglyceride yield with different 20 wt.%-HPW/DS loadings.

difference in the conversion profiles was observed. Generally, lauric acid conversion increased with increasing catalysts loading in the reactor. This could be simply explained based on the fact that with increasing amount of catalyst available in the system, more acid site is available to catalyze the reaction. Thus, higher conversion could be observed. All runs showed increases in conversion with time until the end of the reaction. Interestingly, at the end of the reaction, experimental run with catalyst loading of 2 wt.% showed much higher conversion (around 76%) compared to the rest, which showed conversions in a range of 60–70%.

As the active acid sites were mainly located within the mesopores of the catalyst, the reactants must be able to access the mesopores in order for the reaction to be catalyzed. Thus, diffusion of reactant within the mesoporous matrix was of great importance [3]. Diffusional limiting might occur in this case. As suggested previously, the effect of diffusional limitation in 20 wt.%-HPW/DS would be lower compared with those of higher loading such as 30 wt.%-HPW/DS and 40 wt.%-HPW/DS due to its relatively larger pores. When the same catalyst was used but with different catalyst loadings in the system, such observation might also be due to the formation of other by-products, as suggested by the lower monoglyceride yield in Fig. 11(b).

When monoglyceride yield was studied, it was found that the monoglyceride selectivity in the experimental runs using 2 wt.%

of 20 wt.%-HPW/DS was the lowest, despite showing higher conversion. This clearly showed that monoglyceride was also converted to di- or triglycerides. At other catalyst loadings, the monoglyceride selectivities were almost the same. This observation suggested that high yield of monolaurin could not be achieved by manipulating the catalyst loading. Instead, other parameters such as reaction temperature, reactant's ration and type of catalyst should be considered for such objective. The increase in conversion at the end of the reaction was simply due to the formation of other by-products that had directly contributed to the overall conversion. However, the reason for such drastic increase was not clear. As a conclusion, although the increase in catalyst loading increased the conversion and monoglyceride yield generally, the effect of different catalyst loading was rather minimal. However, an optimum amount of catalyst loading should be used to fully utilize 20 wt.%-HPW/DS without compromising the conversion.

4. Conclusions

The attempt in utilizing HPW superacidity combined with high surfaced silica material, SBA-15 using direct synthesis method was made. Characterization results showed that at suitable HPW loading would be beneficial to acid catalyzed the glycerol esterification process. HPW anions were successfully introduced into SBA-15 but the final surface structure was greatly influenced by the HPW loading. 20 wt.%-HPW/DS showed the most ordered mesoporosity in its pore system while significant surface defects were found in catalysts with high HPW loading (30–40 wt.%). External deposition of HPW also occurred at high loadings and the acid could undergo oxidative decomposition to WO_3 . High lauric acid conversion (70%) and monolaurin yield (50%) were shown in 6 h at 160 °C by this. Its ordered mesoporosity evidently resulted in shape selectivity effect to suppress by-products formation. Effects of reaction temperature (150–170 °C), reactant ratios (1:1–5:1) and catalysts loadings (1–5 wt.%) were thoroughly elucidated and successfully correlated with characteristics of the catalysts.

Acknowledgment

A Research University grant (814181) and a Short Term grant (60311007) from Universiti Sains Malaysia are gratefully acknowledged.

References

- [1] B.M. Bell, J.R. Briggs, R.M. Campbell, S.M. Chambers, P.D. Gaarenstroom, J.G. Hippler, B.D. Hook, K. Kearns, J.M. Kenney, W.J. Kruper, Glycerin as a renewable feedstock for epichlorohydrin production. The GTE process, *Clean* 36 (2008) 657–661.
- [2] N. Rahmat, A.Z. Abdullah, A.R. Mohamed, Recent progress on innovative and potential technologies for glycerol transformation into fuel additives: a critical review, *Renew. Sust. Energy Rev.* 14 (2010) 987–1000.
- [3] W.D. Bossaert, D.E. De Vos, W.M. Van Rhijn, J. Bullen, P.J. Grobet, P.A. Jacobs, Mesoporous sulfonic acids as selective heterogeneous catalysts for the synthesis of monoglycerides, *J. Catal.* 182 (1999) 156–164.
- [4] J. Pérez-Pariente, I. Diaz, F. Mohino, E. Sastre, Selective synthesis of fatty monoglycerides by using functionalised mesoporous catalysts, *Appl. Catal. A* 254 (2003) 173–188.
- [5] S. Abro, Y. Pouilloux, J. Barrault, Selective synthesis of monoglycerides from glycerol and oleic acid in the presence of solid catalysts, *Stud. Surf. Sci. Catal.* 108 (1997) 539–546.
- [6] Y. Pouilloux, S. Abro, C. Vanhove, J. Barrault, Reaction of glycerol with fatty acids in the presence of ion-exchange resins: preparation of monoglycerides, *J. Mol. Catal. A* 149 (1999) 243–254.
- [7] J. Aracil, M. Martínez, N. Sánchez, A. Corma, Formation of a jojoba oil analog by esterification of oleic acid using zeolites as catalyst, *Zeolites* 12 (1992) 233–236.
- [8] M.J.A.S. Phyanalinmat, Biodiesel synthesis from transesterification by clay-based catalyst, *Chiang Mai J. Sci.* 34 (2007) 201–207.
- [9] S.D.F. Barros, A.V. Coelho, E.R. Lachter, R.A.S. San Gil, K. Dahmouche, M.J. Paiva da Silva, A.L.F. Souza, Esterification of lauric acid with butanol over mesoporous materials, *Renew. Energy* 50 (2013) 585–589.
- [10] T. Okuhara, N. Mizuno, M. Misono, Catalysis by heteropoly compounds: recent developments, *Appl. Catal. A* 222 (2001) 63–77.
- [11] D. Zhao, Q. Huo, J. Feng, B.F. Chmelka, G.D. Stucky, Nonionic triblock and star diblock copolymer and oligomeric surfactant syntheses of highly ordered, hydrothermally stable, mesoporous silica structures, *JOACS* 120 (1998) 6024–6036.
- [12] M. Ide, E. Wallaert, I. Van Driessche, F. Lynen, P. Sandra, P. van Der Voort, Synthesis, modification, and characterization of spherical SBA-15 ordered mesoporous silica and evaluation in high performance liquid chromatography, *Micropor. Mesopor. Mater.* 142 (2011) 282–291.
- [13] B. Gagea, Y. Lorguilloux, Y. Altintas, P. Jacobs, J. Martens, Bifunctional conversion of *n*-decane over HPW heteropoly acid incorporated into SBA-15 during synthesis, *J. Catal.* 265 (2009) 99–108.
- [14] A. Tropeccio, M. Casimiro, I. Fonseca, A. Ramos, J. Vital, J. Castanheiro, Esterification of free fatty acids to biodiesel over heteropolyacids immobilized on mesoporous silica, *Appl. Catal. A* 390 (2010) 183–189.
- [15] V. Brahmkhatri, A. Patel, 12-Tungstophosphoric acid anchored to SBA-15: an efficient, environmentally benign reusable catalysts for biodiesel production by esterification of free fatty acids, *Appl. Catal. A* 403 (2011) 161–172.
- [16] X. Sheng, Y. Zhou, Y. Zhang, M. Xue, Y. Duan, Immobilization of 12-tungstophosphoric acid on LaSBA-15 and its catalytic activity for alkylation of *o*-xylene with styrene, *Chem. Eng. J.* 179 (2012) 295–301.
- [17] Y. Park, S.S. Won, C. Sang-June, Ammonium salt of heteropoly acid immobilized on mesoporous silica (SBA-15): an efficient ion exchanger for cesium ion, *Chem. Eng. J.* 220 (2013) 204–213.
- [18] L. Hermida, A.Z. Abdullah, A.R. Mohamed, Synthesis of monoglyceride through glycerol esterification with lauric acid over propyl sulfonic acid post-synthesis functionalized SBA-15 mesoporous catalyst, *Chem. Eng. J.* 174 (2011) 668–676.
- [19] X. Wang, X. Zhang, Y. Wang, H. Liu, J. Qiu, J. Wang, W. Han, K.L. Yeung, Investigating the role of zeolite nanocrystal seeds in the synthesis of mesoporous catalysts with zeolite wall structure, *Chem. Mater.* 23 (20) (2011) 4469–4479.
- [20] B.B. Dong, B.B. Zhang, H.Y. Wu, S.D. Li, K. Zhang, X.C. Zheng, Direct synthesis, characterization and application in benzaldehyde oxidation of HPWA-SBA-15 mesoporous catalysts, *Micropor. Mesopor. Mater.* 176 (2013) 186–193.
- [21] A. Galameau, H. Cambon, F. Di Renzo, R. Ryoo, M. Choi, F. Fajula, Microporosity and connections between pores in SBA-15 mesostructured silicas as a function of the temperature of synthesis, *New J. Chem.* 27 (1) (2003) 73–79.
- [22] J.P. Thielemann, F. Girgsdies, R. Schlögl, C. Hess, Pore structure and surface area of silica SBA-15: influence of washing and scale-up, *Beilstein J. Nanotechnol.* 2 (1) (2011) 110–118.
- [23] C. Rocchiccioli-Deltcheff, M. Fournier, R. Franck, R. Thouvenot, Vibrational investigations of polyoxometalates. 2. Evidence for anion-anion interactions in molybdenum (VI) and tungsten (VI) compounds related to the Keggin structure, *Inorg. Chem.* 22 (1983) 207–216.
- [24] D.P. Sawant, A. Vinu, N.E. Jacob, F. Lefebvre, S. Halligudi, Formation of nanosized zirconia-supported 12-tungstophosphoric acid in mesoporous silica SBA-15: a stable and versatile solid acid catalyst for benzylation of phenol, *J. Catal.* 235 (2005) 341–352.
- [25] Á. Molnár, C. Keresszegi, B. Török, Heteropoly acids immobilized into a silica matrix: characterization and catalytic applications, *Appl. Catal. A* 189 (2) (1999) 217–224.
- [26] L. Yang, Y. Qi, X. Yuan, J. Shen, J. Kim, Direct synthesis, characterization and catalytic application of SBA-15 containing heteropolyacid $H_3PW_{12}O_{40}$, *J. Mol. Catal. A* 229 (1) (2005) 199–205.
- [27] R. Sakhivel, E. Kemnitz, Acetylation of anisole on TPA/ZrO_2 , *Ind. J. Chem. Technol.* 15 (1) (2008) 36–43.
- [28] Y.M. Wang, Z.Y. Wu, L.Y. Shi, L.H. Zhu, Rapid functionalization of mesoporous materials: directly dispersing metal oxides into as-prepared SBA-15 occluded with template, *Adv. Mater.* 17 (2005) 323–327.
- [29] L. Yang, Y. Qi, X. Yuan, J. Shen, J. Kim, Direct synthesis, characterization and catalytic application of SBA-15 containing heteropolyacid $H_3PW_{12}O_{40}$, *J. Mol. Catal. A* 229 (2005) 199–205.
- [30] P. Madhusudhan Rao, A. Wolfson, S. Kababya, S. Vega, M. Landau, Immobilization of molecular $H_3PW_{12}O_{40}$ heteropolyacid catalyst in alumina grafted silica-gel and mesostructured SBA-15 silica matrices, *J. Catal.* 232 (2005) 210–225.
- [31] G.R. Rao, T. Rajkumar, Investigation of 12-tungstophosphoric acid supported on $Ce_{0.5}Zr_{0.5}O_2$ solid solution, *Catal. Lett.* 120 (2008) 261–273.
- [32] G.R. Rao, T. Rajkumar, Interaction of Keggin anions of 12-tungstophosphoric acid with $Ce_{0.5}Zr_{0.5}O_2$ solid solutions, *J. Colloid Interface Sci.* 324 (2008) 134–141.
- [33] D. Zhao, J. Feng, Q. Huo, N. Melosh, G.H. Fredrickson, B.F. Chmelka, G.D. Stucky, Triblock copolymer syntheses of mesoporous silica with periodic 50 to 300 angstrom pores, *Science* 279 (1998) 548–555.
- [34] L. Hermida, A.Z. Abdullah, A.R. Mohamed, Post synthetically functionalized SBA-15 with organosulfonic acid and sulfated zirconia for esterification of glycerol to monoglyceride, *J. Appl. Sci.* 10 (2010) 3199–3206.
- [35] L.H. Wee, T. Festouet, J. Fritsch, F. Bonino, M. Rose, Z. Sun, E. Garrier, D. Packet, S. Bordiga, S. Kaskel, Synthesis of monoglycerides by esterification of oleic acid with glycerol in heterogeneous catalytic process using tin-organic framework catalyst, *Catal. Lett.* (2013) 1–8.
- [36] M. Trautz, Evaluation of Arrhenius frequency factor (A) by simple collision theory, *Chemistry* 96 (1) (1916) 1–28.



Dealing with the surplus of glycerol production from biodiesel industry through catalytic upgrading to polyglycerols and other value-added products



Zahra Gholami, Ahmad Zuhairi Abdullah*, Keat-Teong Lee

School of Chemical Engineering, Universiti Sains Malaysia, Engineering Campus, 14300 Nibong Tebal, Penang, Malaysia

ARTICLE INFO

Article history:

Received 27 January 2014
Received in revised form
19 May 2014
Accepted 7 July 2014

Keywords:

Glycerol surplus
Biodiesel industry
Catalytic conversion
Etherification
Polyglycerols

ABSTRACT

An increase in glycerol production is expected because of the increasing use of fuel additives such as methyl esters. This increase can enhance the importance of glycerol as a cheap raw material for producing value-added products. Future scenarios for worldwide glycerol market will mostly be related to the supply and demand of glycerol and its application in other industries. Much research have been developed and continuously investigated to convert low-value glycerol using different strategies and approaches. Due to the unique structure of glycerol, properties and renewability feature of it, new opportunities for the transformation of glycerol into high-valued chemicals have merged in recent years. This paper provides a review on glycerol, global market of glycerol and conversion of glycerol to value-added products. Catalytic etherification of glycerol to value-added products such as polyglycerols is particularly reviewed.

© 2014 Elsevier Ltd. All rights reserved.

Contents

1. Introduction	327
2. Glycerol	328
2.1. Glycerol supply drivers	329
2.2. Glycerol market and its oversupply problem	329
2.3. Effect of glycerol price on biodiesel production cost	330
2.4. Application of biodiesel-based glycerol and its derivatives	330
3. Polyglycerols	331
3.1. Diglycerol	331
3.2. Application of polyglycerol	332
3.3. Production of diglycerol	332
4. Processes used to produce value-added products from glycerol	332
4.1. Catalytic etherification	334
4.2. Acid catalyzed etherification of glycerol	336
4.3. Base catalyzed etherification of glycerol	336
4.4. Metal oxides as catalysts in etherification of glycerol	337
5. Mechanism of base-catalyzed etherification of glycerol	338
6. Conclusions	339
Acknowledgment	339
References	339

1. Introduction

An increase in glycerol production is expected because of the increasing use of fuel additives such as methyl esters. This increase

* Corresponding author. Tel.: +60 4 559 6411; fax: +60 4 594 1013.
E-mail address: ahzohairi@usm.my (A.Z. Abdullah).

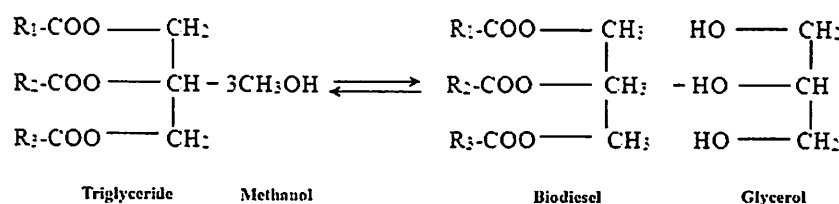


Fig. 1. Glycerol as a by-product of the methanolysis of vegetable oils.

Table 1
Typical elemental analysis results of crude glycerol from biodiesel industries [10].

Element	Weight %
Carbon (C)	52.8
Hydrogen (H)	11.1
Nitrogen (N)	< 0.0001
Sulfur (S)	–
Balance oxygen (O)	36.2

can enhance the importance of glycerol as a cheaper raw material for new products used in surfactants, lubricants, cosmetics, food additives, etc. [1]. To deal with the major excess of glycerol and develop the “green” credentials of the compound, innovative and greener catalytic processes should be developed to convert glycerol into higher value products. The synthesis of value-added molecules from crude glycerol is an attractive replacement to disposal by incineration [2]. Fig. 1 shows the schematic of the biodiesel production through vegetable oil (triglyceride) methanolysis. Homogeneous acid and base solutions are commonly used as catalysts. In a stoichiometric reaction, 1 mole of glycerol is obtained for every 3 mole of fatty acid methyl esters (biodiesel) produced.

It is anticipated that the development of crude glycerol bio-refineries benefit the economy of overall biodiesel industry through the reduction of the disposal costs of residues and increase in production of high value chemicals [3]. The process of biodiesel production starts with the purification of crude vegetable oil. The refined oil then undergoes transesterification to produce biodiesel with glycerol as the waste by-product. In a typical process, the glycerol layer (containing about 80% glycerol) [4] must be removed to enable the use of the esters as fuel. Selling of the waste glycerol solution can reduce the production cost of biodiesel by 6% [5].

Recently, biodiesel has been promoted as a means toward energy independence, rural development, and reduction of greenhouse gas emission. Biodiesel can be produced through the reaction between feedstock oil with either methanol or ethanol. The solubility of oil in methanol is less than that in ethanol. Its rate of reaction is mass transfer-limited, and methanol enables higher equilibrium conversion because of the higher reactive intermediate i.e. methoxide. Most of the biodiesel production processes use methanol, which is obtained from the petrochemical industry. This dependence on methanol can be considered a non-renewable one [6–9].

The objective of this work is to provide a review catalytic upgrading of glycerol to value-added products through etherification reaction. An overview to the relevant research topics is given in Section 1. The formation of glycerol as main by-product of biodiesel industry, investigation of the impact of this glycerol over the biodiesel production cost and glycerol market is reviewed in Section 2. This study also provides a view of transformation of this low value glycerol to upgraded products such as diglycerol using various heterogeneous catalysts as discussed in Section 3. Polyglycerols are biodegradable and biocompatible products that can be used in various industries. Various catalytic routes to produce

Table 2
Differences between types of glycerol [12].

Parameter	Crude glycerol	Purified glycerol	Refined/commercial glycerol
Glycerol content (%)	60–80	99.1–99.8	99.20–99.98
Moisture content (%)	1.5–6.5	0.11–0.8	0.14–0.29
Ash (%)	1.5–2.5	0.054	< 0.002
Soap (%)	3.0–5.0	0.1–0.16	0.04–0.07
Acidity (pH)	0.7–1.3	0.10–0.16	0.04–0.07
Chloride (ppm)	ND	1.0	0.6–9.5
Color (APHA)	Dark	34–45	1.8–10.3

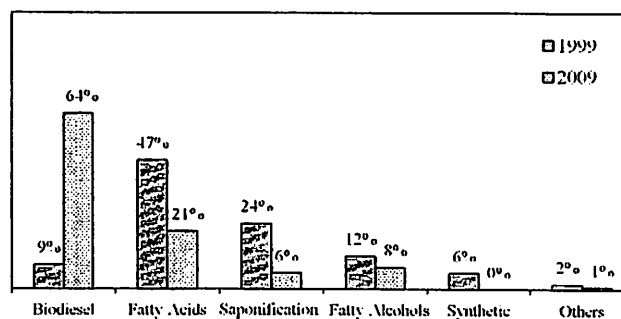


Fig. 2. Changes in glycerol supply drivers from 1999 to 2009 [14].

polyglycerols and the performance of catalysts reported in literature so far are reviewed in Section 4. Section 5 provides a review on the reaction mechanism involved in base-catalyzed etherification process.

2. Glycerol

Glycerol is a material which has numerous uses mainly because of its physical and chemical properties. Table 1 shows typical the elemental analysis results of crude glycerol produced in biodiesel industries, indicating that C, H, and O are the main elemental contents of this material [10]. Glycerol is a good renewable energy source for various applications which might be due to its high carbon content (52.8%). Furthermore, its high oxygen content (36.2%) to indicate that it is a valuable compound [11].

Glycerol can be classified into three main categories: crude, purified/refined, and commercially synthesized. Table 2 shows the major differences between these three types of glycerol from biodiesel industries. This table shows that the differences between purified and commercial glycerol are insignificant, while considerable differences can be observed between crude and purified glycerol. Actually, purified or refined glycerol is often prepared with qualities nearly equivalent to that of commercially synthesized glycerol because of its applications in sensitive fields, such as medicine, food, and cosmetics. Furthermore, Table 2 shows that

crude glycerol has about 60–80% purity, whereas purified or synthesized glycerol is generally almost 100% pure [12]. Likewise, ash, soap, and moisture could present at high quantities in crude glycerol. The acidic value of crude glycerol is slightly higher than the acidic value of the others. Its color is also darker, which may be due to the aforementioned attribute, along with some other minor impurities.

2.1. Glycerol supply drivers

A vast change has been observed among glycerol sources in the last 10 years. After 2003, changes in glycerol drivers became noticeable, at which point quick increase started until they became the largest sources in 2008. These drivers are also predicted to be the strongest future glycerol sources [13]. The fatty acid industry was considered as the main source of glycerol until 2003. However, the contribution of the said source gradually decreased, and in 2008, biodiesel became the primary glycerol source. The reason of this increasing trend of glycerol production was due to an increase in the consumption and production of biodiesel in the last few years [13].

Glycerol supply drivers shifted from one of the most popular driver i.e. the fatty acid industry, to biodiesel industry during the past 10 years, as shown in Fig. 2 [14]. From this figure, fatty acid and soap manufacturing can be seen as the two main sources of glycerol before the boom in biodiesel industry in the past few years.

In 1999, the major glycerol supply drivers were fatty acids, soaps, fatty alcohols, and biodiesel processes. The production percentages for these sources were 47%, 24%, 12% and 9%. In 2009, these sources completely changed, with the production percentages shifting to 21%, 6%, 8%, and 64%. Therefore, the biodiesel industry posed the biggest change as glycerol supply driver, from 9% to 64%, whereas fatty acid industry dropped from 47% to 21% within the same period. The increasing worldwide population may have been a factor in the increasing fuel energy consumption, i.e., increasing fuel demand. Thus, fuel energy is shifting from petroleum to biofuel to overcome this energy crisis. Biodiesel production is increasing day by day, and becoming the biggest driver of glycerol in the last few years.

2.2. Glycerol market and its oversupply problem

Until 2003, the supply of raw glycerol in the market remained relatively stable despite the start of the increase in the production of biodiesel in the United States [15]. Thereafter, the availability of crude glycerol almost doubled, but the demand remained almost unchanged. Thus, the combined effect of supply excess and limited demand of raw glycerol has led to low prices. Although pure

glycerol is an important feedstock in many industrial sectors, raw glycerol must be refined by large-scale biodiesel producers using traditional separation processes to remove impurities such as fatty acids, alcohol and catalyst. Some of these processes are filtration, chemical additions, and fractional vacuum distillation. Generally, these processes are expensive to conduct so that they are economically impossible for small- and medium-scale plants.

Since 2006, the glycerol oversupply has forced biodiesel producers to settle for raw product sale prices of 2 cents per pound or even lower. However, in mid-2007, prices were between 6 cents and 10 cents per pound [6]. In 2008, the amount of glycerol that went into annual technical applications was estimated to be approximately 160,000 t and this amount is expected to further grow at an annual rate of 2.8% [16]. Refined glycerin prices have shown a similar behavior with prices as low as 20 cents to 30 cents per pound, depending on the quality and purity [6,17]. In this sense, the raw glycerin market will continue to remain weak despite large amounts of this raw component being made available. Therefore, glycerol is a key problem in biodiesel production at present. The low sale price could convert this by-product into a residue. Thus, alternative uses must be discovered by biodiesel producers to avoid the continuous fall of glycerol price.

As the glycerol commodity market is limited to a few applications, studies suggest that any increase in biodiesel production may result in a price decline by 60% [18]. By 2016, the world biodiesel market is estimated to be at 37 billion gal. This means that every year, more than 4 billion gal of crude glycerol will be produced. The potential sale of this product could make biodiesel cheaper [19,20].

In the past few years, biodiesel production increased considerably along with the amount of residues generated during production (Fig. 3). Europe is still the largest biodiesel producer, and Brazil has the highest increase in production rate in recent years compared with the United States and Europe, that is, from 736 m³

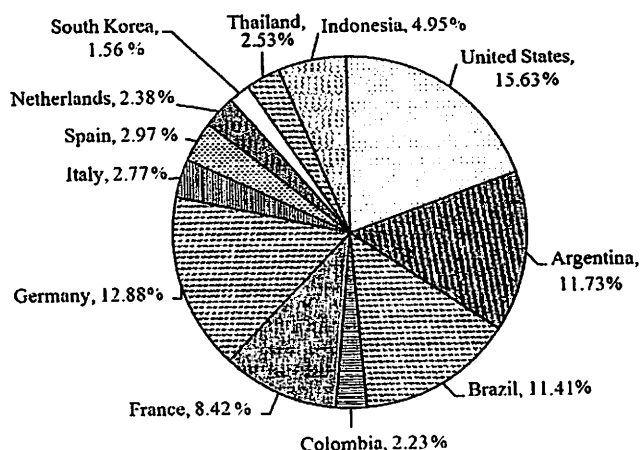


Fig. 4. Top biodiesel producing countries in 2011 [21].

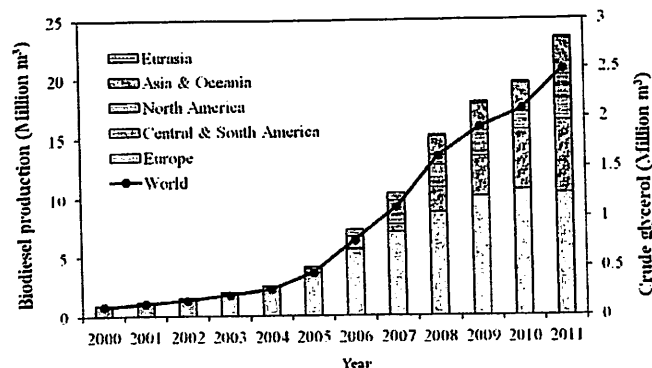


Fig. 3. World biodiesel (bars) and crude glycerol (lines) productions between 2000 and 2010 [21].

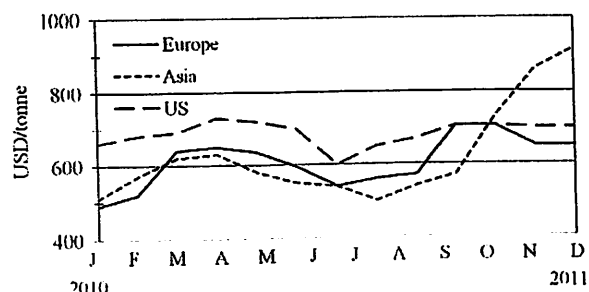


Fig. 5. Refined glycerol prices between 2010 and 2011 [26].

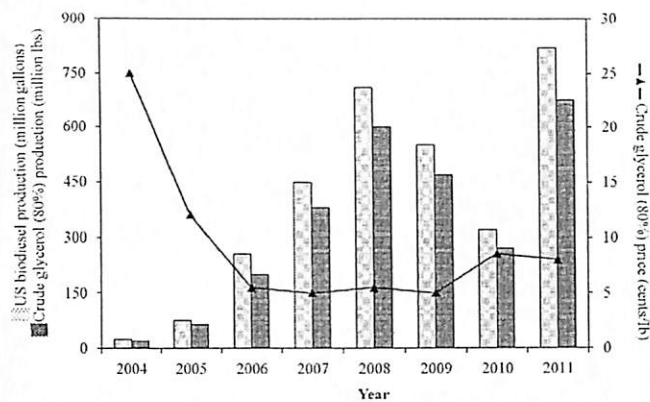


Fig. 6. US biodiesel production and crude glycerol price [36].

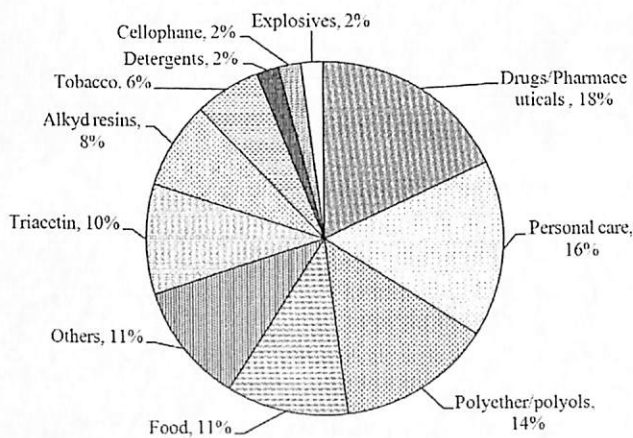


Fig. 7. Glycerol market by industry [16].

in 2005 to 2,670,000 m³ in 2011 (Fig. 4). The concentration and presence of each contaminant vary drastically from one industry to another because of the differences in the parameters, including oil source and reaction conditions. Glycerol and water content can vary from 6–92% [22] to 26–65% respectively, in crude glycerol samples [23]. The existence of these contaminations in crude glycerol samples is expected to negatively influence the bioconversion process of this co-product. However, note that the excess crude glycerol produced in the biodiesel industry leads to a decrease in glycerol prices and to the consideration of glycerol as a waste instead of a co-product [24].

2.3. Effect of glycerol price on biodiesel production cost

Currently, biodiesel production results in the rapid increase in the availability of crude glycerol worldwide. Refineries could have reached the limits of their capacity. The prices of crude glycerol have fallen down to virtually zero and even to a negative mark as producers of glycerol (particularly biodiesel) are forced to pay to have it taken away from their plants and incinerated [25].

The glycerol market is unstable as it depends on many factors such as petroleum and biodiesel production as well as its global supply and demand [26,27]. Fig. 5 shows the refined glycerol prices between 2010 and 2011 [26]. Taking the Asia market for example, the price increased from US\$ 520 to US\$ 640 per ton in the first quarter of the year 2010, and subsequently dropped to US\$ 503 per ton in August. At the beginning of 2011, glycerol price reached US\$ 858 per ton, almost twice the price in mid-2010. The

spot prices of refined glycerol in 2012 are in the range of US\$ 838–948 per ton [28]. Moreover, limited market information is available for glycerol because of its relative small scale against the global basis (approximately 1000 kt annually) [27]. The constantly changing and small markets make it difficult to predict glycerol prices in the future, resulting in the lack of reliable economic analysis of the application of glycerol. Crude glycerol has a more stable price, which is less than one-third of the cost of purified glycerol [27]. However, the downstream treatments (e.g., distillation) required to refine crude glycerol are expensive, particularly for small-scale biodiesel plants [16]. Therefore, the economic assessment of crude glycerol utilization is a challenging task.

Previous studies [29–31] show that the production cost of biodiesel varies inversely and linearly with the variations in the market value of glycerol. A report from Woo [32] indicates that the price trend of glycerol decreased over the last decade, while the production of glycerol increased because of the increase in biodiesel production. According to Fan and Burton [33], biodiesel production cost could be reduced by 25% by increasing the value of crude glycerol as its feedstock.

A promising path for the coupling of processes within a biorefinery is the employment of glycerol as a substrate for the production of biochemicals and biofuels. Glycerol is an unavoidable by-product generated in bioethanol and biodiesel production processes [34–36]. Fig. 6 shows the remarkable growth of these industries, which has led to a dramatic decrease in crude glycerol prices over the past few years [36].

These results show that the amount of crude glycerol produced as a by-product has a significant effect on the net value of the total manufacturing cost of biodiesel. However, glycerol is a valuable by-product with considerable potential as a feedstock to various value-added products. Therefore, its successful application in non-conventional uses could add a noticeable credit to the reduction of the total cost of biodiesel fuel production.

2.4. Application of biodiesel-based glycerol and its derivatives

The current market is saturated with crude glycerol because of the exponential growth of the biodiesel production. Therefore, new value-added applications of crude glycerol are being considered by biodiesel producers. The cost of converting and purifying crude glycerol into conventional materials that are applicable in food, cosmetic, or drug industries is usually high [37,38].

Glycerol has a wide range of applications, from energy bars to cough syrups and even boat coatings. According to an SDA report [10], glycerol has more than 1500 uses. Crude glycerol, resulting from biodiesel production, can be used for these applications after several purification processes. The purity of 99% or higher is used for the cosmetic and pharmaceutical markets which can be obtained by complex operation and distillation of glycerol [10]. Thus, development of new outlets for crude glycerol is essential for the present and future markets. Equally important is the development of more sustainable refining processes and more economical plants.

With respect to the research and development of new applications of glycerol, industries generally hope to increase crude glycerol prices [39]. The success of large-scale utilization of glycerol can assure the stability of the market and the increase in price [40]. The glycerol market will be stronger with the introduction of new applications of crude glycerol and these new usages may indirectly support the reduction of biodiesel production cost. Other opportunities to explore the most valuable applications of crude glycerol are available [41]. These opportunities can boost biodiesel production and transform crude glycerol into a vital part of renewable energy [24,42–46].

Establishing the new outlets for the glycerol may increase the price of crude glycerol. If new outlets for glycerol, specifically

crude glycerol is unsuccessful, glycerol prices will continue to lag. As a result, surplus amount of crude glycerol may be sold as a waste product or may be used only in incinerators to heat industrial boilers [42,47]. Nevertheless, glycerol is a main chemical compound in the world economy. Therefore, new prospects for the glycerol industry should be continuously ventured into to help in improving the economics of biodiesel production.

Glycerol is traditionally used either as food, tobacco, and drug additive or as raw material in the synthesis of trinitroglycerine, alkyd resins, and polyurethanes [16]. The usage of low-grade quality glycerol obtained from biodiesel production is a huge challenge because this type of glycerol cannot be used for food and cosmetic purposes without further purification. An effective use or conversion of crude glycerol into specific products will decrease the biodiesel production costs [48].

The oleochemical industry is a major source of glycerol. The process requires fat splitting of glycerides and biofuels such as biodiesel [49]. The widespread use of glycerol in the cosmetic, soap, pharmaceutical, food, and tobacco industries is shown in Fig. 7 [16]. In the glycerol pharmaceutical market, toothpaste and cosmetics account for 28%, tobacco for 15%, foodstuff for 13%, and manufacture of urethanes for 11%. The remainder is used in the manufacture of lacquers, varnishes, inks, adhesives, synthetic plastics, regenerated cellulose, explosives, and other industrial uses. Furthermore, glycerol is increasingly used as a substitute for propylene glycol [50]. Therefore, glycerol has become a popular research topic, and researchers are keen on discovering alternate applications in fuels and chemicals [51–53].

The required purity is a deterrent future in the use of glycerol from biodiesel production in pharmaceuticals and cosmetics. However, several factors such as low price, availability, and functionalities make glycerol an attractive choice for various industrial processes. Developing selective glycerol-based catalytic processes has become a major challenge as suggested by the high number of patents and research papers being published about it [54,55].

The purification of glycerol using the distillation method is a costly process, and the low price of glycerol makes it uneconomical [56]. Moreover, glycerol exhibits low volatility due to its high boiling point (290 °C), and it does not directly burn in either petrol or diesel engine [18]. Consequently, the idea of converting glycerol into value-added products becomes attractive because it presents a tremendous opportunity for the biodiesel industry to increase revenue and expand its product market.

3. Polyglycerols

Polyglycerol is a highly branched polyol that is clear and viscous, highly soluble in water and in other polar organic solvents such as methanol, and essentially non-volatile at room temperature [57]. At room temperature, polyglycerol is highly viscous, and the viscosity increases with molecular weight. Its high compound functionality combined with the versatile and well-investigated reactivity of hydroxyl groups forms the basis for a variety of derivatives. A number of polyglycerols are commercially available for different applications, ranging from cosmetics to controlled drug release [58,59].

Biocompatibility is an attractive feature of aliphatic polyether structures containing hydroxyl end-groups, including polyglycerols or linear polyethylene glycerols (PEGs), which are approved for a wide variety of medical and biomedical applications. Controlled etherification of glycerol to form polyglycerols with a narrow molecular weight distribution in the range of 1000–30,000 g/mol is done through the anionic polymerization of glycidol in rapid cation exchange equilibrium. Partial esterification of polyglycerols with fatty acids yields amphiphilic materials that behave as nanocapsules [57]. Linkage of individual glycerol monomers to obtain polyglycerol is one of the routes that can be used to physically upgrade the structure of glycerol. Branched isomers are created from secondary hydroxyls, whereas cyclic isomers result from the intramolecular condensation of the previous ones [60].

In several previous articles [1,61–63], producing oligomers using the transformation of glycerol is referred to as etherification. Often, oligomers with 2–4 glycerol units are viewed as polyglycerols, without a strict differentiation as to where the oligomers end and the polyglycerol begins, while bearing the inherent possibility of confusion with high-molecular weight, branched polyglycerol produced through anionic polymerization [64].

Table 3 shows the variations in the physical properties of glycerol and its higher oligomers [65]. Generally, with increasing oligomer molecular weight, the density correspondingly increases with the addition of glycerol units in the chain. The ability to break ether bonds is also more difficult due to the effects of chain structure. Thus, the correlation between pressure and temperature must be considered. Hydroxyl number can be measured experimentally and is defined as the amount of KOH (mg) equivalent to the hydroxyl content of 1 g of sample. The hydroxyl number generally decreases with increasing number of glycerol units, which also results in variations to polarity, solubility, viscosity and color (from water clear to dark yellow) [65,66].

3.1. Diglycerol

Diglycerol (DG) is a clear viscous liquid and very similar to glycerol, but with higher molecular weight and less volatility. DG is water soluble and can be combined with aqueous systems. Table 4 compares the physico-chemical properties of DG and glycerol, which are important in understanding the behavior of DG to explain its kinetic activity in the etherification reaction [67]. The properties of DG are more desirable compared with glycerol. In addition, DG products are conferred with properties that are more applicable and valuable for use in many applications.

Diglycerol is envisaged to be the most plentiful product formed from a pool of isomers during the reaction. Linear, branched, and cyclic dimers are formed, and their formation depends on the location of the interacting hydroxyl groups from different individual monomers. Coupling of primary to primary, primary to secondary, and secondary to secondary locations, as well as second-generation etherification products, results in the formation of prim–prim, prim–sec, sec–sec, and cyclic dimers, respectively [68]. The dimension and basal spacing value (d) of each dimer are shown in Fig. 8 [69].

Table 3
Physical data of glycerol, diglycerol and higher oligomers [65].

Name	Molecular formula/weight (g/mol)	Refractivity n_D^{20} (-)	Density (g/cm ³)	Boiling point (°C)/(Pa)	Hydroxyl number (mg KOH/g)
Glycerol	C ₃ H ₈ O ₃ 92	1.4720	1.2560	290	1830
Diglycerol	C ₆ H ₁₄ O ₅ 166	1.4897	1.2790	205/133	1352
Triglycerol	C ₉ H ₂₀ O ₇ 240	1.4901 (40 °C)	1.2646 (40 °C)	> 250/13.3	1169
Tetraglycerol	C ₁₂ H ₂₆ O ₉ 314	1.4940 (40 °C)	1.2687 (40 °C)	69–73 (melting point)	1071

Table 4
Physico-chemical properties of glycerol and diglycerol [67].

Property	Unit	Diglycerol	Glycerol
Molecular formula	–	C ₆ H ₁₄ O ₅	C ₃ H ₈ O ₃
Molecular weight	g/mol	166	92
Density	g/ml	1.276	1.256
Dynamic viscosity	Pa s	13	1
Refractive index	–	1.487	1.472
Dielectric constant	–	34	46
Boiling point	°C	205 (1.3 mbar)	290
Heat of dissolution in water	J/g	–52	–62
Specific heat capacity	J/g K	2.28	2.38
Thermal conductivity	W/m K	0.28	0.29
Thermal expansion coefficient	°C	0.00053 (20–60 °C)	0.00052 (20–60 °C)
Flash point	°C	230	199
Fire point	°C	264	204
Autoignition	°C	380	370

3.2. Application of polyglycerol

In the current polyglycerol market, this product generally includes different oligomer mixtures such as diglycerol, triglycerol, tetraglycerol, hexaglycerol and decaglycerol. Polyglycerols can be transformed to polyglycerol esters to use as an emulsifier in the cosmetic/food and plastic industries. A main potential market for polyglycerol is polyglycerol ester which can be used as non-ionic surfactant. Due to the amphiphilic character of polyglycerols, these materials are capable to be used in the stabilization of different suspensions and emulsions [70].

Polyglycerols are used to control viscosity, emulsify and stabilize product formulae. They are incorporated into moisturizing sunscreens, sun protective sticks, hair-styling gels, long-acting hand creams, skin treatment gels, skin cleansers and baby creams. In the food industry, polyglycerol esters are used as emulsifying agents in the production of fine bakery products, fat replacement products and chewing gum [70].

In 2012, natural emulsifiers accounted for about one-third of the total emulsifier market, whereas synthetic emulsifiers held the rest. Among the synthetic segment, di-glycerides and derivatives constitute the largest share and are expected to grow at a modest pace. Other synthetic emulsifier which comprises of polyglycerol esters, sucrose esters and polyglycerol polyricinoleate (PGPR) is expected to drive the market for emulsifiers. However, palm oil and other vegetable oil prices are highly volatile and ascertaining accurate future prices would be difficult [71].

Europe generated maximum revenue in global food emulsifier market. The U.S., however, is the leader in the segment in the global market. North America, hence, is the second largest market of the segment. China drives the Asia-Pacific market with the highest annual growth rate globally. Germany generated maximum revenue in European market, followed by Italy. ROW emulsifier market, led by Brazil, is also given a boost by the promising growth in South Africa and Middle East [71].

According to a new market research report [71], "Food Emulsifiers Market By Types (Mono, Di-Glycerides and Derivatives, Lecithin, Sorbitan Esters, Stearoyl Lactylates and Others), Applications (Bakery & Confectionery, Convenience Foods, Dairy Products, Meat Products and Others) and Geography – Global Trends and Forecast To 2018", published by Markets and Markets [71], the food emulsifiers market will grow from an estimated level of \$ 2108.9 million in 2012 to \$ 2858.6 million by 2018 with an annual growth rate of 5.2% from 2013 to 2018. Europe led the global market followed by North America and Asia-Pacific in terms of revenue in the year 2012.

3.3. Production of diglycerol

Different methods or routes can be used to synthesize pure diglycerol, either from glycerol itself or from other substances. In laboratory-scale production, direct synthesis routes were described by Wittcoff et al. [72,73]. Fig. 9 shows several conventional processes for diglycerol synthesis.

All reported processes thus far have the disadvantage of requiring the use of starting substances that are difficult to obtain or synthesis procedures that require several intermediate steps that produces great amounts of salts as by-products [66]. Such methods mostly consist of non-catalytic processes involving allylation, hydroxylation, and hydrolysis. In thermal conversion of glycerol, the reaction is generally performed at specified temperatures under an inert protecting atmosphere [65]. A purely thermal conversion without the addition of a catalyst is set above 200 °C; at 290 °C in the dark, strongly smelling products are formed. At low temperature (180 °C) and in the presence of alkaline, only a small amount of diglycerol is formed with a low conversion degree. Traces of oxygen that present could result in the formation of acrolein and other condensation products. Thus, air should be eliminated from the system during the reaction [74].

During the basic hydrolysis of epichlorohydrin 10 (Fig. 8) by NaOH, an intermediary glycidol 11 is assumed to form aside from glycerol 8, and this intermediary reacts with non-converted 10 or 8 to form diglycerol 1. The residual glycerol has to be separated and water should be removed from raw diglycerol. The reactions of glycidol or epichlorohydrin with glycerol similarly exhibit coupling of the OH groups that is not confined to the terminal positions, with the middle OH groups being involved as well. These events lead to the formation of α, β - and β, β' -diglycerol, aside from α, α' -diglycerol [65,66,75].

Methods of catalyzed glycerol oligomerization have been developed. The process of synthesizing diglycerol has also improved with the application of simple processing techniques, including the use of affordable materials and equipment. Many studies on these catalysts, as well as the improvement of catalytic reactions, have been done. Such works include the study on homogeneous and heterogeneous acid or basic catalysts. The highlights of this related topic in the etherification reaction will be discussed in the following section.

4. Processes used to produce value-added products from glycerol

The superiority of biodiesel over petroleum products with regard to health and environmental concerns (i.e., no sulfur content; low harmful emission of particulate matter, HC, CO, etc.; and better CO₂ lifecycle for global warming alleviation), as well as to engine performance, has encouraged Asian countries to use biodiesel as an alternative fuel source and as an innovative solution to curb the air pollution caused by the growing number of vehicles in the population. In recent years, the availability of glycerol has significantly increased because of the immense growth in biodiesel production [63], with glycerol formation equivalent to 10 wt% of the total biodiesel produced [76]. This development has resulted in a glycerol surplus, which has considerably affected the glycerol market and caused extreme decrease in glycerol prices [77]. The conversion of surplus glycerol to value-added chemicals is important [78,79]. To tackle excess glycerol obtained from vegetable oil transesterification and to build on the green credentials of the compound, a new, innovative, and greener catalytic process that can transform glycerol into high-value products is required [79].

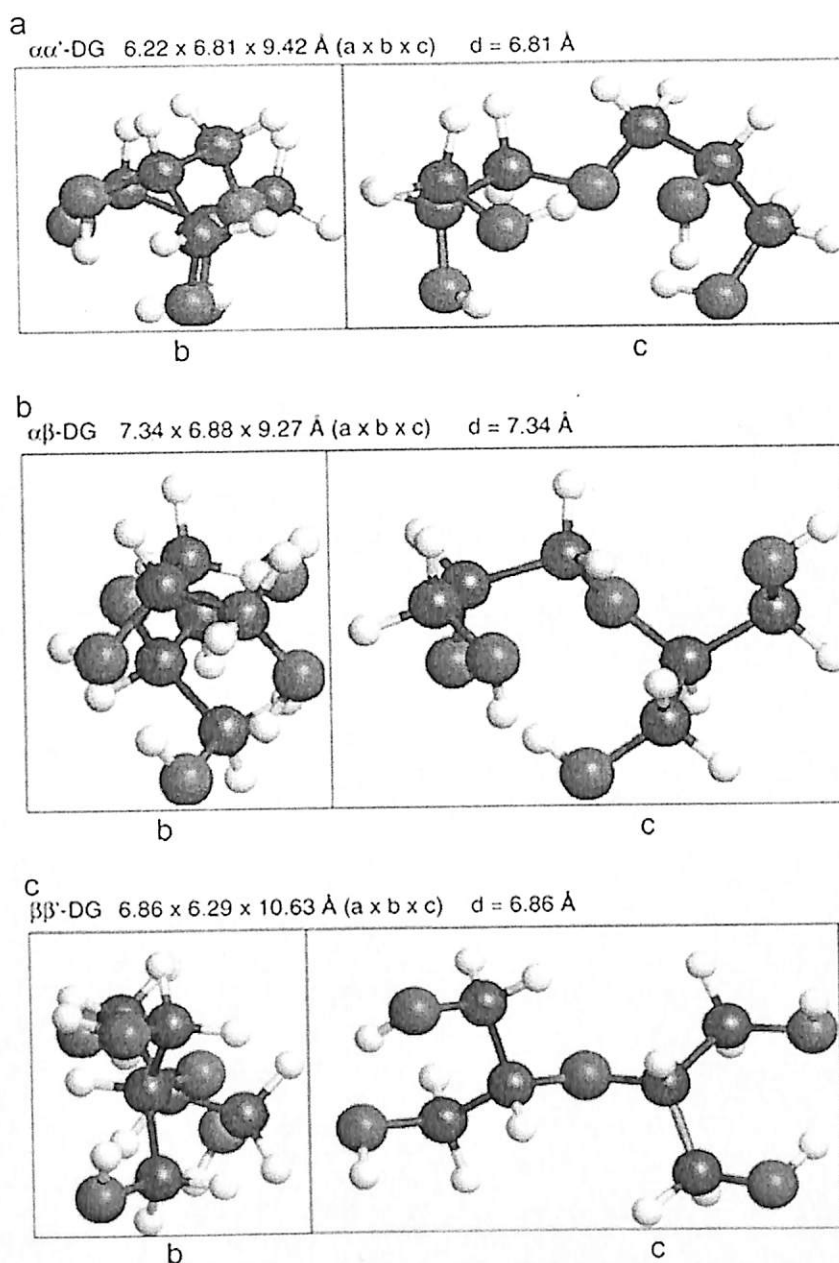


Fig. 8. Spatial properties of the three constitutional diglycerol isomers ($\alpha\alpha'$, $\alpha\beta$, $\beta\beta'$) [69].

Investigating processes with glycerol as a raw material necessitates knowledge on fundamental industrial processes, such as oxidation, hydrogenation, hydrolysis, chlorination, etherification and esterification [80–85]. Most of the products manufactured from glycerol are based on unmodified glycerol or modified glycerol molecules when the production of more complex chemical compounds has become too costly. However, with abundant glycerol in the commodity market, this compound could potentially be used in manufacturing polymers, ethers, and other fine chemicals.

One of the possibilities for converting glycerol into a value-added product is its conversion to acrolein, which is used in many fine chemical products. Catalytic dehydration of glycerol offers an alternative route to the production of acrolein. The said glycerol derivative is a versatile intermediate used in the synthesis of pharmaceuticals, detergents, and polymers [86]. Polyglycerol is a useful derivative of glycerol, which is extensively employed in

controlled drug release and cosmetics. This derivative comprises several units of glycerol that form a branched ether structure with terminal hydroxyl groups [87,88]. The multifunctional structure and properties of glycerol allows it to be easily converted into various products through different reaction pathways. This process was comprehensively reviewed recently [18,84,85].

To utilize excess glycerol produced from biodiesel production, industries are developing innovative methods that can use glycerol as a building block for the production of value added chemicals. The use of glycerol provides a promising possibility of being independent from fossil fuels. However, reports show the cost competitiveness between petroleum-derived products and products obtained from glycerol [84]. The balance can only be maintained when the cost price of glycerol is significantly lower than that of its petroleum-based counterparts. The unique structure of glycerol makes it possible to conduct a heterogeneous

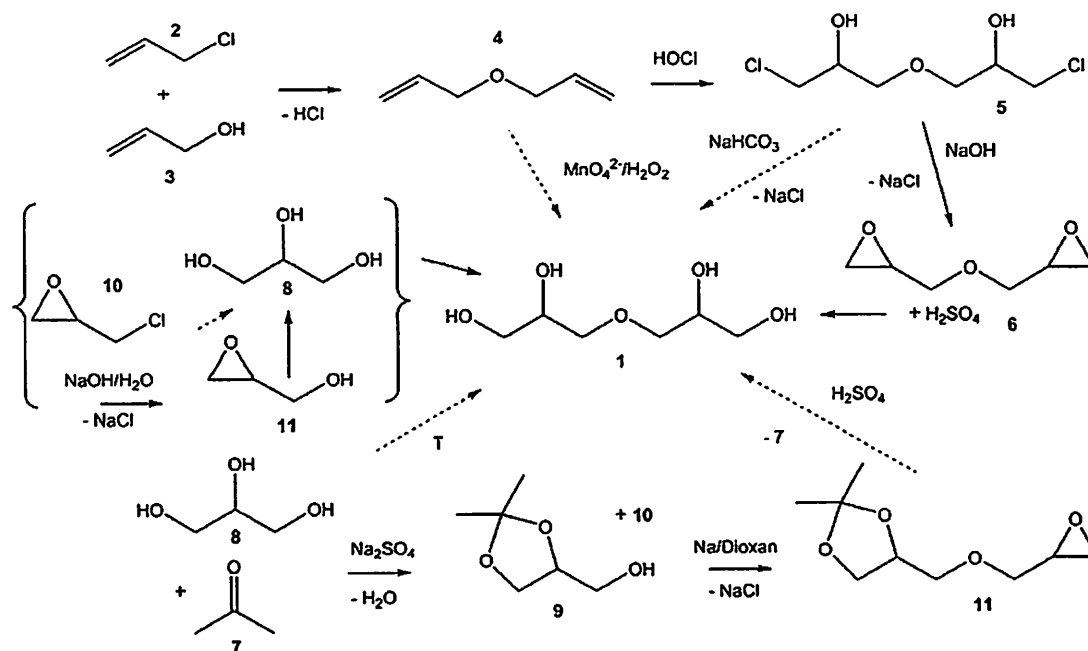


Fig. 9. Different synthesis routes of diglycerol [65].

catalytic oxidation reaction using a cheaper oxidizing agent such as air, oxygen, and hydrogen peroxide [89].

The catalytic transformation of glycerol into various chemicals by hydrogenolysis [80,90–93], polymerization [66,94], etherification [95–98], oxidation [99–101], dehydration [86,102,103], acetylation [84,104], and transesterification [105–107] has been reported. Of these processes, etherification is the most promising option because it can directly yield compounds that can be used as fuel additives [108]. Moreover, they can also be used as intermediates in the pharmaceutical industry, agrochemicals, and non-ionic surfactants [1].

Much research have been developed and continuously investigated to transform low-value glycerol using different strategies and approaches. To help make biodiesel plants more profitable, converting glycerol into chemical commodities of higher price and larger market is desirable. Generally, the conversion of glycerol can be broken down into two classes: (1) oxidation or reduction of glycerol into other three carbon compounds and (2) reaction of glycerol with other molecules to form new species. As the first step, a product with a sufficiently large market was chosen that can absorb the added glycerol to impose a higher price [109]. For a quick understanding of what that can be done to crude glycerol, its derivative products along with their corresponding methods/processes are summarized in Table 5. This listing may be helpful for biodiesel technocrats, giving them a choice for which compound they want to go for in place of crude glycerol.

Various heterogeneous catalysts have been employed in the etherification process [17,63,77,79,110–113]. Heterogeneous catalysts can be acidic or basic in nature. The use of acidic catalyst, in which the reaction products formed are cyclic polyglycerols, has several disadvantages. Deterioration of product quality will occur because of the secondary reactions produced, such as dehydration and oxidation of the intermediate product. Although the conversion of the reaction is relatively higher and faster, the selectivity remains low. Thus, the use of a basic rather than an acidic catalyst is preferred, as the product is more selective (avoids higher oligomers) and shows higher etherification activity. The basic catalysis of glycerol seems to be effective, as the product is more selective and possesses a high degree of conversion.

The etherification process proceeds through the stepwise reaction between the functional reactant groups. The size of polymer molecules increases at a relatively slow pace in such polymerization processes. One proceeds from monomer to dimer, trimer, tetramer, pentamer, and so on until, eventually, large-sized polymer molecules are formed. Step polymerization can be distinguished from chain polymerization by the reaction occurring between any of the different-sized species present in the reaction system [114].

The linkage of individual glycerol monomers in the etherification reaction will create one molecule of water as a side product. This reaction confers certain changes in the physical properties of glycerol, making it more viscous, causing color change from water clear to dark yellow, and affecting polarity. With increasing molecular weight, the hydroxyl number (diglycerol with 4 hydroxyls, triglycerol 5, tetraglycerol 6, etc.) decreases. This increase causes a change in the polarity of oligomers, that is, low oligomers are more hydrophilic than higher ones so that they have better solubility in polar solvents such as water. The viscosity increases with higher degree of oligomerization, often accompanied by a color change from water clear (glycerol) to dark yellow. Presumably, this coloration occurs due to dehydration side-reactions [66].

In etherification, glycerol can be converted into branched, oxygen-containing components through the reaction with either alcohols or alkenes. The reaction products could potentially be used as valuable fuel additives, such as *tert*-butyl ethers. Acidic homogenous catalysts and heterogeneous catalysts such as zeolites can be employed in this process. Karinen and Krause [115] reported that liquid-phase etherification of glycerol with isobutene in the presence of an acidic ion-exchange resin catalyst can yield up to five ether products, with side products in the form of C8 to C16 hydrocarbons.

4.1. Catalytic etherification

Glycerol etherification with or without organic solvents has been intensively studied using different homogeneous alkali catalysts such as hydroxides and carbonates. Recently, research

Table 5
Derivative products from glycerol along with their corresponding production methods.

Product name	Process method/nature	Reference
1,3-Propanediol	Selective hydroxylation technique involving three stages of acetalization, tosylation, and detosylation. Dehydroxylation of glycerol to 1,3-propanediol over a Pt/WO ₃ /ZrO ₂ catalyst Pt/WO ₃ /TiO ₂ /SiO ₂ catalyst in aqueous media. Batch and continuous microbial fermentations by <i>Clostridium butyricum</i> , <i>Citrobacter freundii</i> , <i>Klebsiella pneumoniae</i> . The cultures are specified by nutrient. Microbial and glycerol concentrations. The key parameters are temperature, time and pH.	[110], [90,111] [112] [113,114] [115] [113,116] [113,117]
Hydrogen	Steam reforming of glycerol in the gas with Group 8–10 metal catalysts. Catalytic steam reforming of glycerol using a commercial Ni-based catalyst. Calcined dolomite sorbent and calcium oxide sorbent, in a continuous flow fixed-bed reactor. Microbial fermentation of glycerol by <i>Enterobacter aerogenes</i> HU-101, in a continuous packed-bed reactor. Hydrogen production from glycerol using microbial electrolysis cells (MECs). Hydrogen production from steam-glycerol reforming, the results show that high temperature, low pressure, low feeding reactants to inert gas ratio and low gas flow rate are favorable for steam reforming of glycerol for hydrogen production. There is an optimal water to glycerol feed ratio for steam reforming of glycerol for hydrogen production which is about 9.0. Hydrogen production via glycerol steam reforming with CO ₂ . Production of renewable hydrogen from aqueous-phase reforming of glycerol over Pt-based catalysts supported on different oxides (Al ₂ O ₃ , ZrO ₂ , MgO and CeO ₂). Production of hydrogen from steam reforming of glycerol using nickel catalysts supported on Al ₂ O ₃ , CeO ₂ and ZrO ₂ . Production of hydrogen from steam reforming of glycerol using Pt-based catalysts supported on Al ₂ O ₃ , SiO ₂ , AC, MgO, HUSY, and SAPO-11. Aqueous-phase reforming of biomass-derived oxygenated hydrocarbons over a tin-promoted Raney-nickel catalyst.	[118] [119,120] [119] [121] [122] [123] [124,125] [126] [127] [128] [129] [130]
Succinic acid	Bacterial fermentation use of several promising succinic acid producers including <i>Actinobacillus succinogenes</i> , <i>Anaerobiospirillum succiniciproducens</i> , <i>Mannheimia succiniciproducens</i> and recombinant <i>Escherichia coli</i> .	[131]
1,2-Propanediol	Glycerol hydrogenolysis over the Ru/C catalyst using an ion-exchange resin. Dehydration–hydrogenation of glycerol at ambient hydrogen pressure over supported copper metal catalysts. Aqueous phase hydrogenolysis of glycerol catalyzed by an admixture of 5 wt% Ru/Al ₂ O ₃ and 5 wt% Pt/Al ₂ O ₃ catalysts, without external hydrogen addition. Hydrogenolysis of glycerol using bi-functional Co/MgO catalysts, where the solid MgO acts as the basic component and the support of cobalt nanoparticles. Low-pressure hydrogenolysis of glycerol to propylene glycol using nickel, palladium, platinum, copper, and copper-chromite catalysts. Selective hydrogenolysis with Raney nickel catalyst in an autoclave with hydrogen.	[132,133] [134] [135] [136] [137] [138]
Dihydroxyacetone (DHA)	Overexpression of glycerol dehydrogenase in an alcohol dehydrogenase-deficient (ADH-deficient) mutant of <i>Gluconobacter oxydans</i> . Bioconversion of glycerol with immobilized <i>Gluconobacter oxydans</i> cell in the air-lift reactor. Chemoselective catalytic oxidation with Air on platinum metals. Selective oxidation of glycerol with platinum-bismuth (BiPt) catalyst. Microbial fermentation of DHA by <i>Gluconobacter oxydans</i> in a semi-continuous two-stage repeated fed-batch process.	[131] [121] [51] [116] [116]
Polyesters	Reacting glycerol and aliphatic dicarboxylic acids of various length. Synthesis and characterization of elastic aliphatic polyesters from sebacic acid, glycol and glycerol through a two-step process. Reacting glycerol and adipic acid without any solvents in the presence of tin catalysts.	[131] [121] [111]
Polyglycerols	Etherification of glycerol over MgAl mixed oxides without solvent in a batch reactor Selective etherification of glycerol over impregnated basic MCM-41 type mesoporous catalysts.	[127] [1]
Polyhydroxyalkanoates (PHAs)	Submerged and solid-state fermentation processes using inexpensive carbon sources (from waste materials and by-products). Fermentation of hydrolyzed whey permeate and glycerol liquid phase using a highly osmophilic organism (production of polyhydroxyalkanoates from agricultural waste and surplus materials).	[121] [131]

attention has been shifted toward heterogeneous catalysts such as zeolites, mesoporous silica, and metal oxides [76,79,116].

Chemical reaction takes place on the active sites on the catalyst surface. For the reaction to occur, one or more reactants must diffuse to the catalyst surface and adsorb onto the surface. After the reaction, the products must desorb from the surface and diffuse from the solid surface. This transport of reactants and products from one phase to another frequently has a significant role in limiting the reaction rate.

To find the suitable catalysts for the etherification of polyhydroxy compounds, particularly of glycerol and ethylene glycol, optimization of reaction conditions and procedure has been a subject of several patents. Glycerol etherification by isobutylene established by Behr and Obenorf [117] and homogeneous and heterogeneous catalysts for glycerol etherification were studied. The commercial strong acid ion-exchange resin Amberlyst 15 have shown the best results among heterogeneous catalysts and the best homogeneous catalyst was p-toluenesulfonic acid. The change in concentration with the time at which the individual

components were reacted in the mixture was evaluated by the simplified kinetic model, considering only the main reactions that lead to ether formation.

Klepáčová et al. [118] discussed in detail the study of catalytic activity and selectivity of ion-exchange resins of Amberlyst type and large-pore zeolites on tert-butylation of glycerol with isobutylene and tert-butyl alcohol. Glycerol condensation (etherification) was studied in the presence of alkaline exchange zeolites and mesoporous basic catalysts. The selectivity of diglycerol increased when X zeolites were exchanged with cesium, whereas the selectivity of Cs-ZSM5 was comparable to that of Na₂CO₃. Over mesoporous M-La or M-Mn materials, the formation of triglycerol and tetraglycerol was more significant. Such results could be due to the changes in both pore size and basicity of the catalysts [61].

Glycerol etherification involves polyglycerols, which are oxygenated compounds used as surfactants, lubricants, cosmetics, and food preservatives. Polyglycerols have a low level of polymerization that can be obtained in linear, cyclic, and branched chains. However, research efforts have been focused on selective

production of di- and/or tri-glycerols. The selectivity of glycerol etherification is like pseudo-polymerization, where a mixture of lineal and cyclic polyglycerols is generally obtained, particularly in the presence of homogeneous catalysts, such as sodium, potassium and carbonate hydroxide [60]. Etherification selectivity in the first reaction step of acid catalysts was not controlled, and thus, resulted in a mixture of di- to hexa-glycerols (lineal or cyclic), polyglycerol esters, and acroleine as by-products. Nonetheless, selectivity in the first step could be slightly improved by modifying the pseudo-pore size in the mesoporous materials [1]. Likewise, Na_2CO_3 improved glycerol conversion, although low selectivities with regard to di- and tri-glycerols were obtained. Subsequently, alkaline exchange zeolites were studied, and selectivity was increased [60]. The incorporation of elements such as Al, Mg, and La on mesoporous catalytic structure modified only the activity, and selectivity was set to be almost constant. Clacens et al. [1] found that other methods of impregnation method produced materials that were more stable and selective than incorporation. Among the impregnated materials, La was most active but it had the worst selectivity. In contrast, a positive behavior was observed in Mg, which was highly selective.

Solid catalysts are good alternatives for homogeneous catalysts in the etherification of glycerol to produce polyglycerol because the former do not dissolve in the reactant mixture, thus eliminating the separation issues associated with the conventional homogeneous process. However, the removal of homogenous catalysts is technically difficult because this process produces a large amount of wastewater that needs to be treated via neutralization. In the near future, conventional homogeneous catalysts are expected to be replaced with solid catalysts due to economic and environmental reasons [119,120].

The advantages of heterogeneous catalysts include low cost, reusability, possibility of recovery after the reaction process, and easy separation from the reaction [121,122]. Moreover, heterogeneous catalysts can be designed to provide higher activity and selectivity, eliminate corrosion problems, and improve thermal stability; they have low diffusion resistance (for highly porous materials) and generally longer lifetime [123,124].

Conventional methods for polyglycerol synthesis remain difficult because this reaction requires drastic conditions, namely, high reaction temperature and caustic environment [60]. For example, the use of Na_2CO_3 as a homogeneous catalyst results in high conversion but quite low selectivity. Additionally, several steps that include filtration, purification, and neutralization are required to recover almost pure diglycerol [66]. This procedure produces large amounts of basic aqueous waste which are environmentally damaging [61]. Therefore, for this important catalytic process, heterogeneous catalysts that are highly active, selective, and stable must be identified. Although most research studies conducted in this field are patented, some are reported in open literature.

4.2. Acid catalyzed etherification of glycerol

The glycerol will convert to various products of glycerol ether. In these reactions, the reaction occurs very fast and conversion is usually high. Usually, within 2 h, approximately all glycerol can be converted to products [69]. The non-selective product is formed due to the high-reaction temperature that favors the dehydration of primary oligomer to produce higher oligomers. Homogeneous catalyst has a rapid reaction rate which causes fast depletion of glycerol while being used to create higher oligomers [69]. Moreover, the color of the ether product obtained from the acid-catalyzed etherification shows its quality. When the product deteriorated and secondary product such as cyclic glycerol created, a dark and cloudy color could be observed [65,69].

Acid catalytic etherification is upgraded by changing homogeneous with heterogeneous acid catalysts. The use of a reactant and a catalyst in different phases is very interesting. Utilization of modified zeolite beta, MCM-41 and Amberlyst 16 as catalysts in glycerol etherification studied has been reported recently [125]. By using zeolite beta at various Si/Al molar ratios different products formed such as linear diglycerol, cyclic diglycerol, cyclic triglycerol and higher oligomers.

Further investigation on the performance of the acid catalyst included the use of MCM-41 as a catalyst [126]. For this particular catalyst, the production of higher oligomers was successfully supported, thus representing better selectivity to diglycerol. However, the conversion of glycerol was still low for MCM-41. The structure and the better porous system that are offered by MCM-41 allowed glycerol to access the internal pores to undergo reaction. This porous structure of MCM-41 was responsible for the increase of diglycerol formation and the large porous structure in meso-size range allowed fast internal diffusion of reactants and products.

4.3. Base catalyzed etherification of glycerol

The role of bases as active sites in enhancing the etherification reaction and improvement of catalyst performance has been investigated and several series of homogeneous and heterogeneous basic catalysts have been identified in previous studies. Several bases have been examined as homogeneous catalysts for the conversion of glycerol to polyglycerols. Oxides such as ZnO, MgO, and CaO are less active in the aforementioned reaction due to solubility issues. Nevertheless, these reactions are often not sufficiently fast (in terms of glycerol conversion) or do not selectively produce DG apart from difficulties in filtration, neutralization, and product purification [61]. Aslan [127] reported that 96% glycerol conversion with a corresponding selectivity to DG of 24% was achieved using 2% Na_2CO_3 catalyst at 260 °C for 24 h. Alkaline metals impregnated into mesoporous catalysts were reported to achieve 80% conversion of glycerol with a selectivity to DG of no less than 40% at 260 °C and a long reaction period of 24 h [1]. In 2005, the use of zeolitic catalysts for glycerol etherification was attempted and it resulted in 80% glycerol conversion and less than 20% selectivity to DG at 260 °C [128]. Recently, glycerol etherification was performed using Mg Al mixed oxide catalyst at a lower reaction temperature of 220 °C. For this mixed oxide catalyst, a maximum conversion of 50% was recorded with a high selectivity to DG of approximately 90% after 24 h [129]. Evidently, different catalysts demonstrate different activities and capacities to produce the desired product.

Further theoretical studies of alkaline earth metals have been focused on the role of surface basicity and Lewis acidity of the catalyst. The catalytic behavior of metal oxide surfaces are often explained by the acid/base characteristics [130]. Generally, for acid/base characterizations of surface sites on oxides the adsorption of probe molecules, such as ammonia, pyridine and carbon dioxide is used, and these characterizations usually have been used to explain the catalytic behavior of oxide surfaces. The nature of acidic and basic sites on oxide surfaces can be described in Lewis and Brønsted terms. On metal oxides, coordinated unsaturated metal cations are generally considered as Lewis acid sites, whereas the oxygen anions are regarded as Lewis base sites [131,132]. The electron-deficient metal cations exhibit acidic, electron-acceptor characteristics, whereas the electron-rich oxygen anions exhibit basic, electron-donor characteristics [131].

Alkali-modified zeolites, MCM-41 silica materials and alkaline earth-based mesoporous solids were studied, and partial or complete collapse of the porous structure were observed for all these catalysts [133]. The structural collapse can be resolved through grafting

Table 6
Operating conditions of glycerol etherification process using different catalysts.

Catalyst	Glycerol conversion	Selectivity	Reaction conditions	Ref.
Cs impregnated MCM-41	80%	Diglycerol: 75% Triglycerol: 25%	Glycerol etherification is carried out at 260 °C in a batch reactor at atmospheric pressure under N ₂ in the presence of 2 wt% of catalyst.	[62]
La incorporated MCM-41	90%	Diglycerol: 40% Triglycerol: 23%		
Cs exchanged X zeolite	80%	Diglycerol: 65% Triglycerol: 20%		
CsZSM-5(Si/Me ratio: 1000)	13%	Diglycerol: 100% Triglycerol: 0%	Selective etherification of glycerol to polyglycerols over impregnated basic MCM-41 type mesoporous catalysts, homogeneous and modified zeolite catalysts. 8 h, 260 °C.	[1]
CsZSM-5 (Si/Me ratio: 1000)	12%	Diglycerol: 94% Triglycerol: 6%		
CsX (impregnated)	36%	Diglycerol: 88% Triglycerol: 12%		
CsX (exchanged)	51%	Diglycerol: 83% Triglycerol: 17%		
Heterogeneous (Cs ₂₅ Al(20))	80%	Diglycerol: 55% Triglycerol: 25%	Heterogeneous, 15 h, 260 °C.	
MgAl–Na	50%	Diglycerol: 85% Triglycerol: 15%	Etherification of glycerol to polyglycerols over MgAl mixed oxides, glycerol 15 g, catalyst weight 300 mg, 220 °C, 24 h.	[129]
Amberlyst 15	68%	Not indicate in figures	Investigation on etherification of glycerol and ethylene glycol with isobutylene using strong acid ion-exchange resins (Amberlyst 15 and 35) and two large-pore zeolites H-Y and H-Beta.	[134]
Amberlyst 35	71%		The highest glycerol conversion 88.7% was achieved over zeolite H-Y after 8 h. The highest amount of TTBG was observed over A 35. The most appropriate temperature for etherification of glycerol and ethylene glycol is 60 °C.	
Zeolite H-beta	65%			
Zeolite H-Y	88.7%			
Pr-SBA-15	90%	MTBG: 9% DTBG: 56% TTBG: 35%	Acid catalyzed, etherification of bio-glycerol over sulfonic mesostructured silicas, 75 °C, 4 h.	[135]
Ar-SBA-15	100%	MTBG: 5% DTBG: 54% TTBG: 41%		
Alkaline earth metal oxides MgO, CaO, SrO, BaO	60%	Diglycerol + triglycerol: 90%	Glycerol etherification is carried out at 220 °C, in the presence of 2 wt% of catalyst, 20 h.	[63]
Ca _{1.6} Al _{0.4} La _{0.6} O ₃	91%	Diglycerol: 53.2% Triglycerol: 37.8%	Glycerol etherification is carried out at 250 °C, in the presence of 2 wt% of catalyst, 8 h.	[136]
Montmorillonite K-10 modified with LiOH (Clay Li/MK-10)	98%	Diglycerol: 53%	Glycerol etherification is carried out at 240 °C, in the presence of 2 wt% of catalyst, 12 h.	[137]
Hydrotalcite	77.7%	Diglycerol: 76% Triglycerol: 25%	Glycerol etherification is carried out at 240 °C, in the presence of 2 wt% of catalyst, 16 h.	[138]

(impregnating) the mesoporous solids with certain promoters [66]. However, even with the successful increase of conversion (94% in 24 h), significant formation of acrolein observed.

In another study on mesoporous materials, Clacens et al. [1] analyzed the different techniques for addition of several alkaline earth elements to mesoporous MCM-41, which include incorporation, impregnation and exchange. The best compromise between activity, selectivity, and catalyst leaching was observed with cesium impregnated on pure mesoporous silica presented. High selectivity of 90% to [di- + triglycerol] was obtained at a conversion rate of 80% over such catalysts.

As shown in Table 6, the optimum amount of catalyst used in glycerol etherification is around 2 wt%, although some reports that used higher catalyst reached 4 wt% [133]. Therefore, an increase in the catalyst amount does not necessarily lead to a better production yield, whereas an optimum amount is more favorable for the reaction. Thus, in that study, the optimum amount of catalyst was determined and used in the reaction process to study the effect of other parameters on the reaction.

The use of a suitable solid catalyst in etherification reactions that can replace the rather cumbersome homogeneous processes has been a subject of interest [65]. Using various solid catalysts, potential green catalytic production routes have been reported, with or without solvent. However, the high selectivity of DG at higher levels of glycerol conversion remains a challenge. Compared with homogeneous processes, heterogeneously catalyzed processes have slower

reaction rates [134]. Therefore, to improve the low reaction rates the reaction conditions of heterogeneous catalysis must be enhanced by increasing the reaction temperature and the amount of catalyst used. Another challenge that has to be addressed in heterogeneous processes is the dissolution of the active species into the reaction medium, which results in the partial homogeneity of the process. This phenomenon increases the difficulty in product separation and results in lower product quality, thus limiting the reusability of the catalyst [63]. Furthermore, preparing new catalysts with large porous frameworks is a challenging task because of the difficulty in controlling the resulting pore sizes and structures. In addition, large-pore catalyst materials will enhance mass transfer to overcome diffusion resistance [134].

4.4. Metal oxides as catalysts in etherification of glycerol

Metal oxide catalysts [111] have been used for etherification. The use of an alkaline binary metal oxide catalyst will produce a large amount of linear polyglycerols. Barrault et al. [66] studied the catalytic behavior of zeolitic and mesoporous catalysts with alkaline metals in glycerol etherification. Additionally, glycerol etherification over mesoporous materials, such as MCM-41 impregnated with metals, was studied. Clacens et al. [61,62] used mesoporous catalysts (MCM-41 type) and a Cs-ZSM5 catalyst for glycerol etherification. They observed that an increase in glycerol conversion resulted in loss of selectivity, which subsequently lowered the selectivity to DG.

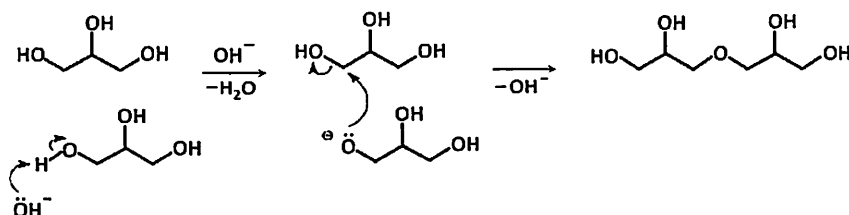


Fig. 10. Reaction scheme for the base-catalyzed glycerol etherification [63].

However, this increase in glycerol conversion increased the formation of triglycerol (TG). Ruppert et al. [63] investigated the use of CaO-based catalysts as heterogeneous catalysts in glycerol etherification to DG and TG. In addition, in the absence of a solvent, MgAl has been used in the formation of polyglycerols from glycerol [129].

Solid basic materials such as MgO, Al–Mg hydrotalcites, Cs-exchanged sepiolite, and mesoporous MCM-41 have been used as catalysts for glycerol transesterification with triglycerides. However, with MgO catalysts a glycerol/fat molar ratio of 12 at 240 °C was required to achieve a monoglyceride yield of 70% at a conversion rate of 97% [106,135]. Metal oxides such as MgO, CeO₂, La₂O₃, and ZnO have been used as solid base catalysts for the transesterification of glycerol with stoichiometric amounts of methyl stearate in the absence of solvent [88,121,136]. The catalysts were active, but the selectivity to mono-, di-, and triesters is similar to that obtained by homogeneous basic catalysts (40% monoester at 80% conversion).

Various microporous and mesoporous crystalline materials have been studied with and without different promoter elements [1,60,61,66]. Several modified zeolites and MCM-41-type mesoporous catalysts with different elements incorporated in their framework have also been investigated. Zeolites show severe limitations when involved large reactant molecules, especially in liquid-phase systems, which is frequently the case in the synthesis of fine chemicals. This observation is ascribed to the severe mass transfer limitations in the microporous solids. Microporous solids have a narrow and uniform micropore size distribution due to their crystallographically defined pore system. The reaction seems to have occurred mainly at the external surface of the catalyst; that is, the pore size of the modified zeolites was too small, which was one of the reasons behind the motivation in the preparation of basic mesoporous materials and the exchange or impregnation of basic elements. The impregnation method provides the most important activity, which is correlated with important active species incorporation. With regard to selectivity, mesoporous solids modified with cesium impregnation or exchanged with other substances lead to the best selectivity and yield to (di-+tri-) glycerol. The exchanged catalysts are most stable, and even if they are less stable, the impregnated catalysts can be reused without major modifications in their selectivity to the (di-+tri-) glycerol fraction.

With regard to microporous solids, Cs-exchanged X zeolites appeared to be active and selective catalysts, with glycerol conversion and (di- and tri-) glycerol selectivity of 79% and 95%, respectively, at a reaction temperature of 260 °C. By contrast, Cs-exchanged ZSM-5 materials proved to be less active. Using mesoporous MCM-41 catalysts loaded with Cs showed the most favorable results, which provided a (di- and tri-) glycerol selectivity of 97% at a conversion of 80% [61]. Clacens et al. [1] noted that the optimum results for catalyst leaching and stability were obtained using grafted solids that preserved their structure and specific area, properties which were not observed for their impregnated mesoporous catalysts. Finally, in the case of Mg- and La-containing mesoporous catalysts, the formation of acrolein due to the double dehydration as catalyzed by acid sites was found to

be significant. Thus, these catalysts were excluded as potential selective catalysts for the synthesis of di- and triglycerol [1,62].

Glycerol etherification reaction over alkaline earth metal oxides (BaO, SrO, CaO, and MgO) as promising heterogeneous catalysts with high activity has been studied. Previous studies have explored the catalytic potential of different CaO materials as examples of environmentally friendly and the most stable materials among the alkaline earth oxides [68]. By increasing glycerol conversion, the selective reaction that would yield the desired product should also be emphasized.

The additional criteria to be considered during the synthesis of heterogeneous catalysts include the availability of materials, ease of handling during preparation, affordability, thermal stability as measured by reusability, and regeneration. Moreover, developing and synthesizing heterogeneous catalysts that will bridge the gap created by the existing catalysts in terms of reusability are very important because they generate minimal leaching and are suitable for etherification reaction.

5. Mechanism of base-catalyzed etherification of glycerol

Oxidation and reduction occur at the same time during the etherification of glycerol, which includes the gain and loss of oxygen and hydrogen molecules between the hydroxyl group and glycerol. The mechanism of the etherification of glycerol using a basic catalyst has been studied by Ruppert et al. [63]. The mechanism includes two mechanistic schemes: deprotonation of the hydroxyl group and attack of the formed alkoxy anion on the carbon of the other glycerol molecule.

Surface properties, such as Lewis acidity, may perhaps have a role in the etherification of glycerol. As outlined in Fig. 10, it is difficult to explain the mechanism of a base-catalyzed etherification without the participation of the Lewis acid sites through the activation of a hydroxyl group as a leaving group [63]. Examples of such dual mechanism involving both basic and Lewis acid active sites have been reported for other heterogeneous catalytic reactions, for example, the destructive adsorption of chlorinated hydrocarbons on lanthanide oxide and oxide chloride materials [137,138].

In Fig. 10, when the basic condition provides adequate hydroxyl ions the reaction starts and one of hydroxyl groups in the glycerol molecule to be protonated. At that time, the protonated molecule of glycerol is ready to be combined with another molecule. Subsequently, the hydroxyl group of another molecule of glycerol is subjected to a nucleophilic attack of the protonated glycerol molecule. The formation of a water molecule after the attack properly recommends that the etherification reaction is a condensation reaction. Diglycerol molecule produces by the attack which combines two glycerol molecules into one longer molecule. Type of dimer produced is determined by the attachment point of one glycerol to another based on the positions of the primary and secondary hydroxyl groups.

6. Conclusions

Glycerol formation is equivalent to 10 wt% of the total biodiesel produced. Crude glycerol from biodiesel plant has low commercial value due to the presence of impurities of between 20% and 40%. In order to upgrade this low value product to the commercial grade, it should be purified through the costly refining process. Possible alternative technologies for the conversion of glycerol to value-added products are a subject of interest. Production of polyglycerols from glycerol provides interesting solutions to the problem as well as providing opportunities. Polyglycerols and their derivatives have vast applications in food, pharmaceutical and cosmetics industries. The most important product is diglycerol. Nature of the process, technical requirements and process behaviors of selective production of diglycerol and high oligomers through acid and base catalyzed processes are discussed in detail. Performance of different catalysts is reviewed and compared. Catalysts reported generally show diglycerol and triglycerol selectivities in the range of 50–80% and 20–40%, respectively at conversions values above 70%. An attempt to elucidate the reaction mechanism involved is also made. The mechanism is based on two mechanistic schemes i.e. deprotonation of the hydroxyl group and attack of the formed alkoxy anion on the carbon of the other glycerol molecule. The role of Lewis acid is also discussed in detail.

Acknowledgment

Research University grants (814144 and 814181) to support our oleochemical research works are gratefully acknowledged.

References

- [1] Clacens JM, Pouilloux Y, Barrault J. Selective etherification of glycerol to polyglycerols over impregnated basic MCM-41 type mesoporous catalysts. *Appl Catal A Gen* 2002;227:181–90.
- [2] Liu X, Ma H, Wu Y, Wang C, Yang M, Yan P, et al. Esterification of glycerol with acetic acid using double SO₃H-functionalized ionic liquids as recoverable catalysts. *Green Chem* 2011;13:697–701.
- [3] Koutinas AA, Wang R-H, Webb C. The biochemurgist-bioconversion of agricultural raw materials for chemical production. *Biofuels Bioprod Biorefin* 2007;1:24–38.
- [4] Gerpen JV. Biodiesel processing and production. *Fuel Process Technol* 2005;86:1097–107.
- [5] Haas MJ, McAloon AJ, Yee WC, Foglia TA. A process model to estimate biodiesel production costs. *Bioresour Technol* 2006;97:671–8.
- [6] Ito T, Nakashimada Y, Senba K, Matsui T, Nishio N. Hydrogen and ethanol production from glycerol-containing wastes discharged after biodiesel manufacturing process. *J Biosci Bioeng* 2005;100:260–5.
- [7] Dharmadi Y, Murarka A, Gonzalez R. Anaerobic fermentation of glycerol by *Escherichia coli*: a new platform for metabolic engineering. *Biotechnol Bioeng* 2006;94:821–9.
- [8] Shams-Yazdani S, Gonzalez R. Engineering *Escherichia coli* for the efficient conversion of glycerol to ethanol and co-products. *Metab Eng* 2008;10:340–51.
- [9] da Silva CJ, Mack M, Contiero J. Glycerol: a promising and abundant carbon source for industrial microbiology. *Biotechnol Adv* 2009;27:30–9.
- [10] You YD, Shie JL, Chang CY, Huang SH, Pai CY, Yu YH, et al. Economic cost analysis of biodiesel production: case in soybean oil. *Energy Fuels* 2007;22:182–9.
- [11] You Y-D, Shie J-L, Chang C-Y, Huang S-H, Pai C-Y, Yu Y-H, et al. Economic cost analysis of biodiesel production: case in soybean oil. *Energy Fuels* 2007;22:182–9.
- [12] Hazimah AH, Ooi TL, Salmiah A. Recovery of glycerol and diglycerol from glycerol pitch. *J Oil Palm Res* 2003;15:1–5.
- [13] Ayoub M, Abdullah AZ. LiOH-modified montmorillonite K-10as catalyst for selective glycerol etherification to diglycerol. *Catal Commun* 2013;34:22–5.
- [14] Bogaart V. Glycerin market brief. In: *Proceedings of the 7th ICIS world oleochemicals conference. Germany; 2009*.
- [15] Ott L, Bieker M, Vogel H. Catalytic dehydration of glycerol in sub- and supercritical water: a new chemical process for acrolein production. *Green Chem* 2006;8:214–20.
- [16] Pagliaro M, Rossi M. The future of glycerol: new uses of a versatile raw material. Cambridge: Royal Society of Chemistry; 2008.
- [17] Rahmat N, Abdullah AZ, Mohamed AR. Recent progress on innovative and potential technologies for glycerol transformation into fuel additives: a critical review. *Renew Sustain Energy Rev* 2010;14:987–1000.
- [18] Zhou C-H, Beltramini JN, Fan Y-X, Lu G-Q. Chemoselective catalytic conversion of glycerol as a biorenewable source to valuable commodity chemicals. *Chem Soc Rev* 2008;37:527–49.
- [19] Wang L, Du W, Liu D, Li L, Dai N. Lipase-catalyzed biodiesel production from soybean oil deodorizer distillate with absorbent present in tert-butanol system. *J Mol Catal B Enzym* 2006;43:29–32.
- [20] Fan X, Burton R, Zhou Y. Glycerol (by-product of biodiesel production) as a source for fuels and chemicals – mini review. *Open Fuels Energy Sci* 2010;3:17–22.
- [21] (<http://www.eia.gov>, International Energy Outlook: 2013 [accessed December 2013]).
- [22] Rywińska A, Rymowicz W. High-yield production of citric acid by *Yarrowia lipolytica* on glycerol in repeated-batch bioreactors. *J Ind Microbiol Biotechnol* 2010;37:431–5.
- [23] Papanikolaou S, Fakas S, Firk M, Chevalot I, Galiotou-Panayotou M, Konaitis M, et al. Biotechnological valorisation of raw glycerol discharged after bio-diesel (fatty acid methyl esters) manufacturing process: production of 1,3-propanediol, citric acid and single cell oil. *Biomass Bioenergy* 2008;32:60–71.
- [24] Yazdani SS, Gonzalez R. Anaerobic fermentation of glycerol: a path to economic viability for the biofuels industry. *Curr Opin Biotechnol* 2007;18:213–9.
- [25] Miller-Klien Associates. Impact of biodiesel production on the glycerol market. http://publications.hgca.com/publications/documents/Impact_of_Biodiesel_Production_on_the_Glycerol_Market.pdf [accessed on 10 May 2014].
- [26] Guzman DD, Taylor J, Seng S. Oleochemicals bounce back. *ICIS Chem Bus* 2011;279:28–30.
- [27] Lin Y-C. Catalytic valorization of glycerol to hydrogen and syngas. *Int J Hydrog Energy* 2013;38:2678–700.
- [28] (<http://www.icis.com/chemicals/glycerine/>, Pricing 1. Glycerine. 2012 [accessed September 2013]).
- [29] Haas M. The interplay between feedstock quality and esterification technology in biodiesel production. *Lipid Technol* 2004;16:7–10.
- [30] Chiu CW, Dasari MA, Sutterlin WR, Suppes GJ. Removal of residual catalyst from simulated biodiesel's crude glycerol for glycerol hydrogenolysis to propylene glycol. *Ind Eng Chem Res* 2005;45:791–5.
- [31] Mu Y, Teng H, Zhang DJ, Wang W, Xiu ZL. Microbial production of 1,3-propanediol by *Klebsiella pneumoniae* using crude glycerol from biodiesel preparations. *Biotechnol Lett* 2006;28:1755–9.
- [32] Woo C. Clean fuel trends in Asia: contribution of MTBE. *Hydrocarb Process* 2007;86:85–8.
- [33] Fan X, Burton R. Recent development of biodiesel feedstocks and the applications of glycerol: a review. *Open Fuels Energy Sci J* 2009;2:100–9.
- [34] Khanal SK, Rasmussen M, Shrestha P, Van Leeuwen HJ, Visvanathan C, Liu H. Bioenergy and biofuel production from wastes/residues of emerging biofuel industries. *Water Environ Res* 2008;80:1625–47.
- [35] Rausch KD, Relyea RL. The future of coproducts from corn processing. *Appl Biochem Biotechnol* 2006;128:47–86.
- [36] Clomburg JM, Gonzalez R. Anaerobic fermentation of glycerol: a platform for renewable fuels and chemicals. *Trends Biotechnol* 2013;31:20–8.
- [37] Tsobanakis P. Glycerin – new applications & markets. *Biofuels and feed stocks*. 2007.
- [38] Brady S, Tam K, Leung G, Salam C. Zero waste biodiesel: using glycerin and biomass to create renewable energy. *UCR Undergrad Res J* 2008;2:5–11.
- [39] Mannazzu I, Budroni M, Zara S, Zara G, Ciani M, Comitini F. Utilization of raw glycerol from biodiesel industry for the production of yeast biomass and secondary metabolites. *J Biotechnol* 2010;150(Supplement):S323.
- [40] Baba Y, Tada C, Watanabe R, Fukuda Y, Chida N, Nakai Y. Anaerobic digestion of crude glycerol from biodiesel manufacturing using a large-scale pilot plant: methane production and application of digested sludge as fertilizer. *Bioresour Technol* 2013;82:232–40.
- [41] Vlysidis A, Binns M, Webb C, Theodoropoulos C. Glycerol utilisation for the production of chemicals: conversion to succinic acid, a combined experimental and computational study. *Biochem Eng J* 2011;58–59:1–11.
- [42] Gupta M, Kumar N. Scope and opportunities of using glycerol as an energy source. *Renew Sustain Energy Rev* 2012;16:4551–6.
- [43] Leoneti AB, Aragão-Leoneti V, de Oliveira SVWB. Glycerol as a by-product of biodiesel production in Brazil: alternatives for the use of unrefined glycerol. *Renew Energy* 2012;45:135–45.
- [44] Medeiros MA, Leite CMM, Lago RM. Use of glycerol by-product of biodiesel to produce an efficient dust suppressant. *Chem Eng J* 2012;180:364–9.
- [45] Zhang Z, Xin L, Li W. Electrocatalytic oxidation of glycerol on Pt/C in anion-exchange membrane fuel cell: cogeneration of electricity and valuable chemicals. *Appl Catal B Environ* 2012;119–120:40–8.
- [46] Hernández D, Fernández JJ, Mondragón F, López D. Production and utilization performance of a glycerol derived additive for diesel engines. *Fuel* 2012;92:130–6.
- [47] Bohon MD, Metzger BA, Linak WP, King CJ, Roberts WL. Glycerol combustion and emissions. In: *Proceedings of the combustion institute, vol. 33; 2011*. p. 2717–24.
- [48] Pachauri N, He B. Value added utilization of crude glycerol from biodiesel production: a survey of current research activities. In: *Proceedings of the ASABE Annual International Meeting, Portland, Oregon: 9–12 July, American*

- society of agricultural and biological engineers (ASABE), St. Joseph, Missouri, USA; 2006.
- [49] Gunstone F, Heming M. Glycerol – an important product of the oleochemical industry. *Lipid Technol* 2004;16:177–9.
- [50] Hájek M, Škopál F. Treatment of glycerol phase formed by biodiesel production. *Bioresour Technol* 2010;101:3242–5.
- [51] Garcia R, Besson M, Gallezot P. Chemoselective catalytic oxidation of glycerol with air on platinum metals. *Appl Catal A Gen* 1995;127:165–76.
- [52] Bühler W, Dinjus E, Ederer HJ, Kruse A, Mas C. Ionic reactions and pyrolysis of glycerol as competing reaction pathways in near- and supercritical water. *J Supercrit Fluids* 2002;22:37–53.
- [53] Cortright RD, Davda RR, Dumesic JA. Hydrogen from catalytic reforming of biomass-derived hydrocarbons in liquid water. *Nature* 2002;418:964–7.
- [54] Guerrero-Pérez MO, Rosas J M, Bedia J, Rodriguez-Mirasol J, Cordero F. Recent inventions in glycerol transformations and processing. *Recent Pat Chem Eng* 2009;2:11–21.
- [55] Jagadeeswarajah K, Balaraju M, Prasad PSS, Lingaiah N. Selective esterification of glycerol to bioadditives over heteropoly tungstate supported on Cs-containing zirconia catalysts. *Appl Catal A Gen* 2010;386:166–70.
- [56] Khanna S, Goyal A, Moholkar VS. Microbial conversion of glycerol: present status and future prospects. *Crit Rev Biotechnol* 2012;32:235–62.
- [57] Oudshoorn MHM, Rössmann R, Bouwstra JA, Hennink WE. Synthesis and characterization of hyperbranched polyglycerol hydrogels. *Biomaterials* 2006;27:5471–9.
- [58] Sunder A, Mülhaupt R, Haag R, Frey H. Hyperbranched polyether polyols: a modular approach to complex polymer architectures. *Advanc Mater* 2000;12:235–9.
- [59] Frey H, Haag R. Dendritic polyglycerol: a new versatile biocompatible material. *Rev Mol Biotechnol* 2002;90:257–67.
- [60] Barrault J, Pouilloux Y, Clacens JM, Vanhove C, Bancquart S. Catalysis and fine chemistry. *Catal Today* 2002;75:177–81.
- [61] Clacens JM, Pouilloux Y, Barrault J, Linares C, Goldwasser M. Mesoporous basic catalysts: comparison with alkaline exchange zeolites (basicity and porosity). Application to the selective etherification of glycerol to polyglycerols. *Stud Surf Sci Catal* 1998;118:895–902.
- [62] Clacens JM, Pouilloux Y, Barrault J. Synthesis and modification of basic mesoporous materials for the selective etherification of glycerol. *Stud Surf Sci Catal* 2000;143:687–95.
- [63] Ruppert AM, Meeldijk JD, Kuipers BWM, Erné BH, Weckhuysen BM. Glycerol etherification over highly active CaO-based materials: new mechanistic aspects and related colloidal particle formation. *Chem – Eur J* 2008;14:2016–24.
- [64] Richter M, Krisnandi YK, Eckelt R, Martin A. Homogeneously catalyzed batch reactor glycerol etherification by CSHCO_3 . *Catal Commun* 2008;9:2112–6.
- [65] Martin A, Richter M. Oligomerization of glycerol – a critical review. *Eur J Lipid Sci Technol* 2011;113:100–17.
- [66] Barrault J, Clacens JM, Pouilloux Y. Selective oligomerization of glycerol over mesoporous catalysts. *Top Catal* 2004;27:137–42.
- [67] Solvay CL. Polyglycerols-general overview 2008. Solvay Chemicals International SA, Belgium.
- [68] Granados ML, Poves MDZ, Alonso DM, Mariscal R, Galisteo FC, Moreno-Tost R, et al. Biodiesel from sunflower oil by using activated calcium oxide. *Appl Catal B Environ* 2007;73:317–26.
- [69] Medeiros MA, Araújo MH, Augusti R, LCAO Oliveira, Lago RM. Acid-catalyzed oligomerization of glycerol investigated by electrospray ionization mass spectrometry. *J Braz Chem Soc* 2009;20:1667–73.
- [70] Nek Mat Din NSNM, Abu Bakar Z, Seng Soi H, Idris Z, Kian YS. Glycerol to polyglycerol: value-addition of biodiesel by-product. *MPOB Inf Ser* 2010;462:1–4.
- [71] Dallas TMRCAcF. Food Emulsifiers Market worth \$2858.6 Million by 2018; 2012.
- [72] Wittcoff H, Roach JR, Miller SE. Polyglycerols I. The identification of polyglycerol mixtures by the procedures of allylation and acetonation: isolation of pure diglycerol. *J Am Chem Soc* 1947;69:2655–7.
- [73] Wittcoff H, Roach JR, Miller SE. Polyglycerols II. Syntheses of diglycerol. *J Am Chem Soc* 1949;71:2666–8.
- [74] Gauri N, Aserin A, Zaidman B. Polyglycerol esters: optimization and techno-economic evaluation. *J Am Chem Soc* 1981;58:878–83.
- [75] Jakobson G. Diglycerin und höhere Oligomere des Glycerins als Synthesebausteine. *Fette Seifen Anstrichm* 1986;88:101–6.
- [76] Khayoon MS, Hameed BH. Synthesis of hybrid SBA-15 functionalized with molybdophosphoric acid as efficient catalyst for glycerol esterification to fuel additives. *Appl Catal A Gen* 2012;433–434:152–61.
- [77] Melero JA, Vicente G, Paniagua M, Morales G, Muñoz P. Etherification of biodiesel derived glycerol with ethanol for fuel formulation over sulfonic modified catalysts. *Bioresour Technol* 2012;103:142–51.
- [78] Zheng Y-F, Lin J-D, Li C-P, Li J-H. Friedel-Crafts allylation of 2-(benzyloxy)-3,4,5-trimethoxytoluene catalyzed by a metal trifluoromethanesulfonic salt: synthesis of coenzyme Q10. *J Chem Res* 2007;686–8.
- [79] Shi Y, Dayoub W, Chen G-R, Lemaire M. Selective synthesis of 1-n-alkyl glycerol and diglycerol ethers by reductive alkylation of alcohols. *Green Chem* 2010;12:2189–95.
- [80] Behr A, Eiling J, Irawadi K, Leschinski J, Lueder F. Improved utilisation of renewable resources: new important derivatives of glycerol. *Green Chem* 2008;10:13–30.
- [81] Behr A, Johnen L. Alternative feedstocks for synthesis. *Handbook of Green Chemistry*. Wiley VCH Verlag GmbH & Co. KGaA; 2010.
- [82] Zhao H, Zhou CH, Wu LM, Lou JY, Li N, Yang HM, et al. Catalytic dehydration of glycerol to acrolein over sulfonic acid activated montmorillonite catalysts. *Appl Clay Sci* 2012;74:154–62.
- [83] Gallezot P. Conversion of biomass to selected chemical products. *Chem Soc Rev* 2012;41:1538–58.
- [84] Zhou L, Nguyen T-H, Adesina AA. The acetylation of glycerol over Amberlyst-15: Kinetic and product distribution. *Fuel Process Technol* 2012;104:310–8.
- [85] Zhou L, Al-Zaini E, Adesina AA. Catalytic characteristics and parameters optimization of the glycerol acetylation over solid acid catalysts. *Fuel* 2013;103:617–25.
- [86] Corma A, Huber GW, Sauvinaud L, O'Connor P. Biomass to chemicals: catalytic conversion of glycerol/water mixtures into acrolein, reaction network. *J Catal* 2008;257:163–71.
- [87] Sunder A, Hanselmann R, Frey H, Mülhaupt R. Controlled synthesis of hyperbranched polyglycerols by ring-opening multibranching polymerization. *Macromolecules* 1999;32:4240–6.
- [88] Márquez Álvarez C, Pérez Pariente J, Sastre de Andrés E. Solid catalysts for the synthesis of fatty esters of glycerol, polyglycerols and sorbitol from renewable resources. *Top Catal* 2004;27:105–17.
- [89] Zakaria ZY, Amin NAS, Linnekoski J. A perspective on catalytic conversion of glycerol to olefins. *Biomass Bioenergy* 2013;55:370–85.
- [90] Kurosaka I, Maruyama H, Naribayashi I, Sasaki Y. Production of 1,3-propanediol by hydrogenolysis of glycerol catalyzed by $\text{Pt}/\text{WO}_3/\text{ZrO}_2$. *Catal Commun* 2008;9:1360–3.
- [91] Huang Z, Cui F, Kang H, Chen J, Xia C. Characterization and catalytic properties of the CuO/SiO_2 catalysts prepared by precipitation-gel method in the hydrogenolysis of glycerol to 1,2-propanediol: effect of residual sodium. *Appl Catal A Gen* 2009;366:288–98.
- [92] Dam JT, Kapteijn F, Djanashvili K, Hancfeld U. Tuning selectivity of Pt/CaCO_3 in glycerol hydrogenolysis – a design of experiments approach. *Catal Commun* 2011;13:1–5.
- [93] Kwak BK, Park DS, Yun YS, Yi J. Preparation and characterization of nanocrystalline CuAl_2O_4 spinel catalysts by sol-gel method for the hydrogenolysis of glycerol. *Catal Commun* 2012;24:90–5.
- [94] Martin A, Checinski MP, Richter M. Tuning of diglycerol yield and isomer distribution in oligomerization of glycerol supported by DFT-calculations. *Catal Commun* 2012;25:130–5.
- [95] Frusteri F, Arena F, Bonura G, Cannilla C, Spadaro L, Di Blasi O. Catalytic etherification of glycerol by tert-butyl alcohol to produce oxygenated additives for diesel fuel. *Appl Catal A Gen* 2009;367:77–83.
- [96] Chang J-S, Chen D-H. Optimization of the etherification of glycerol with tert-butyl alcohol. *J Taiwan Inst Chem Eng* 2011;42:760–7.
- [97] Frusteri F, Frusteri I, Cannilla C, Bonura G. Catalytic etherification of glycerol to produce biofuels over novel spherical silica supported Hyllon[®] catalysts. *Bioresour Technol* 2012;118:350–8.
- [98] Viswanadham N, Saxena SK. Etherification of glycerol for improved production of oxygenates. *Fuel* 2013;103:980–6.
- [99] Liang D, Gao J, Sun H, Chen P, Hou Z, Zheng X. Selective oxidation of glycerol with oxygen in a base-free aqueous solution over MWNTs supported Pt catalysts. *Appl Catal B Environ* 2011;106:423–32.
- [100] Ketchic WC, Murayama M, Davis RJ. Selective oxidation of glycerol over carbon-supported AuPd catalysts. *J Catal* 2007;250:264–73.
- [101] Liang D, Gao J, Wang J, Chen P, Hou Z, Zheng X. Selective oxidation of glycerol in a base-free aqueous solution over different sized Pt catalysts. *Catal Commun* 2009;10:1586–90.
- [102] Kim YT, Jung K-D, Park ED. Gas-phase dehydration of glycerol over ZSM-5 catalysts. *Microporous Mesoporous Mater* 2010;131:29–36.
- [103] Lourenço JP, Macedo MI, Fernandes A. Sulfonic-functionalized SBA-15 as an active catalyst for the gas-phase dehydration of glycerol. *Catal Commun* 2012;19:105–9.
- [104] Balaraju M, Nikhitha P, Jagadeeswarajah K, Sripathi K, Sai Prasad PS, Lingaiah N. Acetylation of glycerol to synthesize bioadditives over niobic acid supported tungstophosphoric acid catalysts. *Fuel Process Technol* 2010;91:249–53.
- [105] Li J, Wang T. Coupling reaction and azeotropic distillation for the synthesis of glycerol carbonate from glycerol and dimethyl carbonate. *Chem Eng Process Intensif* 2010;49:530–5.
- [106] Álvarez MC, Chimentão RJ, Figueras F, Medina F. Tunable basic and textural properties of hydrotalcite derived materials for transesterification of glycerol. *Appl Clay Sci* 2012;58:16–24.
- [107] Gonçalves CE, Laier LO, Cardoso AL, da Silva MJ. Broadly additive synthesis from H3PW12O40-catalyzed glycerol esterification with HOAc under mild reaction conditions. *Fuel Process Technol* 2012;102:46–52.
- [108] Olutoye MA, Hameed BH. $\text{K}_2\text{Mg}_2\text{Zr}_2\text{O}_{10}$ as a heterogeneous catalyst in the transesterification of palm oil to fatty acid methyl esters. *Appl Catal A Gen* 2009;371:191–8.
- [109] Johnson DT, Tacomi KA. The glycerol glut: options for the value-added conversion of crude glycerol resulting from biodiesel production. *Environ Prog* 2007;26:338–48.
- [110] Klepáčová K, Mravec D, Bajus M. Etherification of glycerol with tert-butyl alcohol catalyzed by ion-exchange resins. *Chem Pap* 2006;60:224–30.
- [111] Pariente S, Tanchoux N, Hájala F. Etherification of glycerol with ethanol over solid acid catalysts. *Green Chem* 2009;11:1256–61.
- [112] Silva CRBd, Gonçalves VLC, Lachter FR, Mota CJA. Etherification of glycerol with benzyl alcohol catalyzed by solid acids. *J Brazil Chem Soc* 2009;20:201–4.

- [113] Gaudin P, Jacquot R, Marion P, Pouilloux Y, Jérôme F. Acid-catalyzed etherification of glycerol with long-alkyl-chain alcohols. *ChemSusChem* 2011;4:719–22.
- [114] Odian G. Principles of polymerization, fourth ed.. New York, USA: John Wiley & Sons, Inc.; 2004.
- [115] Karinen RS, Krause AOI. New biocomponents from glycerol. *Appl Catal A Gen* 2006;306:128–33.
- [116] Lee H-G, Hong J-M. Algebraic conditions for state equivalence to a discrete-time nonlinear observer canonical form. *Syst Control Lett* 2011;60:756–62.
- [117] Behr A, Obendorf L. Development of a process for the acid-catalyzed etherification of glycerin and isobutene forming glycerin tertiary butyl ethers. *Eng Life Sci* 2002;2:185–9.
- [118] Klepáčová K, Mravec D, Bajus M. tert-Butylation of glycerol catalyzed by ion-exchange resins. *Appl Catal A Gen* 2005;294:141–7.
- [119] Ono Y, Baba T. Selective reactions over solid base catalysts. *Catal Today* 1997;38:321–37.
- [120] Hattori H. Solid base catalysts: generation of basic sites and application to organic synthesis. *Appl Catal A Gen* 2001;222:247–59.
- [121] Corma A, Iborra S, Miquel S, Primo J. Catalysts for the production of fine chemicals: production of food emulsifiers, monoglycerides, by glycerolysis of fats with solid base catalysts. *J Catal* 1998;173:315–21.
- [122] Mat R, Samsudin RA, Mohamed M, Johari A. Solid catalysts and their application in biodiesel production. *Bull Chem React Eng Catal* 2012;7:142–9.
- [123] Helwani Z, Othman MR, Aziz N, Kim J, Fernando WJN. Solid heterogeneous catalysts for transesterification of triglycerides with methanol: a review. *Appl Catal A Gen* 2009;363:1–10.
- [124] Chopade SG, Kulkarni KS, Kulkarni AD, Topare NS. Solid heterogeneous catalysts for production of biodiesel from Trans-esterification of triglycerides with methanol: a review. *Acta Chim Pharm Indica* 2012;2:8–14.
- [125] Vladimir KD, Bullock RM. A recyclable catalyst that precipitates at the end of the reaction. *Nature* 2000;424:530–2.
- [126] Gallezot P. Selective oxidation with air on metal catalysts. *Catal Today* 1997;37:405–18.
- [127] Aslan N. Application of response surface methodology and central composite rotatable design for modeling and optimization of a multi-gravity separator for chromite concentration. *Powder Technol* 2008;185:80–6.
- [128] Hutchings GJ. Catalysis by gold. *Catal Today* 2005;100:55–61.
- [129] García-Sánchez C, Moreno-Tost R, Mérida-Robles JM, Santamaría-González J, Jiménez-López A, Torres PM. Etherification of glycerol to polyglycerols over MgAl mixed oxides. *Catal Today* 2011;167:84–90.
- [130] Conte RV. The best test preparation & review course: FE/EIT fundamentals of engineering/engineer-in-training: PM exam in mechanical engineering. Piscataway, N.J.: Research & Education Association; 1999.
- [131] Abro S, Pouilloux Y, Barrault J. Selective synthesis of monoglycerides from glycerol and oleic acid in the presence of solid catalysts. In: Blaser AB, Prins R, editors. *Studies in surface science and catalysis*. Amsterdam: Elsevier; 1997. p. 539–46.
- [132] Sakhivel A, Nakamura K, Komura K, Sugi Y. Esterification of glycerol by lauric acid over aluminium and zirconium containing mesoporous molecular sieves in supercritical carbon dioxide medium. *J Supercrit Fluids* 2007;42:219–25.
- [133] Sivaiah MV, Robles-Manuel S, Valange S, Barrault J. Recent developments in acid and base-catalyzed etherification of glycerol to polyglycerols. *Catal Today* 2012;198:305–13.
- [134] Tseng Y-H, Wang M-L. Kinetics and biphasic distribution of active intermediate of phase-transfer-catalytic etherification. *J Taiwan Inst Chem Eng* 2011;42:129–31.
- [135] National Research C. *Bulletin of the National Research Council. Bulletin of the National Research Council*; 1919.
- [136] Pyykkö P, Atsumi M. Molecular double-bond covalent radii for elements Li–E112. *Chemistry* 2009;15:12770–9.
- [137] van der Heijden AWAM, Bellière V, Alonso LE, Daturi M, Manoilova OV, Weckhuysen BM. Destructive adsorption of CCl₄ over lanthanum-based solids: linking activity to acid–base properties. *J Phys Chem B* 2005;109:3993–4001.
- [138] van der Heijden AWAM, Garcia RM, Weckhuysen BM. Intermediates in the destruction of chlorinated C1 hydrocarbons on La-based materials: mechanistic implications. *Chem – Eur J* 2007;13:9561–71.



Deoxygenation of fatty acid to produce diesel-like hydrocarbons: A review of process conditions, reaction kinetics and mechanism



Lilis Hermida^{a,b}, Ahmad Zuhairi Abdullah^{a,*}, Abdul Rahman Mohamed^a

^a School of Chemical Engineering, Universiti Sains Malaysia, 14300 Nibong Tebal, Penang, Malaysia

^b Department of Chemical Engineering, Universitas Lampung, Bandar Lampung 35145, Indonesia

ARTICLE INFO

Article history:

Received 1 June 2014

Received in revised form

3 September 2014

Accepted 28 October 2014

Keywords:

Deoxygenation

Renewable resource

Fatty acid

Diesel-like hydrocarbons

Operating conditions

ABSTRACT

Deoxygenation process of fatty acid as a renewable resource to produce diesel-like hydrocarbons is one of the alternatives to address drastic shortage of crude oil-based fuels in the near future. Catalytic deoxygenation process of fatty acid is getting attention from both academia and industry. Researchers have tried different techniques in the fatty acid deoxygenation to enhance the production of diesel-like hydrocarbons. This review paper elucidates the influence of main operating conditions towards achieving optimum yield and selectivity of desired products. The reaction pathways, the reaction kinetics as well as recent progress in deoxygenation of fatty acid for production of diesel-like hydrocarbons are also reviewed.

© 2014 Elsevier Ltd. All rights reserved.

Contents

1. Introduction	1223
2. Reaction pathways and kinetic models of deoxygenation of fatty acid to produce diesel-like hydrocarbons	1224
3. Factors influencing the deoxygenation process	1227
3.1. Supported metal catalyst type	1228
3.2. Feed types	1228
3.3. Reaction atmosphere	1228
3.4. Reaction temperature	1229
3.5. Catalyst amount	1229
3.6. Feed rate (residence time)	1230
3.7. Use of solvent	1230
4. Recent progress in deoxygenation of fatty acid	1230
5. Conclusions	1232
Acknowledgements	1232
References	1232

1. Introduction

Growth in road transportation sector is currently steering the demand for fuel oils. It has been predicted that the world demand for diesel fuel will grow faster than any other refined oil products toward 2035, as illustrated in Fig. 1 [1]. Diesel fuel demand is

predicted to grow from 26 million barrels per day in 2012 to around 36 million barrels per day by 2035. Meanwhile, the demand for gasoline will moderately increase from about 23 million barrels per day in 2012 to 27 million barrels per day by 2035. In the same period, slight increases in demand will occur for ethane/LPG, naphtha, bitumen, lubricants waxes still gas, coke, direct use of crude oil, etc. On the other hand, demand for residual fuel will globally decrease in the coming years [1].

Due to consumption of diesel fuel derived from diminishing conventional crude oil that will continue in the next decades,

* Corresponding author. Tel.: +604 599 6411; fax: +604 594 1013.

E-mail address: chzuhairi@usm.my (A.Z. Abdullah).

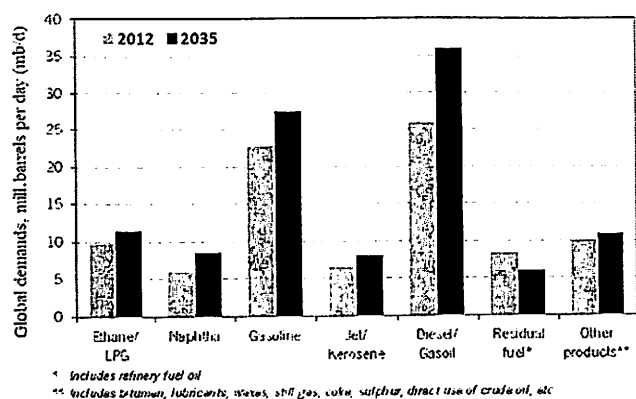


Fig. 1. Global demands for diesel fuel in 2012 and forecast in 2035 compared to other refined oil products [1].

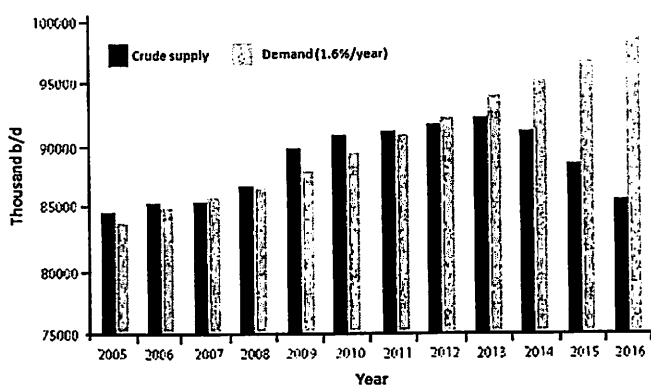


Fig. 2. Global crude oil supply and projected demand [2].

exhaustion of fossil fuels is predicted. Comparison between the most probable crude oil supply and the most likely demand requirements has been reported by the International Energy Agency (IEA) [2], as can be seen in Fig. 2. Conventional crude oil supply exceeded the demand from 2009 to 2011. However, in 2012 and 2013, the demand consistently exceeded supply. Then, from 2014 onwards, the conventional crude oil supply will be shortfall. Meanwhile, the demand will constantly increase due to rapid growth in human population.

Therefore, extensive studies on biofuels productions from various renewable feed stocks and related technologies have been carried out for many years [3–8]. Among others, fatty acids are renewable resources that can be produced in mass scale and used as feedstock for deoxygenation reactions to synthesize diesel-like hydrocarbons [9–14]. Diesel-like hydrocarbons contain *n*-alkanes and alkenes that are hydrocarbons similar to those found in diesel fuel obtained by refining crude oil in petroleum refineries [15]. Thus, this option provides interesting alternative to support future energy demand.

Fatty acids are found in plant oils/fats and animal oils/fats [16–21]. Besides of fatty acids, plant oils/fats and animal oils/fats contain triglycerides with the main constituent. Fatty acids are formed during enzymatic hydrolysis of triglyceride especially when the oils are kept in humid atmosphere [22–27]. Fatty acid can also be formed during purification of vegetable oils and fats [28–30]. It can be produced at a sufficiently high rate in many countries. For example, in the United States, tall oil fatty acid can be obtained by vacuum distillation of crude tall oil which is side stream from pulp and paper industry [31]. Tall oil fatty acid mainly consists of palmitic acid, oleic acid and linoleic acid. The total production of tall oil in the United States was 845,000 t in 2004 [32]. Meanwhile, Malaysia and Indonesia, as the world's top-two

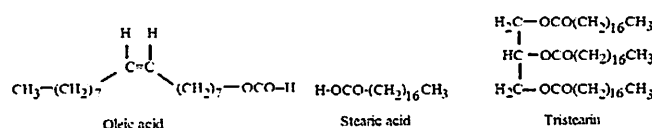


Fig. 3. Molecular structures of stearic acid, oleic acid and tristearin.

largest crude palm oil (CPO) producers, produce palm fatty acid distillate (PFAD) which is the by-product of physical refining process of CPO [33]. Malaysian refineries produced PFAD with the total amount of 750,000 t in 2008 [34]. PFAD contains more than 90% palmitic acid and is comparatively far cheaper than CPO. It is generally sold as a source of industrial fatty acids for non-food applications such as laundry soap industries [35–38]. It can also be used to produce renewable energy sources through suitable thermochemical means.

Fatty acids are carboxylic acids with long aliphatic chains, which are either saturated or unsaturated [39]. Saturated fatty acids are fatty acid that have no carbon–carbon double bond such as palmitic acid, stearic acid and lauric acid. Unsaturated fatty acids are fatty acids with one or more carbon–carbon double bonds for example: oleic acid, myristoleic acid and linoleic acid. Meanwhile, triglycerides are esters derived from glycerol and three fatty acids. They are named according the fatty acid components, for example, tristearin contains three molecules of stearic acid. Other examples of triglyceride are trilaurin, tripalmitin and triolein. Molecular structures of stearic acid, oleic acid and tristearin can be seen in Fig. 3.

There are several alternative techniques recently developed to produce diesel like-hydrocarbon using fatty acid such as catalytic cracking, hydrotreating and catalytic deoxygenation. Catalytic cracking technology is used to break down high-molecular-mass into fragments of lower molecular mass [40–45]. Hydrotreating process involves the removal of oxygen through the introduction of hydrogen into the fatty acid or triglyceride molecules either using metal catalyst or oxide catalysts to produce *n*-alkanes [46–50]. Meanwhile, deoxygenation involves removal of the carboxyl group in the fatty acid as carbon and/or carbon monoxide using a supported metal catalyst, thereby producing alkane and alkene as diesel-like hydrocarbons [51]. Very encouraging results have been reported recently [46–48].

During the past few year, researchers reported mechanism and kinetic model of fatty acid deoxygenation over supported metal catalyst to produce diesel-like hydrocarbons. It also reported that operating parameters were important to optimize selectivity/yield of diesel like-hydrocarbon in the deoxygenation process. The operating parameters include supported metal catalyst type, feed type, temperature, reaction atmosphere, feed rate (residence time), catalyst amount and the presence of solvent. This review summarizes reaction pathways and kinetic models of deoxygenation fatty acid. Subsequently, the roles of the operating conditions that are employed for optimum yield and selectivity of diesel-like hydrocarbon are highlighted. This paper also highlights recent progress in deoxygenation of fatty acid to produce diesel-like hydrocarbons. In addition, highlights on future directions for this option are also provided.

2. Reaction pathways and kinetic models of deoxygenation of fatty acid to produce diesel-like hydrocarbons

Lestari et al. [51] proposed general saturated fatty acid deoxygenation reaction steps under inert atmosphere over supported metal catalyst that involve several reaction pathways, as can be seen in Fig. 4. Under inert atmosphere, the presence of hydrogen during the process is achieved via dehydrogenation of unsaturated

compound [52]. The reaction pathways consist of liquid and gas phase reactions. Liquid phase reactions of the fatty acid deoxygenation process involve direct decarboxylation and decarbonylation reactions that occur simultaneously, as illustrated in reactions 1 and 2 in Fig. 4. Direct decarboxylation removes carboxyl group in the fatty acid to produce *n*-alkane by releasing carbon dioxide molecule. Meanwhile, direct decarbonylation removes carboxyl groups by releasing carbon monoxide and water molecules to produce alkenes. Furthermore, deoxygenation of saturated fatty acid in the presence of hydrogen involves indirect decarboxylation and direct hydrogenation to produce *n*-alkanes, as illustrated in reactions 3 and 4. Furthermore, CO₂, CO, hydrogen and water produced from the liquid phase decarboxylation/ decarbonylation will undergo gas phase reactions. The gas phase reactions include methanation of CO₂ and CO as shown in reactions 5 and 6, respectively. Besides, water-gas-shift reaction also occurs during the deoxygenation process, as shown in reaction 7.

Reaction pathway of deoxygenation of a specific saturated fatty acid has been proposed by Snare et al. [53] who used stearic acid

as reactant. Fig. 5 shows the reaction pathway of stearic acid deoxygenation over various supported metal catalysts under inert atmosphere at 300 °C. First, main reactions of decarboxylation and decarbonylation of stearic acid simultaneously occur to produce *n*-hexadecane (C₁₇H₃₆) and 1-hexadecene (C₁₇H₃₄), respectively, as can be seen in reactions 1 and 2. Then, some of the *n*-hexadecane and 1-hexadecene are isomerized and/or hydrogenated/dehydrogenated, as can be seen in reactions 5–9, to generate minor amounts of C₁₇ cyclic and aromatic molecules as well as hydrogen source. Subsequently, some of stearic acid is hydrogenated using the hydrogen source to produce minor amount of another alkane (C₁₈H₃₈), as in reactions 3. Some of 1-hexadecene will undergo hydrogenation/dehydrogenation to produce *n*-hexadecane, as in reaction 3. Cracking reaction of stearic acid (reaction 10) may also occur leading to the production of lower fatty acids (C₁₀–C₁₇ acid) and shorter hydrocarbons (C₁₃–C₁₆). Besides, conversion of stearic acid to symmetrical ketone and dehydrogenation of stearic acid and unsaturated hydrocarbons can occur to the formation of heavier products, as shown in reaction 11, 12, and 13 in Fig. 5. Thus, fatty acid provides alternatives to produce various hydrocarbons as fuels in the future should some technical hurdles in the processes involved can be properly managed.

For unsaturated fatty acid deoxygenation under inert atmosphere, its reaction pathway has also been proposed by Snare et al. [54]. The unsaturated fatty acid type that they used was oleic acid. Fig. 6 shows the reaction pathway of oleic acid deoxygenation. This can be explained as follows: positional and geometrical isomerizations of oleic acid initially occur to generate elaidic and vaccenic acid. Then, oleic acid and its isomer are dehydrogenated to form polyunsaturated and aromatic by-products as well as source of hydrogen. Subsequently, the double bond (the remaining oleic acid and its isomer) are hydrogenated to generate stearic acid by using the source of hydrogen. Further deoxygenation reaction results in heptadecane hydrocarbon fuel as the main product and minor amounts of unsaturated positional isomers (1-, 3-, and 8-heptadecene) as well as C₁₇ aromatics. Thus, more unsaturated hydrocarbons can be produced when unsaturated fatty acid is used as feedstock.

Furthermore, Kitiyanan et al. [55] reported that kinetic model for oleic acid deoxygenation under inert atmosphere can be

a

Liquid-phase reactions

1. Decarboxylation: $R\text{-COOH} \rightarrow R\text{-H} + \text{CO}_2$
2. Decarbonylation: $R\text{-COOH} \rightarrow R\text{-H} + \text{CO} + \text{H}_2\text{O}$
3. $R\text{-COOH} + \text{H}_2 \rightarrow R\text{-H} + \text{CO} + \text{H}_2\text{O}$
4. Hydrogenation: $R\text{-COOH} + 3\text{H}_2 \rightarrow R\text{-CH}_3 + 2\text{H}_2\text{O}$

R = saturated alkyl group; R' = unsaturated alkyl group

b

Gas-phase reactions

5. Methanation: $\text{CO}_2 + 4\text{H}_2 \rightleftharpoons \text{CH}_4 + 2\text{H}_2\text{O}$
6. Methanation: $\text{CO} + 3\text{H}_2 \rightleftharpoons \text{CH}_4 + \text{H}_2\text{O}$
7. Water-gas shift: $\text{CO} + \text{H}_2\text{O} \rightleftharpoons \text{H}_2 + \text{CO}_2$

Fig. 4. General saturated fatty acid deoxygenation reaction steps under inert atmosphere over supported metal catalyst adapted from [51].

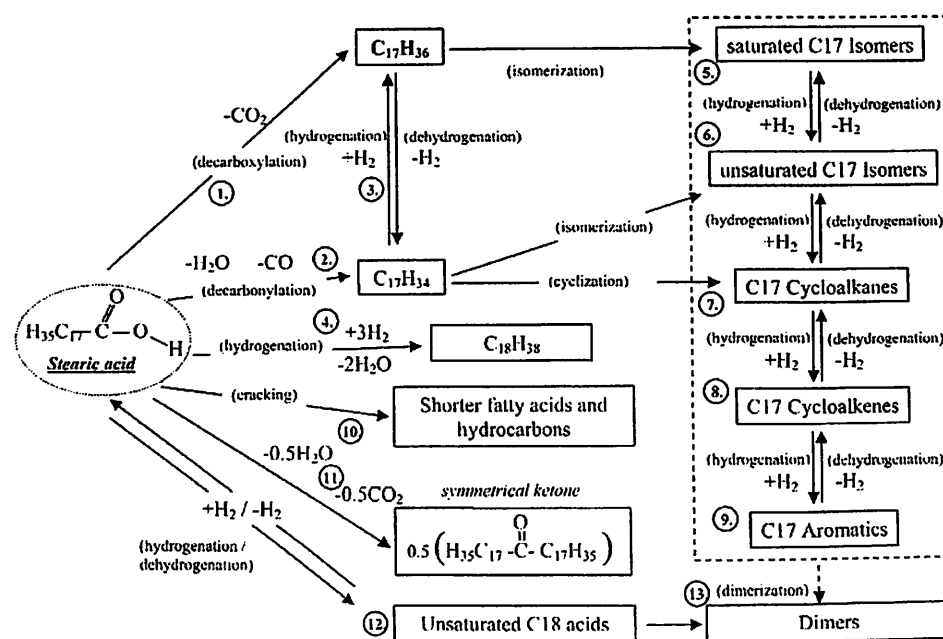


Fig. 5. Reaction pathway of stearic acid deoxygenation over supported metal catalysts under inert atmosphere [53].

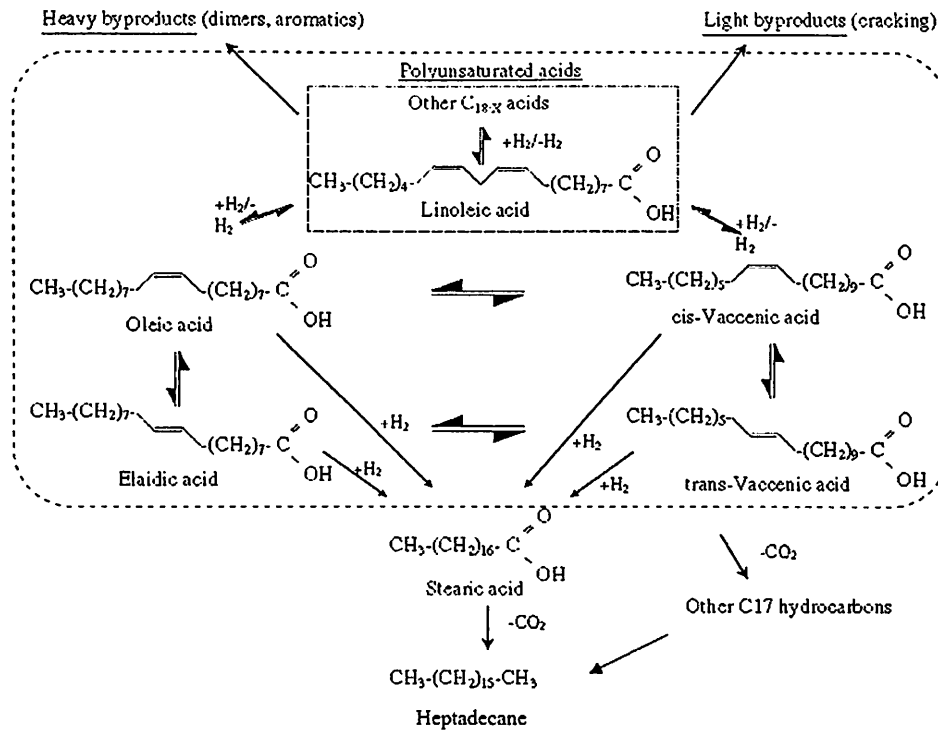


Fig. 6. Reaction pathway of oleic acid deoxygenation over supported metal catalysts under inert atmosphere [54].

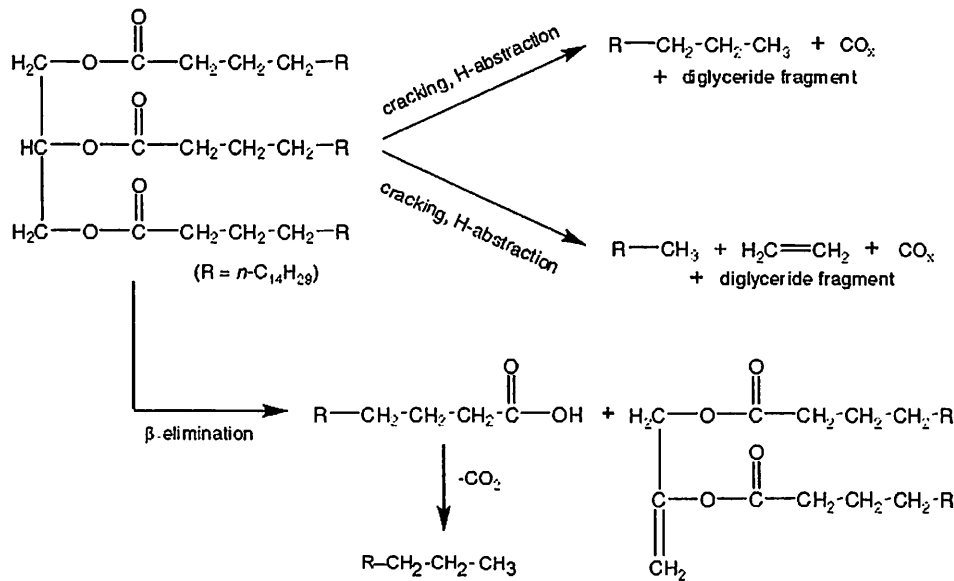


Fig. 7. Reaction pathway for tristearin deoxygenation over supported metal catalyst under inert atmosphere [56].

suggested to follow the first order with respect to oleic acid, as in Eq. (1):

$$\text{Rate} = \frac{-d[\text{COA}]}{dt} = k[\text{COA}] \quad \text{or} \quad \text{Rate} = \frac{-d[\text{COA}]}{[\text{COA}]} = kdt \quad (1)$$

where, k is rate constant, t is reaction time and $[\text{COA}]$ is concentration of oleic acid.

Reaction pathway of tristearin deoxygenation over various supported metals (Ni, Pt, and Pd) under inert atmosphere at 300 °C has been proposed by Morgan et al. [56] as in Fig. 7. First, some tristearins liberated stearic acid via a β -elimination process. This also generates unsaturated glycol difatty ester as a co-product. Subsequently, the stearic acid is decarboxylated to give n -heptadecane.

Meanwhile, the other tristearins can undergo cracking reactions that involve either scission of the C–C bond between the ester carbonyl carbon and a carbon of the hydrocarbon chain, or scission between the β and γ carbon atoms to produce C17 and C15 hydrocarbons, respectively as well as diglyceride fragment and CO_x gas.

The C17 and C15 hydrocarbons correspond to n -heptadecane and n -pentadecane, respectively, as the main products. Besides, the C17 and C15 might correspond to heptadecene and pentadecene that lead to the hydrogen generation during bond scission. It has been reported that hydrogen is consistently detected in the gaseous products. Scission between the β and γ carbon atoms forms ethene as a co-product. It is assumed that the unsaturated glycerol units (diglyceride fragments) produced from reactions 1,

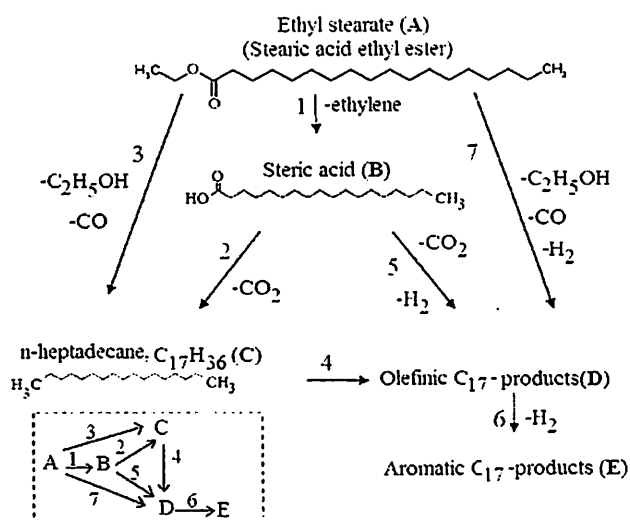


Fig. 8. Reaction pathway for deoxygenation of stearic acid ethyl ester over a commercial Pd/C catalyst [58].

2 and 3 in Fig. 5 will undergo cracking reactions to the formation of volatile products, e.g., C1–C3 hydrocarbons and hydrogen abstraction [40].

In addition, it has been reported by Chiappero et al. [57] that a kinetic model for triglyceride deoxygenation under inert atmosphere in a semi-batch mode is suggested to follow the first order with respect to triglyceride as in Eq. (2).

$$\text{Rate} = -dC_{TG}/dt = k dC_{TG} \quad (2)$$

where k is the rate constant and C_{TG} is the concentration of triglyceride. The kinetic behavior has been reported to be successfully identified for several types of triglyceride such as trilaurin and trimyristin. By using Eq. (1), trilaurin and trimyristin had reaction rates of 1.2×10^{-2} /min and 1.16×10^{-2} /min, respectively.

Meanwhile, reaction pathway of deoxygenation of fatty acid ester in a semi-batch reactor over a commercial Pd/C catalyst at 300 °C has been verified using stearic acid ethyl ester as reactant [58]. The reaction pathway is shown in Fig. 8 and can be explained as follows: stearic acid ethyl ester initially liberates stearic acid (reaction 1). Subsequently, stearic acid is decarboxylated to form *n*-heptadecane (reaction 2). However, dehydrogenation of the produced *n*-heptadecane concurrently occurs to form heptadecene (reaction 4) and aromatic compound (reaction 6). Besides, stearic acid can be directly converted into heptadecene (reaction 5) via dehydrogenation of the stearic acid to generate unsaturated fatty acid intermediate followed by a fast decarboxylation reaction [54]. Stearic acid ethyl ester is also be directly converted into *n*-heptadecane via reaction 3 and into heptadecene via reaction 7.

Additionally, kinetic model for stearic acid ethyl ester deoxygenation under inert atmosphere has been suggested to follow the first order with respect to stearic acid ethyl ester as in Eq. (3):

$$\text{Rate} = -dC_{SAEE}/dt = k dC_{SAEE} \quad (3)$$

where, k is rate constant and C_{SAEE} is the concentration of stearic acid ethyl ester. The rate constant, k is related to an Arrhenius equation, which gives the relationship between pre-exponential factor (A) and activation energy (E) in Eq. (4). The activation energy (E) based on Eqs. (3) and (4) has been reported to be 57.3 kJ/mol [58].

$$k = A \exp [-E/(RT)] \quad (4)$$

Furthermore, a kinetic model has been developed for deoxygenation of stearic acid ethyl ester with intermediate products on

the basis of the reaction pathway in Fig. 6 using Langmuir–Hinshelwood mechanism. Langmuir–Hinshelwood mechanism assumes that the reactant must first adsorb on the catalyst surface. Subsequently, the reaction takes place at the active site, and the product then desorbs from the catalyst [59]. A reasonable simplification is made by disregarding adsorption constants for gaseous products (i.e., CO₂, ethylene, etc.) in the denominator. It was also assumed that surface reactions are rate limiting and adsorption reactions are more rapid than the surface reactions. The rates of reaction steps, r_i ($i=1, 2, 3, 4, 5, 6, 7$), based on Fig. 6 are proposed as follow:

$$r_1 = \frac{K_1 C_A}{1 + K_A C_A + K_B C_B + K_A C_C + K_D C_D + K_E C_E} \quad (5)$$

$$r_2 = \frac{K_2 C_B}{1 + K_A C_A + K_B C_B + K_A C_C + K_D C_D + K_E C_E} \quad (6)$$

$$r_3 = \frac{K_3 C_A}{1 + K_A C_A + K_B C_B + K_A C_C + K_D C_D + K_E C_E} \quad (7)$$

$$r_4 = \frac{K_4 C_C}{1 + K_A C_A + K_B C_B + K_A C_C + K_D C_D + K_E C_E} \quad (8)$$

$$r_5 = \frac{K_5 C_B}{1 + K_A C_A + K_B C_B + K_A C_C + K_D C_D + K_E C_E} \quad (9)$$

$$r_6 = \frac{K_6 C_D}{1 + K_A C_A + K_B C_B + K_A C_C + K_D C_D + K_E C_E} \quad (10)$$

$$r_7 = \frac{K_7 C_A}{1 + K_A C_A + K_B C_B + K_A C_C + K_D C_D + K_E C_E} \quad (11)$$

where A=stearic acid ethyl ester, B=stearic acid, C=*n*-heptadecane, D=olefinic C₁₇ products, E=aromatic C₁₇ products, K_i =equilibrium reaction constant, k_i =apparent reaction constant, C_i =concentration of lance.

A system of ordinary differential equations (ODE) that is obtained by using the kinetic rate expressions into the mass balances of components on the basis of reactions in Fig. 6 can be seen in the following expressions:

$$\frac{1}{\rho_B} \frac{dc_A}{dt} = -r_1 - r_3 - r_7 \quad (12)$$

$$\frac{1}{\rho_B} \frac{dc_B}{dt} = r_1 - r_2 - r_5 \quad (13)$$

$$\frac{1}{\rho_B} \frac{dc_C}{dt} = r_2 + r_3 - r_4 \quad (14)$$

$$\frac{1}{\rho_B} \frac{dc_D}{dt} = r_4 + r_5 - r_6 + r_7 \quad (15)$$

$$\frac{1}{\rho_B} \frac{dc_E}{dt} = r_6 \quad (16)$$

where ρ_B =catalyst amount used in the reaction.

3. Factors influencing the deoxygenation process

Achieving high content of diesel-like hydrocarbons in liquid products is important in deoxygenation of fatty acid and triglyceride in order to avoid further separation step such as distillation to meet a quality standard as a fuel [10]. Process conditions significantly influence yield and selectivity of diesel-like hydrocarbon as well as product composition. The process conditions reported in the literature include the use of supported metal catalyst type, feed type, temperature, reaction atmosphere, residence time,

catalyst loading and type of feed. Mature understandings on the influences of specific process conditions are yet to be established in view of the complex reactions involved. However, some recent works reported managed to shed some light on this area [48,50,60].

3.1. Supported metal catalyst type

Various supported metal catalysts i.e. Pd, Pt and Ni on γ -Al₂O₃ have been investigated for deoxygenation of waste fat containing a mixture of oleic acid and tripalmitin in the presence of solvent under hydrogen atmosphere. It has been observed that Pd/ γ -Al₂O₃ catalyst is more active than the Pt/ γ -Al₂O₃ catalyst and also more selective for production of the C17 and C15 diesel-like hydrocarbons [60]. The higher activity was due to the higher content of active metal (Pd) in the Pd/ γ -Al₂O₃ catalyst than the active metal (Pt) in the Pt/ γ -Al₂O₃ catalyst. However, although Ni/ γ -Al₂O₃ catalyst contained the highest active metal (Ni) among the three catalysts, it showed the poorest activity for production of C17 and C15 diesel-like hydrocarbons. This result was attributed to the largest particle size of active metal (Ni) in Ni/ γ -Al₂O₃ catalyst. The average particle size of Ni in Ni/ γ -Al₂O₃ catalyst was 8.2 nm. Meanwhile, Pd and Pt had the average particle sizes of 4.6 nm and 5.4 nm, respectively. The result was in agreement with reports [52–53] that Ni/ γ -Al₂O₃ was less active catalyst than Pd/ γ -Al₂O₃ and Pt/ γ -Al₂O₃.

Meanwhile, Ni supported on mesoporous carbon (Ni/C) has been reported to be more active and selective catalyst for diesel-like hydrocarbons compared to Pd or Pt supported on mesoporous carbon in deoxygenation of triglycerides (tristearin, triolein and soybean oil) under inert atmosphere (N₂) [56]. The higher activity of the nickel supported on mesoporous carbon was due to its higher content of Ni as active metal (20 wt%) with small particle size (4 nm) in the Ni/C catalyst. Pd/C had active metal content of 5 wt% with particle size of 6 nm while Pt/C had metal content of 1 wt% with particle size of 3.7 nm. Furthermore, various Ni functionalized mesostructured cellular foam silica (NiMCF) with different characteristics have been investigated as catalysts for solventless deoxygenation of palmitic acid under inert atmosphere [61]. It was found that NiMCF catalyst that had the highest nickel content (17.57 wt%) with the smallest particle sizes (1 to 3 nm) was the highest active and selective catalyst for solventless palmitic acid deoxygenation to produce diesel-like hydrocarbons. Metal particles were active sites to produce *n*-alkane and alkene in fatty acid deoxygenation through decarboxylation and decarbonylation reaction, respectively [62]. In general, it can be concluded that metal incorporated mesoporous materials having high metal content with small particle sizes are suitable catalysts for fatty acid deoxygenation to produce diesel-like hydrocarbons.

3.2. Feed types

Various feeds, i.e. saturated fatty acid (behenic acid, C₂₁H₄₃COOH and stearic acid, C₁₇H₃₅COOH) and fatty acid ester (stearic acid ethyl ester, C₁₇H₂₅COOC₂H₅) have been deoxygenated over commercial Pd/C catalyst in the presence of dodecane as solvent at 300 °C under 5% H₂ in argon for 360 min [52]. It was found that initial reaction rate for stearic acid (0.63 mmol/min-g_{cat}) was higher than that for behenic acid (0.36 mmol/min-g_{cat}), while initial reaction rate for stearic acid ethyl ester (0.70 mmol/min-g_{cat}) was slight higher compared to stearic acid. However, deactivation of Pd/C catalyst was more severe for deoxygenation of stearic acid ethyl ester than for that of stearic acid. It was observed that after a prolonged reaction time of 360 min, the conversion of stearic acid ethyl ester was only 38%, while the conversion of stearic acid was 60%. The more severe deactivation of the Pd/C

catalyst was mainly ascribed to higher amounts of unsaturated products that were produced through stearic acid ethyl ester deoxygenation.

The large quantities of unsaturated compounds decreased the selectivity to *n*-alkane. At a conversion of 30%, deoxygenation of stearic acid ethyl ester gave *n*-alkane selectivity of 40% which was much lower than that of stearic acid (86%). Meanwhile, deoxygenation of behenic acid achieved *n*-alkane selectivity of 78% at the conversion of 30%. This indicated that decarboxylation reaction was more dominant in fatty acid deoxygenation than in fatty acid ester deoxygenation. This was due to the easier breaking the COO–H bond in fatty acid compared to the COO–R bond in fatty acid ester, because the alkyl group in ester is a nucleophilic group as reported in the literature [63]. It was also reported that deoxygenation of stearic acid ethyl ester produced CO as the predominant gaseous compound because of the stability of the ethoxy group in ester. It can be concluded from the results that deoxygenation of fatty acid (such as behenic acid and stearic acid) was more selective to produce *n*-alkane as diesel-like hydrocarbons through decarboxylation when compared to deoxygenation of fatty acid ester (stearic acid ethyl ester). Deoxygenation of saturated fatty acid with a shorter chain achieves a bit higher *n*-alkane selectivity.

Furthermore, deoxygenations of palmitic acid has been compared with deoxygenation of stearic acid using Pd supported on mesoporous carbon catalyst in the presence of dodecane as solvent in a semi batch reactor at 300 °C under 5% H₂ in argon [64]. Reaction rate of palmitic acid deoxygenation was found to be the same as reaction rate of stearic acid deoxygenation. deoxygenation of palmitic. This result was in agreement with those reported for deoxygenations of heptadecanoic acid, stearic acid, nonadecanoic acid, arachidic acid and behenic acid [65]. The catalytic deoxygenations of palmitic acid and stearic acid resulted in formation of *n*-pentadecane and *n*-heptadecane, respectively, as the main liquid products.

3.3. Reaction atmosphere

Effect of reaction atmosphere on conversion and yield/selectivity of desired products (*n*-undecane (n-C₁₁H₂₄) and undecene (C₁₁H₂₂) in deoxygenation of lauric acid (C₁₂H₂₄O₂) has been studied using two different reaction atmospheres, i.e. pure Ar (Inert) and pure H₂ [66]. The reactions were carried out in a semi-batch reactor under the presence of hexadecane as a solvent using Pd supported on mesoporous carbon as catalyst. It was found that in the first 100 min of reaction, yields of the desired products using the experiment in inert atmosphere were higher than those obtained in the experiment carried out in hydrogen rich atmosphere. On the other hand, from 100 min until 300 min of reaction, the yields obtained in the experiment under inert atmosphere were lower than those under hydrogen rich atmosphere.

The lower yields in the reactions under the rich hydrogen in the first 100 min of reaction were due to initial high formation of intermediates which were gradually converted into the desired products. Meanwhile, in the reaction under inert atmosphere, the desired products were formed via decarboxylation and decarbonylation. Fatty acid deoxygenation pathways under the rich hydrogen atmosphere, as can be seen in Fig. 9. These can be explained as follows: with high saturation of the palladium surface with hydrogen, hydrogenation of carboxylic group in fatty acid primarily occurs forming an aldehyde (R–CHO) as an intermediate (reaction 1). The aldehyde highly decomposes through decarbonylation reaction producing hydrocarbon and CO (reaction 2 and 3). Some of the aldehydes can be further hydrogenated to lauryl alcohol, R–CH₂–OH, (reaction 4). Subsequently, decomposition of lauryl alcohol forming mainly undecane is a more favorable step

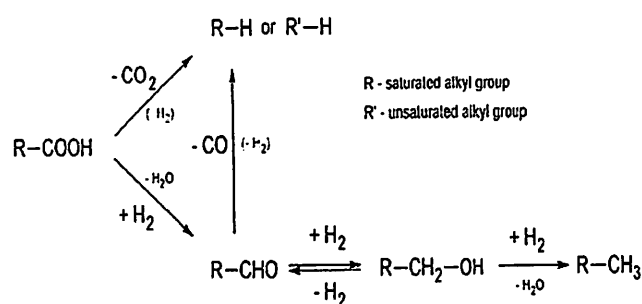


Fig. 9. Fatty acid deoxygenation pathways under rich hydrogen atmosphere in a batch reactor using Pd/C catalyst in the presence of solvent [66].

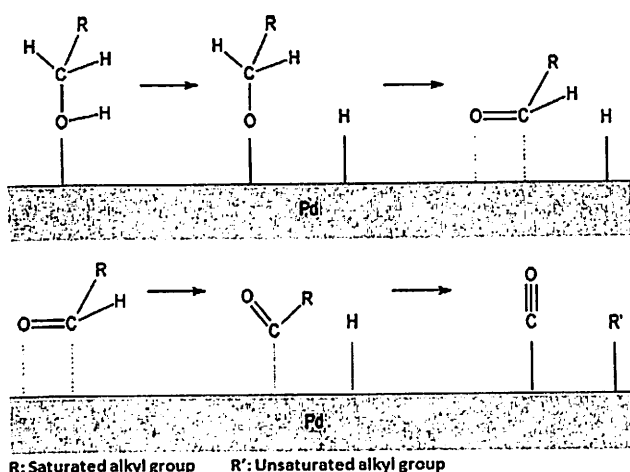
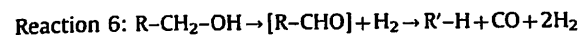
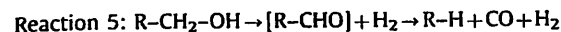
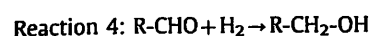
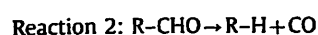
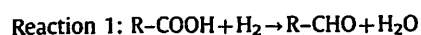


Fig. 10. Lauryl alcohol decomposition mechanism over Pd catalyst [66].

than further hydrodeoxygenation of alcohol to dodecane (R-CH₃). Lauryl alcohol decomposes through dehydrogenation to the aldehyde intermediate (reaction 5) and thereafter decarbonylate to hydrocarbon over Pd surface (reaction 6). Decomposition of lauryl alcohol is illustrated in Fig. 10.



Furthermore, Kubickova et al. [67], Lestari et al. [64] and Madsen et al. [60] reported that fatty acid deoxygenation in the presence of Pd/C catalyst using reaction atmosphere with small quantity of H₂ in inert gas (5% H₂ in argon or 5% H₂ in helium) gave higher catalytic activities compared to those using inert or rich hydrogen atmospheres. This was because the presence of a small quantity of H₂ in inert gas in the reactions generated lower amounts of unsaturated hydrocarbons and aromatic hydrocarbons leading to coke formation and also generated a smaller molecular weight compounds in the product mixture. The coke formation and accumulation of different compounds on the catalyst surface can contribute to catalyst deactivation. As such, the presence of a small quantity of H₂ in inert gas is expected to preserve the catalytic activity for a longer time.

3.4. Reaction temperature

Bernas et al. [68] reported that reaction temperature significantly affected conversion and yield/selectivity of diesel-like hydrocarbon in deoxygenation of diluted dodecanoic acid over 1% Pd/C catalyst in a continuous reactor under inert atmosphere. The increase in temperature from 300 to 360 °C resulted in the increase in conversion from 10% to 60% with undecane and undecene as the main products. Meanwhile, for deoxygenation of diluted stearic acid over 4% Pd/C in a semi-batch reactor under inert atmosphere, the increase in temperature from 270 to 330 °C made time needed for 100% conversion shorter i.e. from 270 min to 20 min and *n*-heptadecane selectivities generated were nearly the same i.e. around 50% [69]. Furthermore, the increase in temperature from 300 to 360 °C for deoxygenation of diluted ethyl stearate resulted in an increase in conversion (from 40 to 100%). On the other hand, *n*-heptadecane selectivity decreased from 70 to 40%. The deoxygenation was carried out in a semi-batch reactor under the flow of 5% H₂ in argon for 360 min [67].

Effect of temperature in deoxygenation of tall oil fatty acid (TOFA) over Pd/C catalyst has been studied at various temperatures from 300 °C to 350 °C in the presence of dodecane as a solvent under the flow of 1% H₂ in argon for 360 min [31]. It was found that total conversion of the fatty acid increased with an increase in reaction temperature and only minor sintering of Pd/C (Sibunit) occurred at a reaction temperature of 350 °C. The main products in the liquid phase at temperature reaction of 300 °C were desired products (*n*-heptadecane and *n*-heptadecene) with a higher amount of *n*-heptadecane compared to *n*-heptadecene.

At higher reaction temperatures, 325 °C and 350 °C, the ratio between *n*-heptadecane and *n*-heptadecene was lower. This indicated that dehydrogenation occurred to a larger extent [40]. Selectivity to the desired products decreased with the increase in temperature due to the more extensive catalyst deactivation at higher temperatures because of enhanced formation of an aromatic C17 compound. The aromatic compound was typically undecylbenzene type. Aromatic compound is formed after the deoxygenation via dehydrogenation of *n*-C17-heptadecane leading to cyclization. Besides that, conversion of linoleic acid in TOFA into its C18 fatty acid isomers was enhanced at higher temperatures.

3.5. Catalyst amount

Catalyst amount used for stearic acid deoxygenation significantly can influence reaction rates and selectivity of the desired products (*n*-heptadecane and heptadecene) [52]. The effect of catalyst amount in stearic acid deoxygenation has been studied at 300 °C under 6 bar of helium in dodecane by using Pd/C catalyst at different amounts (0.2, 0.5, and 1 g). It was reported that the reaction rates and conversion increased linearly with the amount of the catalyst in the range. Besides that, the increase in catalyst amount resulted in a slower catalyst deactivation and a higher selectivity to *n*-heptadecane. Thus, this parameter is critical in optimizing the yield of the desired products.

Furthermore, Kwon et al. [70] studied the effect of catalyst amount in deoxygenation of methyl laurate at 350 °C in a batch reactor in the presence of H₂ using various amounts of NiMo/Al₂O₃ catalyst (0–0.126 g). They found that the conversion and selectivity of linear hydrocarbons (undecane and dodecane) increased with the catalyst amount. Meanwhile, lauric acid as an intermediate product and undesired products decreased when the catalyst amounts was increased. This result indicated that the use of smaller amounts of catalyst in the presence of H₂ led to higher polymerization of methyl laurate toward the formation of undesired products.

3.6. Feed rate (residence time)

Maki-Arvela et al. [71] studied the effect of feed rate on the activities in lauric acid deoxygenation using four different volumetric feed flow rates, i.e. 0.1 ml/min, 0.25 ml/min, 1 ml/min and 1.5 ml/min. The reaction was carried out using Pd/C catalyst under the presence of dodecane as solvent in a continuous reactor. It was found that when the feed rate was decreased from 1 ml/min to 0.25 ml/min, the conversion level increased from 4% to 45% because of the increase in the residence time of feed in the reactor. Feed rate is inversely proportional to residence time. The increase in feed rate resulted in the decrease in the conversion level due to a shorter residence time that resulted in extensive catalyst deactivation. It can be concluded that, catalyst deactivation during lauric acid deoxygenation was significant when contacting the catalyst with a large quantity of lauric acid.

3.7. Use of solvent

Effect of solvent on catalytic activity has been studied for deoxygenation of methyl stearate over catalyst of 5% Pd/BaSO₄ under hydrogen atmosphere in a batch reactor at 270 °C for 6 h [72]. It was reported that deoxygenation reaction carried out without using a solvent produced no alkanes, although the methyl stearate conversion was nearly 100%. This could be due to formation of macromolecules via coupling reactions among intermediates on the catalyst surface. This result agreed with that of solventless deoxygenation of sunflower oil as reported in the literature [73].

Meanwhile, when organic solvents such as hexane was used for the methyl stearate deoxygenation, high stearic acid conversion (99.5%) with high yield of *n*-alkane (95.7%) were achieved. Furthermore, using hexane as solvent in deoxygenation of sunflower oil over catalyst of 5% Pd/BaSO₄ under hydrogen atmosphere also successfully gave high yield of desired products of around 79.2% [72]. This result was because the high diffusivity of supercritical hexane that could reduce mass-transfer resistance of reactants in the reactions, which facilitated the contact of hydrogen and the reactants with the catalyst. Besides that, the solvent has high solubility with alkanes. The high solubility enhances desorption of alkanes generated on the catalyst surfaces. As such, the coupling reactions among alkyl intermediates adsorbed on the active sites of the catalysts to form unidentified macromolecules were effectively inhibited. However, the presence of an excess of solvent made the deoxygenation slow due to a volume expansion reaction.

4. Recent progress in deoxygenation of fatty acid

Initially, Snare et al. [53] studied stearic acid deoxygenation in the presence of dodecane as solvent in a semi-batch reactor using noble metals (Pd, Pt, Ru, Ir, Os and Rh) as well as non-noble metal (Ni) as active components. The catalyst supports explored were Al₂O₃, SiO₂ and activated carbon. It was found that Pd supported on mesoporous carbon (5 wt% Pd/C) was the most efficient catalyst for stearic acid deoxygenation in especially through decarboxylation to produce *n*-heptadecane. The 5 wt% Pd/C catalyst successfully converted stearic acid completely with > 98% selectivity toward deoxygenated C₁₇ products. It was also reported that activities of metals incorporated on the same support for the deoxygenation increased in the order of Os < Ru < Ir < Rh < Ni < Pt < Pd. A continuous process of ethyl stearate deoxygenation was also successfully carried out using the 5 wt% Pd/C catalyst at 360 °C that gave 100% of conversion with 95% of *n*-heptadecane selectivity [58]. Since then, a number of works in the literatures

reported deoxygenation of various fatty acids to produce diesel like hydrocarbons over supported metal catalysts under various operating conditions and various reactor types. These works are summarized in Table 1.

As can be seen from Table 1, Maki-Arvela et al. [52] observed deoxygenation of various fatty acids and their derivative using 5 wt% Pd/C catalyst in a semi-batch reactor for 5 h under various operating conditions i.e. temperatures (300 to 320 °C), gas atmosphere (argon, nitrogen and hydrogen), solvents (dodecane, mesitylene) and initial feed concentrations (0.2–1.0 g). It was reported that high yields of the desired product, *n*-heptadecane were achieved in stearic acid deoxygenation at 300 °C under helium. Moreover, deoxygenations of a saturated fatty acid i.e. lauric acid over 1 wt% Pd/C catalyst were carried out in continuous process using various solvents (dodecane, mesitylene and decane) at lower temperatures (255–300 °C) to study the stability and deactivation of the catalyst [71]. Catalyst deactivation was identified to be the most prominent when using solvents such as mesitylene and dodecane. The deactivation of catalyst resulted from poisoning by gas products of CO and CO₂ and coking.

Subsequently, 5 wt% Pd/C were examined in deoxygenations of unsaturated fatty acids (oleic acid, linoleic acid) and unsaturated fatty acid ester (methyl oleate) either in a semi-batch or in a continuous reactor under various operating conditions i.e. atmospheres (argon, hydrogen and synthetic air), temperatures (300–360 °C) and pressures (15–27 bar) [54]. It was found that the unsaturated fatty acids and unsaturated fatty acid ester were successfully deoxygenated to produce diesel-like hydrocarbons via initial hydrogenation of double bonds and subsequent deoxygenation of corresponding saturated feeds. Then, the application of continuous process for the reaction confirmed stability of the catalyst. Arend et al. [74] studied solventless deoxygenation of oleic acid over 2 wt% Pd/C in a continuous reactor under hydrogen atmosphere at various conditions. Deoxygenations of dodecanoic acid over 1 wt% Pd/C were also carried out in a continuous reactor [68]. Furthermore, tall oil fatty acid and lauric acid deoxygenations over Pd/C catalysts were successfully demonstrated in a semi-batch reactor with encouraging results [31,66,75].

Pd supported on SBA-15 mesoporous silica was also studied for deoxygenation of stearic acid using dodecane as solvent in a semi-batch reactor at 300 °C under a flow of 5% H₂ in Ar [76]. The catalyst achieved stearic acid conversion of 94% with *n*-heptadecane selectivity of 94% for a reaction time of 5 h. Meanwhile, when 4 wt% Pd/C catalyst was used, deoxygenation of a mixture of stearic acid and palmitic acid using the same conditions achieved a total conversion of about 97% with *n*-heptadecane and *n*-pentadecane selectivity of 99% for a reaction time of 2 h [64]. Furthermore, Pd incorporated on different supports (i.e. Pd/C, Pd/SiO₂, and Pd/Al₂O₃) was demonstrated to be promising catalyst for stearic acid deoxygenation in a semi-batch reactor at 300 °C using dodecane as solvent under flow of 10% hydrogen in helium [77].

Immer et al. [78] observed stearic acid deoxygenation using Pd/C catalyst in the presence of dodecane or heptadecane using a semi-batch reactor. Complete stearic acid conversion with 98% selectivity to *n*-heptadecane was achieved after 5 h. Besides, the use of Pd/C catalyst for deoxygenation of C₁₈ free fatty acid in heptadecane has also been studied using fed-batch reactor [79]. Continuous processes of solventless deoxygenations of stearic acid over Pd/C catalyst were successfully carried out either under inert atmosphere or under the flow of H₂ in Ar [60,80]. Stearic acid conversions of around 12–15% with *n*-heptadecane (C₁₇H₃₆) as the main liquid product were achieved using these processes.

Besides using catalysts derived from Pd which is high price-rare metal, some researchers also investigated fatty acid deoxygenation using low cost catalysts such as Ni/MgO–Al₂O₃, Ni/Al₂O₃ and MgO/Al₂O₃ in a batch reactor under solvent free and inert

Table 1
Fatty acid deoxygenation over various supported metal catalysts to produce diesel-like hydrocarbons.

Catalyst	Feed	Solvent	Reactor type	Conditions	Reference
5 wt% Pd/C	Stearic acid Ethyl stearate Behenic acid Nonanoic acid Oleic acid Lauric acid	Dodecane Mesitylene	Semi-batch	T=300–320 °C Atmosphere=argon; nitrogen; hydrogen Initial feed concentration=0.1–1.6 mol/l Catalyst amount=0.2–1 g Reaction time=5 h	[52]
1 wt% Pd/C	Lauric acid	Dodecane Mesitylene Decane	Continuous	T=255–300 °C; feed rate=0.1–1.5 ml/min Atmosphere=argon; hydrogen; synthetic air Initial feed concentration=0.22; 0.35;0.44 mol/l Catalyst amount=0.3–0.5 g	[71]
5 wt% Pd/C	Oleic acid Linoleic acid Methyl oleate	Solvent free Mesitylene	Semi-batch	T=300–360 °C; Catalyst amount=1 g Atmosphere=argon (25 ml/min) Initial feed concentration=0.83 mol/l and 100 wt% (solvent free) Reaction time=6 h	[54]
			Continuous	T=300 °C; Atmosphere=argon Catalyst amount=0.2 g Residence time = 8 min Liquid flow rate=0.05 ml/min	
2 wt% Pd/C	Oleic acid	Solvent free	Continuous	T=380–450 °C; Catalyst amount=1–5 g Atmosphere=hydrogen (5–95 ml/min) Residence time=0.5–15 s WHSV=1.6 and 7.9 h ⁻¹	[74]
1 wt% Pd/C	Dodecanoic Acid	Solvent free, Dodecane	Continuous	T=300–360 °C; Atmosphere=argon Initial feed concentration=0.5–4.4 mol/l Catalyst amount=2–12 g Residence time = 0.5–15 s WHSV=0.8–1.7 h ⁻¹	[68]
1 wt % Pd/C 4 wt% Pd/C	Tall oil fatty Acid	Dodecane	Semi-batch	T=300–350 °C Atmosphere=1% H ₂ in Ar; 100% H ₂ Reaction time=360 min Amount of catalyst=0.5 g Feed concentration=0.15–0.6 mol/L	[75]
5 wt% Pd/C	Lauric acid Lauric aldehyde Lauric alcohol Tall oil fatty Acid	Hexadecane	Semi-batch	T=300 °C ; Atmosphere=100%Ar;100 % H ₂ Reaction time=5 h Feed concentration=0.05 mol/L Amount of catalyst=0.1 g	[66]
1 wt% Pd/C	Tall oil fatty Acid	Dodecane	Semi-batch	T=300–350 °C; Atmosphere= 100 % H ₂ Reaction time = 330 min Feed concentration=0.15–0.6 mol/L Amount of catalyst=0.5 g	[31]
3 wt% Pd- SBA-15	Stearic acid	Dodecane	Semi-batch	T=300 °C ; Atmosphere=5 % H ₂ in argon Reaction time=5 h Feed concentration=0.05 mol/l Amount of catalyst=0.5 g	[76]
4 wt % Pd/C	A mixture of Palmitic acid (PA) and Stearic acid (SA)	Dodecane	Semi-batch	T=300 °C ; Atmosphere=5 % H ₂ in argon Reaction time=180 min Feed concentration=0.05 mol/l Amount of catalyst=0.5 g	[64]
5 wt% Pd/C 5 wt % Pd/SiO ₂ 5 wt% Pd/Al ₂ O ₃	Stearic acid	Dodecane	Semi-batch	T=300 °C Atmosphere=5–10 % hydrogen in argon Solvent amount=22.5 g; feed amount=5.6 Mmol Catalyst amount = 336 mg Reaction time=5 h	[77]
5 wt% Pd/C	Stearic acid Linoleic acid	Dodecane Heptadecane	Semi-batch	T=300 °C; reaction time=5 h Atmosphere=helium ; 10 % H ₂ in Ar. Feed concentration = 1.6 g reactant in 23 g solvent Catalyst amount=350 mg	[78]
5 wt% Pd/C	C18 free fatty acid	Heptadecane	Fed-batch	T=300 °C; reaction time=24 h Atmosphere=5–10 % hydrogen in argon feed flow rate: 6–30 µl/min Solvent amount=12.4 g; catalyst amount=336 mg	[79]
5 wt% Pd/C	Stearic acid	Solvent free	Continuous	T=360 °C ; Atmosphere=Ar; 5 % H ₂ in argon Feed rate=0.075 ml/min; Catalyst amount=10 g	[80]
2 wt% Pd/C	Stearic acid	Dodecane Solvent free	Continuous	T=300 °C; Catalyst amount=10 g Atmosphere=argon; 5 % H ₂ in argon Initial feed concentration=10 wt%; pure stearic acid Feed rate = 42 ml/min	[60]
MgO/Al ₂ O ₃	Oleic acid	Solvent free	Batch	T=300–400 °C; Reaction time=3 h Atmosphere=N ₂ ; feed amount=55 g Catalyst amount=2.75 g	[81]
Ni/MgO–Al ₂ O ₃	Oleic acid	Solvent free	Batch	T=300–400 °C; Reaction time=3 h Atmosphere=N ₂ ; feed amount=55 g Catalyst amount=1.375 g	[62]

atmosphere conditions [62,81]. Solventless deoxygenation of oleic acid through decarboxylation over hydrotalcite catalysts (MgO/Al₂O₃) with different MgO contents that has been carried out in an autoclave reactor at 300 °C for 3 h without the use of hydrogen [81]. However, the results confirmed that during the decarboxylation of oleic acid, saponification reaction of MgO was also involved. Saponification was dominant at 300 °C so that MgO disappeared after the decarboxylation process. Meanwhile, hydrotalcites that catalyzed oleic acid decarboxylation at higher temperatures (350 or 400 °C) exhibited very low selectivity of heptadecane since molecular cracking was dominant mechanism in the reaction during the decarboxylation process.

Roh et al. [62] investigated deoxygenation oleic acid through decarboxylation carried out in an autoclave reactor under solvent free condition without the use of H₂ flow. The catalysts were 20 wt % Ni supported on MgO–Al₂O₃ catalysts with different calcination temperatures (300, 400 and 500 °C). The catalysts achieved oleic acid conversions ranging from 26% to 31% with corresponding heptadecane selectivity ranging from 4.8% to 5.5% at 300 °C for 3 h. These results proved the plausibility of fatty acids as feedstock for production of hydrocarbons to be used as renewable energy sources in the future.

5. Conclusions

As an effort to address the drastic shortages of crude oil supplies in the near future, deoxygenation of fatty acid as a renewable resource using supported metal catalyst to produce diesel-like hydrocarbons is becoming more attractive. It is due to the feedstock availability in many countries and liquid products containing hydrocarbons similar to those found in diesel fuel obtained by refining crude oil in petroleum refineries. Reaction pathways and kinetic models of fatty acid deoxygenations over supported metal catalyst are critically reviewed. The key technology of fatty acid deoxygenation using supported metal catalyst to obtain a high yield or selectivity to the diesel-like hydrocarbons can be constructed by detailed understanding on roles of the operating conditions such as supported metal catalyst type, feed type, temperature, reaction atmosphere, catalyst loading, feed rate (residence time) and the use of solvent.

Metal incorporated mesoporous materials having high metal content with small particle are recommended catalysts for fatty acid deoxygenation to produce high yield or selectivity of diesel-like hydrocarbons. Furthermore, deoxygenation of fatty acid is more selective to produce diesel-like hydrocarbons compared to that of fatty acid ester. Deoxygenation of saturated fatty acid with a shorter chain achieved slightly higher selectivity to diesel-like hydrocarbons. Fatty acid deoxygenation under small quantity of H₂ in inert gas is recommended for higher yield of diesel-like hydrocarbons compared to that under inert or rich hydrogen atmospheres as this condition results in lower coke formation. The recommended temperature for the fatty acid deoxygenation is at around 300 °C for reactions in a batch or semi batch reactor. At higher reaction temperatures, it could lead to dehydrogenation reaction in a larger extent. Meanwhile, the higher amount of the catalyst gives positive effect to the reaction rates and selectivity to diesel-like hydrocarbons of *n*-alkane. Besides that, it resulted in a slower catalyst deactivation.

In general, most of the recently demonstrated catalysts for the deoxygenation process were noble metals (Pd, or Pt) supported on mesoporous carbon. However, catalysts based on noble metals are expensive and unattractive for commercial applications. For future research, more economical catalysts (e.g. Ni, Co, Cu-based catalysts) need to be fully developed to obtain mesoporous catalysts with high metal content with small particles. Besides that,

examination of performance of the catalysts on laboratory scale and on a pilot scale as well as optimized catalyst regeneration method are needed to put the catalytic fatty acid deoxygenation to practical use.

Acknowledgements

Research University grant (no. 814181) from Universiti Sains Malaysia and a Sciencefund grant (no. 6013381) from Ministry of Science, Technology and Innovation (MOSTI) to support this research work are gratefully acknowledged. Lilis Hermida also thanks the Directorate General of Higher Education (DIKTI), Ministry of National Education of Indonesia for her PhD scholarship.

References

- [1] World Oil Outlook. Accessed on December 2013 from http://www.opec.org/opec_web/static_files_project/media/downloads/publications/WOO2012.pdf.
- [2] Leggett, J. The oil crunch securing the UK's energy future. Accessed on December 2013 from <http://peakoiltaskforce.net/wp-content/uploads/2008/10/oil-report-final.pdf>.
- [3] Abbas A, Ansumali S. Global potential of rice husk as a renewable feedstock for ethanol biofuel production. *Bioenergy Res* 2010;3:328–34.
- [4] Liu H, Cheng T, Xian M, Cao Y, Fang F, Zou H. Fatty acid from the renewable sources: a promising feedstock for the production of biofuels and bio-based chemicals. *Biotechnol Adv* 2014;32:382–9.
- [5] Ziolkowska JK. Evaluating sustainability of biofuels feedstocks: a multi-objective framework for supporting decision making. *Biomass Bioenergy* 2013;59 (425–40).
- [6] Sawangkeaw R, Ngamprasertsith S. A review of lipid-based biomasses as feedstocks for biofuels production. *Renewable Sustainable Energy Rev* 2013;25:97–108.
- [7] Bastianoni S, Coppola F, Tiezzi E, Colacevich A, Borghini F, Focardi S. Biofuel potential production from the *Orbetello lagoon* macroalgae: a comparison with sunflower feedstock. *Biomass Bioenergy* 2008;32:619–28.
- [8] Badlay AS, Abdullah AZ, Lee KL. Transesterification of crude *Jatropha* oil by activated carbon-supported heteropolyacid catalyst in an ultrasound-assisted reactor system. *Renewable Energy*. 2014;62 (10–7).
- [9] Santillan Jimenez E, Morgan T, Lacey J, Mohapatra S, Crocker M. Catalytic deoxygenation of triglycerides and fatty acids to hydrocarbons over carbon-supported nickel. *Fuel* 2013;103 (1010–7).
- [10] Sari E, Kim M, Salley SO, Ng KYS. A highly active nanocomposite silica-carbon supported palladium catalyst for decarboxylation of free fatty acids for green diesel production: correlation of activity and catalyst properties. *Appl Catal A*. 2013;467 (261–9).
- [11] Ping EW, Venkatasubbaiah K, Fuller IF, Jones CW. Oxidative heck coupling using Pd(II) supported on organosilane-functionalized silica mesocellular foam. *Top Catal* 2010;53 (1048–54).
- [12] Ping EW, Pierson J, Wallace R, Miller JI, Fuller IF, Jones CW. On the nature of the deactivation of supported palladium nanoparticle catalysts in the decarboxylation of fatty acids. *Appl Catal A*. 2011;396:85–90.
- [13] Shi H, Chen J, Yang Y, Tian S. Catalytic deoxygenation of methyl laurate as a model compound to hydrocarbons on nickel phosphide catalysts: remarkable support effect. *Fuel Process Technol* 2014;118:161–70.
- [14] Chen J, Yang Y, Shi H, Li M, Chu Y, Pan Z, et al. Regulating product distribution in deoxygenation of methyl laurate on silica-supported Ni–Mo phosphides: effect of Ni/Mo ratio. *Fuel* 2014;129:1–10.
- [15] Identity and analysis of total petroleum hydrocarbon. Total petroleum hydrocarbon page. Available at: http://www.bvsde.paho.org/bvsdtx/j/fulltext/tox_profiles/total.pdf. (Accessed January, 2013).
- [16] Faeije A, Alkhezai J, Al Laith AA. Fatty acid composition of three medicinal plants from Bahrain: new potential sources of γ -linolenic acid and dihomo- γ -linolenic. *Ind Crops Prod* 2013;43 (218–24).
- [17] Režanka J, Votruba J. Chromatography of very long-chain fatty acids from animal and plant kingdoms. *Anal Chim Acta* 2002;465 (273–97).
- [18] Encinar JM, Sánchez N, Martínez G, García J. Study of biodiesel production from animal fats with high free fatty acid content. *Bioresour Technol* 2011;102 (10907–14).
- [19] Adewale P, Mba O, Dumont MJ, Ngadi M, Cocciardi R. Determination of the iodine value and the free fatty acid content of waste animal fat blends using FT-NIR. *Vib Spectrosc* 2014;72 (72–8).
- [20] Režanka J, Sigler K. Odd-numbered very long-chain fatty acids from the microbial, animal and plant kingdom. *Prog Lipid Res* 2009;48 (206–35).
- [21] Lopes LS, Martins SR, Chizzotti ML, Busato KC, Oliveira IM, Neto ORM, et al. Meat quality and fatty acid profile of Brazilian goats subjected to different nutritional treatments. *Meat Sci* 2014;97 (602–8).
- [22] Myllyoja J, Aalto P, Savolainen P, Purola VM, Alopaeus V, Gronqvist J. Process for the manufacture of diesel range hydrocarbons. U.S. Patent No. 8,022,258; 2011.

- [23] Sharma A, Chaurasia SP, Dalai AK. Enzymatic hydrolysis of cod liver oil for the fatty acids production. *Catal Today*. 2013;207:93–110.
- [24] Pencic MC, Constenla DT, Carelli AA. Free-fatty acid profile obtained by enzymatic solvent-free hydrolysis of sunflower and soybean lecithin. *Food Chem* 2010;120 (332–8).
- [25] Brijwani K, Vadlani PV. Lipase-mediated hydrolysis of corn DDGS oil: kinetics of linoleic acid production. *Biochem Eng J* 2010;52 (289–95).
- [26] Valladao ABG, Torres AG, Freire DMG, Cammarota MC. Profiles of fatty acids and triacylglycerols and their influence on the anaerobic biodegradability of effluents from poultry slaughterhouse. *Bioresour Technol* 2011;102 (7043–50).
- [27] Parfene G, Horincar V, Tyagi AK, Malik A, Bahrim G. Production of medium chain saturated fatty acids with enhanced antimicrobial activity from crude coconut fat by solid state cultivation of *Yarrowia lipolytica*. *Food Chem* 2013;136 (1345–9).
- [28] Martins PF, Ito VM, Batisstella CB, Maciel MRW. Free fatty acid separation from vegetable oil deodorizer distillate using molecular distillation process. *Sep Purif Technol* 2006;48:78–84.
- [29] Tan CH, Ghazali HM, Kuntom A, Tan CP, Ariffin AA. Extraction and physico-chemical properties of low free fatty acid crude palm oil. *Food Chem* 2009;113 (645–50).
- [30] Hayyan A, Alam MZ, Miqhani MES, Kabbashi NA, NINM Halkimi, Siran YM, et al. Reduction of high content of free fatty acid in sludge palm oil via acid catalyst for biodiesel production. *Fuel Process Technol* 2011;92 (920–4).
- [31] Maki-Arvela P, Rozmyszowicz B, Lestari S, Simakova O, Eranen K, Salmi T, et al. Catalytic deoxygenation of tall oil fatty acid over palladium supported on mesoporous carbon. *Energy Fuels* 2011;25 (2815–25).
- [32] Romney R, Charley R. *Forest chemicals review, International yearbook; New Orleans; Kriedt Enterprises; 2004.*
- [33] Mielke, T. The price outlook of palm and lauric oils and impacts from the global vegetable oil markets—a fundamental approach. In: *Paper presented at the palm and lauric oils conference & exhibition price outlook (POC), Kuala Lumpur, Malaysia, 2010.*
- [34] Top AGM. Production and utilization of palm fatty acid distillate (PFAD). *Lipid Technol* 2010;22(1):11–3.
- [35] Herrick AB, Jungermann E. Manufacture of soap from fatty acid. *JAOCs* 1963;140:616–8.
- [36] Adebajo MO, Akanni MS. The electrical conductance and viscosity of Nigerian traditional soaps in alcoholic media. *Colloids Surf A*. 2001;194:97–110.
- [37] Kuntom A, Kifli H, Iim PK. Chemical and physical characteristics of soap made from distillates fatty acids of palm oil and palm kernel oil. *JAOCs* 1996;73 (1):105–8.
- [38] Kuntom A, Kifli H. Properties of soaps derived from distilled palm stearin and palm kernel fatty acids. *J Surf Deter* 1998;1(3):329–34.
- [39] Chupa J, Sachdev A, Misner S, Smith GA. Soap, fatty acids, and synthetic detergents. In: James AK, editor. *Kent and Riegel's handbook of industrial chemistry and biotechnology*. New York: Springer Science + Business Media; 2007.
- [40] Li S, Wang Y, Dong S, Chen Y, Cao F, Chai F, et al. Biodiesel production from *Eruca sativa* Gars vegetable oil and motor, emissions properties. *Renewable Energy*. 2009;34 (1871–6).
- [41] Ooi YS, Zakaria R, Mohamed AR, Bhatia S. Catalytic conversion of palm oil-based fatty acid mixture to liquid fuel. *Biomass Bioenergy* 2004;27 (477–84).
- [42] Billaud F, Guilard Y, Minha AKT, Zahraa O, Lozano P, Pioch D. Kinetic studies of catalytic cracking of octanoic acid. *J Mol Catal* 2003;192 (281–8).
- [43] Asomaning J, Mussone P, Bressler DC. Pyrolysis of polyunsaturated fatty acids. *Fuel Process Technol* 2014;120:89–95.
- [44] Doronin VP, Potapenko OV, Lipin PV, Sorokina TP. Catalytic cracking of vegetable oils and vacuum gas oil. *Fuel* 2013;106 (757–65).
- [45] Kalnes T, Marker T, Shonnard DR. Green diesel: a second generation biofuel. *Int J Chem Reaction Eng* 2007;5:1542–80.
- [46] Yang Y, Wang Q, Zhang X, Wang L, Li G. Hydrotreating of C18 fatty acids to hydrocarbons on sulphided NiW/SiO₂-Al₂O₃. *Fuel Process Technol* 2013;116:165–74.
- [47] Srifa A, Faungnawakij K, Itthubenchapong V, Viriya-empikul N, Charinpanitkul T, Assabumrungrat S. Production of bio-hydrogenated diesel by catalytic hydrotreating of palm oil over NiMoS₂/γ-Al₂O₃ catalyst. *Bioresour Technol* 2014;158:81–90.
- [48] Pinto F, Varela FF, Goncalves M, Andre RN, Costa P, Mendes B. Production of bio-hydrocarbons by hydrotreating of pomace oil. *Fuel* 2014;116:84–93.
- [49] Bezergianni S, Dimitriadis A, Kaiogianni A, Pilavachi PA. Hydrotreating of waste cooking oil for biodiesel production. Part I: effect of temperature on product yields and heteroatom removal. *Bioresour Technol* 2010;101:6651–6.
- [50] Lestari S, Maki-Arvela P, Beltramini J, Lu GQM, Murzin DY. Transforming triglycerides and fatty acids into biofuels. *ChemSusChem* 2009;2:1109–19.
- [51] Maki-Arvela P, Kubickova I, Snare M, Eranen K, Murzin DM. Catalytic deoxygenation of fatty acids and their derivatives. *Energy Fuels* 2007;21:30–41.
- [52] Snare M, Kubickova I, Maki-Arvela P, Eranen K, Murzin DY. Heterogeneous catalytic deoxygenation of stearic acid for production of biodiesel. *Ind Eng Chem Res* 2006;45 (5708–15).
- [53] Snare M, Kubickova I, Maki-Arvela P, Chichova D, Eranen K, Murzin DY. Catalytic deoxygenation of unsaturated renewable feedstocks for production of diesel fuel hydrocarbons. *Fuel* 2008;87 (933–45).
- [54] Kitiyanan B, Ung-Jinda C, Meeyoo V, Rirkosomboon T, Rangsunvigit P. Catalytic deoxygenation of oleic acid over ceria-zirconia catalysts. In: *Proceeding of AIChE annual meeting, Philadelphia; 2008.*
- [55] Morgan T, Grubb D, Santillan-Jimenez E, Crocker M. Conversion of triglycerides to hydrocarbons over supported metal catalysts. *Top Catal* 2010;53 (820–9).
- [56] Chiappero M, Do PFM, Crossley S, Lobban LL, Resasco DE. Direct conversion of triglycerides to olefins and paraffins over noble metal supported catalysts. *Fuel* 2011;90 (1155–65).
- [57] Snare M, Kubickova I, Maki-Arvela P, Eranen K, Warna J, Murzin DY. Production of diesel fuel from renewable feeds: kinetics of ethyl stearate decarboxylation. *Chem Eng J* 2007;134:29–34.
- [58] Rothenberg G. *Catalysis*. In: Kirk-Othmer, editor. *Encyclopedia of chemical technology*. New York: John Wiley & Sons, Inc.; 2001.
- [59] Madsen AT, Rozmyszowicz B, Simakova IL, Kilpio I, Anne-Riikka L, Kordas K, et al. Step changes and deactivation behavior in the continuous decarboxylation of stearic acid. *Ind Eng Chem Res* 2011;50 (11049–58).
- [60] Hermida I, Abdullah AZ, Mohamed AR. Nickel functionalized mesostructured cellular foam (MCF) silica as a catalyst for solventless deoxygenation of palmitic acid to produce diesel-like hydrocarbons. In: *Mendez-Vilas A, editor. Materials and processes for energy: communicating current research and technological developments*. Boca Raton, USA: Brown Walker Press; 2013. p. 312–9.
- [61] Roh HS, Eum IH, Jeong DW, Yi BE, Na JG, Ko CH. The effect of calcination temperature on the performance of Ni/MgO-Al₂O₃ catalysts for decarboxylation of oleic acid. *Catal Today*. 2011;164 (457–60).
- [62] Santiago N, Sanchez-Castillo MA, Corright RD, Dumesic JA. Catalytic reduction of acetic acid, methyl acetate, and ethyl acetate over silica-supported copper. *J Catal* 2000;193:16–28.
- [63] Lestari S, Maki-Arvela P, Simakova I, Beltramini J, Lu GQM, Murzin DY. Catalytic deoxygenation of stearic acid and palmitic acid in semibatch mode. *Catal Lett* 2009;130:48–51.
- [64] Simakova I, Simakova O, Maki-Arvela P, Murzin DY. Decarboxylation of fatty acids over Pd supported on mesoporous carbon. *Catal Today*. 2010;150:28–31.
- [65] Rozmyszowicz B, Maki-Arvela P, Tokarev A, Anne-Riikka L, Eranen K, Murzin DY. Influence of hydrogen in catalytic deoxygenation of fatty acids and their derivatives over Pd/C. *Ind Eng Chem Res* 2012;51 (8922–7).
- [66] Kubickova I, Snare M, Eranen K, Maki-Arvela P, Murzin DY. Hydrocarbons for diesel fuel via decarboxylation of vegetable oils. *Catal Today*. 2005;106:197–200.
- [67] Bernas H, Eränen K, Simakova I, Anne-Riikka L, Kordas K, Myllyoja J, et al. Deoxygenation of dodecanoic acid under inert atmosphere. *Fuel* 2010;89 (2033–9).
- [68] Lestari S, Simakova I, Tokarev A, Maki-Arvela P, Eranen K, Murzin DY. Synthesis of biodiesel via deoxygenation of stearic acid over supported Pd/C catalyst. *Catal Lett* 2008;122 (247–51).
- [69] Kwon KC, Mayfield H, Marolla I, Nichols B, Mashburn M. Catalytic deoxygenation of liquid biomass for hydrocarbon fuels. *Renewable Energy*. 2011;36 (907–15).
- [70] Maki-Arvela P, Snare M, Eränen K, Myllyoja J, Murzin DY. Continuous decarboxylation of lauric acid over Pd/C catalyst. *Fuel* 2008;87 (3543–9).
- [71] Han J, Sun H, Ding Y, Lou H, Zheng X. Palladium-catalyzed decarboxylation of higher aliphatic esters: towards a new protocol to the second generation biodiesel production. *Green Chem*. 2010;12:463–7.
- [72] Ji Y, El-Sayed MA. The effect of stabilizers on the catalytic activity and stability of Pd colloidal nanoparticles in the Suzuki reactions in aqueous solution. *J Phys Chem B*. 2001;105 (8938–43).
- [73] Arend M, Nonnen T, Hoelderich WF, Fischer J, Groos J. Catalytic deoxygenation of oleic acid in continuous gas flow for the production of diesel-like hydrocarbons. *Appl Catal A*. 2011;399:198–204.
- [74] Rozmyszowicz B, Maki-Arvela P, Lestari S, Simakova O, Eranen K, Simakova I, et al. Catalytic deoxygenation of tall oil fatty acids over a palladium-mesoporous carbon catalyst: a new source of biofuels. *Top Catal* 2010;53 (1274–7).
- [75] Lestari S, Maki-Arvela P, Eranen K, Beltramini J, Lu GQM, Murzin DY. Diesel-like hydrocarbons from catalytic deoxygenation of stearic acid over supported Pd nanoparticles on SBA-15 catalysts. *Catal Lett* 2010;134 (250–7).
- [76] Ford JP, Immer JC, Lamb HH. Palladium catalysts for fatty acid deoxygenation: influence of the support and fatty acid chain length. *Top Catal* 2012;55 (175–84).
- [77] Immer JC, Kelly MJ, Lamb HH. Catalytic reaction pathways in liquid-phase deoxygenation of C18 free fatty acids. *Appl Catal A*. 2010;375 (134–9).
- [78] Immer JC, Lamb HH. Fed-batch catalytic deoxygenation of free fatty acids. *Energy Fuels* 2010;24 (5291–9).
- [79] Lestari S, Maki-Arvela P, Bernas H, Simakova O, Sjöholm R, Beltramini J, et al. Catalytic deoxygenation of stearic acid in a continuous reactor over a mesoporous carbon-supported Pd catalyst. *Energy Fuels* 2009;23:3842–5.
- [80] Na JG, Yi BE, Kim JN, Yi KB, Park SY, Park JH, et al. Hydrocarbon production from decarboxylation of fatty acid without hydrogen. *Catal Today*. 2010;156:44–8.

Kinetics Modeling and Mechanism Study for Selective Esterification of Glycerol with Lauric Acid Using 12-Tungstophosphoric Acid Post-Impregnated SBA-15

Pengyong Hoo* and Ahmad Zuhairi Abdullah

School of Chemical Engineering, Engineering Campus, Universiti Sains Malaysia, Seri Ampangan, 14300 Nibong Tebal, Pulau Pinang, Malaysia

S Supporting Information

ABSTRACT: Multiple kinetics models including simple power law model and mechanism-based models (nucleophilic substitution, Langmuir–Hinshelwood, and Eley–Rideal kinetics models) were investigated for selective esterification of glycerol with lauric acid using post-impregnated 12-tungstophosphoric acid SBA-15. Rate equations for all suggested models and mechanisms were derived, and appropriate experimental works were carried out. The model that best describes the studied reaction is found to be a combination of both a nucleophilic substitution mechanism and the Langmuir–Hinshelwood kinetics model with high accuracy and reliability of the model observed. The mechanism scheme describing the reaction from the bulk up to reactant molecular level and the interaction between reactant molecules on catalyst surface was outlined. Activation energy (E_a) of the studied reaction is found to be 35.62 kJ mol⁻¹ with an Arrhenius constant, A , of 1141.2 L mol⁻¹ g cat⁻¹ h⁻¹, which shows 40 wt %-HPW/IM to have a relatively low activation energy compared with that reported for catalyst on the same or reaction.

1. INTRODUCTION

In the attempt to tackle global glycerol oversupply caused by increased oleochemical, soap making, and biodiesel industrial production, value-added chemicals such as monoglyceride, epichlorohydrin, mesoxalic acid, allyl alcohol, and glycidol were synthesized to increase glycerol sales potential.^{1–3} As one of the many useful glycerol-derived chemicals, monoglyceride is traditionally synthesized via direct esterification of glycerol with fatty acid in the presence of homogeneous acid (sulfuric acid, phosphoric acid, or organic sulfonic acid).^{4,5} However, heterogeneous catalysts are favored for having higher monolaurin selectivity, being more environmental friendly, and having an ease of separation of catalyst that could be achieved with less expensive product purification processes.⁶

Keggin-type heteropoly acids (HPA), especially 12-tungstophosphoric acid (HPW, H₃PW₁₂O₄₀) were often chosen to be incorporated as acid sites for many organic reactions owing to its high Brønsted acidity.^{7–9} Incorporation of HPW onto an inert support such as SBA-15 or MCM-41 via various techniques was reported to show superior catalyst activity with a high conversion of the tested reactions.^{10,11} Modification of catalyst material was also reported to reduce and eliminate the leaching of HPW from the supported catalyst.^{12,13} In our unpublished work, post-impregnated 12-tungstophosphoric acid supported on SBA-15 had shown promising catalytic performance on selective esterification of glycerol with lauric acid, forming monolaurin. Our effort is now focused on the investigation of kinetics modeling and mechanism study of the mentioned reaction.

Despite different catalysts used in earlier investigations, direct esterification of glycerol with lauric acid is traditionally assumed to be a nonreversible parallel reaction.¹⁴ Thus, an irreversible second-order power law model is suggested.^{14–16} However, simplified power law model could not accurately represent the

actual reaction. In fact, the models derived are also not related to any proposed mechanism. Motivated by this scenario, this work concentrates on the investigation of possible reaction pathways with the use of 12-tungstophosphoric acid (HPW)-incorporated SBA-15. Possible reaction pathways including nucleophilic (glycerol) substitution (NS) mechanism and Langmuir–Hinshelwood (LH) and Eley–Rideal (ER) kinetics models are the focus of this investigation.

2. EXPERIMENTAL METHODS

Typical SBA-15 was synthesized as reported in literature.¹⁷ HPW was incorporated into SBA-15 at 40 wt % loading via an incipient wetness impregnation method.¹⁸ A batch reactor with temperature controller and magnetic stirrer and connected to the vacuum pump was used. Samples were collected and analyzed using Agilent Technologies 7890A GC equipped with a CP-Sil SCB (15 m x 0.32 mm x 0.1 mm) column. To perform kinetics study for the designated reaction and catalyst, the rate equations for simple power law model, NS mechanism model, LH kinetics model, and ER kinetics model were derived and are summarized in Table 1. Parity plots for each of the derived models were plotted to check their accuracy and reliability. Also, the activation energy of the reaction using the mentioned catalyst is calculated from the Arrhenius plot using experimental rate constants (k) from a range of reaction temperatures. The obtained activation energy is then compared with other results reported for the same reaction to show the potential of the studied catalyst and process.

Received: June 24, 2015

Revised: July 30, 2015

Accepted: July 30, 2015

Published: July 30, 2015

Table 1. List of Models Proposed along with the Assumptions Made

model name	assumptions made	models derived
simple power law (SP)	(i) nonreversible parallel esterification reaction (ii) irreversible second-order power law model	(i) $-r_{FA} = -\frac{1}{W} \frac{dC_{FA}}{dt} = kC_G C_{FA}$ (ii) For $R = 1$, $\frac{1}{C_{FAD}} \frac{X_{FA}}{(1 - X_{FA})} = kWt$ (iii) For $R \neq 1$, $\ln \left(\frac{(R - X_{FA})}{R(1 - X_{FA})} \right) = kW(R - 1)C_{FAD}t$
nucleophilic substitution mechanism (NS)	(i) Nucleophile (glycerol) is substituted to form ester and remove water. (ii) Nucleophilic substitution of glycerol is rate determining. (iii) All other diffusion steps are considered fast and rapid step. (iv) Concentration of water in reactor is considered negligible because of continuous water removal.	(i) $r_{II} = k_{II}C_A \cdot C_G - k_{-II}C_E C_{H_2O} C_{II}$ (ii) $r_{II} = k' C_{II} \left[C_A C_G - \frac{C_E C_{H_2O}}{K_E} \right]$ (iii) For $R = 1$, $\frac{1}{C_{FAD}} \frac{X_{FA}}{(1 - X_{FA})} = kWt$ (iv) For $R \neq 1$, $\ln \left(\frac{(R - X_{FA})}{R(1 - X_{FA})} \right) = kW(R - 1)C_{FAD}t$
Langmuir–Hinshelwood mechanism (LH)	(i) Both reactant (lauric acid and glycerol) are adsorbed on catalyst surface. (ii) Reaction occurred between both adsorbed reactant on surface. (iii) All diffusion process are considered relatively rapid compared with the surface reaction between adsorbed reactants.	(i) $r_A = -\frac{dC_A}{dt} = +\frac{dC_C}{dt} = k_T \theta_A \theta_B$ (ii) For neither A nor B is strongly adsorbed, $r_A = k_T b_A b_B C_A C_B = k' C_A C_B$ (iii) For only A is strongly adsorbed, $r_A = \frac{k_T b_A b_B C_A C_B}{(b_B C_B)^2} = k'' \frac{C_A}{C_B}$ $(R - 1) \ln \left(\frac{1}{1 - X_A} \right) + X_A = \frac{k'' W}{C_{AD}} t$
Eley–Rideal mechanism (ER)	(i) Only one reactant is adsorbed on the catalysts surface. (ii) Reaction occurred between adsorbed reactant with another reactant from the bulk. (iii) All diffusion steps are rapid and considered relatively fast compared with surface reaction. (iv) Only lauric acid is covered on the catalyst surface, whereas glycerol react with adsorbed lauric acid from the bulk.	(i) $r_A = -\frac{1}{W} \frac{dC_A}{dt} = k_T \theta_A C_A$ (ii) $\left(\frac{X_A}{1 - X_A} \right) = k_T b_A C_{AD} \left[Wt - \ln \left(\frac{1}{1 - X_A} \right) \right]$

7853



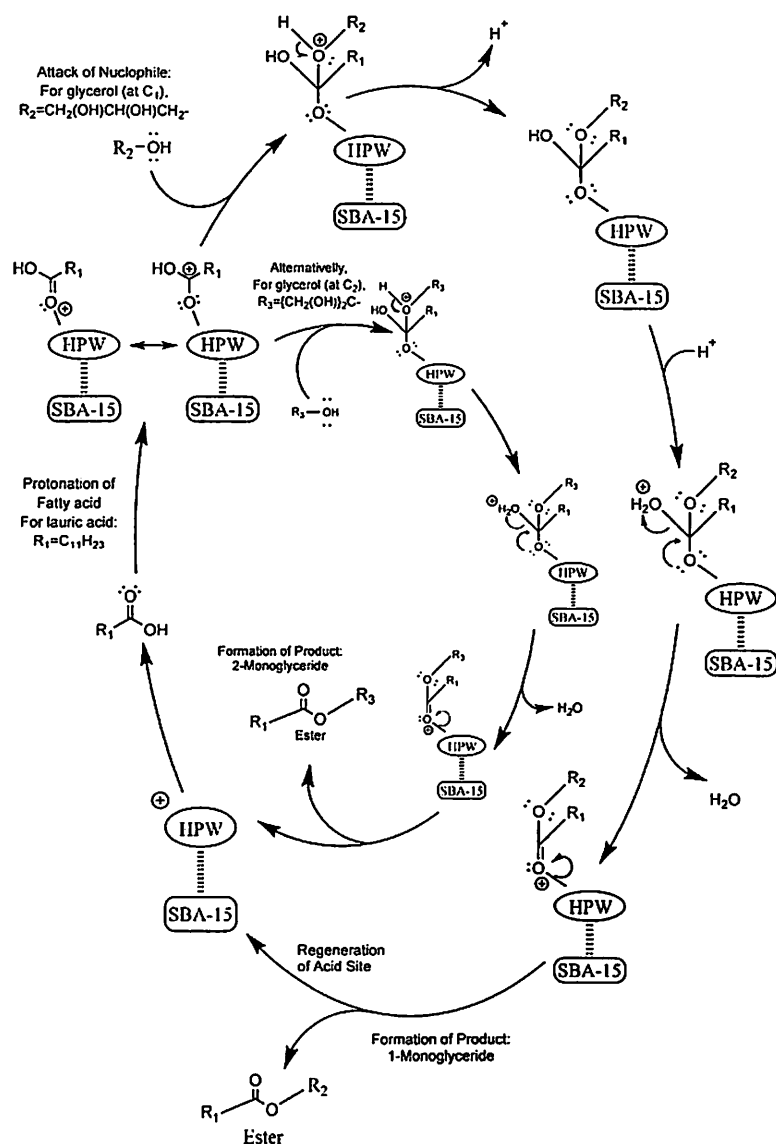


Figure 1. Proposed nucleophilic substitution mechanism producing 1-monolaurin and 2-monolaurin.

3. THEORETICAL BASIS

Historically, the simple power law model has been frequently used in the investigation of activation energy (E_a) of a heterogeneous catalyst, especially those that involve esterification. Though it enables rapid investigation to obtain the rate constant (k) and activation energy of developed catalysts, no mechanism details can be derived from the model. However, it is still mentioned in this text to provide a means of comparison with the rest of mechanism-based models proposed. In contrast, the mechanism of esterification between alcohol and carboxylic acid is well-known to be nucleophilic substitution. However, long-chain fatty acid esterification with glycerol catalyzed by synthesized catalysts has yet to be investigated under such a mechanism. Thus, a NS mechanism-based model has been derived and investigated in this work.

Two other mechanism-based models that are widely associated with heterogeneous catalysis, the LH and the ER kinetics models, have been explored as well. The most distinct

difference between these two models is the species adsorbed on the heterogeneous catalyst surface (acid site). Both reactants are assumed to be adsorbed for the LH model, whereas only one of the reactants is adsorbed for the ER model. All the proposed models of interest along with their respective assumptions made during derivation are shown in Table 1.

4. RESULTS AND DISCUSSION

Prior to investigating the irreversible second power law model, attempts in applying zero- and first-order power rate models to fit the same experiment data were done and ended with a disappointing result. When higher catalyst loadings were used, the second-order power model clearly demonstrated deviation. Such an observation suggests significance influence by the catalyst weight to the order of reaction. In fact, the order of reaction might not always be an integral value, as reported previously.^{19,20} Nevertheless, the second-order power model appeared to best fit most experimental data compared to both

zero- and first-order power law models. Thus, the second power model is chosen for further comparison to other mechanism-based models.

Moving on to the NS mechanism, the mechanism of selective esterification of glycerol with fatty acid could be related to nucleophile (alcohol) substitution.²¹ The reaction involves activation of reactants and attack of a nucleophile, followed by elimination of water, the formation of ester, and finally regeneration of catalyst.¹⁸ In this study, the possible mechanism paths concentrating on the formation of monolaurin while relating to the catalytic property of the synthesized catalyst are illustrated in Figure 1. Without discrimination between 1-monolaurin or 2-monolaurin, the rate equation of the mechanism in Figure 1 is derived and shown in Table 1. From the NS eq iv, the rate of the limiting reaction (II) is first-order with respect to both lauric acid and the available acid sites, making the overall order of the reaction a second-order reaction. A graph of $\ln[(R - X_{FA})/(R(1 - X_{FA}))]$ at different reaction temperatures versus t is plotted in Figure 2. The model was found to be of great fit (high

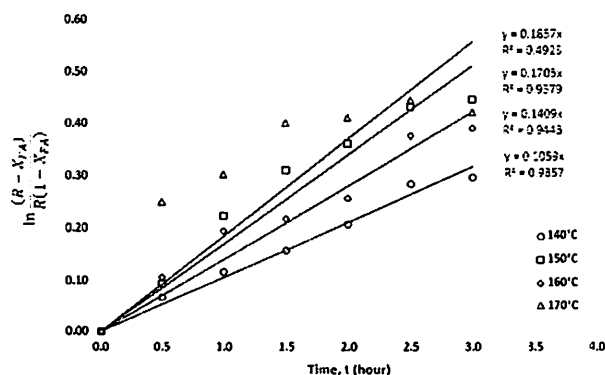


Figure 2. Nucleophilic substitution second-order model at different temperature.

R^2 value) at lower reaction temperatures (140–160 °C), whereas deviation is observed at higher reaction temperature (170 °C) as much lower R^2 value (0.4923) was found.

The high R^2 value suggested that at moderate reaction temperature (140–160 °C) selective esterification of glycerol with lauric acid forming monolaurin that was catalyzed by the synthesized catalyst follows the NS mechanism proposed in Figure 1. At higher reaction temperatures, the rate of esterification would increase because of the increment of the forward reaction rate constant, k . Because of the reaction endothermic nature, a higher conversion rate could be observed as well at the elevated reaction temperatures.^{22,23} At the same time, it was known that further esterification of monolaurin would occur.^{16,17} Thus, further esterification of monolaurin to form dilaurin or even trilaurin could have occurred at the higher reaction temperature, causing such deviation when experiment data were fitted into the proposed model.

The LH kinetics model describes the reaction of two reactant molecules on a heterogeneous catalyst surface. The derived model, LH eq iii, was fitted with experimental data and is illustrated in Figure 3. The experimental data are found to be well-fitted to the proposed kinetics model, with high R^2 values ($R^2 > 0.90$). Similarly, the deviation of experimental data found at the higher reaction temperature, 170 °C, had an R^2 value of only 0.4438. Such observations suggested that the model could not be used to correctly predict the reaction at the elevated reaction

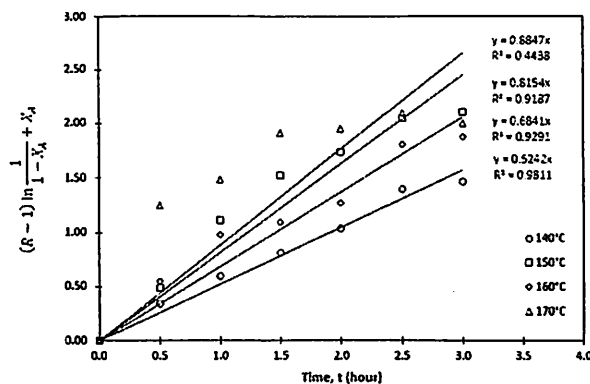


Figure 3. Langmuir-Hinshelwood (LH) kinetics model fitted at different temperatures.

temperature, which was attributed to the further esterification of dilaurin or trilaurin. Additionally, an elevated reaction rate could hinder the absorption strength of lauric acid and glycerol, which were assumed to be strongly adsorbed on the surface. At high temperatures, both lauric acid and glycerol would be weakly adsorbed compared to adsorption at lower temperatures. Thus, the derived model is more suitable for describing the reaction at moderate temperatures.

Similar to the LH kinetics model, the ER kinetics model describes the reaction between two reactant molecules on a heterogeneous catalyst surface, but only one of these is adsorbed (or strongly adsorbed) on the catalyst surface. Its kinetics model was derived as ER eq ii, and the result is plotted in Figure 4. From

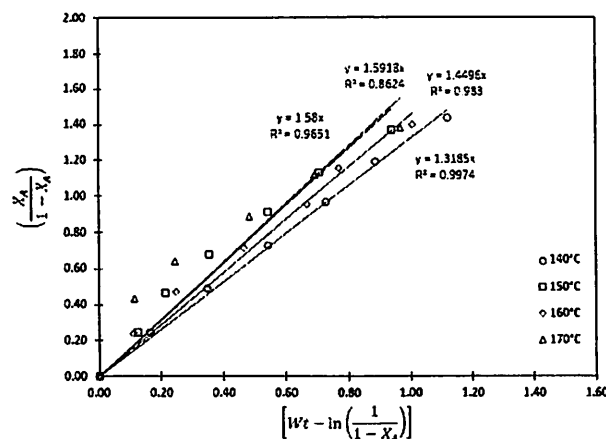


Figure 4. Eley-Rideal (ER) kinetics model fitted at different temperatures.

Figure 4, it is noted that the data fit the proposed ER model reasonably well with high R^2 values (0.8624–0.9974). Again, it is also inevitable that the lack of fit of the model is significant at high reaction temperatures. As discussed earlier, such deviation could be due to the effect of temperature toward the adsorption of reactant onto the catalyst surface. In ER kinetics models, it is assumed that lauric acid is adsorbed on the surface and reacts with glycerol from the bulk. Because the adsorption of lauric acid is exothermic, the effect of elevated temperature would have significant adverse effect on the lauric acid adsorption, thus

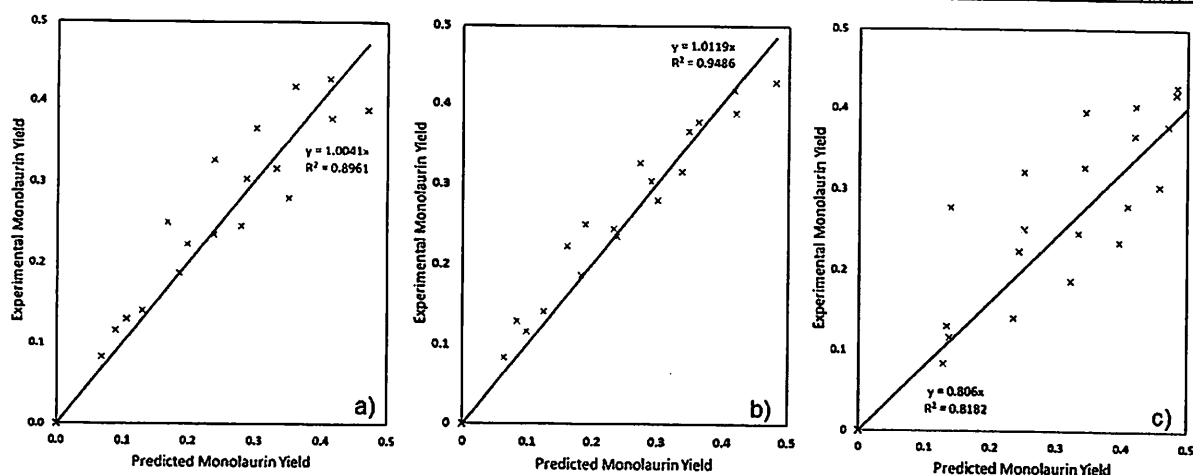


Figure 5. Parity plots of (a) nucleophilic substitution mechanism model, (b) Langmuir–Hinshelwood kinetics model, and (c) Eley–Rideal kinetics model.

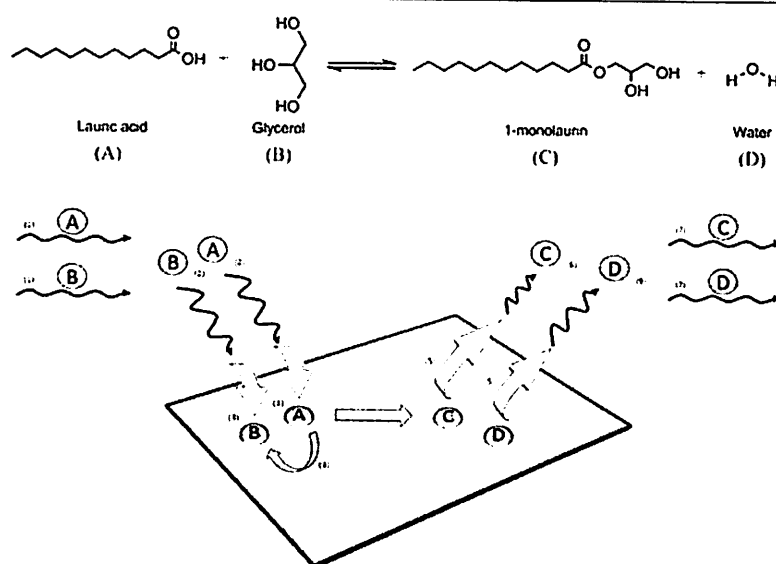


Figure 6. Proposed Langmuir–Hinshelwood kinetics model and its mechanism.

making the model less likely to correctly describe the actual case.²¹

Comparison of actual data to predicted result from each respective model was represented in the parity plot in Figure 5. The parity plots showed that both NS and LH kinetics models (Figure 5a,b, respectively) have high accuracy in representing the actual monolaurin yield because both models show slopes that are very near to unity (1.0041 for NS and 1.0119 for LH kinetics model). In contrast, despite having the highest R^2 value when plotted in its derived model, the ER model showed significant deviation of the predicted data from the actual ones (only 0.806 compared to unity) as shown in Figure 5c. Such findings suggest that the ER model does not accurately represent the studied reaction compared to the earlier two models.

On the basis of both actual experimental data fitting and parity plots, it is suggested that the actual mechanism for the studied reaction could be combination of both NS and LH mechanisms. Such claim could be justified by the observation that both models show high accuracy when comparing both experimental data and

predicted results. In fact, the combination of both models could lead to an overall mechanism that describes the reaction from the reactants' bulk to the molecular interaction between acid sites and reactant molecules. Revisiting the derivation of the LH kinetics model, it is assumed that only lauric acid molecules are strongly adsorbed on the catalyst surface whereas glycerol molecules are weakly adsorbed on the surface. It is understood that for both models, the esterification of glycerol with lauric acid occurs on the catalyst surface. The NS mechanism suggests that lauric acid molecules are activated by the vacant acid sites on the catalyst surface provided by HPW-impregnated SBA-15. The interaction between HPW-impregnated SBA-15 and the lauric acid molecule is predicted to be a strong ionic bond; thus, it is valid to make the assumption that lauric acid is strongly adsorbed on the surface. As such, combining both assumptions from both models, the actual mechanism is suggested to follow the NS mechanism presented in Figure 1 under the condition that glycerol molecules are weakly adsorbed on the catalyst surface. The attack of the nucleophile (glycerol) occurs after glycerol

from the bulk is weakly adsorbed on the surface. All steps involved in the reaction and its description are illustrated in Figure 6 and are as follows: (1) External diffusion of both lauric acid and glycerol from the bulk fluid to the fluid–solid interface between bulk and 40 wt %-HPW/IM and finally to the external surface of the catalyst. (2) Internal diffusion of lauric acid and glycerol to the internal surface (mesopores) of 40 wt %-HPW/IM. (3) Adsorption and activation of lauric acid by active acid sites (HPW) impregnated on the surface of the SBA-15 simultaneous to weak adsorption of glycerol on vacant sites. (4) Surface reaction between both adsorbed and activated lauric acid with weakly adsorbed glycerol on the catalyst surface, forming ester and water (Figure 1). (5) Desorption of both esters and water from the internal surface of the 40 wt %-HPW/IM that simultaneously regenerates vacant acid sites (HPW) on SBA-15. (6) Internal diffusion of both ester and water from the internal surface of the catalyst to the external surface. (7) External diffusion of both ester and water from external surface of the catalyst to fluid–solid interface between bulk and catalyst and finally into the bulk fluid.

5. CONCLUSIONS

The model that best describes the studied selective esterification of glycerol with lauric acid producing monolaurin is found to be a combination two mechanisms. The investigated models from NS mechanism with LH kinetics model showed high accuracy and reliability. The mechanism scheme describing the reaction from the bulk down to the reactant molecule level and the interaction between reactant molecules on the catalyst surface are proposed. Of course, the development of a final mathematical model combining both of the proposed mechanisms is not near completion in this study. However, such derivation works are beyond the scope of the current report. The authors understand the potential novelty to further investigate such matter and reserve the development of such work for the future.

■ ASSOCIATED CONTENT

● Supporting Information

The Supporting Information is available free of charge on the ACS Publications website at DOI: 10.1021/acs.iecr.5b02304.

Derivation of all involved models: (A) irreversible second order power model, (B) nucleophilic substitution mechanism, (C) Langmuir–Hinshelwood kinetics model, and (D) Eley–Rideal kinetics model. (PDF)

■ AUTHOR INFORMATION

Corresponding Author

*E-mail: arthur.py.hoo@gmail.com.

Funding

A Research University grant (814181) from Universiti Sains Malaysia and Transdisciplinary Research Grant Scheme (6762001) from Malaysian Ministry of Education are gratefully acknowledged.

Notes

The authors declare no competing financial interest.

■ ACKNOWLEDGMENTS

We thank the Universiti Sains Malaysia (USM) and School of Chemical Engineering for all the financial and technical support.

■ ABBREVIATIONS

- HPA = heteropoly acid
 HPW = 12-tungstophosphoric acid
 SBA-15 = Santa-Barbara Amorphous No. 15
 MCM-41 = Mobil Composition of Matter No. 41
 GC = gas chromatography
 k = rate constant
 E_a = activation energy
 SP = simple-power law
 NS = nucleophilic substitution
 LH = Langmuir–Hinshelwood
 ER = Eley–Rideal
 $-r_{FA}$ = rate of reaction with respect to fatty acid
 R = ratio of glycerol to lauric acid
 W = weight of catalyst (g)
 C_{FA} = instantaneous concentration of fatty acid (mol/L)
 C_G = instantaneous concentration of glycerol (mol/L)
 t = time (s)
 C_{PAD} = initial concentration of fatty acid (mol/L)
 X_{FA} = fatty acid conversion with respect to monoglyceride formation
 C_{H_2O} = instantaneous concentration of water (mol/L)
 C_{H^+} = instantaneous concentration of proton (mol/L)
 C_E = instantaneous concentration of ester
 K_E = equilibrium constant with respect to ester
 θ_A = coverage of reactant A molecules on the available active surface sites
 θ_B = coverage of reactant B molecules on the available active surface sites

■ REFERENCES

- (1) Johnson, D. T.; Taconi, K. A. The Glycerin Glut: Options for the Value-Added Conversion of Crude Glycerol Resulting from Biodiesel Production. *Environ. Prog.* **2007**, *26*, 338–348.
- (2) Valliyappan, T.; Bakhshi, N.; Dalai, A. Pyrolysis of Glycerol for the Production of Hydrogen or Syn Gas. *Bioresour. Technol.* **2008**, *99*, 4476–4483.
- (3) Bell, B. M.; Briggs, J. R.; Campbell, R. M.; Chambers, S. M.; Gaarenstroom, P. D.; Hippler, J. G.; Hook, B. D.; Kearns, K.; Kenney, J. M.; Kruper, W. J.; et al. Glycerin as a Renewable Feedstock for Epichlorohydrin Production. The Gte Process. *Clean: Soil, Air, Water* **2008**, *36*, 657–661.
- (4) Bossaert, W. D.; De Vos, D. E.; Van Rhijn, W. M.; Bullen, J.; Grobet, P. J.; Jacobs, P. A. Mesoporous Sulfonic Acids as Selective Heterogeneous Catalysts for the Synthesis of Monoglycerides. *J. Catal.* **1999**, *182*, 156–164.
- (5) Formo, M. W. Ester Reactions of Fatty Materials. *J. Am. Oil Chem. Soc.* **1954**, *31*, 548–559.
- (6) Pérez-Pariente, J. n.; Díaz, L.; Mohino, F.; Sastre, E. Selective Synthesis of Fatty Monoglycerides by Using Functionalised Mesoporous Catalysts. *Appl. Catal., A* **2003**, *254*, 173–188.
- (7) Gagea, B.; Lorgouilloux, Y.; Altintas, Y.; Jacobs, P.; Martens, J. Bifunctional Conversion of N-Decane over HPW Heteropoly Acid Incorporated into SBA-15 During Synthesis. *J. Catal.* **2009**, *265*, 99–108.
- (8) Hoo, P.-Y.; Abdullah, A. Z. Direct Synthesis of Mesoporous 12-Tungstophosphoric Acid SBA-15 Catalyst for Selective Esterification of Glycerol and Lauric Acid to Monolaurate. *Chem. Eng. J.* **2014**, *250*, 274–287.
- (9) Tropecêlo, A. I.; Casimiro, M. H.; Fonseca, I. M.; Ramos, A. M.; Vital, J.; Castanheiro, J. E. Esterification of Free Fatty Acids to Biodiesel over Heteropolyacids Immobilized on Mesoporous Silica. *Appl. Catal., A* **2010**, *390*, 183–189.
- (10) Dong, B.-B.; Zhang, B.-B.; Wu, H.-Y.; Li, S.-D.; Zhang, K.; Zheng, X.-C. Direct Synthesis, Characterization and Application in Benzalde-

hyde Oxidation of HPWA-SBA-15 Mesoporous Catalysts. *Microporous Mesoporous Mater.* 2013, 176, 186–193.

(11) Sheng, X.; Kong, J.; Zhou, Y.; Zhang, Y.; Zhang, Z.; Zhou, S. Direct Synthesis, Characterization and Catalytic Application of Sba-15 Mesoporous Silica with Heteropolyacid Incorporated into Their Framework. *Microporous Mesoporous Mater.* 2014, 187, 7–13.

(12) Sheng, X.; Zhou, Y.; Zhang, Y.; Duan, Y.; Zhang, Z.; Yang, Y. Immobilization of 12-Tungstophosphoric Acid in Alumina-Grafted Mesoporous LaSBA-15 and Its Catalytic Activity for Alkylation of O-Xylene with Styrene. *Microporous Mesoporous Mater.* 2012, 161, 25–32.

(13) Park, Y.; Shin, W. S.; Choi, S.-J. Ammonium Salt of Heteropoly Acid Immobilized on Mesoporous Silica (SBA-15): An Efficient Ion Exchanger for Cesium Ion. *Chem. Eng. J.* 2013, 220, 204–213.

(14) Sánchez, N.; Martínez, M.; Aracil, J. Selective Esterification of Glycerine to 1-Glycerol Monooleate. 2. Optimization Studies. *Ind. Eng. Chem. Res.* 1997, 36, 1529–1534.

(15) Aracil, J.; Martínez, M.; Sánchez, N.; Corma, A. Formation of a Jojoba Oil Analog by Esterification of Oleic Acid Using Zeolites as Catalyst. *Zeolites* 1992, 12, 233–236.

(16) Hermida, L.; Abdullah, A. Z.; Mohamed, A. R. Synthesis of Monoglyceride through Glycerol Esterification with Lauric Acid over Propyl Sulfonic Acid Post-Synthesis Functionalized SBA-15 Mesoporous Catalyst. *Chem. Eng. J.* 2011, 174, 668–676.

(17) Hermida, L.; Abdullah, A. Z.; Mohamed, A. R. Sulfated Zirconia for Esterification of Glycerol to Monoglyceride. *J. Appl. Sci.* 2010, 10, 3199–3206.

(18) Brahmkhatri, V.; Patel, A. 12-Tungstophosphoric Acid Anchored to SBA-15: An Efficient, Environmentally Benign Reusable Catalysts for Biodiesel Production by Esterification of Free Fatty Acids. *Appl. Catal., A* 2011, 403, 161–172.

(19) Blackmond, D. G. Reaction Progress Kinetic Analysis: A Powerful Methodology for Mechanistic Studies of Complex Catalytic Reactions. *Angew. Chem., Int. Ed.* 2005, 44, 4302–4320.

(20) Xu, F.; Ding, H. A New Kinetic Model for Heterogeneous (or Spatially Confined) Enzymatic Catalysis: Contributions from the Fractal and Jamming (Overcrowding) Effects. *Appl. Catal., A* 2007, 317, 70–81.

(21) Murzin, D. Y.; Salmi, T. *Catalytic Kinetics*; Elsevier: Amsterdam, The Netherlands, 2005.

(22) Kotwal, M.; Deshpande, S. S.; Srinivas, D. Esterification of Fatty Acids with Glycerol over Fe–Zn Double-Metal Cyanide Catalyst. *Catal. Commun.* 2011, 12, 1302–1306.

(23) Baroi, C.; Mahto, S.; Niu, C.; Dalai, A. K. Biofuel Production from Green Seed Canola Oil Using Zeolites. *Appl. Catal., A* 2014, 469, 18–32.

Monolaurin yield optimization in selective esterification of glycerol with lauric acid over post impregnated HPW/SBA-15 catalyst

Pengyong Hoo[†] and Ahmad Zuhairi Abdullah

School of Chemical Engineering, Universiti Sains Malaysia, Engineering Campus, Seri Ampangan,
14300 Nibong Tebal, Pulau Pinang, Malaysia

(Received 28 June 2015 • accepted 17 November 2015)

Abstract—Process optimization of selective esterification of glycerol with lauric acid catalyzed by highly uniformed SBA-15 catalysts post impregnated with 12-tungstophosphorus acid (HPW) has been elucidated via response surface methodology (RSM). The significance of factors including reaction time (*t*), reactants ratio (*R*) and temperature (*T*) was investigated and led to the development of response models for lauric acid conversion (*R*₁) and monolaurin yield (*R*₂). The optimized monolaurin yield operating condition (50% yield at *t*=3.18 h, *R*=4.6 and *T*=175 °C) was identified by using the developed models with high accuracy (98% confidence level, small standard deviation and error) and reproducibility (3 times). Comparison done with reported results showed the good performance of developed catalyst with significant reduction in reaction time needed to achieve similar lauric acid conversion and monolaurin yield.

Keywords: 12-Tungstophosphoric Acid, Mesoporous SBA-15, Response Surface Methodology, Yield, Optimization

INTRODUCTION

Optimization of chemical processes is an important goal for both academic and industrial purposes. In an effort to tackle glycerol oversupply from oleochemical, soap making and biodiesel industries, its conversion to other value added chemicals such as monoglyceride is necessary [1-3]. Whereas the use of homogeneous catalysts (sulfuric acid or phosphoric acid) is common in monoglyceride production, a greener approach with the use of novel heterogeneous acidic catalysts is actively investigated [4,5]. High monoglyceride selectivity, environmental friendliness, ease of catalyst separation and hence inexpensive product purification processes could be achieved with the use of high performance heterogeneous catalysts under their optimized operation conditions [6-8]. With such motivation, an investigation on optimization of lauric acid conversion and monolaurin yield was performed in this study.

In our previous report, supporting Keggin type heteropoly acids (HPA), especially 12-tungstophosphoric acid (HPW, H₃PW₁₂O₄₀) onto mesoporous SBA-15 could produce high performance heterogeneous catalyst for the esterification [9-11]. Due to its high Brønsted acidity, HPW is often reported to catalyze organic acid transformation, though systematic process optimization is rarely reported [12,13]. As such, to further exploit the superacidity of HPW impregnated on mesoporous SBA-15, a preliminary screening of the catalytic performance of post impregnated HPW/SBA-15 was performed [11]. Factors including HPW loading (10-40 wt%), reaction temperature (140-180 °C), glycerol to lauric acid ratio (1-6), catalyst loading (1-5 wt% with respect to lauric acid) and reaction duration (1-6 hours) were investigated. The results

suggested that the 40 wt% HPW impregnated on SBA-15 resulted in the most potential catalyst (40 wt%-HPW/SBA-15) in terms of lauric acid conversion (up to 80%) and monolaurin yield (up to 50%). Meanwhile, reaction time, reactant ratio and reaction temperature were observed to have significant effects on both of the responses of interest.

Extensive kinetic and mechanism studies at the fundamental molecular level were done upon the same catalyst [10]. It was found that the catalyst had lower activation energy (35.62 kJ mol⁻¹) as compared to the reported ones available in the literature. This result suggested that the catalyst could further improve the monolaurin productivity. However, optimized lauric acid conversion and monolaurin yield using this catalyst have yet to be reported. As a continuous effort to further improve the findings from our previous report [10], we are eager to further investigate and report the optimum catalytic performances that could be delivered by the catalyst of interest. The findings of this report could provide results in the practicability of this catalyst complementary to the fundamental mechanism studies as reported previously. As such, with this report, the overall picture of the catalytic performance of post impregnated HPW/SBA-15 mesoporous catalyst on both fundamental and practical point of views is presented to wider science audiences.

Motivated to fill in the gap of knowledge that is missing in the literature, the optimization of lauric acid conversion and monolaurin yield using 40 wt%-HPW/IM is attempted. Previously, non-optimized results shown by the catalyst was found to be rather inferior to those reported ones. Thus, the results of this optimization study could also be used for fair comparison with reported results. The optimized results and models using 40 wt%-HPW/IM in esterification could also be useful for future work involving the design of larger scale reactor and also for developing heterogeneous catalysts for similar reactions. At the same time, interac-

[†]To whom correspondence should be addressed.

E-mail: arthur.py.hoo@gmail.com

Copyright by The Korean Institute of Chemical Engineers.

tions between significant parameters or factors for both lauric acid conversion and monolaurin yield catalyzed by acidic heterogeneous catalysts have also been elucidated in this study.

By using Design Expert software package (version 8.0.6), response surface methodology (RSM) was applied for the development of experimental responses so that numerical experimented modeling could be performed. Along with obtaining the highest possible lauric acid conversion and monolaurin yield, mathematical models that can describe the significant of factors on the responses could be derived. Preliminary screenings suggested that 40 wt%-HPW/IM showed the highest conversion and monolaurin yield, while reaction time (A), reactant ratio (B) and reaction temperature (C) were observed to have significant effects on both responses. Thus, these factors were selected as the main focus in this investigation. The statistical models generated in this investigation could be useful in two ways: predicting the responses with known operating conditions and knowing the required operating conditions to achieve certain required responses. Thus, with this essential information, the developed models might be eventually useful in the design of a reactor for the reaction.

MATERIALS AND METHODS

1. Synthesis of Post Impregnated HPW/SBA-15

SBA-15 support was synthesized based on a reported method with minor modification [14]. In a typical preparation, 4.0 g Pluronic P123 (Sigma-Aldrich, Germany) was dissolved in 30 ml of deionized water and 120 ml of 2 M hydrochloric acid (R & J Chemicals) under stirring at 35 °C. The mixture was heated to 60 °C followed by the addition of 8.50 g of tetraethyl orthosilicate (TEOS, Alfa Aesar). Then, the solution was stirred rapidly for 30 minutes followed by slow stirring for the following 20 h. The content was transferred into a polyethylene bottle and aged for 48 h at 80 °C. After cooling to room temperature, the white precipitation was filtered, washed and dried at room temperature for 12 h, followed by another 12 h at 100 °C in an oven. The solid was then calcined in a furnace at 300 °C for 30 min and 500 °C for 6 h. The white powder obtained was SBA-15. HPW was incorporated into SBA-15 at 40 wt% loadings via incipient wetness impregnation method [12, 15]. SBA-15 was first hydrated with deionized water at a ratio of 2.5 ml/g of SBA-15. HPW solution with appropriate amount of HPW in deionized water was then added to the wet SBA-15 dropwise. The solid was then dried at 60 °C for 12 h, followed by at 100 °C for another 12 h.

2. Product Analysis

Selective esterification of glycerol (R & J Chemicals) with lauric acid (R & J Chemicals) to selectively form monolaurin was carried out in a batch system that consisted of a heating mantle with stirring and a three-necked flask as the reaction vessel. One of the necks was connected to a vacuum pump and another neck was fitted with a thermocouple for temperature measurement and control. Product mixtures were analyzed by a gas chromatograph (Agilent Technologies 7890A GC system) equipped with a CP-Sil 5CB (15 m×0.32 mm×0.1 mm) column. The lauric acid conversion and monolaurin selectivity were calculated as proposed by Pouilloux et al. [16].

Table 1. List of numeric factors and responses defined in design expert V8.0.6

Numeric factors	Name	Units	Low	High
A	Reaction time	Hour	3	6
B	Reactant ratio		1	5
C	Temperature	°C	150	180
Responses				
Y1	Fatty acid conversion	%		
Y2	Monoglyceride yield	%		

3. Response Surface Methodology (RSM)

Prior to RSM, a carefully designed DoE was preliminarily performed to decide significant design variables to be studied. Parameters including catalyst loading (1-5 wt%), reaction temperature (140-180 °C), reaction time (1-6 hours) and reactant ratio (glycerol: lauric acid; 6-1) were investigated. After reviewing the responses (both lauric acid conversion and monolaurin yield), we selected the three most significant factors--reaction time, *t*; reactant ratio, *R*; and reaction temperature, *T*--for further investigation. These factors and responses as defined in Design Expert V8.0.6 are of shown in Table 1.

Results for both responses were analyzed using sequential model sum of squares (Type I), lack of fit test, model summary statistics and analysis of variance (ANOVA). Plots and graphs, as well as 2D and 3D contours for all respective factors and responses were studied. The significance of each factor towards respective responses was determined and the final empirical model for each response was developed. The investigation was followed by optimization of the derived models by minimizing reaction time, reactant ratio and reaction temperature to achieve highest monolaurin yield. The derived model as well as the optimized factors were evaluated by repeating experiments using the optimized. Lastly, the accuracy of the models are also analyzed.

RESULTS AND DISCUSSION

1. Lauric Acid Conversion, Y1

Lauric acid conversion responses were in the range of 75.1-96.3% with small value of max to min ratio (1.282). Thus, no transformation of the responses was needed [17]. The sequential model sum of squares (Type I), lack of fit tests and model summary statistics are tabulated in Table 2, 3 and 4, respectively.

As a rule of thumb, the suggested model has to be the highest order model that is significant (represented by small *P*-value), not aliased, no lack of fit (with *P*-value>0.10) and small difference between adjusted *R*-squared and predicted *R*-squared values (within 0.20) [18]. In this case, quadratic polynomial model (Eq. (1)) is chosen. Eq. (1) also shows the lowest standard error, high *R*-squared (*R*²) value and lowest predicted residual sum of squares (PRESS) compared to all other models which are not aliased [19]. The observed differences between adjusted *R*-squared and predicted *R*-squared values are much less than 0.2 (only 0.0285, see Table 4), showing that the high *R*² values are not artificially improved by additional insignificant terms of the model [20].

Table 2. Sequential model sum of squares (type I) for lauric acid conversion, R1

Source	Sum of squares	df	Mean square	F value	P-value Prob>F
Mean vs total	2.375E+005	1	2.375E+005		
Linear vs mean	600.02	3	200.01	20.18	<0.0001
2FI vs linear	74.53	3	24.84	3.15	0.0453
<u>Quadratic vs 2FI</u>	<u>148.68</u>	<u>3</u>	<u>49.56</u>	<u>38.02</u>	<u><0.0001</u>
<i>Cubic vs quadratic</i>	15.73	7	2.25	2.98	0.0465
Residual	9.04	12	0.75		
Total	2.383E+005	29	8217.68		

Table 3. Lack of fit test results for lauric acid conversion, R1

Source	Sum of squares	df	Mean square	F value	P-value Prob>F
Linear	244.32	20	12.22	16.69	0.0027
2FI	169.79	17	9.99	13.64	0.0045
<u>Quadratic</u>	<u>21.11</u>	<u>14</u>	<u>1.51</u>	<u>2.06</u>	<u>0.2184</u>
<i>Cubic</i>	5.38	7	0.77	1.05	0.4963
Pure error	3.66	5	0.73		

Lauric Acid Conversion (%), (R1)

$$\begin{aligned}
 &= -603.5 + 26.87(A) + 15.24(B) + 6.877(C) \\
 &- 0.4927(A)(B) - 0.1172(A)(C) - 0.0499(B)(C) \\
 &- 0.4196A^2 - 0.5608B^2 - 0.01737C^2
 \end{aligned} \quad (1)$$

Next, ANOVA analysis was performed on Eq. (1), and the results are in Table 5. The quadratic model shows F-value of 70.16 with a very small P-value (<0.0001). Such result suggests that the model has significant effect on the response, with only 0.01% chance that the F-value is due to noise signals. Thus, the derived model has a significant effect in predicting the lauric acid conversion given that the reaction time, reactant ratio and reaction temperature are defined within the experimental ranges.

By evaluating the terms P-value, it is found that all terms are significant as they have P-values less than 0.05 [21,22]. Thus, no term needs to be removed from Equation 1. In accordance with the high R-squared value (97%), the lack of fit F-value of 2.06 shown in Table 5 implies that the lack of fit is not significant relative to the pure error [19,23]. The quadratic model also shows high signal to noise ratio (31.4, much greater than 4). Such result indi-

Table 4. Model summary statistics for lauric acid conversion, R1

Source	Standard deviation	R-square	Adjusted R-squared	Predicted R-squared	PRESS
Linear	3.15	0.7076	0.6725	0.5960	342.63
2FI	2.81	0.7955	0.7397	0.6138	327.48
<u>Quadratic</u>	<u>1.14</u>	<u>0.9708</u>	<u>0.9570</u>	<u>0.9285</u>	<u>60.60</u>
<i>Cubic</i>	0.87	0.9893	0.9751	0.8823	99.84

Table 5. Analysis of variance (ANOVA) results for lauric acid conversion, R1

Source	Sum of squares	df	Mean square	F value	P-value Prob>F
Model	823.23	9	91.47	70.16	<0.0001
<i>A - Reaction time</i>	174.75	1	174.75	134.04	<0.0001
<i>B - Reactant ratio</i>	79.98	1	79.98	61.35	<0.0001
<i>C - Temperature</i>	487.05	1	487.05	373.58	<0.0001
<i>AB</i>	20.17	1	20.17	15.47	0.0009
<i>AC</i>	64.20	1	64.20	49.24	<0.0001
<i>BC</i>	12.08	1	12.08	9.26	0.0067
<i>A²</i>	5.73	1	5.73	4.39	0.0497
<i>B²</i>	29.15	1	29.15	22.36	0.0001
<i>C²</i>	88.48	1	88.48	67.87	<0.0001
Residual	24.77	19	1.30		
<i>Lack of fit</i>	21.11	14	1.51	<u>2.06</u>	0.2184
<i>Pure error</i>	3.66	5	0.73		
Cor. total	848.00	28			

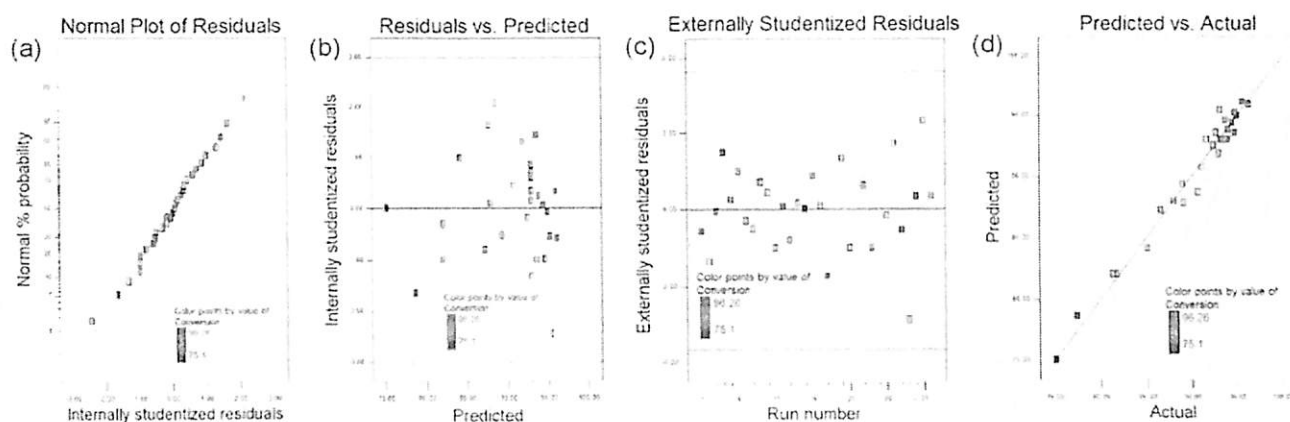


Fig. 1. Collective graphical diagnostics for Eq. (1).

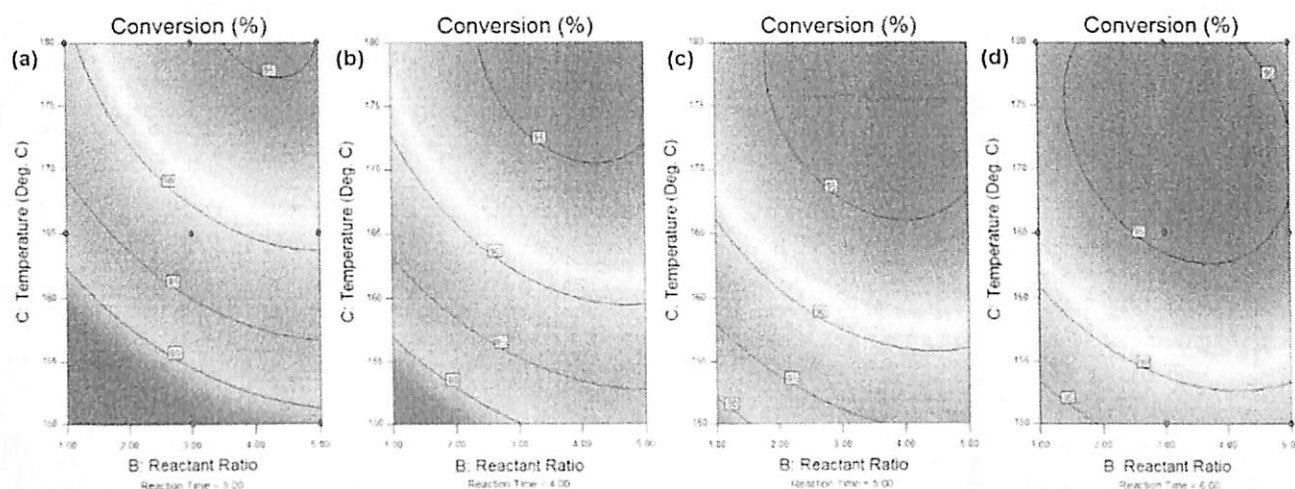


Fig. 2. Two dimensional contour model graphs (B & C) for lauric acid conversion (R1) at reaction time of (a) 3.0 hr, (b) 4.0 hrs, (c) 5.0 hrs and (d) 6.0 hrs.

icates that the model (Eq. (1)) can be used to navigate through the design space [24].

A series of graphical diagnostics (Fig. 1) are studied to further discuss the validity of the derived equation. First, the studentized normal plot of residuals (Fig. 1(a)) shows a straight line, suggesting the data residuals follow a normal distribution [25]. The scattering of data points near the line also indicates that there is no need for the transformation of the response to get better analysis. The random scattering of data points found in residuals VS predicted plot (Fig. 1(b)) verifies the constant variance assumption while not indicating the need for power transformation. From the externally studentized residuals plot in Fig. 1(c), it is concluded that all the data points do not deviate far from the values predicted. Similarly, the evenly split data points by the 45 degree line, which are seen in Fig. 1(d), describe high accuracy of the model. As a conclusion, the derived model (Eq. (1)) is statistically proven as an accurate model in representing response R1, i.e., the lauric acid conversion.

A set of two-dimensional contour plots describing the interaction between reactant ratio and reaction temperature towards lau-

ric acid conversion at different reaction times is shown in Fig. 2. High conversion (95%) was reached at the shortest reaction time available but with only relatively high reactant temperature ratio, as shown in Fig. 2(a). Generally, at longer reaction times, the 95% conversion contour is shifted in such a way that both reactant ratio and reaction temperature needed to reach 95% conversion are lowered. Interestingly, at the longest reaction time (6 hours), the 95% conversion contour shows two boundaries (Fig. 2(d)), rather than one as seen in Fig. 2(a) and 2(b). Such observation suggests that the conversion could not increase up to 100% even with the combination of the longest reaction time, the highest reaction temperature and the highest reactant ratio used in this study. It is also suggested that a maximum or optimum condition for highest conversion could be found in this RSM analysis, as two boundaries are found within the tested parameter ranges.

Based on the observation, the reaction temperatures can be identified to have much greater significance towards lauric acid conversion, followed by reactant duration and lastly reactant ratio used in the experiment. Such statement could be observed in Fig. 2(a), where both maximum and minimum could be found at all ranges

Table 6. Sequential model sum of squares (type I) for monolaurin yield, R2

Source	Sum of squares	df	Mean square	F value	P-value Prob>F
Mean vs total	51217.34	1	51217.34		
Linear vs mean	617.46	3	205.82	12.85	<0.0001
2FI vs linear	175.49	3	58.50	5.72	0.0047
<u>Quadratic vs 2FI</u>	<u>186.09</u>	<u>3</u>	<u>62.03</u>	<u>30.28</u>	<u><0.0001</u>
<i>Cubic vs quadratic</i>	9.76	7	1.39	0.57	0.7645
Residual	29.16	12	2.43		
Total	52235.30	29	1801.22		

of reactant ratio at the shortest reaction time. At any tested reactant ratio, the change in reaction temperature could drastically affect the lauric acid conversion even at the shortest reaction time. For a reaction to occur, effective collisions between reactants must occur. As such, increased reaction temperature enables higher kinetic energy and potential energy possessed by the reactant molecules. These energized reactant molecules could easily overcome the energy barrier for esterification to occur and ultimately increase in effective collisions frequency to form the products [26]. In fact, the use of 40 wt%-HPW/IM catalyst has allowed the reaction to occur at lower activation energy [10]. Thus, more reactant molecules now possesses sufficient energy to overcome the activation energy barrier for the esterification reaction as suggested in the shifting of the Maxwell-Boltzmann distributions [26]. On the other hand, at longer reaction time, the lauric acid conversion is shifted towards the maximum and the minimum response disappears. Thus, the prolonged reaction time allows more lauric acid to be converted to the product regardless of the reaction temperature and reactant ratio. Lastly, though reactant ratio shows significance effect towards lauric acid, it is highly dependent on the other two factors to achieve high lauric acid conversion. As a conclusion, when lauric acid is of main interest, reaction temperature is identified as the major factor affecting the outcome, followed by reaction duration and reactant ratio.

In short, the developed mathematical model from statistical analyses based on the actual experimental data is verified to be reliable and accurate. It also verifies that all tested factors (temperature, reaction time and reactant ratio) have significant effect towards lauric acid conversion. Due to its high reliability, the model could be used to provide rapid and accurate prediction within the tested experimental data ranges without the need for actual experimental work. In fact, by using the model, lauric acid conversion using the catalyst studied could be easily obtained by other researchers testing different catalysts for the same reaction. Thus, the availability

Table 7. Lack of fit tests for monolaurin yield, R2

Source	Sum of squares	df	Mean square	F value	P-value Prob>F
Linear	396.26	20	19.81	23.35	0.0012
2FI	220.77	17	12.99	15.30	0.0034
<u>Quadratic</u>	<u>34.68</u>	<u>14</u>	<u>2.48</u>	<u>2.92</u>	<u>0.1214</u>
<i>Cubic</i>	24.92	7	3.56	4.20	0.0668
Pure error	4.24	5	0.85		

of this model in the literature and the ease of using it provides the opportunity to exchange and compare results in a convenient way.

2. Monolaurin Yield, Y2

As the monolaurin yields occur within a range of 25.7-51.6% with small max to min ratio (2.006), no response transformation is needed [17]. Sequential model sum of squares (Type I), lack of fit tests and model summary statistics for R2 are tabulated in Tables 6, 7 and 8, respectively. The quadratic model is chosen as the suggested model to represent R2 due to its low P-value (<0.0001) (Table 6) with the highest P-value (0.1214) showing no lack of fit compared to other models as seen in Table 7 [18]. The suggested quadratic polynomial model also shows the lowest standard deviation (1.43), high R-squared (R2) values (adjusted and predicted) with the lowest predicted residual sum of squares (PRESS) (112.73) compared to all other models which are not aliased as shown in Table 8 [19].

In contrast to Eq. (1), the ANOVA analysis suggests that the response surface quadratic model consisted of insignificant terms with their respective P-value exceeding 0.10 [27,28]. Terms AB, A2 and C2 are removed from the model after reviewing their respective P-values. The updated ANOVA analysis for the reduced model is reported in Table 9. The new quadratic model is found to have significant effect on the response R2 with high F-value 66.46 while

Table 8. Model summary statistics for monolaurin yield, R2

Source	Standard deviation	R-square	Adjusted R-squared	Predicted R-squared	PRESS
Linear	4.00	0.6066	0.5594	0.4505	559.36
2FI	3.20	0.7790	0.7187	0.5606	447.32
<u>Quadratic</u>	<u>1.43</u>	<u>0.9618</u>	<u>0.9437</u>	<u>0.8893</u>	<u>112.73</u>
<i>Cubic</i>	1.56	0.9714	0.9332	0.6258	380.95

Table 9. Analysis of variance (ANOVA) (partial sum of squares - type III) result for reduced quadratic model of monolaurin yield, R2

Source	Sum of squares	df	Mean square	F value	P-value Prob>F
Model	964.73	6	160.79	66.46	<0.0001
A - Reaction time	16.46	1	16.46	6.81	0.0160
B - Reactant ratio	429.18	1	429.18	177.40	<0.0001
C - Temperature	1.00	1	1.00	0.42	0.5260
AC	22.57	1	22.57	9.33	0.0058
BC	48.34	1	48.34	19.98	0.0002
B ²	177.46	1	177.46	73.35	<0.0001
Residual	53.23	22	2.42		
Lack of fit	48.98	17	2.88	3.40	0.0907
Pure error	4.24	5	0.85		
Cor. total	1017.96	28			

maintaining its low P-value (<0.0001). All terms in the model are now significant except the experimental factor C, which must not be removed. The difference between the new adjusted R2 (0.9335) and predicted R2 (0.8877) is only 0.0458, which is smaller than 0.2 [20]. Thus, the quadratic model could be used to represent response R2 and fit the experimental data to a reasonable extent. Furthermore, the quadratic model also shows high signal to noise ratio (30.6, much greater than 4), implying that the model (Eq. (2)) could be used to navigate the design space [24]. The quadratic model representing R2 is labelled as Eq. (2).

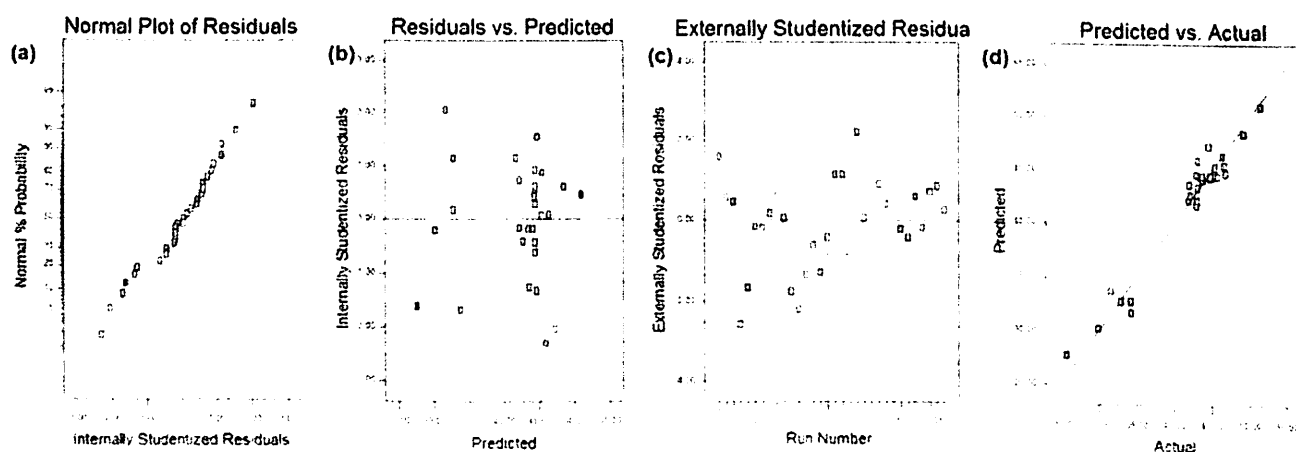
$$\begin{aligned} \text{Monoglyceride Yield (\%), R2} \\ = 19.18 + 10.47(A) - 4.37(B) + 0.041(C) \\ - 0.068(A)(C) + 0.095(B)(C) - 1.349B^2 \end{aligned} \quad (2)$$

A series of graphical analyses for response model R2 are illustrated in Fig. 3. From Fig. 3(a), data points are scattered near the straight line of the studentized normal plot of residuals, suggesting the data points form a normal distribution [25]. Random scattering of the data points found in Fig. 3(b) verifies the constant variance assumption and not suggesting the need for power transformation [29]. No deviation of data point is observed from externally studentized residuals plot (Fig. 3(c)) and residual vs predicted

plot (Fig. 3(d)). Data points in the predicted vs actual plot (Fig. 3(d)) scatter evenly around the 45 degree line, indicating all points are accurately predicted by the model derived. Thus, the derived quadratic response model (Eq. (2)) is verified to be a reliable model to represent the monolaurin yield, R2.

Essentially, a simplified monolaurin yield representing model has been developed using statistical data from the actual experimental data. Different from the lauric acid conversion model developed earlier, we found that by removing some of the terms from the equation, better reliability and accuracy of the model could be obtained. Similar to the lauric acid response model, this monolaurin yield statistical model is found to be more simplified without a compromise for accuracy. The model could be translated as a simple tool to accurately predict the monolaurin yield, which is of the most importance in the study of material catalyzing the esterification of glycerol with long chain fatty acid. As such, the development of Eq. (2) would make a good addition to the current gap of knowledge specifically in this field of study.

The interaction between reactant ratio (B) and reaction temperature (C) was investigated by 2-D contours of monolaurin yield (R2) at different reaction times as shown in Fig. 4. Interestingly, the highest monolaurin yield is obtained only at the shortest reac-


Fig. 3. Collective graphical diagnostics for Eq. (2).

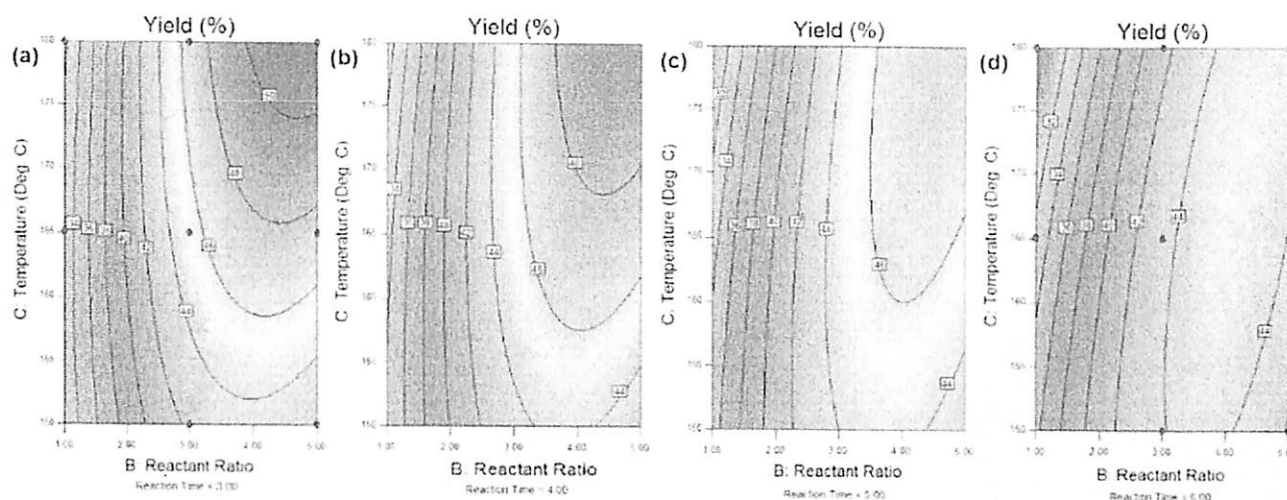


Fig. 4. Two-dimensional contour model graphs (B & C) for monolaurin yield (R2) at (a) 3.0 hrs, (b) 4.0 hrs, (c) 5.0 hrs and (d) 6.0 hrs.

tion time (3 hours) compared to the rest of the 2-D contour graphs at longer duration. From Fig. 4(a), the monolaurin yield contour is shifted towards higher reactant ratio and reaction temperature for higher reactant yield. Also, high yield contour could only be found at reactant ratios higher than 3. The minimum temperature point was found with increasing the reactant ratio. For instance, to achieve 44% yield, a minimum of 153 °C and a reactant ratio of 4 are required, and for 46% yield, a minimum of 158 °C and reactant ratio of 4.1 are needed. However, with increasing the reaction time, the higher yield contour begins to disappear, suggesting a decrease in yield.

To understand the disappearance of high monolaurin yield contour at longer reaction time, one must first understand the possible products formed in the reaction mixture. Monolaurin produced by esterification between glycerol and lauric acid could undergo further esterification with or without catalyst, as lauric acid itself could autocatalyze the reaction [30]. At longer reaction, though high concentrations of monolaurin occur in the reaction mixture, this monolaurin is vulnerable to the attack of other lauric acid, thus forming dilaurin or even trilaurin. Although the employment of heterogeneous catalyst (in this case 40 wt%-HPW/IM) could significantly limit the formation of dilaurin and trilaurin, these two compounds are still able to form within the reaction mixture. Thus, at longer reaction times, more and more monolaurin is converted into dilaurin and even trilaurin, resulting in a reduction in monolaurin yield. As such, the most significant factor towards monolaurin yield could be suggested to be the reaction time.

On the other hand, the reactant ratio was found to have high significance towards monolaurin yield as well. Interestingly, at low reactant ratio (below 3), the reaction temperature is observed to be insignificant towards monolaurin yield as seen in Fig. 4(a). On the other hand, at higher reactant ratio (above 3), the effect of temperature becomes very significant towards monolaurin yield. Such observation suggests that the effect of temperature is highly dependent on reactant ratio, and the mode of interaction between these two factors is dictated by reactant ratio. At very low reactant ratio ($R=1$), poor dispersion of glycerol among activated lauric acid on

catalyst surfaces could be less effective as compared to that at higher reactant ratio [15]. Thus, longer time to achieve high yield is required. Furthermore, as most acid sites were located within the catalysts where reactant would need to diffuse into the pores of the catalysts where most acid sites were located in order to undergo the reaction [31]. At higher reactant ratio, more glycerol was used, thus increasing the probability of effective collisions within the mesopore channels [26]. Besides, higher glycerol concentration would also bring about the dilution effect of lauric acid within the reaction, thus decreasing the formation of di- or trilaurin during the reaction [32].

In short, the same factors are investigated for both responses, and their significance towards each response could be very different. For the interest of lauric acid conversion, reaction temperature is identified as the major factor affecting the outcome, followed by reaction duration and reactant ratio. However, as far as monolaurin yield is concerned, reaction time is deemed to have the most significant effect, followed by reactant ratio and reaction temperature. As mentioned earlier, all three factors are found to be significant towards both responses. When compared among themselves, interactions between these factors resulting in significance difference in responses have been elucidated and could be useful for future investigation.

Next, a collection of 3D response surface plots for R2 at different combination of factors are shown in Fig. 5 to enable study on the trend, minimum and maximum of the response with different combinations. Most importantly, the 3D response surfaces allow the observation on the monolaurin yield profiles that evolved with time, reactant ratio and temperature. 3D response surfaces showing interaction between reaction time (A) and reactant ratio (B) at different reaction temperatures are plotted in Fig. 5(a)-(c). A maximum point could be found in both Fig. 5(a) and (b) at a reactant ratio of 4 for different reaction times. Interestingly, both extreme (maximum and minimum) yields are shown in Fig. 5(c). Thus, it could be concluded that increased reaction temperature is only beneficial to our system for the right combination of reactant ratio and reaction time, allowing the possibility of optimum oper-

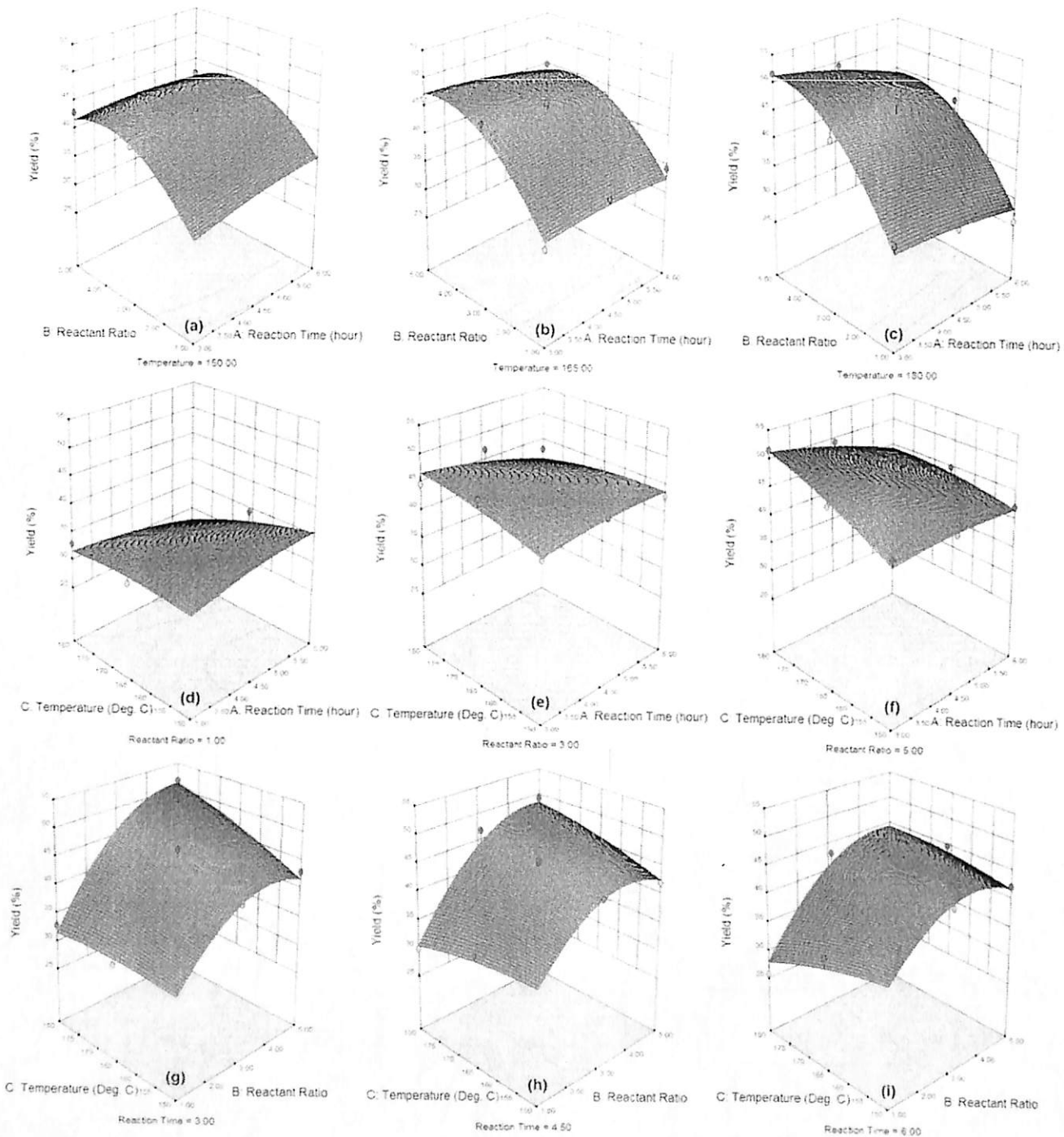


Fig. 5. Three-dimensional response surface model plots for monolaurin yield (R2) at (a) 150°C, (b) 165°C, (c) 180°C, (d) R=1, (e) R=3, (f) R=5, (g) 3 hrs, (h) 4.5 hrs, (i) 6 hrs.

ational conditions to be identified.

On the other hand, Fig. 5(d)-(f) show that the overall monolaurin yield increases with increasing reactant ratio. However, "flat" types of response surface are obtained, leading to the understanding that only minor interaction occurs between the reaction time and temperature when the reactant ratio is fixed. It is also understood that the effects of reaction time and temperature are less sig-

nificant when the reactant ratio is fixed. Thus, the reactant ratio should be the governing factor among all the three. Fig. 5(g)-(i) shows the 3D response surface graphs with varying reactant ratio and temperature at 3, 4.5 and 6 hours of reaction time. From these graphs, it is obvious that the 3-D surface curves show both maximum and minimum points with varying reactant ratio and temperature. Again, such observation suggests that an optimum point

must be available within the range of experimental work done. Besides, the range of monolaurin yield was wider at shorter reaction time when comparing all three plots in the last row. Such finding suggested that at the shortest tested reaction time, a maximum yield could be achieved using the optimum reactant ratio and reaction temperature. Though, such result is highly desirable due to high production rate. The higher production cost might be the drawback due to the higher reactant ratio or higher reaction temperature used. Thus, carefully optimized operating conditions should be studied to identify the optimum point to maximize the monolaurin yield in this case.

3. Process Optimization Based on Monolaurin Yield, R2

Knowing the possible existence of an optimum point in monolaurin yield, numerical optimization in RSM is employed to inves-

tigate and identify such an optimum point. All constraints are set to obtain the maximum possible monolaurin yield. The goals are set to be in the range of lower and upper limits for all three factors (A, B and C). As maximizing the conversion would not always return with maximized yield, conversion is removed from the criteria by setting its goal to none. The yield is set to reach its target, i.e. 50% yield, to avoid any extreme parameter points chosen (at the lower or upper limit of each factor). Fifty-four solutions are returned when such constraints are used. The selected solution with the highest desirability suggests that 50% yield could be achieved by using a reactants ratio of 4.6, at 175 °C in a 3.18 hours of reaction time.

The optimized experimental conditions are confirmed by repeating the experiment for three times using the proposed optimized

Table 10. Statistical analysis for confirmatory runs of optimized conditions

Statistical analysis	Experiment #1	Experiment #2	Experiment #3
Monolaurin yield (%)	49.22	49.93	50.41
Difference from predicted value	-0.78	-0.07	+0.41
Percentage difference (%)	-1.56	-0.14	+0.82
Mean (%)		49.85	
Variance (% ²)		0.2390	
Standard deviation (%)		0.4888	

Table 11. Comparison between the obtained catalyst activities with reported results

Catalyst	Reactant ratio (R)	Reaction temperature (°C)	Catalysts loading (wt%)	Reaction time (hour)	Lauric acid conversion (%)	Monolaurin yield (%)	Remarks	References
HFAU 1	1 : 1	112	2	9	20.0	88.0	Zeolite Y; Addition of 10 wt% Monolaurin	[33]
M10H	1 : 1	120	5	8	92.0	62.0	Hybrid MCM-41 material containing simultaneous alkyl (methyl or propyl) and sulfonic acid groups	[34]
HB400	1 : 1	100	5	10	32.5	59.5	Modified Zeolite Beta: different Si/Al ratio (15, 50, 400)	[35]
H-Beta	1 : 1	100	5	24	20.0	60.0	Zeolite Y; Addition of 10 wt% Monolaurin	[36]
F10MH-C	1 : 1	100	5	7	50.0	73.0	Chlorosulfonic functionalized SO ₃ H-phenyl-MCM-41	[37]
M40H	1 : 1	100	5	8	61.0	56.7	Hybrid MCM-41 material containing methyl and sulfonic acid groups	[38]
TBMMT	6 : 1	130	5	8	80.0	58.4	Montmorillonite modified with tetra-n-butylammonium bromide (TBAB)	[32]
DMC-50 °C	1 : 1	180	7	1	75.0	49.5	Fe-Zn double-metal cyanide catalyst	[39]
HSO ₃ -SBA-15	4 : 1	160	5	7	95.0	68.0	Propyl sulfonic acid functionalized SBA-15 mesoporous catalysts	[30]
SBA-15-SO ₃ -H(1)	4 : 1	160	14	20	95.0	67.0	Propyl sulfonic acid -modified SBA-15 with different acid weight	[40]
40 wt%-HPW/DS	4 : 1	160	2.5	6	73.0	52.0	Direct synthesized 12-tungstophosphoric acid SBA-15	[9]
40 wt%-HPW/IM	4.6 : 1	175	2.5	3.18	92.0	49.9	Optimized reaction conditions	This study

conditions. The results are shown in Table 10. It is obvious that the optimized conditions suggested are highly accurate as the responses found from the three confirmatory runs are very close to the desired yield (50%). Differences between the predicted yield and the experimental yield are found to be within 98% confidence level. Only small standard deviation is shown by the three experimental responses to suggest high repeatability of the experiments with very small error.

4. Comparison of Optimized Catalytic Performance

As the optimum point has been identified, the reported results from the literature can be compared. The past reported results based on conversion and yield of monolaurin together with our optimized results are compared in Table 11. Though slightly higher temperature was used as compared to some previously reported studies, the duration of reaction required was greatly reduced from around 20 hours down to only less than 4 hours by using 40 wt%-HPW/IM. Even though different reactors and catalysts were used, significant reduction in reaction time would be a major advantage from a chemical engineering point of view. The reduction of reaction time as well as reactant ratio could be translated into much better industrial manufacture of monolaurin in terms of time and energy consumed. In short, the applicability of the statistical models developed in this study as well as its high reliability and accuracy justifies this approach to modeling the process.

CONCLUSIONS

The development of both lauric acid conversion and monolaurin yield response models was achieved by the use of RSM method. Highly accurate empirical quadratic response models for both lauric acid conversion and monolaurin yield were developed as Eqs. (1) and (2). The significance of factors including reaction time, reactant ratio and reaction temperature was successfully elucidated. All three factors examined were found to have significant effect towards both responses. Optimized monolaurin yield was achieved at a reactant ratio of 4.6, 175 °C in 3.18 hours. The optimized conditions resulted in 50% monolaurin yield with high repeatability and confidence level (98%) with very low level of error. When compared with reported catalysts, the use of 40 wt%-HPW/IM enables low catalyst loading and short reaction time to reach high lauric acid conversion and monolaurin yield as compared to those reported ones. Moreover, the contribution of developed responses models as a rapid and accurate prediction tools could fill in the gap specifically in this area of study. These statistically accurate models could provide supplementary information on the catalytic performance of the developed catalyst and correlation with the characteristics of the catalyst as reported in our past publication. The behavior of each factor towards both responses and the interaction between these factors are successfully explained. This results could provide useful information regarding the esterification of glycerol with long chain fatty acid to be extended to other setup and catalyst system.

ACKNOWLEDGEMENT

A Research University Individual (RUI) grant (814181) and Dana

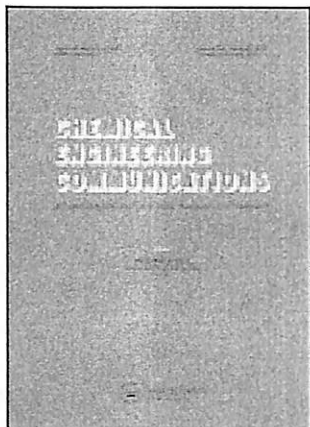
Inovasi Awal (AUPI 00234) from Universiti Sains Malaysia and Transdisciplinary Research Grant Scheme (6762001) from Malaysian Ministry of Education are gratefully acknowledged.

REFERENCES

1. B. M. Bell, J. R. Briggs, R. M. Campbell, S. M. Chambers, P. D. Gaarenstroom, J. G. Hippler, B. D. Hook, K. Kearns, J. M. Kenney and W. J. Kruper, *CLEAN-Soil, Air, Water*, **36**, 657 (2008).
2. D. T. Johnson and K. A. Taconi, *Environ. Prog.*, **26**, 338 (2007).
3. T. Valliyappan, N. Bakhshi and A. Dalai, *Bioresour. Technol.*, **99**, 4476 (2008).
4. M. W. Formo, *J. Am. Oil Chem. Soc.*, **31**, 548 (1954).
5. A. Carlos, *Catalytic processing of glycerol to fuels and chemicals*, in *Next Generation Biofuels and bio-based Chemicals* (2009), Trieste.
6. J. n. Pérez-Pariente, I. Díaz, F. Mohino and E. Sastre, *Appl. Catal., A*, **254**, 173 (2003).
7. P. Kumar, V. Srivastava and I. Mishra, *Korean J. Chem. Eng.*, **32**, 1774 (2015).
8. W. Wan Abdullah, W. Wan Abu Bakar and R. Ali, *Korean J. Chem. Eng.*, **32**, 1999 (2015).
9. P.-Y. Hoo and A. Z. Abdullah, *Chem. Eng. J.*, **250**, 274 (2014).
10. P.-Y. Hoo and A. Z. Abdullah, *Ind. Eng. Chem. Res.*, **54**, 7852 (2015).
11. P.-Y. Hoo and A. Z. Abdullah, *Characteristics of post-Impregnated SBA-15 with 12-tungstophosphoric acid and correlation with catalytic activity in selective esterification of glycerol to monolaurate*, in *Extended Abstracts, International Conference on Chemical and Biochemical Engineering* (2015), Paris. Available online: <http://goo.gl/yPTzy3>.
12. B. Gagea, Y. Lorgouilloux, Y. Altintas, P. Jacobs and J. Martens, *J. Catal.*, **265**, 99 (2009).
13. A. I. Tropecêlo, M. H. Casimiro, I. M. Fonseca, A. M. Ramos, J. Vital and J. E. Castanheiro, *Appl. Catal., A*, **390**, 183 (2010).
14. L. Hermida, A. Z. Abdullah and A. R. Mohamed, *J. Appl. Sci.*, **10**, 3199 (2010).
15. V. Brahmkhatri and A. Patel, *Appl. Catal., A*, **403**, 161 (2011).
16. Y. Pouilloux, S. Abro, C. Vanhove and J. Barrault, *J. Mol. Catal. A: Chem.*, **149**, 243 (1999).
17. M. S. Bhatti, A. S. Reddy and A. K. Thukral, *J. Hazard. Mater.*, **172**, 839 (2009).
18. E. M. Ejikeme, L. E. Aneke, G. N. Okonkwo, P. C. N. Ejikeme and N. Abalu Benjamin, *Int. J. Eng. Sci. Res. Technol.*, **2**, 442 (2013).
19. R. H. Myers and C. M. Anderson-Cook, *Response surface methodology: Process and product optimization using designed experiments*, **705**, Wiley (2009).
20. R. Azargohar and A. Dalai, *Micropor. Mesopor. Mater.*, **85**, 219 (2005).
21. B. Kiran and K. Thanasekaran, *Int. Biodeterior. Biodegrad.*, **65**, 840 (2011).
22. S. Cox and N. Abu-Ghannam, *Int. Food Res. J.*, **20**, 1537 (2013).
23. Y. Wu, S. Zhou, F. Qin, X. Ye and K. Zheng, *J. Hazard. Mater.*, **180**, 456 (2010).
24. A. Hafizi, A. Ahmadpour, M. Koolivand-Salooki, M. Heravi and F. Bamoharram, *J. Ind. Eng. Chem.*, **19**, 1981 (2013).
25. A. Panda, S. Chen, A. C. Shaw and H. G. Allore, *J. Immunol. Methods*, **398-399**, 19 (2013).

26. M. E. Starzak, *Maxwell-Boltzmann Distributions, in Energy and Entropy*. Springer (2010).
27. N. I. Bukhari, S. Kaur, S. H. Bai, Y. K. Hay, A. Bakar, A. Majeed, Y. B. Kang and M. J. Anderson. *Statistical Design of Experiments on Fabrication of Starch Nanoparticles-A Case Study for Application of Response Surface Methods (RSM)*, 2008; Available online: <http://goo.gl/AGF3jd>.
28. M. Demirel and B. Kayan, *Int. J. Ind. Chem.*, **3**, 1 (2012).
29. J. W. Osborne, *Pract. Assess. Res. Eval.*, **15**, 1 (2010).
30. L. Hermida, A. Z. Abdullah and A. R. Mohamed, *Chem. Eng. J.*, **174**, 668 (2011).
31. J. J. Chiu, D. J. Pine, S. T. Bishop and B. F. Chmelka, *J. Catal.*, **221** (2004).
32. M. Kotwal, S. S. Deshpande and D. Srinivas, *Catal. Commun.*, **12**, 1302 (2011).
33. E. Heykants, W. H. Verrelst, R. F. Parton and P. A. Jacobs, *Stud. Surf. Sci. Catal.*, **105**, 1277 (1997).
34. I. Díaz, C. Márquez-Alvarez, F. Mohino, J. n. Pérez-Pariente and E. Sastre, *J. Catal.*, **193**, 295 (2000).
35. M. da Silva-Machado, D. Cardoso, J. Perez-Pariente and E. Sastre, *Stud. Surf. Sci. Catal.*, **130**, 3417 (2000).
36. M. S. Machado, J. Perez-Pariente, E. Sastre, D. Cardoso and A. de Guereñu, *Appl. Catal., A*, **203**, 321 (2000).
37. F. Mohino, I. Díaz, J. Pérez-Pariente and E. Sastre, *Stud. Surf. Sci. Catal.*, **142**, 1275 (2002).
38. I. Díaz, F. Mohino, J. Pérez-Pariente and E. Sastre, *Appl. Catal., A*, **242**, 161 (2003).
39. T. Y. Wibowo, A. Z. Abdullah and R. Zakaria, *Appl. Clay Sci.*, **50**, 280 (2010).
40. L. Hermida, A. Z. Abdullah and A. R. Mohamed, *J. Porous Mater.*, **19**, 835 (2012).

This article was downloaded by: [Universiti Sains Malaysia]
On: 01 June 2015, At: 18:39
Publisher: Taylor & Francis
Informa Ltd Registered in England and Wales Registered Number: 1072954 Registered office: Mortimer House,
37-41 Mortimer Street, London W1T 3JH, UK



Chemical Engineering Communications

Publication details, including instructions for authors and subscription information:
<http://www.tandfonline.com/loi/gcec20>

Catalytic Etherification of Glycerol to Diglycerol Over Heterogeneous Calcium-Based Mixed-Oxide Catalyst: Reusability and Stability

Zahra Gholami^a, Ahmad Zuhairi Abdullah^b & Keat Teong Lee^b

^a Centralized Analytical Laboratory, Universiti Teknologi PETRONAS, Bandar Seri Iskandar, Perak Darul Rizduan, Malaysia

^b School of Chemical Engineering, Universiti Sains Malaysia, Engineering Campus, Nibong Tebal, Penang, Malaysia

Accepted author version posted online: 09 Sep 2014.



CrossMark

[Click for updates](#)

To cite this article: Zahra Gholami, Ahmad Zuhairi Abdullah & Keat Teong Lee (2015) Catalytic Etherification of Glycerol to Diglycerol Over Heterogeneous Calcium-Based Mixed-Oxide Catalyst: Reusability and Stability, *Chemical Engineering Communications*, 202:10, 1397-1405, DOI: [10.1080/00986445.2014.952812](https://doi.org/10.1080/00986445.2014.952812)

To link to this article: <http://dx.doi.org/10.1080/00986445.2014.952812>

PLEASE SCROLL DOWN FOR ARTICLE

Taylor & Francis makes every effort to ensure the accuracy of all the information (the "Content") contained in the publications on our platform. However, Taylor & Francis, our agents, and our licensors make no representations or warranties whatsoever as to the accuracy, completeness, or suitability for any purpose of the Content. Any opinions and views expressed in this publication are the opinions and views of the authors, and are not the views of or endorsed by Taylor & Francis. The accuracy of the Content should not be relied upon and should be independently verified with primary sources of information. Taylor and Francis shall not be liable for any losses, actions, claims, proceedings, demands, costs, expenses, damages, and other liabilities whatsoever or howsoever caused arising directly or indirectly in connection with, in relation to or arising out of the use of the Content.

This article may be used for research, teaching, and private study purposes. Any substantial or systematic reproduction, redistribution, reselling, loan, sub-licensing, systematic supply, or distribution in any form to anyone is expressly forbidden. Terms & Conditions of access and use can be found at <http://www.tandfonline.com/page/terms-and-conditions>

Catalytic Etherification of Glycerol to Diglycerol Over Heterogeneous Calcium-Based Mixed-Oxide Catalyst: Reusability and Stability

ZAHRA GHOLAMI¹, AHMAD ZUHAIRI ABDULLAH², and KEAT TEONG LEE²

¹Centralized Analytical Laboratory, Universiti Teknologi PETRONAS, Bandar Seri Iskandar, Perak Darul Rizduan, Malaysia

²School of Chemical Engineering, Universiti Sains Malaysia, Engineering Campus, Nibong Tebal, Penang, Malaysia

The activities of different heterogeneous alkaline-earth metal oxide catalysts and mixed-metal oxide catalysts were investigated. Glycerol etherification was carried out at 250°C in a three-necked glass reactor vessel at atmospheric pressure. In a typical experiment, 50 g of anhydrous glycerol was loaded into the reactor. Then, 2 wt.% of catalyst was added to the reactor. The reactor was then heated to the appropriate reaction temperature in nitrogen atmosphere under continuous stirring. The heterogeneous CaO catalyst showed the highest catalytic conversion (72%) compared with other alkaline-earth metal oxides, with a diglycerol yield of 19%. The highest glycerol conversion of 96% and diglycerol yield of 52% were observed for the mixed-metal oxide catalyst (Ca_{1.6}Al_{0.4}La_{0.6}O₃). Reusability and stability of this catalyst were tested. The ICP-AES analysis was performed to confirm the leaching of the metal species in the liquid phase of the reaction mixture.

Keywords: Alkaline-earth metal oxide; Catalyst; Etherification; Glycerol; Leaching; Mixed Oxides; Reusability

Introduction

An increase in glycerol production is expected because of the increasing use of fuel additives such as methyl esters (Soares et al., 2011). This increase can enhance the importance of glycerol as a cheaper raw material for new products used in surfactants, lubricants, cosmetics, food additives, etc. (Clacens et al., 2002). The synthesis of value-added molecules from crude glycerol is an attractive replacement to disposal by incineration (Liu et al., 2011). Etherification of glycerol has been studied with or without the use of organic solvents in the presence of different homogeneous or heterogeneous catalysts (Clacens et al., 2002; Jerome et al., 2008; Martin and Richter, 2011; Gholami et al., 2014a). Polyglycerols, especially diglycerol and triglycerol, are the main products of glycerol etherification. The use of solvent could lead to some difficulties in the production process, leading to a more complex overall process (Ayoub et al., 2012). In this respect, solventless etherification process could promise several advantages.

Various heterogeneous catalysts have been employed in the etherification process (Klepáčová et al., 2006; Ruppert et al., 2008; Pariente et al., 2009; Silva et al., 2009; Rahmat et al., 2010; Shi et al., 2010; Gaudin et al., 2011; Melero et al., 2012). However, the high selectivity of diglycerol at higher levels of glycerol conversion remains a challenge. Compared

with homogeneous processes, heterogeneously catalyzed processes have slower reaction rates (Tseng and Wang, 2011). Glycerol etherification at 260°C and 24 h over mesoporous materials, such as MCM-41 impregnated with cesium, resulted in 75% and 22% selectivities to di- and triglycerol at 80% glycerol conversion. Clacens et al. (1998, 2000, 2002) used mesoporous catalysts (MCM-41 type) and a Cs-ZSM5 catalyst for glycerol etherification at 260°C for 24 h and subsequently obtained 80% glycerol conversion with 40% corresponding diglycerol selectivities. Catalytic etherification over the CaLa/MCM-41 resulted in the highest glycerol conversion of 91% at a diglycerol yield of 43% (Gholami et al., 2014b). Etherification of glycerol to diglycerol isomers in a solvent-free reaction system by Li-Mg/SBA-15 catalyst was studied by Admiral and Abdullah (2013). The reaction was carried out at 240°C with 2 wt.% of catalyst and the highest diglycerol yield of 63% was obtained after 18 h of reaction.

Etherification of glycerol using alkaline earth metal oxides as heterogeneous catalysts with high activity has been reported in the literature and it has been concluded that different CaO materials are examples of the most stable and environmentally friendly materials among alkaline earth oxides (Granados et al., 2007). The yield of diglycerol, as a desirable product, was significantly affected by catalyst loading, reaction temperature, and reaction time. It is necessary to identify a suitable type of mesoporous material with suitable pore size that can stand the harsh reaction conditions while having the capability to accommodate diglycerol molecules. Therefore, a suitable heterogeneous catalyst was required for the selective etherification of glycerol to diglycerol. The stability of the

Address correspondence to Ahmad Zuhairi Abdullah, School of Chemical Engineering, Universiti Sains Malaysia, Engineering Campus, 14300 Nibong Tebal, Penang, Malaysia. E-mail: chzuhairi@usm.my

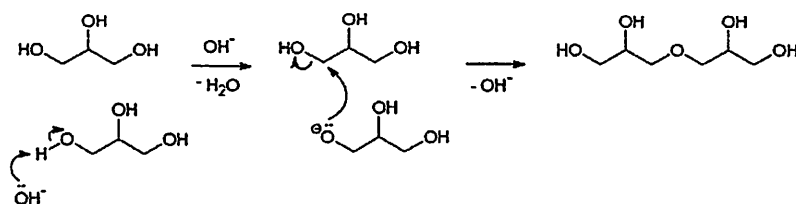


Fig. 1. Base-catalyzed glycerol etherification of glycerol to diglycerol (Ruppert et al., 2008).

structure under high temperature and long-time reaction might be improved using the catalyst with mostly meso-size-range pores (Ayoub and Abdullah, 2013a, 2013b). The structure of this catalyst should be able to withstand the reaction conditions. Furthermore, at the end of reaction, the catalyst should be easily separated from the product mixture so that it can be used for several cycles of reaction. It has been reported that binary oxides containing alkali and alkaline earth metals can increase the stability and improve catalytic behavior. The strength and number of basic sites of the mixed oxide of La_2O_3 were higher than those of single oxide (Choudhary et al., 1998). Some factors were considered to be of paramount importance for catalyst modification. First is the addition of Al into the catalyst matrix in the form of stable aluminum compound (Al_2O_3). Another consideration is the improvement on the surface area as a consequence of the inclusion of Al into the matrix of the solid catalyst to increase the number of available active sites during reaction.

Base-Catalyzed Etherification of Glycerol

Oxidation and reduction occur at the same time during the etherification of glycerol, which includes the gain and loss of oxygen and hydrogen molecules between the hydroxyl group and glycerol. Ruppert et al. (2008) studied the mechanism of glycerol etherification over a basic catalyst. The mechanism includes two mechanistic schemes: (1) deprotonation of the hydroxyl group and (2) attack of the formed alkoxy anion on the carbon of the other molecule of glycerol. As shown in Figure 1, it is difficult to explain the mechanism of a base-catalyzed etherification without the participation of the Lewis acid sites through the activation of a hydroxyl group as a leaving group (Ruppert et al., 2008). Examples of such dual mechanism involving both basic and Lewis acid active sites have been reported for other heterogeneous catalytic reactions, for example, the destructive adsorption of

chlorinated hydrocarbons on lanthanide oxide and oxide chloride materials (van der Heijden et al., 2005, 2007).

Further theoretical studies of alkaline earth metals have focused on the importance of surface basicity and Lewis acidity of the catalyst. The catalytic behavior of metal oxide surfaces is often explained by the acid/base characteristics (Conte, 1999). The nature of acidic and basic sites on oxide surfaces can be described in Lewis and Brønsted terms. On metal oxides, coordinated unsaturated metal cations are generally considered as Lewis acid sites, whereas the oxygen anions are regarded as Lewis base sites (Abro et al., 1997; Sakthivel et al., 2007). As shown in Figure 2, it was reported that the role of coordinative unsaturated surface metal ions was to facilitate the hydroxyl leaving process in the glycerol etherification reaction (Ruppert et al., 2008). The electron-deficient metal cations exhibit acidic, electron-acceptor characteristics, whereas the electron-rich oxygen anions exhibit basic, electron-donor characteristics (Abro et al., 1997).

In our previous study (Gholami et al., 2013), the activity of novel $\text{Ca}_{1-x}\text{Al}_x\text{La}_x\text{O}_3$ ($0.1 \leq x \leq 0.9$) heterogeneous catalyst in glycerol etherification into polyglycerols in a solventless system was investigated. The characterization of catalysts such as SEM, BET, FTIR, and XRD was also studied and the effects of the reaction conditions on the process were determined to identify the highest conversion and selectivity that can be achieved. In this study, the effects of shape selectivity in the distribution of diglycerol isomers, and the stability and reusability of alkaline earth metal oxides and the mixed-oxide catalyst are investigated.

Materials and Methods

Materials

Anhydrous glycerol of high purity (>99%) was purchased from R&M Chemicals, Ltd., whereas lanthanum nitrate hexahydrate (99.9%) was supplied by Sigma Sdn. Bhd.

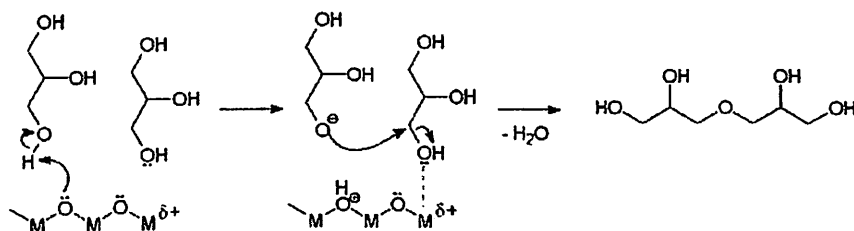


Fig. 2. Potential reaction scheme for base-catalyzed glycerol etherification involving Lewis acidity (Ruppert et al., 2008).

Potassium hydroxide (85%), aluminum nitrate nonahydrate (>98.5%), calcium nitrate tetrahydrate (>99%), and strontium nitrate (>99%) were obtained from Sigma–Aldrich, Malaysia, and magnesium nitrate (>99%) was purchased from ACROS organics. Meanwhile, glycerol (99%) and triglycerol (>90%) obtained from Sigma–Aldrich and diglycerol (>90%) from Solvay Chemicals were used as GC standards. Moreover, chlorotrimethylsilane (98%), hexamethyldisilazane (99%), pyridin, analytical reagent (99.99%), and toluene, anhydrous (99.8%) were supplied by Aldrich, Fulka, Fisher Scientific, and Sigma–Aldrich, respectively, which were used as GC analysis solutions. These chemicals were used without further purification.

Catalyst Preparation

The catalysts were synthesized based on our previous study (Gholami et al., 2013). Heterogeneous catalysts $\text{Ca}_{1.6}\text{La}_{0.4}\text{Al}_{0.6}\text{O}_3$ were synthesized using a co-precipitation method from the nitrate compounds of calcium, aluminum, and lanthanum. In a typical batch preparation, based on 10 g of the final catalyst, 50 mL of mixed salt solution containing 3.07 M of $\text{Ca}(\text{NO}_3)_2$, 1.14 M of $\text{Al}(\text{NO}_3)_3$, and 0.33 M of $\text{La}(\text{NO}_3)_3$ was prepared. The solution was then precipitated with a controlled pH of 10 using 2 M KOH to obtain a mixed-hydroxide solution. During the precipitation step, the mixture was continuously stirred at 600 rpm for 6 h at 80°C on a magnetic hot plate-stirrer until the solution was homogenized. The resulting mixture was subsequently filtered, dried, and then thermally treated at 560°C for 6 h to obtain the composite mixed-metal oxide catalyst. The same method was employed for preparation of single-oxide catalysts (CaO, MgO, and SrO), whereas the proper amount of nitrate was precipitated with 2.0 M KOH.

Reaction Procedure

The catalytic activity of the heterogeneous catalysts was tested using solvent-free etherification of glycerol. The reaction was carried out in a three-necked glass reactor vessel (250 mL) at atmospheric pressure in the presence of 2 wt.% of catalyst (based on glycerol weight). The reactor was placed on a stirring-heating mantle equipped with a proportional–integral–derivative (PID) temperature controller. The reaction was carried out at 250°C for up to 10 h and it was performed under a continuous flow of nitrogen gas to avoid glycerol oxidation. Water that was produced was eliminated and collected using a Dean–Stark system. In the experimental run, the reactor was charged with 50 g of anhydrous glycerol and 2 wt.% of catalyst was then added to it. Then, the reaction vessel was heated up to the desired reaction temperature.

Catalyst Characterization

The surface area, pore volume, and pore size distribution of the synthesized catalyst were measured based on nitrogen adsorption/desorption isotherms at –196°C using an ASAP 2020 Micromeritics instrument. Powder X-ray diffraction (XRD) patterns recorded using a diffractometer (Phillips

PW 1710) with Cu K α radiation were used to determine the purity and the unit cell parameters of the developed oxides catalyst. The elemental analysis of metals was performed using an inductivity coupled plasma atomic-emission spectrometer (Perkin Elmer Optima 3000 DV ICP-AES Spectrophotometer).

Analytical Methods

The samples obtained from the etherification of glycerol using the synthesized catalysts were collected at specific intervals during the reaction and were qualitatively analyzed using the GC analysis. Analysis was performed using the GCD 7890A System (Agilent Technologies, USA) with flame ionization detectors. The system was equipped with a capillary polyethylene glycol column (Agilent technologies) with the following dimensions: 30 m length, 0.32 mm i.d., and 0.25 μm film thickness. The temperature limit was from –60°C to 325°C. Nitrogen was used as the carrier gas. The injector temperature was set at 100°C, and the detector temperature was maintained at 250°C. The column temperature was kept constant at 100°C. The products were analyzed with GC after silylation.

The silylation preparation procedure was performed based on the method reported by Sweeley et al. (1963). First, 0.050 g of the produced sample was mixed with 1.5 mL of dried pyridine in a screw-capped septum vial (4 mL). 0.2 mL of hexamethyldisilazane was added into this solution and the vial was shaken well and then 0.1 mL of trimethylchlorosilane was added. To allow large particles in the mixture to settle down, the obtained solution was heated to 70°C for 1 h. Later, the top layer of the mixture was taken and centrifuged to separate the remaining solid particles. Then, 0.05 mL of the final solution was diluted into 2 mL of dried toluene. Finally, 1 μL of this liquid was injected into the GC. Additional information about calculations of conversion of glycerol, selectivity and yield towards diglycerol and triglycerol have been provided in the supplemental data.

Results and Discussion

Catalytic Activity

Performance of Alkaline Earth Oxide Catalysts in Etherification Reaction

The activity of the synthesized catalysts was examined based on the yield of the desired product (diglycerol) in the etherification reaction. The reaction was carried out at 250°C for 10 h, and the effects of the different reaction parameters were investigated. Figures 3(a) and (b) show the performance of different catalysts used for the solventless etherification of glycerol. Figure 3(a) indicates that in the etherification reaction over SrO catalyst, the highest glycerol conversion was achieved after 8 h. The etherification of glycerol using alkaline-earth metal oxide catalysts was affected by both their surface basicity and Lewis acidity (Ruppert et al., 2008). The conversion of glycerol increased in the order of $\text{MgO} < \text{CaO} < \text{SrO}$ when the catalyst basicity theoretically

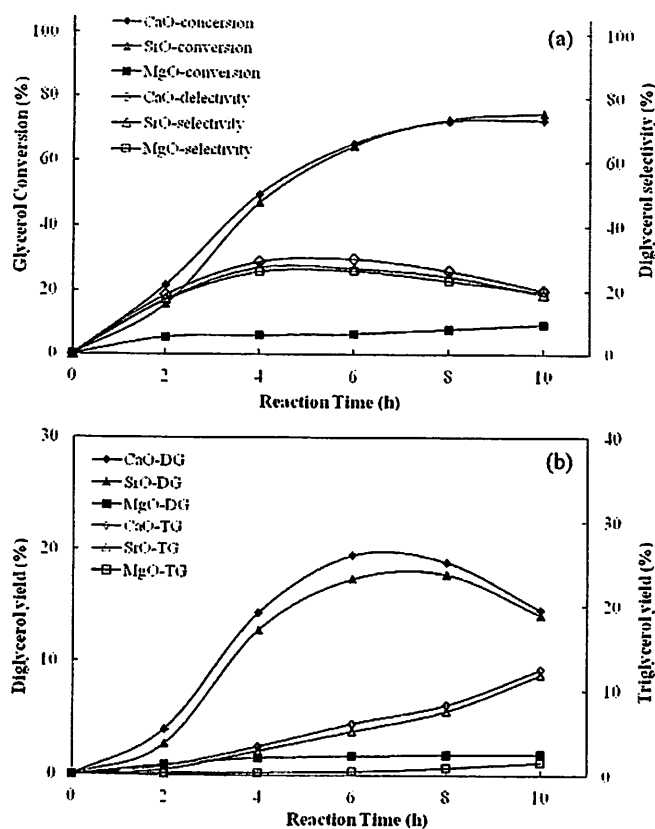


Fig. 3. Performance of heterogeneous catalysts in the (a) conversion of glycerol and diglycerol selectivity, (b) yield of di-, tri-glycerol in the etherification reaction (reaction temperature: 250°C; catalyst loading: 2 wt.%).

increases. The order of conversion is thus in accordance with their basicity, that is $MgO < CaO < SrO$.

To evaluate the selectivity behavior of unsupported MgO, CaO, and SrO, the selectivities versus reaction time is also plotted in Figure 3(a). No significant differences in the selectivity behavior are observed for the different catalyst materials investigated. With an increase in the glycerol conversion, the selectivity towards triglycerol gradually increased at the expense of the selectivity towards diglycerol. Furthermore, from Figure 3(b) it can be seen that the yield towards triglycerol steadily increased with increasing glycerol conversion, due to the polymerization of diglycerol to higher oligomers at the prolonged reaction, whereas a decrease in the yield towards diglycerol was observed after 6 h of reaction. Notably, MgO revealed rather low conversion in the etherification of glycerol (9% after 10 h). The glycerol conversion over CaO catalyst gradually reached a final value of about 72% after 10 h of reaction.

The results revealed that the basic strength, the Lewis acid sites, and the surface area are important, and the catalyst with the precise balance of Lewis acidity and basicity shows the highest glycerol etherification activity. The basic strength, surface basicity, and BET surface area of the catalysts are presented in Table I. The surface area and basicity of the

Table I. Basic strength and surface basicity of the catalysts

Catalyst	Basic strength	Surface basicity ($\mu\text{mol/g}$)	BET surface area (m^2/g)
SrO	$15.0 < H_- < 18.4$	1250	8.8
CaO	$9.3 < H_- < 15.0$	985	14.3
MgO	$7.2 < H_- < 9.3$	575	24.7

catalyst are important parameters in the etherification reaction. However, the basicity and basic strength have significant impact on the activity of the catalyst in this reaction. The comparison between surface properties of MgO and CaO shows that the activity of the catalyst considerably increased (from 9% to 72%) by increasing the basicity of the catalyst, whereas by increasing the basicity of the SrO catalyst, there was no significant difference in the catalytic activity.

Mixed oxide of CaLa showed a low surface area of $20 \text{ m}^2/\text{g}$ and to improve the surface area of this catalyst, aluminum was considered for integration into the catalyst structure. Heterogeneous mixed-metal oxide catalysts are considered as a potential alternative for use as basic heterogeneous catalysts for the selective etherification of glycerol. Specifically, it is expected that the catalyst materials consisting of calcium, aluminum, and lanthanum elements show higher stability and basicity. Particularly, this type of catalyst has received significant attention in various reactions (Muroi, 2012; Olutoye and Hameed, 2010) due to their mesostructure, low cost, environmental friendly nature, simple method of preparation, and reusability.

Performance of Mixed-Oxide Catalyst ($Ca_{1.6}Al_{0.4}La_{0.6}O_3$) in Etherification Reaction

In the etherification reaction of glycerol, a high level of glycerol conversion with high corresponding selectivity to diglycerol is very important. The above facts establish the basis for further study in the synthesis of heterogeneous catalysts, which was carried out in this work to improve the process. Mixed-metal oxides composite of La, Ca, and Al were synthesized in this part of the study. These metals were selected based on their suitable characteristics that can favorably enhance the process by providing the basic conditions during the solventless etherification of glycerol. These mixed-oxide catalysts were used in the etherification reaction due to their high stability to enhance the selective oligomerization of glycerol under various reaction conditions.

Effect of Reaction Variables

Catalyst Loading

The effect of catalyst loading on the etherification reaction at 250°C and 8 h was also investigated. Concentration of the catalyst ($Ca_{1+x}La_{1-x}Al_xO_3$ at $x=0.6$) in the reaction medium was in the range of 0.5–5 wt.%, whereas the other reaction variables were kept constant. Different catalyst loadings resulted in different activities and selectivities (Figure 4). The conversion of glycerol reached its highest level of 96% after 8 h while the maximum yield of diglycerol of approximately 52% was attained with 2 wt.% of the

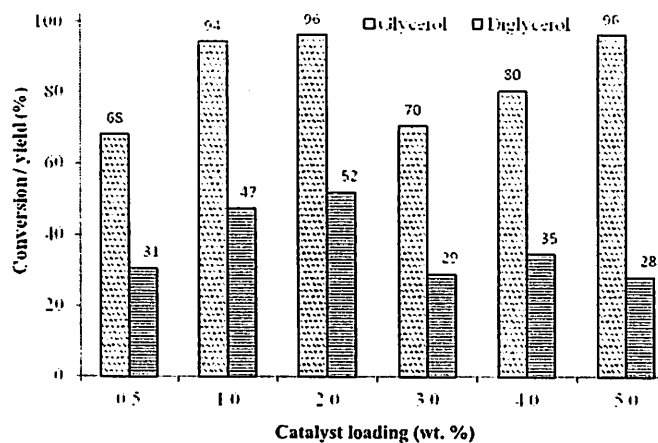


Fig. 4. Effect of catalyst loading on glycerol conversion and yield of diglycerol for $\text{Ca}_{1.6}\text{La}_{0.4}\text{Al}_{0.6}\text{O}_3$ catalyst (reaction time: 8 h; reaction temperature: 250°C).

catalyst after 8 h. Increasing the catalyst amount from 0.5 to 2 wt.% caused an increase in the glycerol conversion and corresponding diglycerol and triglycerol selectivities. This result was attributed to the dehydration of glycerol molecules. Similarly, the nucleophilic character of the hydroxyl oxygen could have been enhanced by the interaction between O-H bonds of glycerol and the oxide catalyst (Martin and Richter, 2011). Thus, the attack on the polarized glycerol molecule by the hydroxyl group of another molecule of glycerol could have simultaneously split the water molecule to result in diglycerol formation (Martin and Richter, 2011; Ayoub et al., 2012). However, increasing the catalyst amount from 2 to 4 wt.% resulted in decreasing trends as observed in both glycerol conversion and diglycerol selectivity. This observation could be attributed to the back-scission of diglycerol to glycerol (Martin and Richter, 2011).

The effect of catalyst loading on the conversion of glycerol over homogeneous LiOH catalyst in a solventless etherification reaction was studied by Ayoub et al. (2012). They reported that the conversion of glycerol to diglycerol was enhanced by increasing the amount of LiOH from 0.5 to 2 wt.% and they found that 2 wt.% of catalyst loading was a level at which the highest reaction rate was achieved. Further increase in the catalyst amount did not result in higher conversion and selectivity because the reaction could have been limited by the mass transfer during the reaction (Ayoub et al., 2012).

Reaction Time

Figure 5 shows the effect of reaction time on glycerol conversion and the corresponding diglycerol and triglycerol selectivities. Generally, conversion of glycerol increased with an increase in reaction time. Yield of diglycerol reached 28% after 4 h of reaction, and then increased gradually to 52% after 8 h. Because of the prolonged reaction, more glycerol molecules experienced dehydration or other forms of side reaction that increased the conversion of glycerol. The conversion of glycerol molecules might not exactly result in polyglycerols in these reactions. Instead, the double dehydration of glycerol

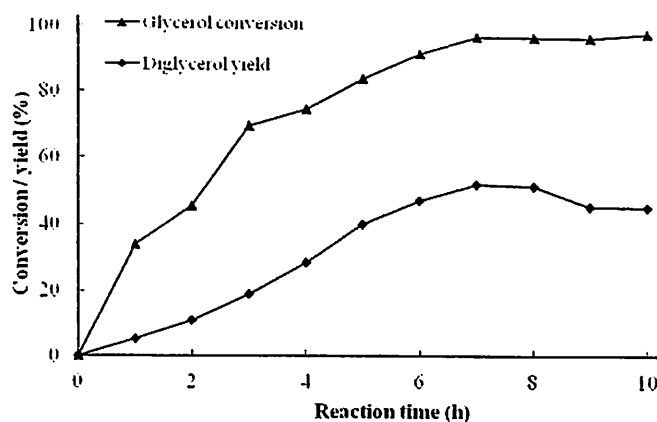


Fig. 5. Effect of reaction time on diglycerol yield for $\text{Ca}_{1.6}\text{La}_{0.4}\text{Al}_{0.6}\text{O}_3$ (2 wt.% catalyst loading, reaction temperature: 250°C).

could convert it to other forms of undesired by-products such as acrolein, which produces harmful products (Clacens et al., 2002). Thus, 8 h was considered as a suitable reaction time to be used in this study. Further investigation revealed that the selectivity of diglycerol increased at a certain rate up to 8 h, and then gradually decreased until the reaction was complete.

Under uncontrolled reaction conditions, diglycerol molecules could be transformed into higher oligomers of glycerol (Ruppert et al., 2008). The weak formation of two polymerized molecules of glycerol (diglycerol isomers) is not highly stable under the specified reaction conditions. Thus, nucleophilic attack at the C-OH bond of the glycerol generates an intermediate phase from which diglycerol and triglycerol are formed. The latter deprotonated the catalyst to regenerate active species capable of further reacting with glycerol molecule. Thus, another catalytic cycle would start and a higher nuclear charge of the as-synthesized catalyst would facilitate stronger attraction between electrons and protons during the reaction (Clacens et al., 2002; Ayoub et al., 2012).

Reaction Temperature

Reaction temperature plays a key role in etherification reaction and based on the highest yield of diglycerol, the optimum temperature must be determined. Thus, the effect of reaction temperature (ranging from 150 to 260°C) on glycerol etherification was studied. Figure 6 shows that the glycerol conversion reached its maximum level (96%) in the presence of the 2 wt.% of $\text{Ca}_{1.6}\text{La}_{0.4}\text{Al}_{0.6}\text{O}_3$ catalyst, at 250°C after 8 h. Increasing the reaction temperature from 220 to 250°C resulted in a significant increase in the glycerol conversion from 39% to 96%.

However, the yield of diglycerol under these conditions was 52%; on increasing the reaction temperature and time, it decreased. These results suggest that reaction temperatures above 250°C might accelerate the conversion of the remaining glycerol to enhance the subsequent etherification of diglycerol to higher glycerol oligomers, which subsequently resulted in a decrease in diglycerol selectivity. Furthermore, discoloration and strong odor generation could occur at such high temperatures to indicate partial decomposition of the

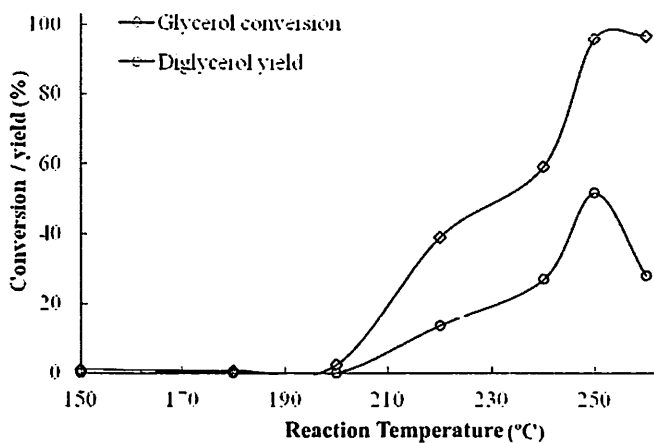


Fig. 6. Effect of reaction temperature on glycerol conversion and diglycerol yield, $\text{Ca}_{1.6}\text{La}_{0.4}\text{Al}_{0.6}\text{O}_3$ catalyst (2 wt.% catalyst loading, reaction time: 8 h).

derived products. On the other hand, glycerol conversion was very low at reaction temperatures below 200°C. These observations were in good agreement with previously reported results (Clacens et al., 1998; Charles et al., 2003).

Reusability and Stability of the Catalyst

Reusability of the catalyst is one of the important factors for the catalytic reactions. This factor was tested in phases for the developed mixed-metal oxide $\text{Ca}_{1.6}\text{La}_{0.4}\text{Al}_{0.6}\text{O}_3$ catalyst. Characterization tests were performed for the mixed-metal oxide $\text{Ca}_{1.6}\text{La}_{0.4}\text{Al}_{0.6}\text{O}_3$ catalyst samples before and after the reaction. The nitrogen adsorption and desorption method, as well as the ICP-AES and XRD analyses, was performed to study the structure variations in the catalysts after etherification. The XRD patterns of the catalyst before and after etherification for one cycle are shown in Figure 7. A rather similar XRD pattern was observed for the catalysts before and after reaction. For both catalysts, the main peaks

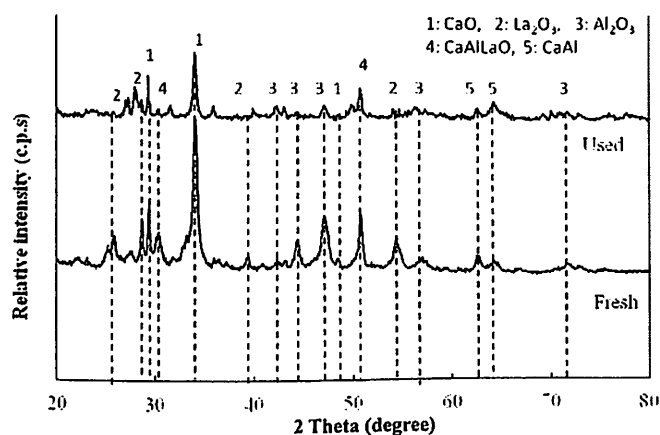


Fig. 7. XRD patterns for the mixed-oxide $\text{Ca}_{1.6}\text{La}_{0.4}\text{Al}_{0.6}\text{O}_3$ catalyst before and after the etherification reaction.

are clearly observed. However, it can be seen that the intensity of prominent peaks decreased after the reaction at $2\theta = 25^\circ, 28^\circ, 29^\circ, 34^\circ, 47^\circ, 51^\circ,$ and 54° . The slight reduction in intensities indicates a satisfactory preservation of the structure so that it appeared quite similar to that of the fresh mixed-oxide $\text{Ca}_{1.6}\text{La}_{0.4}\text{Al}_{0.6}\text{O}_3$ catalyst sample. However, the disappearance or decreasing intensities of these peaks suggested that leaching occurred during the reaction and it caused a reduction in the amount of metals in the catalyst structure.

In general, in the XRD pattern for the catalyst after the reaction, the peaks are shorter than the peaks in the fresh catalyst. Furthermore, the peaks of the Ca component in the catalyst sample after the reaction were found to be weaker and with lower intensities than those of the fresh catalyst before the reaction. This phenomenon might have been caused by the liquid phase reaction and severe reaction conditions (250°C and 10 h reaction time). Hence, the stability of the structure was confirmed by the existence of some basic peaks, which were sufficiently preserved in the catalyst after reaction. The typical peaks of the separate metal contents on the crystalline phases and that of mixed-metal oxides were obviously detected in the obtained patterns (Biswas et al., 2010; Manfro et al., 2013).

The surface properties of the mixed-oxide $\text{Ca}_{1.6}\text{La}_{0.4}\text{Al}_{0.6}\text{O}_3$ catalyst before and after the reaction were evaluated, and the results are shown in Table II. A significant reduction in the surface area, pore size, and pore volume of the catalyst was observed after the etherification reaction. However, the surface area and pore size of the catalyst after the reaction were still high enough for being used as reusable catalyst in the second run of the reaction. The partial blockage of the catalyst by-products might have reduced the surface area and pore size of the catalyst after the reaction. The clogs of the produced oligomers such as diglycerol, triglycerol, and higher oligomers formed during the reaction were deposited on the surface of the catalyst, which might have decreased the number of available active sites for the next catalytic run.

The stability of the catalytic activity of mixed-oxide $\text{Ca}_{1.6}\text{La}_{0.4}\text{Al}_{0.6}\text{O}_3$ catalyst was considered in this study by recycling the catalyst in three successive batch runs at optimum conditions of etherification of glycerol. The catalyst was removed after each catalytic experiment, washed carefully with methanol, and then dried in an oven at 100°C for 10 h. Figure 8 shows the conversion of glycerol and diglycerol yield in three sequential runs. A significant reduction in conversion and yield was observed after each run during the catalytic etherification of glycerol. The yield of diglycerol dropped to 29% in the second run and decreased to 12% after the third run. A similar trend was observed for the glycerol conversion, and it decreased from 96% to 67% after three runs. Thus, the leaching of the active metal caused a

Table II. Surface properties of mixed-oxide $\text{Ca}_{1.6}\text{La}_{0.4}\text{Al}_{0.6}\text{O}_3$ catalyst before and after reaction

Properties	Before reaction	After reaction
BET surface area (m^2/g)	53.9	34.2
Pore volume (cm^3/g)	0.20	0.15
Pore size (nm)	16.8	10.1

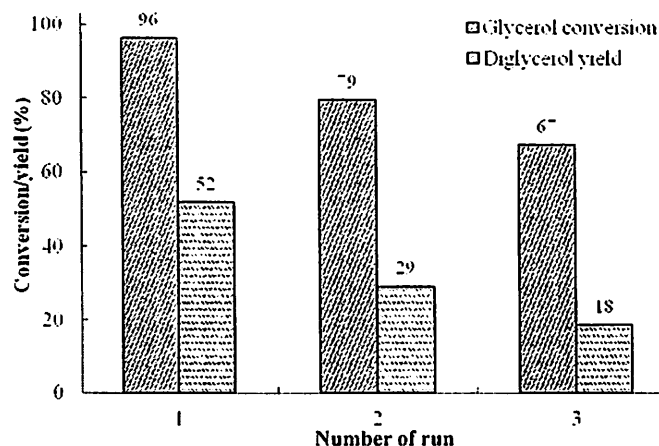


Fig. 8. Glycerol conversion and diglycerol yield versus run number in the etherification of glycerol.

reduction in the catalytic activity throughout the reaction. Ca leaching was confirmed by the results of the characterization of used catalyst after etherification. The lost amount of metals might have been dissolved in the liquid phase of reaction mixture. The leached metals would remain in the reaction and contribute to the homogeneous reaction.

Heterogeneous catalysis is used to avoid metal loss during catalytic reactions. However, a previous study has reported that some metals are leached from the solid catalyst to the liquid product mixture, thus requiring recovery of the metal. Hunter et al. (1987) reported that the metal leaching occurs because some species such as starting material, product, by-product, or intermediate are better ligands, forming a stronger bond with the metal complex than the ligand functionality of the solid support. Therefore, the metal complex is leached out of the solid support and dissolved in the liquid reaction mixture. However, modification of the collected catalyst including filtration, as well as washing and drying after each run, could affect the catalytic activity.

The ICP-AES analysis was performed to confirm the leaching of the metal species in the liquid phase of the reaction mixture, and the results are shown in Table III. The Ca and La contents in the fresh catalyst were measured to be 49 and 7 wt.%, respectively. After the first run, it was observed that the amount of Ca and La in the catalyst was reduced to 22 and 24 wt.% of their amount in the fresh

Table III. Metal contents in the catalyst and final liquid product after the etherification reaction

Component	Run number		
	1	2	3
Calcium			
Remove from catalyst actual (wt.%)	22	12	9
Present in liquid phase ICP-AES (ppm)	16	10	8
Lanthanum			
Remove from catalyst actual (wt.%)	24	15	8
Present in liquid phase ICP-AES (ppm)	13	9	6

catalyst, and after the third run the amount of Ca and La reached 31 and 4 wt.%, respectively, in the used catalyst. At the same time, the amount of metals in the reaction mixture was measured after each run. It was observed that the amounts of Ca and La in the product mixture were 16 and 13 ppm, respectively, after the first run. In the final liquid product after the third run the amounts of Ca and La were found to be 8 and 6 ppm, respectively. These findings prove that Ca, as an active component, was partially dissolved in the liquid phase during the etherification reaction under harsh reaction conditions. The amount of calcium as an active component decreased in the used catalyst after each run, which may be the primary reason for the reduced activity and selectivity of the catalyst in the etherification reaction.

The effect of Ca leaching on diglycerol yield was examined in the etherification reaction over mixed-oxide $\text{Ca}_{1.6}\text{La}_{0.4}\text{Al}_{10.6}\text{O}_{30}$ catalyst, and the results are shown in Figure 9. After 2 h of reaction, the amount of Ca in the liquid phase was approximately 5% of the Ca content in the fresh mixed-oxide catalyst, and these amounts increased steadily on increasing the reaction time. After 10 h of reaction the Ca content in the liquid phase reached 21% and at the same time 24% of La was observed in the liquid phase. Simultaneously, after 8 h reaction the diglycerol yield reached its maximum (52% at 96% glycerol conversion) and then started to decrease and reached to 31 wt.% after 10 h of reaction. A direct relationship between the diglycerol yield and content of active component was observed.

The reaction might occur because of the availability of the active sites on the catalyst, and on increasing the reaction time above 8 h, some dissolved Ca species in the liquid phase might act homogeneously. Thus, the yield of diglycerol reduced by further increase in the reaction time up to 8 h, which might be due to the production of some undesirable products instead of diglycerol. The obtained result for the reusability of the prepared catalyst was compared with those observed by other researchers.

Previous studies could confirm the obtained results in the present study and the suggested hypothesis in this study. Seshu Babu et al. (2008) studied the synthesis of polyfunctionalized pyrans using a heterogeneous strong basic Mg/La

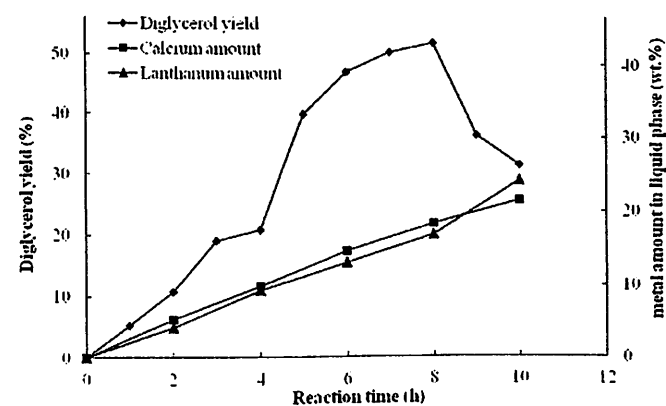


Fig. 9. Calcium leaching effect on yield of diglycerol during the 10 h of reaction.

mixed-oxide catalyst at short reaction times and mild reaction conditions. They reported that Mg/La mixed-oxide catalysts were reusable basic catalysts, and the presence of La enhanced the basicity of the catalyst. The Mg/La catalyst showed strong basic sites compared with other solid base catalysts. The presence of La_2O_3 with MgO led to enhanced basicity. However, given the harsh reaction conditions in the present study, a higher reduction in catalytic activity was observed.

Barrault et al. (2004) studied the selective oligomerization of glycerol over mesoporous catalysts. They reported that polar compounds are well known to create alkaline (earth) and soluble alcoholates. Therefore, the content of the basic element of the catalyst in the presence of glycerol and its oligomers may be decreased. Thus, a reduction in activity and rapid variations in the selectivity were observed upon reuse. The solids were analyzed after the reaction, which showed that the metal content was considerably reduced and dissolved in the liquid phase, and the metals acted as a homogeneous catalyst during the reaction. Ruppert et al. (2008) also studied the etherification of glycerol over CaO-based materials. They observed that catalyst leaching could have occurred. In addition to the CaO solid, the active species involved might be the Ca ions, most probably in the form of Ca diglyceroxide. In this study, after 2 h of reaction approximately 3%–6% of Ca from the original CaO catalyst material was detected in the liquid phase, which steadily increased with reaction time. Thus, the activation of the different catalyst materials is directly related with the increasing amounts of metal content, which could be transferred into the liquid phase in the reaction solution. However, further study should be conducted to minimize leaching and the loss of activity in heterogeneous catalysts.

Conclusion

Solventless etherification of glycerol to diglycerol in the presence of heterogeneous CaO catalyst showed good activity (20% yield of diglycerol at a glycerol conversion of 78%) compared with other unsupported alkaline-earth metal oxide catalysts (MgO and SrO). The yield of diglycerol was affected by the atomic size of the metal oxide (CaO) catalyst and operation parameters of the reaction. The heterogeneous mixed-oxide catalyst showed high diglycerol yield of 52% under similar reaction conditions (250°C, 8 h) compared with the other synthesized catalysts in this study. The high basic strength of this catalyst evidently improved the activity of the catalyst. Moreover, the mixed-oxide catalyst was found to be more stable compared with the other prepared catalysts in this study.

Reusability of the mixed-metal oxide $\text{Ca}_{1.6}\text{Al}_{0.4}\text{La}_{0.6}\text{O}_3$ catalyst was tested in the etherification reaction of glycerol at 250°C using 2 wt.% of catalyst. The reusability of the catalyst was demonstrated for up to three runs, during which the yield of diglycerol potential decreased from 52% for the fresh catalyst to 18% after the third run. The activation of the catalyst was directly related to the increasing amounts of metal content, which was leached into the liquid phase of

the reaction solution. This study still showed that considerable leaching of the active metal during the reaction occurred. In summary, the heterogeneous mixed-metal oxide ($\text{Ca}_{1.6}\text{Al}_{0.4}\text{La}_{0.6}\text{O}_3$) with 96% glycerol conversion and 52% yield of diglycerol was an active catalyst for the solventless etherification of glycerol to diglycerol. However, long-term stability still remains an issue as in the case of other basic catalysts reported in the literature.

Supplemental Material

Supplemental data for this article can be accessed on the publisher's website.

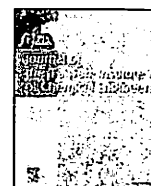
Funding

The authors sincerely acknowledge the financial support provided by Universiti Sains Malaysia in the forms of a Research University (RU) grant.

References

- Abro, S., Pouilloux, Y., and Barrault, J. (1997). Selective synthesis of monoglycerides from glycerol and oleic acid in the presence of solid catalysts, *Stud. Surf. Sci. Catal.*, **108**, 539–546.
- Admiral, A., and Abdullah, A. (2013). Shape selectivity effects in etherification of glycerol by Li–Mg/SBA-15 catalyst, *Catal. Lett.*, **144**, 1–5.
- Ayoub, M., and Abdullah, A. Z. (2013a). Diglycerol synthesis via solvent-free selective glycerol etherification process over lithium-modified clay catalyst, *Chem. Eng. J.*, **225**, 784–789.
- Ayoub, M., and Abdullah, A. Z. (2013b). LiOH-modified montmorillonite K-10 as catalyst for selective glycerol etherification to diglycerol, *Catal. Commun.*, **34**, 22–25.
- Ayoub, M., Khayoon, M. S., and Abdullah, A. Z. (2012). Synthesis of oxygenated fuel additives via the solventless etherification of glycerol, *Bioresour. Technol.*, **112**, 308–312.
- Babu N. S., Pasha, N., Rao, K. T. V., Prasad, P. S., and Lingaiah, N. (2008). A heterogeneous strong basic Mg/La mixed oxide catalyst for efficient synthesis of polyfunctionalized pyrans, *Tetrahedron Lett.*, **49**, 2730.
- Barrault, J., Clacens, J. M., and Pouilloux, Y. (2004). Selective oligomerization of glycerol over mesoporous catalysts, *Top. Catal.*, **27**, 137–142.
- Biswas, K., Sontakke, A., Majumder, M., and Annapurna, K. (2010). Nonisothermal crystallization kinetics and microstructure evolution of calcium lanthanum metaborate glass, *J. Therm. Anal. Calorim.*, **101**, 143–151.
- Charles, G., Clacens, J.-M., Pouilloux, Y., and Barrault, J. (2003). Preparation of diglycerol and triglycerol via direct polymerisation of glycerol with basic mesoporous catalysts, *Ol Corps Gras Lipides*, **10**, 74–82.
- Choudhary, V. R., Mulla, S. A. R., and Rane, V. H. (1998). Surface basicity and acidity of alkaline earth-promoted La_2O_3 catalysts and their performance in oxidative coupling of methane, *J. Chem. Technol. Biotechnol.*, **72**, 125–130.
- Clacens, J. M., Pouilloux, Y., and Barrault, J. (2000). Synthesis and modification of basic mesoporous materials for the selective etherification of glycerol, *Stud. Surf. Sci. Catal.*, **143**, 687–695.
- Clacens, J. M., Pouilloux, Y., and Barrault, J. (2002). Selective etherification of glycerol to polyglycerols over preregnated basic MCM-41 type mesoporous catalysts, *Appl. Catal. A*, **227**, 181–190.
- Clacens, J. M., Pouilloux, Y., Barrault, J., Linares, C., and Goldwasser, M. (1998). Mesoporous basic catalysts: comparison with alkaline

- exchange zeolites (basicity and porosity). Application to the selective etherification of glycerol to polyglycerols, *Stud. Surf. Sci. Catal.*, **118**, 895–902.
- Conte, R. V. (1999). *The Best Test Preparation & Review Course: FE/EIT Fundamentals of Engineering/Engineer-in-Training: PM Exam in Mechanical Engineering*, Research & Education Association, Piscataway, NJ.
- Gaudin, P., Jacquot, R., Marion, P., Pouilloux, Y., and Jérôme, F. (2011). Acid-catalyzed etherification of glycerol with long-alkyl-chain alcohols, *Chem. Sus. Chem.*, **4**, 719–722.
- Gholami, Z., Abdullah, A. Z., and Lee, K. T. (2013). Glycerol etherification to polyglycerols using $\text{Ca}_{1+x}\text{Al}_{1-x}\text{La}_x\text{O}_3$ composite catalysts in a solventless medium, *J. Taiwan Inst. Chem. Eng.*, **44**, 117–122.
- Gholami, Z., Abdullah, A. Z., Lee, K.-T. (2014a). Dealing with the surplus of glycerol production from biodiesel industry through catalytic upgrading to polyglycerols and other value-added products, *Renew. Sust. Energ. Rev.*, **39**, 327–341.
- Gholami, Z., Abdullah, A. Z., and Lee, K. T. (2014b). Heterogeneously catalyzed etherification of glycerol to diglycerol over calcium-lanthanum oxide supported on MCM-41: A heterogeneous basic catalyst, *Appl. Catal. A*, **479**, 76–86.
- Granados, M. L., Poves, M., Alonso, D. M., Mariscal, R., Galisteo, F. C., Moreno-Tost, R., Santamaria, J., and Fierro, J. (2007). Biodiesel from sunflower oil by using activated calcium oxide, *Appl. Catal. B. Environ.*, **73**, 317–326.
- Hunter, D. L., Moore, S. E., and Willis, G. G. (1987). Metal leach control from processes with polymer-supported catalysts, Google Patents. United States Patent, 4647708, USA.
- Jerome, F., Pouilloux, Y., and Barrault, J. (2008). Rational design of solid catalysts for the selective use of glycerol as a natural organic building block, *Chem. Sus. Chem.*, **1**, 586–613.
- Klepáčová, K., Mravec, D., and Bajus, M. (2006). Etherification of glycerol with tert-butyl alcohol catalysed by ion-exchange resins, *Chem. Pap.*, **60**, 224–230.
- Liu, X., Ma, H., Wu, Y., Wang, C., Yang, M., Yan, P., and Welz-Biermann, U. (2011). Esterification of glycerol with acetic acid using double SO_3H -functionalized ionic liquids as recoverable catalysts, *Green Chem.*, **13**, 697–701.
- Manfro, R. L., Nielson, F. P. R., and Mariana, M. V. M. S. (2013). Production of hydrogen from steam reforming of glycerol using nickel catalysts supported on Al_2O_3 , CeO_2 and ZrO_2 , *Catal. Sustainable Energy*, **1**, 60–70.
- Martin, A., and Richter, M. (2011). Oligomerization of glycerol – a critical review, *Eur. J. Lipid. Sci. Technol.*, **113**, 100–117.
- Melero, J. A., Vicente, G., Paniagua, M., Morales, G., and Muñoz, P. (2012). Etherification of biodiesel-derived glycerol with ethanol for fuel formulation over sulfonic modified catalysts, *Bioresour. Technol.*, **103**, 142–151.
- Muroi, T. (2012). Role of precious metal catalysts, in *Noble Metals*, Y.-H. Su (Ed.), InTech, Rijeka, Croatia.
- Olutoye, M. A., and Hameed, B. H. (2010). Transesterification of palm oil on $\text{K}_y\text{Mg}_{1-x}\text{Zn}_{1+x}\text{O}_3$ catalyst: Effect of Mg–Zn interaction, *Fuel Process. Technol.*, **91**, 653–659.
- Pariente, S., Tanchoux, N., and Fajula, F. (2009). Etherification of glycerol with ethanol over solid acid catalysts, *Green Chem.*, **11**, 1256–1261.
- Rahmat, N., Abdullah, A. Z., and Mohamed, A. R. (2010). Recent progress on innovative and potential technologies for glycerol transformation into fuel additives: a critical review, *Renew. Sustainable Energy Rev.*, **14**, 987–1000.
- Ruppert, A. M., Meeldijk, J. D., Kuipers, B. W. M., Ern , B. H., and Weckhuysen, B. M. (2008). Glycerol etherification over highly active CaO-based materials: new mechanistic aspects and related colloidal particle formation, *Chem. Eur. J.*, **14**, 2016–2024.
- Sakthivel, A., Nakamura, R., Komura, K., and Sugi, Y. (2007). Esterification of glycerol by lauric acid over aluminium and zirconium containing mesoporous molecular sieves in supercritical carbon dioxide medium, *J. Supercrit. Fluid.*, **42**, 219–225.
- Shi, Y., Dayoub, W., Chen, G. R., and Lemaire, M. (2010). Selective synthesis of 1-O-alkyl glycerol and diglycerol ethers by reductive alkylation of alcohols, *Green Chem.*, **12**, 2189–2195.
- Silva, C. R. B. d., Gonalves, V. L. C., Lachter, E. R., and Mota, C. J. A. (2009). Etherification of glycerol with benzyl alcohol catalyzed by solid acids, *J. Braz. Chem. Soc.* **20**, 201–204.
- Soares, V. L. P. S., Lachter, E. R. L., Rodrigues, J. R. J. D. A. R. J., Batista, L. N., and Nascimento, R. S. V. (2011). *New Applications for Soybean Biodiesel Glycerol*, 1st ed., InTech, Brazil.
- Sweeley, C. C., Bentley, R., Makita, M., and Wells, W. W. (1963). Gas-liquid chromatography of trimethylsilyl derivatives of sugar and related substances, *J. Am. Chem. Soc.*, **85**, 2497–2507.
- Tseng, Y. H., and Wang, M. L. (2011). Kinetics and biphasic distribution of active intermediate of phase-transfer-catalytic etherification, *J. Taiwan Inst. Chem. Eng.*, **42**, 129–131.
- Van Der Heijden, A. W. A. M., Belli re, V., Alonso, L. E., Daturi, M., Manoilova, O. V., and Weckhuysen, B. M. (2005). Destructive adsorption of CCl_4 over lanthanum-based solids: linking activity to acid–base properties, *J. Phys. Chem. B*, **109**, 23993–24001.
- Van Der Heijden, A. W. A. M., Garcia Ramos, M., and Weckhuysen, B. M. (2007). Intermediates in the destruction of chlorinated C1 hydrocarbons on La-based materials: mechanistic implications, *Chem. Eur. J.*, **13**, 9561–9571.



Catalytic behavior of sulfated zirconia supported on SBA-15 as catalyst in selective glycerol esterification with palmitic acid to monopalmitin



Mohd Hizami Mohd Yusoff*, Ahmad Zuhairi Abdullah

School of Chemical Engineering, Engineering Campus, Universiti Sains Malaysia, 14300 Nibong Tebal, Penang, Malaysia

ARTICLE INFO

Article history:

Received 2 September 2015

Revised 28 October 2015

Accepted 30 November 2015

Available online 23 December 2015

Keywords:

SBA-15

Sulfated zirconia

Urea hydrolysis

Selective esterification

Monopalmitin

ABSTRACT

An active SBA-15 supported sulfated zirconia catalyst was synthesized by urea hydrolysis method and characterized using N_2 adsorption-desorption, SEM, TEM and EDX analyses. The catalyst was used in glycerol esterification with palmitic acid under continuous nitrogen flow and the performance was demonstrated based on palmitic acid conversion and monopalmitin yield. Effects of reaction conditions such as temperature (160–180 °C) and catalyst loading (1–3 wt. %) were elucidated and correlated with the characteristics of the catalyst. Incorporation of SZ into SBA-15 clearly improved the conversion of palmitic acid and monopalmitin yield. Increases in reaction temperature and catalyst loading increased the conversion of palmitic acid but the yield of monopalmitin was limited to less than 50% due to the pore characteristics that limited the diffusion of bulky molecules into the pore. On top of that, high palmitic acid conversion (86%) with monopalmitin yield of 43% was achieved in 3 h at 170 °C using 2 wt. % of SZSBA-15 catalyst. Moreover, the SZSBA-15 catalyst could be reused for up to four times without significant loss of the catalytic activity.

© 2015 Taiwan Institute of Chemical Engineers. Published by Elsevier B.V. All rights reserved.

1. Introduction

Monoglycerides are commonly used in many industries (food, pharmaceutical and cosmetics) due to their unique properties that can be used as surfactants [1]. Generally, monoglycerides can be synthesized via direct esterification of glycerol with various types of fatty acid. Among all the fatty acids available, palmitic acid is considered to be the best option because this low value feed material can be extracted from a sustainable long-term feedstock like palm oil [2].

More recently, functionalized mesoporous silica based catalysts [3,4] have been used in the selective synthesis of monoglyceride due to uniform and large pore size which are beneficial in the reaction involving bulky molecules. Among them, sulfated zirconia (SZ) on SBA-15 (SZSBA-15) is a promising candidate for such reaction due to its superacidic properties. Previously, SZSBA-15 has been used as a comparison with sulfonic acid supported on SBA-15 in the glycerol esterification with lauric acid under vacuum condition [5]. High monolaurin selectivity (68 %) with 62% lauric acid conversion was demonstrated. However, details on the characteristics of SZSBA-15 catalyst and correlation with its activity are hardly addressed. Although the SZSBA-15 catalyst has been studied in many reactions [6–8], our literature review showed that no work has been reported on the application of SZSBA-15 in the synthesis of monopalmitin via glycerol esterification with palmitic acid. It is a great challenge

to catalyze a reaction involving bulky molecules due to diffusional restriction of the reactants into the pores. Therefore, the application of mesoporous superacidic catalyst like SZSBA-15 is expected to enhance the reaction while improving the mass transport of bulky molecules within the pores.

In this paper, catalytic activity of SZSBA-15 in the esterification of glycerol and palmitic acid (C16:0) has been studied under a continuous nitrogen flow. The structural, surface and chemical characteristics of SZSBA-15 catalyst have been investigated and correlated with the catalytic behavior. The main objective of the present work has been to study the performance of the catalyst to generate new understandings on the effects of operating conditions such as reaction temperature and catalyst loading on the palmitic acid conversion and monopalmitin yield. Reusability study has also been performed to investigate the stability of the catalyst in the reaction at high temperature.

2. Experimental

2.1. Preparation of the catalyst

The SBA-15 was prepared according to the surfactant-templating method [9] with some modifications and the incorporation of SZ onto SBA-15 was achieved following a published urea hydrolysis method [7]. 4.0 g of Pluronic P123 was first dissolved in 150 ml of 2 M HCl under vigorous stirring at 40 °C for 2 h. After that, 9.0 ml of TEOS was added into the solution and the solution was stirred for 30 min.

* Corresponding author: Tel. +604 599 6411; fax: +604 594 1013.

E-mail address: jam.053@yahoo.com (M.H.M. Yusoff).

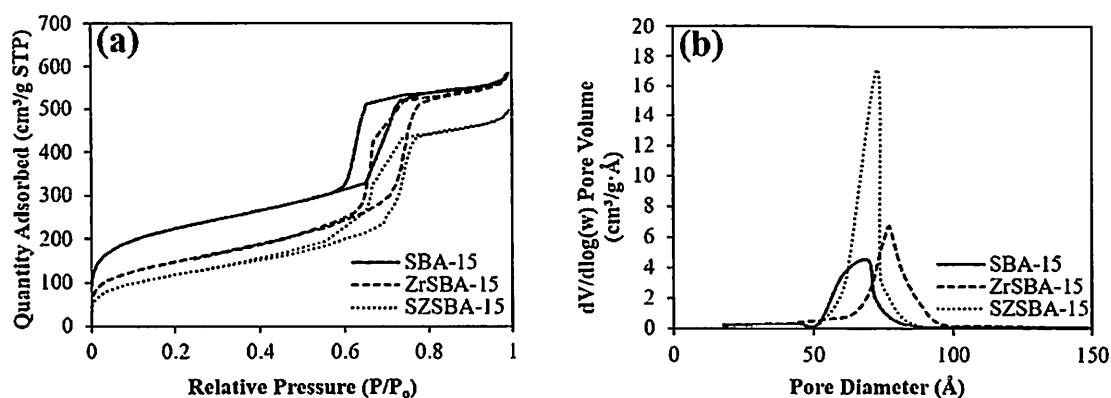


Fig. 1. Profiles of (a) N_2 adsorption–desorption isotherm and (b) pore size distribution of SBA-15, ZrSBA-15 and SZSBA-15.

The stirring rate was then reduced and the reaction system was kept under this condition for another 21.5 h. Then, the content was transferred into a Teflon bottle and subjected to aging at 80 °C for 48 h in an oven. The solid product was then filtered, washed with deionized water, dried in an oven at 80 °C for 24 h and calcined at 500 °C for 6 h. 2.0 g of the calcined SBA-15 was added into a solution containing 0.5812 g of $ZrOCl_2 \cdot 8H_2O$ and 1.083 g of urea in 120 ml of distilled water. The mixture was then refluxed under stirring at 90 °C for 5 h and the resultant gel was filtered and washed to remove excess chloride ions. The filtered gel was dried at 100 °C for 24 h and the product was calcined in the air at 550 °C for 6 h to obtain ZrSBA-15. Sulfation of the solid was carried out by stirring the calcined product with 0.5 M H_2SO_4 (15 ml/g) at room temperature for 3 h. The resultant material was filtered, dried at 100 °C for 2 h and calcined at 550 °C for 3 h.

For comparison, unsupported sulfated zirconia (SZ) was synthesized by calcining $ZrOCl_2 \cdot 8H_2O$ at 600 °C for 5 h to obtain ZrO_2 [10]. The product was sulfated with 0.5 M H_2SO_4 for 3 h at room temperature and calcined at 550 °C for 3 h.

2.2. Catalyst characterization

The catalyst was characterized by N_2 adsorption–desorption analysis, transmission electron microscopy (TEM), scanning electron microscopy (SEM) and energy dispersive X-ray (EDX). N_2 adsorption–desorption analysis was carried out using a Micromeritics ASAP 2020 equipment. The sample was first degassed ($P < 10^{-1}$ Pa) at 270 °C for 6 h. SEM images to study the surface morphology of the catalysts were taken using Quanta FEG 450 SEM and the presence of zirconia and sulfur on the surface was verified using EDX from the same equipment. TEM images were taken using Philips CM12 TEM microscope. The surface acidity of the catalysts was quantitatively estimated using titration method with different acid solutions [11]. 0.5 g catalyst was added into 15 ml of 0.1 M NaOH solution and stirred for 60 min at room temperature. The solid catalyst was then filtered and the solution was titrated using 0.1 M HCl solution with phenolphthalein as an indicator.

2.3. Activity study

The esterification reaction was carried out in a 250 ml three-necked round bottom flask reactor. A continuous nitrogen flow of 10 cm^3/min was used to ensure continuous removal of water. In a typical procedure, palmitic acid (0.0585 mol), glycerol (0.2340 mol) and a specified amount of catalyst (with respect to palmitic acid) were added into the reactor, heated to 170 °C and stirred for 3 h. 1 ml sample was withdrawn from the reactor for every 30 min and kept inside micro centrifuge tubes. Then, 200 μL of the product was withdrawn and added into a vial containing 200 μL water and 200 μL

methyl acetate [12]. The mixture was vortexed and subsequently centrifuged to separate the organic layer and 40 μL of it was diluted with 1000 μL acetone and 100 μL internal standards (10 mg/ml *n*-tetradecane in acetone). Mono-, di- and tripalmitin were analyzed using a gas chromatograph (Agilent 7820A) equipped with a capillary column (15 m \times 0.32 mm \times 0.10 μm CP Sil 5CB). The conversion of palmitic acid and selectivity of the respective glycerides were calculated according to a published literature [13].

3. Results and discussion

3.1. Characterization of catalyst

The physical properties of SBA-15 before and after the incorporation of SZ were investigated using N_2 adsorption–desorption analysis. The isotherms and pore size distributions of the catalysts are illustrated in Fig. 1. Fig. 1a shows that all of the isotherms exhibit a type IV model which represents the typical feature of mesoporous materials [14]. The results suggested that the mesoporous structure of the catalysts was satisfactorily preserved even after the incorporation of SZ which indicates the deposition of active sites on the external surface of silica framework. Furthermore, a clear H1 hysteresis loop with a steep increase in the adsorption value within a relative pressure (P/P_0) ranging from 0.5 to 0.9 was observed indicating that the catalysts had highly ordered mesostructure with cylindrical channels [15]. Meanwhile, Fig. 1b confirms the defined structure of the SZSBA-15 which had narrow pore size distribution in the meso size range.

Table 1 shows the results from the surface analysis. The surface area and average pore diameter of SBA-15 were found to be 769 m^2/g and 57 Å, respectively. The high surface area which is typical for SBA-15 makes it suitable to be used as the support material for better and uniform distribution of zirconia. However, upon introduction of zirconia with subsequent sulfation, the surface area significantly decreased to 419 m^2/g due to the partial collapse of the pore structure. Meanwhile, the pore volume decreased from 0.89 to 0.75 cm^3/g to suggest that some of the sulfated zirconia species were successfully loaded into the mesoporous SBA-15 channels. Nevertheless, the pore diameter increased from 57 Å to 63 Å. The increase in the pore size indicated that the preparation condition used in this study allowed the enlargement of mesoporous structure of SBA-15. This phenomenon was also observed in a reported study [16]. Since larger pores will minimize diffusion limitations for bulkier molecules such as long-chain fatty acid, this phenomenon would give significant effect on the catalytic activity in terms of reactant's conversion and selectivity.

SEM and TEM images of SBA-15 and SZSBA-15 are presented in Fig. 2. As illustrated in Fig. 2a, the prepared SBA-15 support evidently composed of rope-like domains with uniform size (roughly 1 μm) which were aggregated into wheat-like morphology. This was similar

Table 1
Surface characteristics of the catalysts and support.

Material	Surface area (m ² /g)	Pore volume (cm ³ /g)	BJH pore diameter (Å)	Acidity (mmol/g)
SBA-15	769	0.89	57	–
ZrSBA-15	421	0.78	66	2.04
SZSBA-15	419	0.75	63	2.40
SZ	21	0.08	161	0.81

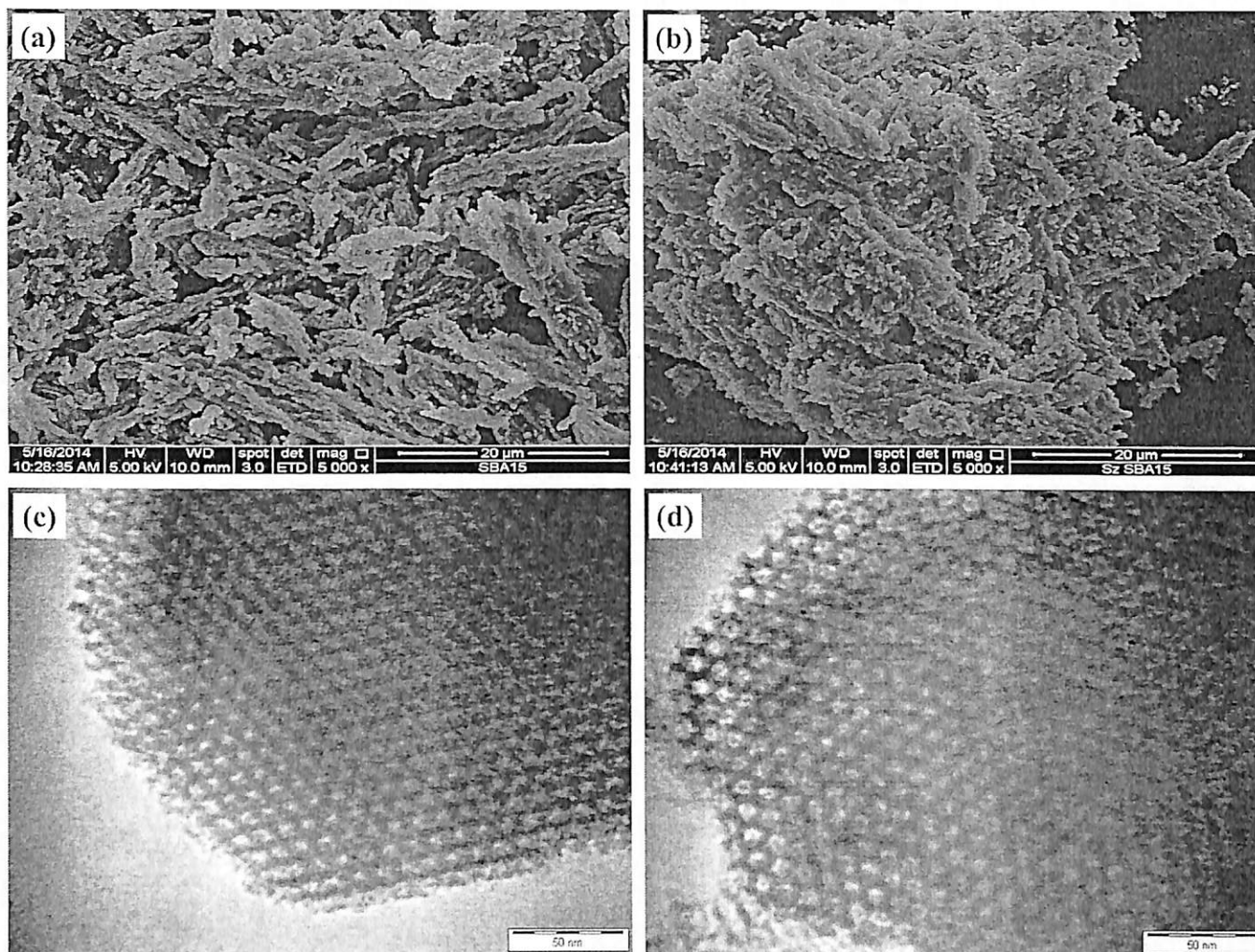


Fig. 2. SEM images of (a) SBA-15, (b) SZSBA-15, and TEM images of (c) SBA-15 and (d) SZSBA-15.

to the conventional SBA-15 structure as reported in a previous work [9]. It is interesting to note that the wheat-like macrostructure agglomerated into a more dense material after sulfation, as shown in Fig. 2b. This was due to the presence of ZrO₂ phase which was attached to the mesopores and in the voids between the wheat-like macrostructure. The agglomeration of the catalyst could explain the formation of bulkier molecules (di- and triglycerides) from the reaction on the external surface and within the voids of SZSBA-15 as observed in the catalytic activity study. Even so, the rope-like domains remain unaffected even after the impregnation of zirconia with subsequent sulfation.

Fig. 2c and d show the TEM images of SBA-15 and SZSBA-15, respectively. As shown in Fig. 2c, SBA-15 exhibits well-ordered hexagonal arrays of uniform mesopores and the structure was consistent with results in a previous report [7]. Meanwhile, Fig. 2d shows that the hexagonal mesoporous structure was preserved after the

incorporation of sulfated zirconia which indicates the high structural stability of silica framework. Furthermore, the enlargement of the pores was observed in the SZSBA-15 sample suggesting the dispersion of sulfated zirconia that mostly occurred outside the pores which resulted in a partial collapse of the pore structure. This result was consistent with the surface analysis in which the pore size enlarged after the incorporation of sulfated zirconia. From the surface analysis, SEM and TEM images, it can be concluded that the SBA-15 and mesoporous SZSBA-15 catalysts were satisfactorily formed in this study.

EDX analysis was performed in order to verify the presence of zirconia and sulfur on the synthesized SZSBA-15. The elemental compositions on the surface of the catalysts are tabulated in Table 2. SBA-15 was found to consist of Si atom (29.74 wt. %) and O atom (70.26 wt. %). After the addition of SZ, the results show the presence of 6.36 wt. % of zirconia (Zr) and 1.61 wt. % of sulfur (S). The composition of Zr slightly decreased from 6.50 to 6.36 wt. % which possibly

Table 2
EDX results of the catalysts and support.

Catalyst	Component							
	O		Si		Zr		S	
	wt.%	at.%	wt.%	at.%	wt.%	at.%	wt.%	at.%
SBA-15	70.26	80.57	29.74	19.43	0.00	0.00	0.00	0.00
ZrSBA-15	60.98	75.62	32.52	22.97	6.50	1.41	0.00	0.00
SZSBA-15	57.52	77.40	34.51	21.23	6.36	0.89	1.61	0.49

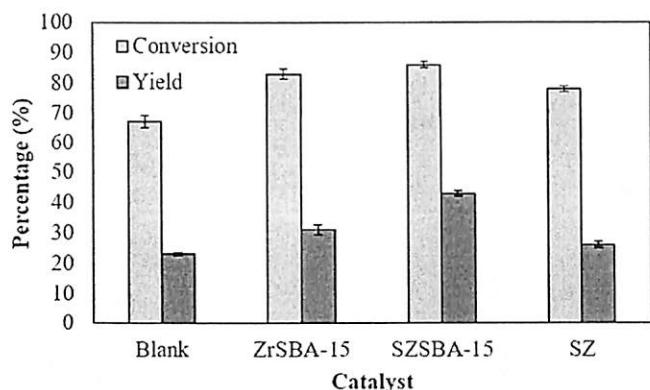


Fig. 3. Performance of SZSBA-15 catalyst in glycerol esterification with palmitic acid.

resulted from the agglomeration of Zr ions into larger domains [8]. Despite these results, the EDX analysis evidently confirmed the presence of zirconia and sulfur which indicates the effectiveness of the preparation method.

3.2. Catalytic activity in glycerol esterification

3.2.1. Performance of the catalyst

The activity of the SZSBA-15 catalyst was investigated in glycerol esterification with palmitic acid and the results are illustrated in Fig. 3. The reaction was conducted at 170 °C for 3 h with a glycerol/palmitic acid molar ratio and catalyst loading of 4:1 and 2 wt. %, respectively. Blank experiment was performed under the same conditions and the result shows that the conversion of palmitic acid and monopalmitin yield in the absence of catalyst were 68% and 23%, respectively. High conversion was attributed to the autocatalytic effect considering the acidic nature of palmitic acid aided by high reaction temperature. However, the reaction could not restrict the formation of higher glycerides (di- and tripalmitin) that led to the low monopalmitin yield. The autocatalytic effect has been previously reported in several studies [17–19] which implied that this spontaneous reaction under acidic condition and high temperature could not be neglected. Meanwhile, the unsupported SZ catalyst exhibited low catalytic activity with 78% conversion (26% yield), which could be ascribed to its low surface area [20]. On the other hand, the activity was enhanced using ZrSBA-15 catalyst due to its high acidity compared to the unsupported catalyst, as shown in Table 1. Interestingly, after sulfation, the activity of the catalyst was significantly improved, and 86% conversion with 43% yield was obtained using SZSBA-15 catalyst. This result could be attributed to the increasing catalyst acidity after sulfation which favorably enhanced the reaction toward the formation of monopalmitin. Therefore, compared to the unsupported and unsulfated catalysts, SZSBA-15 catalyst has successfully enhanced the catalytic activity and improved the monopalmitin yield.

3.2.2. Effect of reaction temperature

The effect of reaction temperature was investigated in the range of 160–180 °C. This study was conducted using a constant glycerol/palmitic acid molar ratio of 4:1 and a constant catalyst loading

of 2 wt. %. As shown in Fig. 4a, the palmitic acid conversion increased with increasing temperature. After 3 h, the conversion of palmitic acid at 160 °C was found to be 76% while the conversion at 170 °C and 180 °C were 86% and 90%, respectively. This finding is consistent with the fact that by increasing the reaction temperature, the mobility of the molecules increases [21]. The kinetic energy is much higher at higher temperature, increasing the frequency of collision between the bulky molecules and subsequently accelerates the reaction rate that led to significant increase in palmitic acid conversion. Monopalmitin yield as a function of reaction time for various reaction temperatures is shown in Fig. 4b. It was found that increasing reaction temperatures significantly improved the monopalmitin yield. The monopalmitin yield at 180 °C was found to be 47% which was higher compared to the other temperatures. At higher temperature, the residence time for the molecules to interact with the active sites on the catalyst was shorter due to the rapid mass transfer of the molecules as a result of high kinetic energy. This consequently increased the number of effective collisions and subsequently improved the catalytic activity [22]. Although catalyst activity was higher at high temperature (180 °C), it is not practical from economic point of view considering high energy consumption. On the contrary, the monopalmitin yield was quite low at 160 °C due to low palmitic acid conversion and monopalmitin selectivity.

3.2.3. Effect of catalyst loading

While varying the catalyst loadings between 1 and 3 wt. % (with respect to palmitic acid), the other reaction parameters such as reaction temperature and reactant molar ratio were fixed at 170 °C and 4:1, respectively. Fig. 5 shows the effect of catalyst loadings on the conversion and monopalmitin yield. As shown in Fig. 5a, increasing the catalyst loading from 1 to 3 wt. % significantly increased the conversion of palmitic acid. This is due to the increasing number of acid sites on the catalyst which could provide effective interaction with the reactant molecules. However, the difference in the conversion was only significant during the first 2 h of the reaction. At longer reaction time, the conversion was found to be leveled off for all catalyst loadings. This observation suggests that there were more acid sites available in the reaction mixture than actually required by the reactant molecules [13]. Thus, increasing catalyst loading above 3 wt. % would no longer improve the conversion. Similar trend was also reported in a previous work [23] which lead to a conclusion that the reaction rate was not significantly influenced by varying catalyst loading.

Fig. 5b shows the effect of catalyst loading on the monopalmitin yield after 3 h of reaction time. As shown in the figure, increasing the catalyst loading from 1 to 3 wt. % significantly increased the monopalmitin yield. Low monopalmitin yield was observed for 1 wt. % of catalyst loading because of the decreasing number of active sites available on the catalyst. Meanwhile, high monopalmitin yield was obtained using 3 wt. % of SZSBA-15 catalyst. However, the yield started to level off after 2 h and finally reached 42% at 3 h which was almost similar to that of 2 wt. % catalyst. This result could be attributed to the formation of higher glycerides on the external surface of the catalyst which in turn, improved the dipalmitin yield. Since the increase in the catalyst amount used did not significantly improve the final conversion, further addition of catalyst was not necessary.

3.2.4. Reusability of the catalyst

The reusability and stability of the catalyst was investigated in glycerol esterification with palmitic acid. After each catalytic run, the catalyst was recovered, washed with 10 ml of methanol and calcined at 450 °C for 2 h. It was found that the monopalmitin yield decreased from 43% to 36% after four consecutive runs, as shown in Fig. 6. The loss of some activity may be explained by the loss of sulfur which consequently reduced the acidity of the catalyst and decreased the

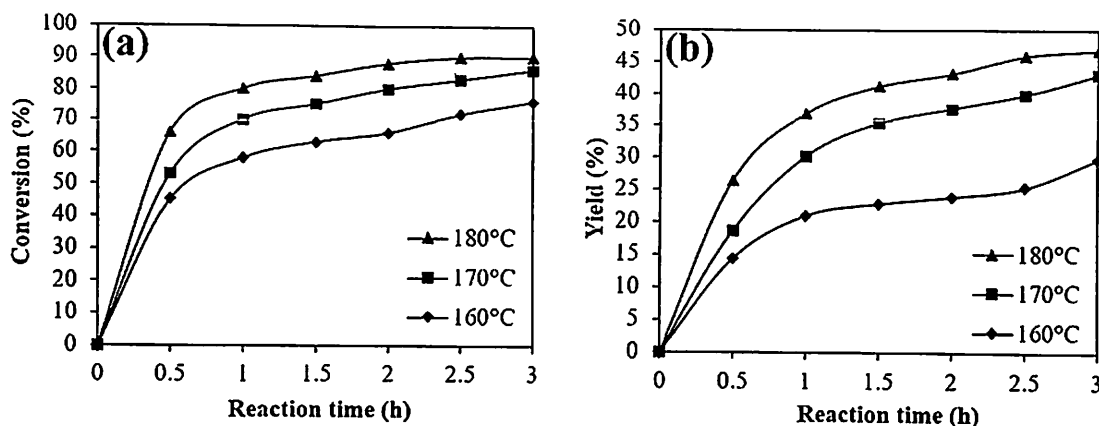


Fig. 4. Effects of reaction temperature on (a) palmitic acid conversion and (b) yield of monopalmitin.

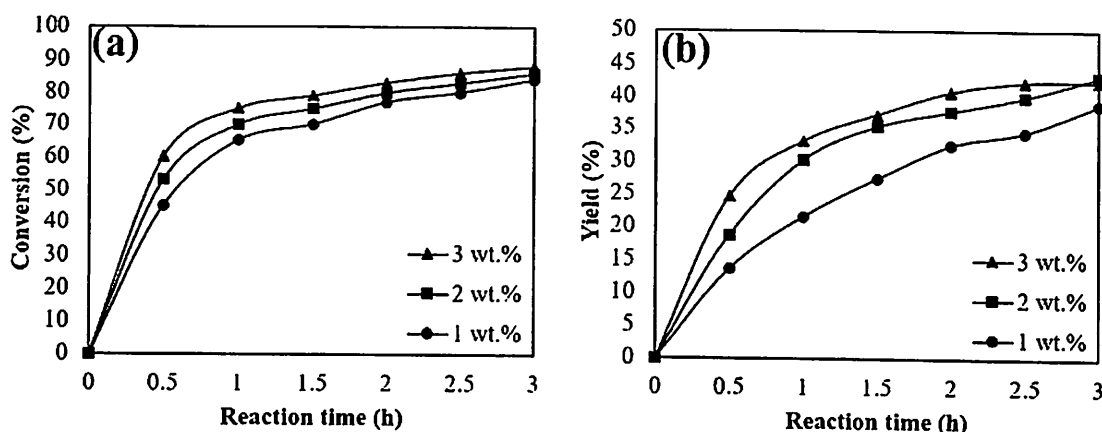


Fig. 5. Effects of catalyst loading on (a) palmitic acid conversion and (b) yield of monopalmitin.

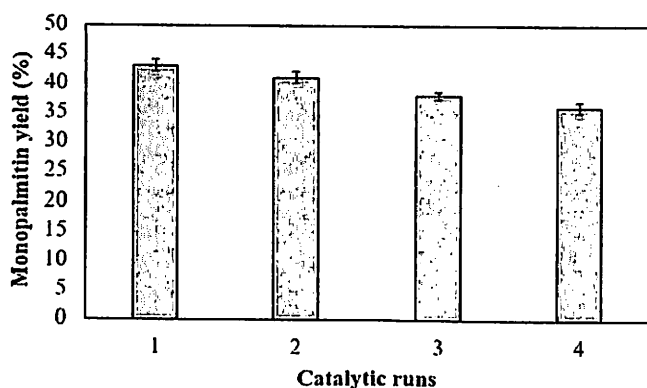


Fig. 6. Reusability of SZSBA-15 catalyst in glycerol esterification with palmitic acid (Reaction temperature = 170 °C, reaction time = 3 h, glycerol/palmitic acid = 4:1, catalyst loading = 2 wt. %).

conversion of palmitic acid. This finding was supported by the result obtained from EDX analysis in which the amount of sulfur reduced from 1.61 wt. % to 0.68 wt. % after four consecutive runs. On the contrary, the amount of zirconia was maintained at around 6.2–6.4 wt. %. N_2 adsorption–desorption analysis for the spent catalysts revealed that the pore diameter remained unchanged even after four consecutive runs. Thus, it can be concluded that the decrease in the monopalmitin yield was mainly due to the reduced acidity as a result of sulfur leaching, not because of the collapse of the pore structure as represented in Table 3. Furthermore, the reusability of this catalyst in

Table 3
Physicochemical properties of the fresh and spent catalysts.

Material	Surface area (m^2/g)	Pore diameter (\AA)	Sulfur content (wt. %)
Fresh	419	63	1.61
Spent 1	406	63	1.23
Spent 2	415	63	0.93
Spent 3	411	64	0.68

this reaction was much better compared to that of in the esterification of oleic acid with methanol [20].

3.3. Comparison with reported catalysts

The results from this study were comparable with those of previous works on glycerol esterification with smaller fatty acid like lauric acid. The monoglyceride yield obtained at 170 °C using this catalyst was higher compared to that of HPA supported on SBA-15 [4]. Less than 30% of monolaurin yield was obtained in their study while 43% of monopalmitin yield was observed in this study. In another study, high fatty acid conversion (94%) was observed using sulfonic acid grafted on SBA-15 [13]. However, the amount of catalyst used was quite high (5 wt. %) compared to this work that required only 2 wt. % of SZSBA-15 to attain 86% conversion. Furthermore, the reaction time was relatively longer (20 h) compared to this work which took only 3 h. The esterification of oleic acid with glycerol in the presence of tin-organic framework (Sn-EOF) was studied and high monoolein selectivity (99% at 26% conversion) was obtained within 8 h [17]. However, the monoolein yield was only about 26% which was lower



Deoxygenation of Palmitic Acid to Produce Diesel-like Hydrocarbons over Nickel Incorporated Cellular Foam Catalyst: A Kinetic Study

Lilis Hermida^{1,2}, H Amani¹, Ahmad Zuhairi Abdullah^{1*} and Abdul Rahman Mohamed¹

¹School of Chemical Engineering, Universiti Sains Malaysia, 14300 Nibong Tebal, Penang, Malaysia

²Department of Chemical Engineering, Universitas Lampung, Bandar Lampung 35145, Indonesia

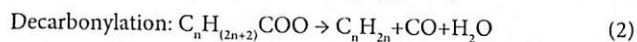
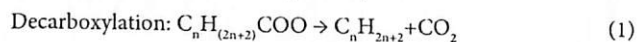
Abstract

Nickel incorporated mesostructured cellular foam (NiMCF) was studied as a catalyst for palmitic acid deoxygenation to primarily synthesize *n*-pentadecane and 1-pentadecene. The kinetic behaviour was tested in a temperature range from 280 to 300°C. The reaction was found to follow a first order kinetic model with respect to the palmitic acid with an activation energy of 111.57 KJ/Mol. In the reusability study, it was found that the average reduction in palmitic acid conversions was about 40.5%, which indicated the occurrence of catalyst deactivation during the deoxygenation. Fresh and spent catalysts were characterized by means of scanning electron microscope. Energy-dispersive X-ray spectroscopy and X-ray powder diffraction correlate their characteristics with catalytic activity and to identify the main catalyst deactivation mechanism. The catalyst deactivation was mainly due to phase transformation of metallic nickel (Ni⁰) to nickel ion (Ni²⁺) and the deposition of organic molecules on the catalyst during the deoxygenation. Regeneration of spent catalyst successfully reduced the drops in the palmitic acid conversions between the reaction cycles from 40.5% to 11.3%.

Keywords: Mesostructured cellular foam catalyst; Palmitic acid deoxygenation; Microstructure; Diesel-like hydrocarbons; Kinetics

Introduction

Exhaustion of petroleum oil or crude oil is predicted in the near future [1]. The shortage of crude oil will have global impact on the economy, culture and health of every nation as in this situation; fuel oil prices will go up. The high fuel oil price will induce other commodities or goods to be sold at relatively high prices. Diesel fuel is a kind of fuel oil that is obtained by refining crude oil in petroleum refineries. It has been predicted that the world demand for diesel fuel will grow faster than any other refined oil products in 2035 [2]. Therefore, renewable sources with related technologies should be identified as alternatives. Extensive studies on biofuels production from various renewable feedstocks have been carried out for many years. Among others, catalytic deoxygenation of fatty acids as renewable resources can be a potential technology to synthesize diesel-like hydrocarbons. During fatty acid deoxygenation, *n*-alkanes and alkenes will be produced through decarboxylation and decarbonylation [3] reactions, respectively;



The *n*-alkanes and alkenes are hydrocarbons that are similar to those found in crude oil derived diesel fuel [4].

Recently, extensive works have been reported on deoxygenation of various fatty acids to produce diesel-like hydrocarbons. They were carried out either in the presence of solvent or solventless condition using various catalysts such as Pd supported on mesoporous carbon [5-11] or on mesoporous silica [12-14]. Although the catalyst derived from Pd exhibited significant activity in the deoxygenation reactions, they are usually expensive. Ni-based catalysts are more practical on an industrial scale due to their availability and economic feasibility [15-18].

The use of Al₂O₃ or MgO-Al₂O₃ supported Ni catalysts for oleic acid deoxygenation in a batch reactor under solvent free and inert atmosphere conditions have been investigated [19]. Ni supported on mesostructured cellular foam (MCF) silica has been reported to be a more effective catalyst compared to Ni supported on Al₂O₃ or SBA-15 catalysts for pyrolytic decomposition of cellulose to produce H₂ [20].

This could be due to the larger pores in MCF silica support to minimize the diffusional effects of reactants as well as the products [21,22].

In our earlier work, various Ni functionalized mesostructured cellular foam (NiMCF) catalysts were used for solventless deoxygenation of palmitic acid at 300°C for 6 h in a semi batch reactor to produce *n*-pentadecane and 1-pentadecene as diesel-like hydrocarbons [23]. The catalysts were synthesized using different structures of MCF silicas prepared under various conditions. It was found that NiMCF catalyst using MCF silica prepared with 9.2 ml of tetra-ethyl-ortho-silicate (TEOS) and subsequently aged for 3 days showed the highest activity for the process. However, no attempt has been made so far to study the reaction kinetic and reusability of the NiMCF catalyst.

In the present study, kinetic of solventless deoxygenation of palmitic acid has been studied in a temperature range from 280 to 300°C. Reusability of NiMCF catalyst has also been evaluated in the deoxygenation process. The main mechanism for the catalyst deactivation has been successfully elucidated based on SEM, XRD and TGA results.

Experimental

Preparation of NiMCF catalyst

NiMCF catalyst was synthesized using MCF silica prepared with 9.2 mL of tetraethyl orthosilicate (TEOS) and aged for 3 days [23]. Nickel incorporation of into the support was achieved through deposition-

*Corresponding author: Ahmad Zuhairi Abdullah, School of Chemical Engineering, Universiti Sains Malaysia, 14300 Nibong Tebal, Penang, Malaysia, Tel:+6045996411; E-mail: chzuhairi@usm.my

Received February 11, 2016; Accepted February 27, 2016; Published March 07, 2016

Citation: Hermida L, Amani H, Abdullah AZ, Mohamed AR (2016) Deoxygenation of Palmitic Acid to Produce Diesel-like Hydrocarbons over Nickel Incorporated Cellular Foam Catalyst: A Kinetic Study. J Adv Chem Eng 6: 144. doi:10.4172/2090-4568.1000144

Copyright: © 2016 Hermida L, et al. This is an open-access article distributed under the terms of the Creative Commons Attribution License, which permits unrestricted use, distribution, and reproduction in any medium, provided the original author and source are credited.

precipitation process and subsequently reduced in hydrogen stream at 550°C for 2.5 h and cooled down under nitrogen flow.

Kinetic of solventless palmitic acid deoxygenation

Kinetic of solventless palmitic acid deoxygenation was performed in a semi-batch mode in which gaseous products (CO₂, CO, etc.) produced during the reaction were continuously removed. The deoxygenation reaction was carried out in a 250 mL three-necked flask reactor equipped with a magnetic stirring bar, reflux condenser and a tube to pass pure nitrogen flow to reaction mixture. During the reaction, nitrogen stream was used to sweep the evolved gaseous products. The reaction vessel was heated with a stirring hot plate. 6 g of palmitic acid and 15 wt% (with respect to palmitic acid) of catalyst amount were then added into the reactor. Before an experiment was started, nitrogen flow was passed through the reaction mixture for 30 min to create an inert reaction environment. Then, the reaction mixture was heated to different temperatures (280-300°C) and maintained for different reaction times (2 to 6 h) under rapid stirring. During the reaction, the gaseous products were collected in a gas-sampling bulb. At the end of the reaction, the mixture was allowed to cool to about 100°C, and then poured through a filter paper to separate the liquid products from the spent catalyst. Analysis of the liquid products was achieved using Agilent Technology 7890A gas chromatograph and then validated using a Perkin Elmer GC-MS system (Clarus 600).

Product analysis

Gas products in were identified by means of a Shimadzu C11484811134 GC system equipped with a thermal conductivity detector (TCD) and a capillary column. A mixture of standard gases with known composition was injected into the GC to identify each of the gas components based on their retention times. The mixture standard gas consisted of 30 vol% CO₂, 30 vol% CO, 30 vol% H₂ and 10 vol% Ar. It should be noted that the palmitic acid conversion and the desired product selectivity were based on the liquid-phase concentrations of the products. The gas-phase analyses were performed only for the confirmation of the presence of CO₂ and CO in the gaseous products.

Meanwhile, liquid product was collected and analyzed by means of an Agilent Technology 7890A GC system equipped with a flame ionization detector and a non-polar capillary column (GsBP-5). The detector and injector temperatures were set at 280°C and 250°C, respectively. The column temperature was set at 135°C for 1 min and was then programmed at 15°C/min to 290°C, and it was maintained constant at this temperature for 2 min. 20 µL sample was dissolved in 200 µL hexane, and then a direct injection into the gas chromatograph was carried out. The 1-pentadecane (CH₃(CH₂)₁₃CH₃) was used as standard to identify substances in a liquid product and to create calibration curves. The calibration curves were used to determine the concentration of substances in the liquid product. Calibration curve was generated using a series of chemical standards with known concentrations. Palmitic acid conversion, product selectivity and product yield were calculated according to Fu et al. [24] using Equations (3), (4) and (5), respectively.

$$\text{Conversion \%}, C = \frac{[C_{PA,0}] - [C_{PA,t}]}{[C_{PA,0}]} \times 100\% \quad (3)$$

$$\text{Selectivity \%}, S = \frac{[C_{PA,t}]}{[C_{PA,0}] - [C_{PA,t}]} \times 100\% \quad (4)$$

$$\text{Yield \%} = C \times S \times 100\% \quad (5)$$

where, [C_{PA,0}]=Concentration of palmitic acid before reaction

[C_{PA,t}]=Concentration of palmitic acid after reaction

[C_{p,t}]=Concentration of a product (*n*-pentadecane or 1-pentadecene) after reaction

Reusability study of NiMCF catalyst

For reusability study of the catalyst, fresh NiMCF catalyst with amount 15 wt.% (with respect to palmitic acid) was used for the solventless deoxygenation of palmitic acid at 300°C for 2, 3, 4, 5 and 6 h. After the experiment, the spent NiMCF catalyst was filtered out from the catalytic reaction mixture, washed thoroughly with dichloromethane, and then dried at 100°C overnight. Then, the washed spent catalyst was directly reused for the following deoxygenation runs using the same procedure.

Meanwhile, in the regeneration of catalyst, the washed spent catalyst was re-reduced under H₂ flow at 550°C for 2.5 h to regenerate it. After that, the spent catalyst was reused for the next deoxygenation run using the same procedure. The regenerated catalyst was characterized by means of TGA, SEM and XRD analyses. For comparison, spent NiMCF catalyst without regeneration was also characterized using the same analytical method.

Characterization of NiMCF catalyst

The SEM images were captured using a Leo Supra 50 VP field emission SEM. Before observations were made at room temperature, the samples were coated with high purity gold for electron reflection at a thickness of 20 nm by using a Polaron SC 515 Sputter Coater. Then, samples were mounted on aluminium stubs with double-sided adhesive tape for the observations carried out at a magnification of 50 kX.

X-ray diffraction (XRD) analysis was performed using a Siemens 2000X system to obtain XRD patterns of fresh, spend and regenerated catalysts in order to identify the different phases in the catalysts. The X-ray diffraction pattern was recorded using Cu-Kα radiation at 2θ angles ranging from 10-100°C. The TGA was carried out to observe the change in weight of the catalyst sample as it was heated in a certain temperature range. The thermal gravimetric analyzer unit coupled with a TG controller (TAC 7/DX) was supplied by Perkin-Elmer, USA. About 5 mg of catalyst sample was heated from 31-840°C at a heating rate of 10°C/min and an airflow rate of 25 ml/min.

Results and Discussion

Mechanisms of palmitic acid deoxygenation over NiMCF catalyst

In this study, the catalyst used was in powder form as obtained from the preparation method. Attempt to measure the particle sizes was not done bearing in mind that the catalyst particles were visibly reduced to even smaller sizes during the reaction under continuous mixing for up to 6 h. The stirring speed was set at about 250 rpm. Under such conditions, no significant external mass transfer effect was expected as generally reported in literatures [10-13].

Solventless palmitic acid deoxygenation over NiMCF catalyst in a semi batch reactor at 300°C produced mainly *n*-pentadecane and 1-pentadecene (Figure 1). In this reaction, *n*-pentadecane and 1-pentadecene were the predominant products so that the concentrations of both products were high at the end of the reaction. In the first 3 h of reaction, palmitic acid was converted

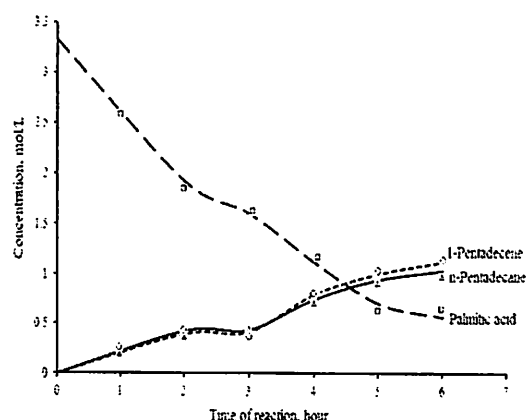


Figure 1: Solventless palmitic acid deoxygenation over NiMCF catalyst at 300°C with catalyst loading of 15 wt%.

into *n*-pentadecane and 1-pentadecene in which concentration of *n*-pentadecane was slightly higher than that of 1-pentadecene. This indicated that decarboxylation reaction was a more favoured reaction than decarbonylation reaction during this period. On the other hand, at reaction times longer than 3 h, concentrations of 1-pentadecene were usually higher than those of *n*-pentadecane. This observation gave the indication that decarbonylation reaction was the more dominant reaction compared to decarboxylation reaction. The lower *n*-pentadecane concentration was ascribed to the higher formation of CO gas that could inhibit the palmitic acid decarboxylation. CO gas which is a by-product from palmitic acid decarbonylation is poison to the catalyst in the decarboxylation reaction [25]. The activity of this catalyst was comparable with that reported by Roh et al. [19] using Ni/MgO-Al₂O₃ catalyst.

CO₂ and CO gases were detected in gaseous product through GC equipped with TCD detector. Meanwhile, *n*-pentadecane and 1-pentadecene were also detected in liquid products through GC-MS analysis. Besides *n*-pentadecane and 1-pentadecene, other products such as cyclopentadecane, ketone, etc. were also present at small quantities in the liquid products. This indicated that deoxygenation of palmitic acid over NiMCF catalyst in this study occurred not only through decarboxylation and decarbonylation reactions, but other reactions could also occur. Based on the reaction products, reaction pathways of solventless palmitic acid deoxygenation reaction could be proposed. Palmitic acid is first deoxygenated through decarboxylation reaction to produce *n*-pentadecane and CO₂ and through decarbonylation reaction to produce 1-pentadecene, CO and H₂O. Besides that, 1-pentadecene can also be produced through dehydrogenation of *n*-pentadecane. Moreover, a part of palmitic acid is converted into *n*-hexadecane (C₁₆H₃₄) through hydrogenation reaction [5].

Kinetic of solventless deoxygenation of palmitic acid over NiMCFcatalyst

Kinetic study of palmitic acid deoxygenation over the synthesized NiMCF catalyst was investigated at three different temperatures (280, 290 and 300°C). 6 g of palmitic acid and catalyst loading of 15 wt% was used in all the experiments. The kinetic model of oleic acid under inert atmosphere is suggested to follow first order with respect oleic acid [26]. Hence, the first order kinetic model for palmitic acid deoxygenation can be expressed as follows;

$$\text{Rate} = \frac{-d[C_{PA}]}{dt} = k[C_{PA}] \quad (6)$$

where, *k* is the rate constant, *t* is reaction time and [C_{PA}] is the concentration of palmitic acid. In the kinetic study, the change in the palmitic acid concentration with the time was followed from the start of the reaction, [C_{PA}]₀ at *t*=0 to [C_{PA}]_{*t*} at time *t*. These are the limits between which integration is performed. Upon integration and rearrangement, the final equation obtained is;

$$\ln = \frac{[C_{PA}]_t}{[C_{PA}]_0} = -kt \quad (7)$$

The experimental results obtained in this study are shown in Figure 2. As can be seen in the figure, the increase in temperature resulted in an increase in the disappearance of palmitic acid concentration. This indicated that the temperature had positive effect in accelerating the reaction rate. Since the kinetic model of the palmitic acid deoxygenation is assumed to follow a first order model with respect palmitic acid, Equation (7) can be used. Figure 2 shows the plot of Equation (7) which ln [C_{PA}]_{*t*}/[C_{PA}]₀ is plotted against the reaction times. All the experimental data obtained for the palmitic acid deoxygenation experiments are found to be in good agreement with the Equation 7 due to the high value of correlation coefficient (R² are above 0.95) for all the straight lines. This indicates that the assumption that was used in this analysis was valid.

The integrated form of the rate law allows us to find the concentration of palmitic acid at any time after the start of the reaction. The slopes of the straight lines obtained by plotting ln [C_{PA}]_{*t*}/[C_{PA}]₀ versus the reaction time give *-k*, as can be seen in Figure 2. The reaction rate constants (*k*) are summarized in Table 1. As can be seen in the table, the increase in temperature resulted in the increase in the reaction rate constant. This was because mobility of reactant molecules was higher when the temperature was increased. The higher mobility of palmitic acid molecules made it easier for the molecules to reach the metallic nickel that might be located in the cell or the window pores in the NiMCF catalyst. The metallic nickel sites were the active sites for catalyzing the palmitic acid deoxygenation to produce diesel-like hydrocarbons of *n*-pentadecane and pentadecene [19].

Phenomenon of molecular diffusion is generally relevant in most liquid phase reactions involving porous catalysts. Furthermore, a rather viscous liquid (palmitic acid) was used as the reactant in this reaction. However, it has been reported that catalyst having a minimum average

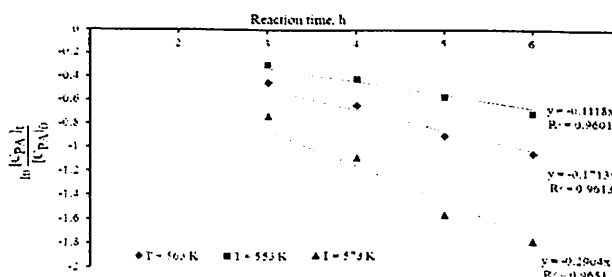


Figure 2: Plot of ln[CPA]_{*t*}/[CPA]₀ versus reaction time at various temperature.

Temperature (K)	Specific rate constant, <i>k_s</i> (h ⁻¹)
553	0.1118
563	0.1713
573	0.2904

Table 1: Specific rate constants for the first order kinetic model.

pore size of 20 Å is required for liquid phase reactions to effectively avoid internal diffusion effect of the reactants and products [22]. In this study, structure of the NiMCF catalyst with large cell size (234 Å) and window pore size (90 Å) in the NiMCF catalyst should favour diffusion of the reactant and product molecules [23]. Thus, the effect of internal diffusion limitation should be negligible considering the small particle sizes of the catalyst. As such, reactant molecules reacted faster in the catalyst when mobility of reactant and product molecules was higher. Feature of molecular diffusions in three-dimensional structure of NiMCF catalyst together with its cell and window pores can be seen in Figure 3.

The rate constant, k , is related to the reaction temperature by the Arrhenius equation. The equation takes into account the rate constant of chemical reactions (k), reaction temperature (T), the activation energy (E_A), the pre-exponential factor (A) and the universal gas constant R . The Arrhenius equation is a relationship for the dependence of a reaction rate on temperature;

$$\ln k = \ln A - E_A/RT \quad (8)$$

where; k = specific rate constant, h^{-1}

A = pre-exponential factor, h^{-1}

E_A = activation energy, J/mol

R = gas constant = $8.314 J/mol.K$

The activation energy, E_A , and pre-exponential factor, A , can be obtained by plotting $\ln k$ versus $1/T$. The plot should produce a straight line in which a slope and intercept equal to $-E_A/R$ and $\ln A$, respectively. On the basis of data obtained from Table 1, a plot of $\ln k$ vs $1/T$ yields a straight line with high value of correlation coefficient ($R^2 > 0.95$). This result shows that the reaction rate constant follows the Arrhenius law, as can be seen in Figure 4. The value of activation energy (E_A) and pre-exponential factor (A) are calculated to be 111.565 kJ/mol and $38 \times 10^8/h$, respectively. The value of E_A for this reaction is relatively lower than that reported in literature for Ni/MgO-Al₂O₃ (123 kJ/mol) to indicate higher activity of the catalyst used in this study [19].

With the kinetic parameters (E_A , A and k) that were obtained, mathematical model of rate expressions can be constructed as follows,

$$-r_{PA} = 38 \times 10^8 \exp\left(-\frac{111565}{RT}\right) [C_{PA}]^{\frac{-1}{h}} \quad (9)$$

The values of palmitic acid concentrations can be calculated using the first order kinetic model using Equation (7). The values of the palmitic acid concentration from the calculation and from the experimental results are presented in Table 2.

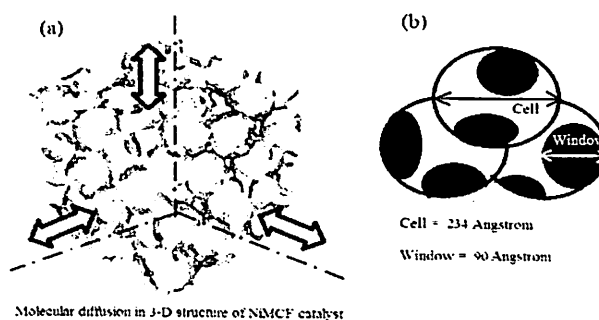
A parity plot between the experimental and calculated values of palmitic acid concentration is showed in Figure 5. As can be seen in the figure, the values of the palmitic acid concentration calculated at any time after the start of the reaction are in good agreement with experimental palmitic acid concentrations with a high value of correlation coefficient ($R^2 > 0.95$). It can be concluded from the results that palmitic acid deoxygenation over NiMCF catalyst satisfactorily followed first order kinetic model with respect to palmitic acid.

Reusability study of NiMCF catalyst

One of the major obstacles in the use of supported metal catalyst in fatty acid deoxygenation for production of diesel-like hydrocarbons is catalyst deactivation. Study of reusability of catalyst is important

for the economic assessment of the catalytic fatty acid deoxygenation process. Through the catalyst reusability study, stability and degree of catalyst deactivation can be examined. In this part of work, reusability of the NiMCF catalyst was studied through experiments in which the NiMCF catalyst after one cycle of use (or spent NiMCF catalyst) was re-used without regeneration for further solventless palmitic acid deoxygenation palmitic cycle. Alternatively, the catalyst was also regenerated as described in section 2.4 and used in the same reaction. Figure 6 shows results of the palmitic acid conversions obtained from various reaction times for the fresh NiMCF and the spent NiMCF catalyst.

As can be seen in Figure 6, palmitic acid conversions decreased after one cycle of use for all reaction times. This indicated the occurrence of significant deactivation of NiMCF catalyst during the palmitic acid



Molecular diffusion in 3-D structure of NiMCF catalyst

Figure 3: (a) Molecular diffusions in 3-D structure of NiMCF catalyst, (b) cell and window pores in NiMCF catalyst.

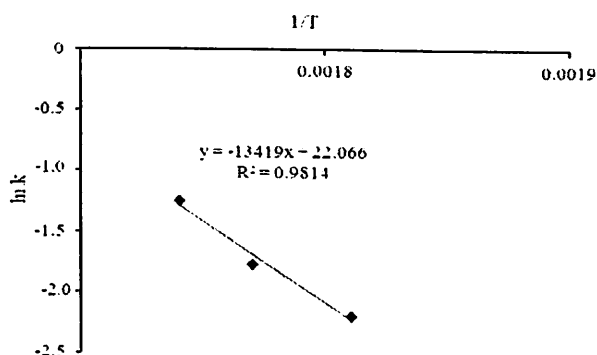


Figure 4: Arrhenius plot for palmitic acid deoxygenation over NiMCF catalyst.

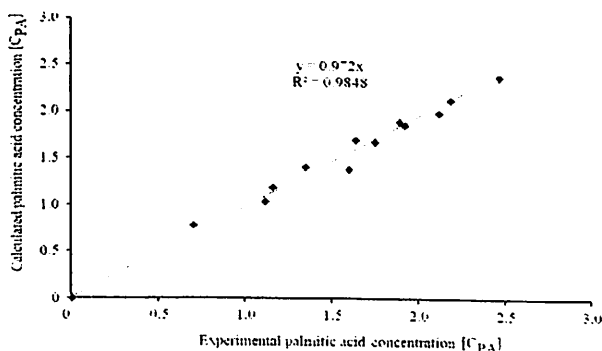


Figure 5: Parity plot between the experimental and calculated values of palmitic acid concentration.

Time (h)	[C _{PA}] at 553 K		[C _{PA}] at 563 K		[C _{PA}] at 573 K	
	Experimental	Calculated	Experimental	Calculated	Experimental	Calculated
2	-	-	-	-	1.92	1.86
3	2.47	2.38	2.12	1.99	1.6	1.39
4	2.19	2.13	1.75	1.68	1.12	1.04
5	1.89	1.9	1.35	1.41	0.7	0.78
6	1.64	1.7	1.16	1.19	0.56	0.58

Table 2: Values of experimental palmitic acid concentrations versus calculated ones.

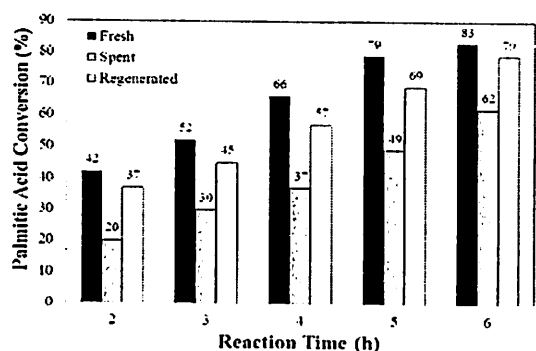


Figure 6: Comparison between solvent less palmitic acid deoxygenation over fresh NiMCF, spent and regenerated NiMCF catalyst.

deoxygenation process after the first cycle. The catalyst deactivation caused reductions on the fatty acid conversion. The spent catalyst achieved palmitic acid conversion of 20% at a reaction time of 2 h. Meanwhile, fresh catalyst achieved palmitic acid conversion of 42% at a reaction time of 2 h. Thus, the reduction in palmitic acid conversion at 2 h of reaction is 52.8%. Meanwhile, reduction of palmitic acid conversion at 3, 4, 5 and 6 h of reaction time were 42.3%, 43.9%, 38.0% and 25.3%, respectively. Hence, average reduction of palmitic acid conversion using spent catalyst was 40.5%.

Figure 6 also shows palmitic acid conversions obtained by using the fresh NiMCF and regenerated NiMCF catalysts in the solventless palmitic acid deoxygenation using the same operating conditions. As can be seen, palmitic acid conversions using the regenerated catalyst were slightly lower than those using fresh catalyst for all reaction times. Reduction of palmitic acid conversion at 2, 3, 4, 5 and 6 h of reaction time were 11.9%, 13.5%, 13.6%, 12.7% and 4.8%, respectively. The average reduction of palmitic acid conversion using a semi-batch reactor was 11.3%.

Despite significant reduction in palmitic acid conversion, the values achieved by the regenerated catalyst were higher than those achieved by the spent catalyst without regeneration. By regenerating the spent catalyst, the extent on the drop in palmitic acid conversion reduced from 40.5% to 11.3%. This indicated that the regeneration of the spent catalyst using this method could improve the performance of the spent catalyst.

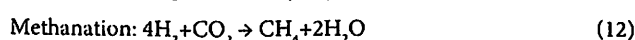
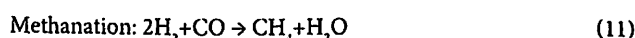
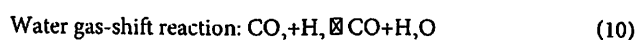
Deactivation of palladium supported on MCF catalyst (PdMCF) has been reported to be severe after one cycle of use for stearic acid deoxygenation in the presence of dodecane as solvent [14]. Almost no conversion of stearic acid was achieved by spent PdMCF catalyst in the deoxygenation reactions at reaction times from 0 until 6 h. PdMCF catalyst was mainly deactivated by significant organic deposition on the catalyst during the reaction. Other deactivation mechanism i.e., oxidation of metallic palladium and agglomeration of palladium particles on the catalyst was insignificant. The catalyst deactivation sources were elucidated based on results of various characterization

tests. Regeneration of the spent PdMCF catalyst was also carried out by sequential hot extractions with solvents tetrahydrofuran (THF), hexane and dichloromethane (DCM) followed by re-reduction process at 300°C. The regenerated catalyst showed a 19-fold increase in decarboxylation activity as compared to the spent PdMCF catalyst.

In order to identify mechanism of catalyst deactivation, several catalyst characterization methods such as XRD, SEM and TGA were performed. Evaluation of the deactivation mechanism involved comparison of the physical and chemical characteristics for the fresh and spent NiMCF catalysts. However, excessive discussion on the catalyst characteristics is avoided as in this liquid phase reaction, changes in the characteristics of the catalyst could significantly occur during the reaction and characteristics that are obtained ex-situ such as surface characteristics etc. could give misleading information on the reaction. In this study, the catalyst was recovered after the reaction by filtration and washed with organic solvents followed by drying. Unfortunately, complete removal of organic substances from the surface of the catalyst was not achieved. These organics would decompose during the degassing step (at 300°C) of surface analysis through nitrogen adsorption-desorption to cause errors in the results. Thus, attempts to measure the surface area after the reaction were unsuccessful. Figure 7 compares the characteristic of the fresh, spent and regenerated NiMCF catalysts by means of an XRD analysis method. For the spent catalyst sample, XRD pattern displays a peak at $2\theta=23^\circ$ that is attributed to the presence of amorphous silica. Besides that, the XRD pattern displays peaks at $2\theta=33$ and 60° that are characteristic of nickel ions (Ni^{2+}) that could be in the form of nickel phyllosilicates [27].

Furthermore, peak at $2\theta=44^\circ$ attributed to metallic nickel particles is almost not detected in the spent catalyst sample. This indicated that metallic nanoparticle sintering, agglomeration and ripening that are common nanoparticles phenomena were not the main cause of deactivation in this system. In fact, higher peaks at $2\theta=33$ and 60° in the XRD pattern of the spent catalyst compared to those in the pattern of fresh catalyst could be due to involvement of water vapour that oxidized the metallic nickel nanoparticles (Ni^0) during the palmitic acid deoxygenation so that they changed into nickel ions (Ni^{2+}) that could be in the form of nickel phyllosilicate or nickel oxide phases.

Water vapour is a by-product in palmitic acid decarbonylation and hydrogenation. It could also be produced through water gas-shift reaction and methanation [28,29] in which molecules of H_2 from dehydrogenation reactions react with molecules of other gaseous products, i.e., CO_2 and CO (by-products from decarboxylation and decarbonylation), as given in the following reactions;



It has been reported in literature that the presence of water vapor reduced the activity iron catalyst in Fischer-Tropsch reaction due to

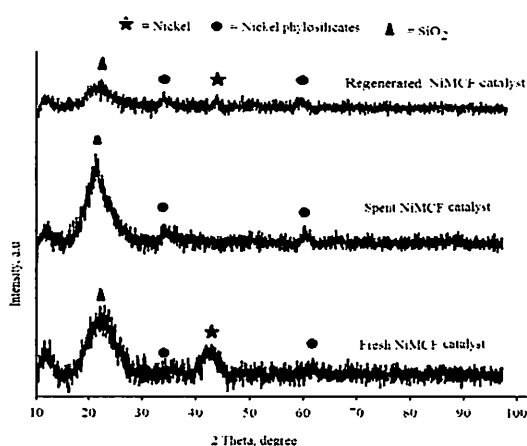


Figure 7: XRD patterns of fresh, spent and regenerated NiMCF catalysts.

the oxidation of iron catalyst by water vapor [30]. Meanwhile, nickel catalyst was found to have low activity for hydrocarbon transformation in the presence of water vapour due to oxidation metallic nickel by water vapour [31]. Through the oxidation reaction, metallic nicks in $\text{Ni}/\text{Al}_2\text{O}_3$ catalyst transformed into nickel ions (Ni^{2+}) in the form of nickelous oxide phases that rapidly re-crystallize [32]. This nickel catalyst deactivation mechanism can be applicable to the deactivation of NiMCF catalyst by water vapor in this study.

For the fresh catalyst sample, the presence of metallic nickel particles was clearly detected through the observation on the XRD pattern, as can be seen in Figure 7. The phase transformation from metallic nickel (Ni^0) into nickel ion (Ni^{2+}) reduced the activity of the spent catalyst in the deoxygenation reaction. This caused the decrease in palmitic acid conversion this system. It can be concluded that metallic particles (Ni^0) in NiMCF catalyst have higher active sites than nickel ion (Ni^{2+}) in NiMCF catalyst for the palmitic acid deoxygenation reaction. This result was in agreement with reports that oxide type catalysts such as MnO_3/C , MnO/C , WO_3/C , $\text{NiOMoO}_3/\text{Al}_2\text{O}_3$ and $\text{V}_2\text{O}_5/\text{C}$ had lower activities compared to metal type catalysts such as Ni/C , Co/SiO_2 , Ni/SiO_2 and $\text{Ni}/\text{Al}_2\text{O}_3$ for deoxygenation of bio-oil [33] and also for deoxygenation of fatty acid methyl ester.

On the basis of the aforementioned characterization results, it is hypothesized that the catalyst deactivation in this study could be attributed to organic molecules derived from reactant and products as well as small deposits of coke on the catalyst. Besides that, phase transformation from metallic nickel (Ni^0) into to nickel ion (Ni^{2+}) was also responsible for the catalyst deactivation. Therefore, regeneration of the spent catalyst was then carried out. Furthermore, the regenerated catalyst was characterized by means of XRD and SEM. Figure 7 also shows the comparison between XRD pattern of spent NiMCF catalyst and that of regenerated NiMCF catalyst.

The XRD pattern of the regenerated catalyst displayed the presence of peak at $2\theta=44^\circ$ that is characteristics to the metallic nickel particles. However, peaks at $2\theta=33$ and 60° that are characteristics of the nickel phyllosilicates are still present with considerable intensities in the regenerated catalyst. This indicated that not all nickel phyllosilicate was reduced into metallic nickel after the re-reduction process. The re-reduction process was carried out at 550°C for 2.5 h in this study. The unreduced nickel phyllosilicate was probably due to very high interactions between nickel phyllosilicates and MCF silica. As such, in order to reduce the more nickel phyllosilicate, the re-reduction process should be carried out at higher temperatures and/or for a longer period.

In order to identify the possibility of catalyst deactivation due to deposition of organic molecules on the spent catalyst, weight loss, thermal behaviour and structural destruction of the spent catalyst were investigated using TGA analysis method. Figure 8 shows a TGA thermo gram of the spent catalyst together with the first derivative whether its weight change from the TGA test. A decomposition region occurred from temperatures of around 250 to 600°C . The derivative of the thermo gram clearly exposes this inflection with maximum peak at around 400°C . The decomposition of the spent catalyst in this region could be attributed to the removal of organic components that were deposited on the catalyst. Removal of organic components deposited in spent Pd functionalized MCF catalyst at the same temperature region was reported in the literature [14].

Morphologies of the fresh and spent NiMCF catalyst were examined by means of SEM. The SEM image results are shown in Figure 9. The SEM image of the spent catalyst clearly confirms layered structures in the spent catalyst. The layered structures contained nickel ions (Ni^{2+}) that could be in the form of nickel phyllosilicate. The SEM image of the spent catalyst also confirmed that the spent catalyst had fewer porous structures compared to the fresh catalyst. Meanwhile, the SEM image of the fresh catalyst reveals high porous structures with Nano worm structures of nickel nanoparticles on the MCF silica.

Figure 9 also shows comparison between SEM images of the fresh NiMCF catalyst and regenerated NiMCF catalysts. The SEM image of the regenerated catalyst confirmed nickel nanoparticles in the form of Nano worm structures with sizes of around 19 nm. The structures in the regenerated catalyst were almost the same with those in fresh catalyst but the nickel nanoparticle sizes in the regenerated catalyst were slightly larger than those in fresh catalyst. Besides that, mesoporous structures in the regenerated catalyst were slightly lower than those in fresh catalyst. Nevertheless, the regenerated catalyst regained nearly all of lost porosity and metallic nickel particles after the sufficient removal of deposited organic molecules and followed by the re-reduction process.

Conclusion

Kinetic of solventless palmitic acid deoxygenation over nickel functionalized mesostructured cellular foam catalyst (NiMCF) to selectively synthesize *n*-pentadecane and 1-pentadecene (diesel-like hydrocarbons) was successfully studied in a temperature range from 280 to 300°C . The deoxygenation reaction satisfactorily followed a first order kinetic with an activation energy of 111.57 kJ/mol. From the reusability studies of the NiMCF catalyst, it was found that palmitic acid conversions significantly decreased after one cycle of use for all reaction times which suggested the occurrence of catalyst deactivation. The average reduction of palmitic acid conversion was about 40.5%. Based on characterizations of the spent catalyst, the main cause for

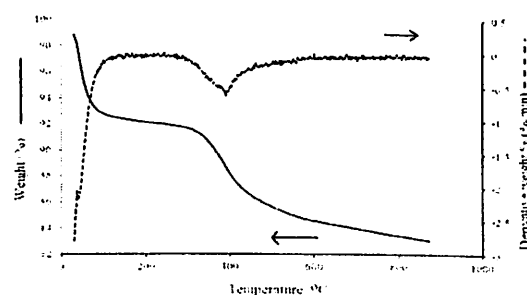


Figure 8: TGA profile (solid line) with its derivative profile (broken line) for spent NiMCF catalyst.

5. Ang GT, Tan KT, Lee KT (2015) Supercritical and Superheated Technologies: Future of Biodiesel Production. *J Adv Chem Eng* 5: e106.

6. Moore M, Herrell B, Counce R, Watson J (2015) A Hierarchical Procedure for Synthesis of a Base Case Solid Oxide Fuel Cell System in Aspen HYSYS. *J Adv Chem Eng* 5: 129.

7. Lee SP, Ramli A (2013) Methyl oleate deoxygenation for production of diesel fuel aliphatic hydrocarbons over Pd/SBA-15 catalysts. *Chem Cent J* 7: 149.

8. Amani H, Ahmad Z, Hameed BH (2014) Highly active alumina-supported Cs-Zr mixed oxide catalysts for low-temperature transesterification of waste cooking oil. *Appl Catal A* 487: 16-25.

9. Maki-Arvela P, Rozmyszowicz B, Lestari S, Simakova O, Eränen K, et al. (2011) Catalytic deoxygenation of tall oil fatty acid over palladium supported on mesoporous carbon. *Energy Fuels* 25: 2815-2825.

10. Amani H, Asif M, Hameed BH (2016) Transesterification of waste cooking palm oil and palm oil to fatty acid methyl ester using cesium-modified silica catalyst. *J Taiwan Inst Chem Eng* 58: 226-234.

11. Mansur AA, Pannirselvam M, Al-Hothaly KA, Adetutu EM, Ball AS (2015) Recovery and Characterization of Oil from Waste Crude Oil Tank Bottom Sludge from Azzawya Oil Refinery in Libya. *J Adv Chem Eng* 5: 118.

12. Albrecht KO, Hallen RT (2011) A Brief Literature Overview of Various Routes to Renewable Fuels from Lipids for the National Alliance for Advanced Biofuels and Bio-products (NABAB) Consortium. Department of Energy, Pacific Northwest National Laboratory.

13. Sivula L, Ilander A, Väisänen A, Rintala J (2010) Weathering of gasification and grate bottom ash in anaerobic conditions. *J Hazard Mater* 174: 344-351.

14. Ping EW, Pierson J, Wallace R, Miller JT, Fuller TF, et al. (2011) On the nature of the deactivation of supported palladium nanoparticle catalysts in the decarboxylation of fatty acids. *Appl Catal A* 396: 85-90.

15. Kho ET, Scott J, Anai R (2016) Ni/TiO₂ for low temperature steam reforming of methane. *Chemical Engineering Science* 140: 161-170.

16. Wang J, Lu AH, Li M, Zhang W, Chen YS, et al. (2013) Thin porous alumina sheets as supports for stabilizing gold nanoparticles. *ACS Nano* 7: 4902-4910.

17. Haltham MA, Bernd H (2015) Template-Assisted Synthesis of Metal Oxide Hollow Spheres Utilizing Glucose Derived-Carbonaceous Spheres As Sacrificial Templates. *J Adv Chem Eng* 5: 116.

18. Oluyoye MA, Wong SW, Chin LH, Amani H, Asif M, et al. (2016) Synthesis of fatty acid methyl esters via the transesterification of waste cooking oil by methanol with a barium-modified montmorillonite K10 catalyst. *Renewable Energy* 86: 392-398.

19. Roh HS, Eum IH, Jeong DW, Yi BE, Na JG, et al. (2011) The effect of calcination temperature on the performance of Ni/MgO-Al₂O₃ catalysts for decarboxylation of oleic acid. *Catal Today* 164: 457-460.

20. Zhao M, Yang X, Church TL, Harris AT (2012) Novel CaO-SiO₂ sorbent and bifunctional Ni/CaO-CaO/SiO₂ complex for selective H₂ synthesis from cellulose. *Environ Sci Technol* 46: 2976-2983.

21. Lam MK, Uemura Y (2015) The Potential of Gamma-Valerolactone (GVL) Production from Oil Palm Biomass. *J Adv Chem Eng* 5: e105.

22. Mahmud GK, Haque MDA, Chowdhury AMS, Ahad MA, Gatut MDA (2014) Preparation and Characterization of Polyester Composites Reinforced with Bleached, Diospyros perfrina (Indian persimmon) Treated and Unbleached Jute Mat. *J Adv Chem Eng* 4: 114.

23. Hermida L, Abdullah AZ, Mohamed AR (2013) Nickel functionalized mesoporous cellular foam (MCF) silica as a catalyst for solventless deoxygenation of palmitic acid to produce diesel-like hydrocarbons. In: *Mendez-Villas A (Ed) Materials and Processes for Energy: Communicating Current Research and Technological Developments*. Brown Walker Press, Boca Raton, USA.

24. Morales G, Meleiro JA, Iglesias J, Paniagua M (2014) Advanced Biofuels from Lignocellulosic Biomass. *J Adv Chem Eng* 4: e101.

25. Immer JG (2010) Liquid-phase deoxygenation of free fatty acids to hydrocarbons using supported palladium catalysts. North Carolina State University, Raleigh.

26. Diaz L, Brito A (2014) FFA Adsorption from Waste Oils or Non-Edible Oils onto an Anion-Exchange Resin as Alternative Method to Esterification Reaction Prior to Transesterification Reaction for Biodiesel Production. *J Adv Chem Eng* 4: 105.

1. Amani H, Ahmad Z, Asif M, Hameed BH (2014) Transesterification of waste cooking palm oil by MnZr with supported alumina as a potential heterogeneous catalyst. *J Ind Eng Chem* 20: 4437-4442.

2. Amani H, Ahmad Z, Hameed BH (2014) Synthesis of fatty acid methyl esters via the methanolysis of palm oil over Ca₃SxZr_{0.5}YAlxO₃ mixed oxide catalyst. *Renewable Energy* 66: 680-685.

3. Ayodele OB, Hamisu U, Jibril MY, Uemurad WM, Dauda AW (2015) Hydrodeoxygenation of oleic acid into n- and iso-paraffin biofuel using zeolite supported fluoro-oxalate modified molybdenum catalyst: kinetics study. *J Taiwan Inst Chem Eng* 50: 142-152.

4. Matzen M, Alhajji M, Yasar D (2015) Demirel Technoeconomics and Sustainability of Renewable Methanol and Ammonia Productions Using Wind Power-based Hydrogen. *J Adv Chem Eng* 5: 128.

deoxygenation in a semi-batch reactor.

spent NiMCF and (c) regenerated NiMCF catalyst obtained from catalytic

of metallic nickel (Ni⁰) into to nickel ion (Ni²⁺) and the deposition

of organic molecules on the NiMCF catalyst during the palmitic

deoxygenation. Regeneration of the spent improved the performance

the spent catalyst in which the extent of drop in the palmitic acid

conversion could be reduced from 40.5% to 11.3%.

Acknowledgments

The authors gratefully acknowledge a Research University grant (No. 814181) from Universiti Sains Malaysia and a Science fund grant (6013381) from MOSTI Malaysia to support this study.

References

1. Amani H, Ahmad Z, Asif M, Hameed BH (2014) Transesterification of waste cooking palm oil by MnZr with supported alumina as a potential heterogeneous catalyst. *J Ind Eng Chem* 20: 4437-4442.

2. Amani H, Ahmad Z, Hameed BH (2014) Synthesis of fatty acid methyl esters via the methanolysis of palm oil over Ca₃SxZr_{0.5}YAlxO₃ mixed oxide catalyst. *Renewable Energy* 66: 680-685.

3. Ayodele OB, Hamisu U, Jibril MY, Uemurad WM, Dauda AW (2015) Hydrodeoxygenation of oleic acid into n- and iso-paraffin biofuel using zeolite supported fluoro-oxalate modified molybdenum catalyst: kinetics study. *J Taiwan Inst Chem Eng* 50: 142-152.

4. Matzen M, Alhajji M, Yasar D (2015) Demirel Technoeconomics and Sustainability of Renewable Methanol and Ammonia Productions Using Wind Power-based Hydrogen. *J Adv Chem Eng* 5: 128.

27. Nares R, Ramirez J, Gutierrez-Alejandre A, Cuevas R (2009) Characterization and Hydrogenation Activity of Ni/Si(Al)- MCM-41 Catalysts Prepared by Deposition-Precipitation. *Ind Eng Chem Res* 48: 1154-1162.
28. Zhao X, Wei L, Cheng S, Huang Y, Yu Y, et al. (2015) Catalytic cracking of camelina oil for hydrocarbon biofuel over ZSM-5-Zn catalyst Original. *Fuel Process Technol* 139: 117-126.
29. Madsen AT, Rozmyszowicz B, Simakova IL, Kipio T, Leino AR, et al. (2011) Step Changes and Deactivation Behavior in the Continuous Decarboxylation of Stearic Acid. *Ind Eng Chem Res* 50: 11049-11058.
30. Hermida L, Abdullah AZ, Mohamed AR (2015) Deoxygenation of fatty acid to produce diesel-like hydrocarbons. *Renewable Sustainable Energy Rev* 42: 1223-1233.
31. Norhasyimi R, Zuhairi A, Abdul Rahman M (2010) Recent progress on innovative and potential technologies for glycerol transformation into fuel additives: A critical review. *Renewable Sustainable Energy Rev* 14: 987-1000.
32. Ullah K, Ahmad M, Sultana S, Teong LK, Sharma VK, et al. (2014) Experimental analysis of di-functional magnetic oxide catalyst and its performance in the hemp plant biodiesel production. *Applied Energy* 113: 660-669.
33. Wolfson A, Yefet E, Alon T, Dlugy C, Tavor D (2015) Glycerolysis of Esters with *Candida antarctica* Lipase B in Glycerol. *J Adv Chem Eng*.

Citation: Hermida L, Amani H, Abdullah AZ, Mohamed AR (2016) Deoxygenation of Palmitic Acid to Produce Diesel-like Hydrocarbons over Nickel Incorporated Cellular Foam Catalyst: A Kinetic Study. *J Adv Chem Eng* 6: 144. doi:10.4172/2090-4568.1000144

OMICS International: Publication Benefits & Features

Unique features:

- Increased global visibility of articles through worldwide distribution and indexing
- Showcasing recent research output in a timely and updated manner
- Special issues on the current trends of scientific research

Special features:

- 700 Open Access Journals
- 50,000 Editorial team
- Rapid review process
- Quality and quick editorial, review and publication processing
- Indexing at PubMed (partial), Scopus, EBSCO, Index Copernicus, Google Scholar etc.
- Sharing Option: Social Networking Enabled
- Authors, Reviewers and Editors rewarded with online Scientific Credits
- Better discount for your subsequent articles

Submit your manuscript at: <http://www.omicsgroup.org/journals/submit.asp>

SELECTIVE ESTERIFICATION OF GLYCEROL WITH LAURIC ACID
TO MONOLAURIN USING H₂-TUNGSTOPHOSPHORIC ACID
INCORPORATED SBA-15

HOO PENG YONG

UNIVERSITI SAINS MALAYSIA
2016

**SELECTIVE ESTERIFICATION OF GLYCEROL WITH
LAURIC ACID TO MONOLAURIN USING
12-TUNGSTOPHOSPHORIC ACID INCORPORATED SBA-15**

by

HOO PENG YONG

Thesis submitted in fulfilment of the requirements

for the degree of

Doctor of Philosophy

MAY 2016

SULFATED ZIRCONIA SUPPORTED ON SBA-15
FOR SELECTIVE GLYCEROL ESTERIFICATION
WITH PALMITIC ACID TO MONOPALMITIN

MOHD E ZAM BIN MOHD YUSOFF

UNIVERSITI SAINS MALAYSIA
2016

**SULFATED ZIRCONIA SUPPORTED ON SBA-15 FOR SELECTIVE
GLYCEROL ESTERIFICATION WITH PALMITIC ACID TO
MONOPALMITIN**

by

MOHD HIZAMI BIN MOHD YUSOFF

**Thesis submitted in fulfillment of the
requirements for the degree of
Doctor of Philosophy**

September 2016

UNIVERSITY OF MALAYA
FACULTY OF EDUCATION
DEPARTMENT OF EDUCATIONAL PSYCHOLOGY

TATAKALANGAN

UNIVERSITI MALAYSIA
2012

**FUNCTIONALIZED MCM-41 WITH ZIRCONIA FOR
ESTERIFICATION OF GLYCEROL TO MONOGLYCERIDE**

By

NATASHA BINTI GHAZALI

**Thesis submitted in fulfillment of the requirements for the degree of
Masters of Science**

AUGUST 2012

SEKOLAH PASAFAKULTAS TEKNIK
POLITEKNIK NEGERI MALANG
CIKUTAN, ANGGREK

SYAFIHA NASHIRUDDIN HANIFFA SAGHI

UNIVERSITI SAINS MALAYSIA
2015

**Cs-HPW/SBA-15 CATALYST FOR SELECTIVE
PRODUCTION OF MONOLAURIN FROM
GLYCEROL AND LAURIC ACID**

by

SYAMIMA NASRIN BT MOHAMED SALEH

**Thesis submitted in fulfillment of the requirements for Master's
Degree**

July 2015

International Conference on Biomass: Technology, Application and Sustainable Development

October 10 – 11th 2016 Salak Tower Hotel, Bogor Indonesia

Secretariate: SBRC-IPB. Kampus IPB Baranangsiang, Jl. Padjajaran No. 1. Bogor

Contact Person: Athin (+62 81282797110), Hendri (+62 81310889744), Email : icbbogor2016@gmail.com,
Website : www.icbbogor2016.com

Bogor, September 17th, 2016

Prof. Dr. Ahmad Zuhairi Abdullah
Universiti Sains Malaysia

Dear Prof. Dr. Ahmad,

We are pleased to inform you that Surfactant and Bioenergy Research Center (SBRC) IPB will conduct the **International Conference on Biomass: Technology, Application and Sustainable Development** on October 10th – 11th, 2016, in Salak Tower Hotel, Bogor, Indonesia.

The themes of the conference will be : **Sharing Knowledge and Experienced on Biomass Technology, Application and Its Sustainable Development**

In this conference, we would like to invite you to join this conference as a **Invited Speaker**. We do hope you are willing to join us in this conference. For further information, you could contact us in our official website at www.icbbogor2016.com or through email at icbbogor2016@gmail.com.

We are looking forward to seeing a positive response from you and your willingness to share your expertise to the audiences.

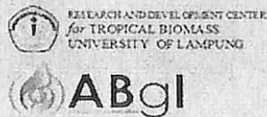
Best Regards,



Dr. Endang Warsiki, STP, M.Si
Chairman

Website : www.icbbogor2016.com
Email : icbbogor2016@gmail.com
Phone : Fifin N. Nisya (+62 81381709617)
Athini Nuryanti (+62 81282797110)
Hendri Wijaya (+62 81310889744)
Adress : Surfactant and Bioenergy Research Center
Kampus IPB Baranangsiang
Jl. Raya Pajajaran No. 1, Bogor, Jawa Barat, Indonesia 16144

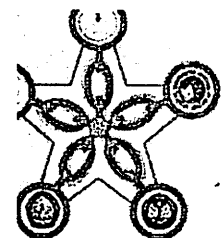
Organized by:



Supported by:



BPDPSawit



11th Joint Conference on Chemistry

in conjunction with

The 4th Regional Biomaterials Scientific Meeting

Purwokerto, 15-16 September 2016



Purwokerto, June 10, 2016

Prof. Dr. Ahmad Zuhairi Abdullah
Universitas Sains Malaysia (USM), Malaysia

Dear Prof. Dr. A Z Abdullah,

We are pleased to invite you to be a **Invited Speaker** on the **"11th Joint Conference on Chemistry 2016 in conjunction with The 4th Regional Biomaterials Scientific Meeting 2016"** scheduled to be held between **September 15-16, 2016** in Horizon Hotel , Purwokerto, Jawa Tengah, Indonesia.

The themes of the conference will be on the following topics:
"Material Chemistry Development for Future Medicine, Industry, Environmental and Biomaterial Application"

We look forward to a positive response, to our organiser for the event and from there we can provide you with any additional information you might require.

Best Regards,

Amin Fatoni, Ph.D
Chairman

Website : jcc.fmipa.unsoed.ac.id
Email : jccunsoed@gmail.com
Phone : +6281327717444 (Amin Fatoni)
+6285814438770 (Anung Riapanitra)
+628170611988 (Hartiwi Diastuti)

Address : Department of Chemistry, Faculty of Mathematics and Natural Sciences, Universitas Jenderal Soedirman. Jl. Dr. Soeparno 61, Karangwangkal, Purwokerto, Jawa Tengah, Indonesia 53125.



Tarikh : 9 Mac 2015

Memorandum

Profesor Dr. Ahmad Zuhairi Abdullah
Pusat Pengajian Kejuruteraan Kimia
Universiti Sains Malaysia
Kampus Kejuruteraan

Universiti Sains Malaysia
Aras 6, Bangunan Canselor
11800, USM Pulau Pinang, Malaysia
T : (6)04-653 3108/3178/3988/5019
F : (6)04-656 6466/8470
: (6)04-653 2350
L : www.research.usm.my
www.usm.my

Tuan,

KEPUTUSAN PERMOHONAN SKIM GERAN PENYELIDIKAN TRANSDISIPLINARI (TRGS) FASA 2/2014

TAJUK PROGRAM : *PRODUCTION OF VALUABLE CHEMICALS FROM CRUDE GLYCEROL USING CATALYTIC AND BIOCHEMICALS METHODS*
JUMLAH PROJEK : 3
JUMLAH PERUNTUKAN : RM755,600.00 (KESELURUHAN PROGRAM)

Dengan segala hormatnya perkara di atas adalah dirujuk.

2. Tahniah diucapkan di atas kejayaan tuan memperolehi geran TRGS Fasa 2/2014 di bawah Kementerian Pendidikan Malaysia (KPM) sebagai **Ketua Program** seperti tajuk di atas. Berikut ialah butiran penting berkaitan projek beserta nombor akaun untuk rujukan dan tindakan oleh pihak tuan.

Ketua Program	Profesor Dr. Ahmad Zuhairi Bin Abdullah	PTJ	Pusat Pengajian Kejuruteraan Kimia
Penyelidik bersama	1. Profesor Dr. Farook Adam 2. Prof. Madya Dr. Mohd Roslee Othman 3. Dr. Melati Khairuddean	PTJ	1. Pusat Pengajian Sains Kimia 2. Pusat Pengajian Kejuruteraan Kimia 3. Pusat Pengajian Sains Kimia
No. Akaun	203 / PJKIMIA / 6762001		
Tajuk Projek	<i>Mesoporous Composite Catalyst for Conversion of Purified Crude Glycerol to Lactic Acid</i>		
Tempoh Projek	36 bulan	Jumlah Peruntukan	RM311,200.00
Tarikh Mula	1 Februari 2015	Tarikh Tamat	31 Januari 2018

3. Senarai tiga buah projek lain di bawah program ini adalah seperti berikut :

Bil.	Ketua Projek/PTJ	Tajuk Projek	Peruntukan (RM)
1.	Profesor Dr. Bassim H. Hameed (Pusat Pengajian Kejuruteraan Kimia)	<i>Development of Highly-Active and Reusable Structured Catalyst for the Conversion of Glycerol as By-Product from Biodiesel Production to Value-Added Glycerol Carbonate</i>	282,000.00
2.	Dr. Noor Aziah Binti Serri (Pusat Pengajian Teknologi Industri)	<i>Enzymatic Esterification for Optimal Production of Monoglycerides via Immobilized Lipase</i>	162,400.00

4. Bersama-sama ini disertakan Garis Panduan Umum Geran Penyelidikan Transdisiplinari (TRGS) seperti di lampiran untuk perhatian pihak tuan.

Sekian, terima kasih.

"BERKHIDMAT UNTUK NEGARA"
'Memastikan Kelestarian Hari Esok'



(PROFESOR DR. LEE KEAT TEONG)

Pengarah

Pejabat Pengurusan dan Kreativiti Penyelidikan

s.k. Timbalan Naib Canselor
(Penyelidikan & Inovasi)
Universiti Sains Malaysia

Dekan
Pusat Pengajian Kejuruteraan Kimia
Universiti Sains Malaysia
Kampus Kejuruteraan

Ketua Penolong Bendahari
Jabatan Bendahari
Universiti Sains Malaysia
Kampus Kejuruteraan



Rujukan Fail : USM/INNOV/DIA2014

Tarikh : 30 September 2014

Building J06
Universiti Sains Malaysia
11800 USM, Penang, Malaysia
T : 604-653 2616 / 3166 / 3038
F : 604-653 4399
W : <http://innovations.usm.my>

Prof. Madya Dr. Ahmad Zuhairi Abdullah
Timbalan Dekan (Penyelidikan)
Pusat Pengajian Kejuruteraan Kimia
Kampus Kejuruteraan
Universiti Sains Malaysia
14300 Nibong Tebal
Pulau Pinang

Tuan,

KEPUTUSAN PERMOHONAN DANA INOVASI AWAL UNIVERSITI SAINS MALAYSIA TAHUN 2014

Dengan hormatnya perkara di atas dirujuk.

2. Sukacita dimaklumkan bahawa Pejabat Inovasi & Pengkomersilan, Bahagian Penyelidikan & Inovasi, Universiti Sains Malaysia telah meluluskan permohonan tuan untuk menjalankan penyelidikan di bawah peruntukan Dana Inovasi Awal Universiti Sains Malaysia seperti berikut :

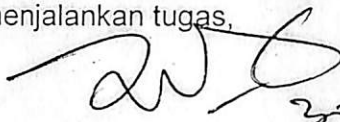
Penyelidik Utama	Prof. Madya Dr. Ahmad Zuhairi Abdullah	PTJ	Pusat Pengajian Kejuruteraan Kimia
Penyelidik Bersama	Prof. Madya Dr. Mohd Azmier Ahmad	PTJ	Pusat Pengajian Kejuruteraan Kimia
Tajuk Projek	<i>Feasibility Demonstration of Palm Oil Based Monoglycerides Production as Halal Emulsifiers using Heterogeneous Catalytic Reactor System</i>		
No. Akaun	1001/PJKIMIA/AUPI00234		
Jumlah Peruntukan Projek	RM 50,000.00	Tempoh Projek	12 bulan
Tarikh Mula	15 September 2014	Tarikh Tamat	14 September 2015

3. Kerjasama tuan untuk mengembalikan Borang Perakuan (**Lampiran A**) dalam tempoh **5 hari bekerja** dari tarikh surat ini amatlah dihargai. Bersama-sama ini disertakan juga **Syarat dan Garis Panduan Dana Inovasi Awal** untuk makluman dan tindakan tuan selanjutnya.

Sekian, terima kasih.

"BERKHIDMAT UNTUK NEGARA"
'Memastikan Kelestarian Hari Esok'

Yang menjalankan tugas,



20/9/2014

PROFESOR DR. RAHMAT AWANG

Pengarah

No. tel : 04-653 2616

E-mel : rahmat@usm.my

s.k. **Ybhg. Profesor Dato' Dr. Muhamad Jantan**
Timbalan Naib Canselor
Penyelidikan & Inovasi

Dekan

Pusat Pengajian Kejuruteraan Kimia
Universiti Sains Malaysia

Unit Belanjawan Kumpulan Wang Penyelidikan dan APEX
Jabatan Bendahari] untuk tindakan
Kampus Kejuruteraan
Universiti Sains Malaysia